DISEÑO DE LA PEROXIGENASA INESPECÍFICA DE *Agrocybe aegerita* MEDIANTE EVOLUCIÓN DIRIGIDA: EXPRESIÓN FUNCIONAL EN LEVADURAS Y SÍNTESIS DE 1-NAFTOL

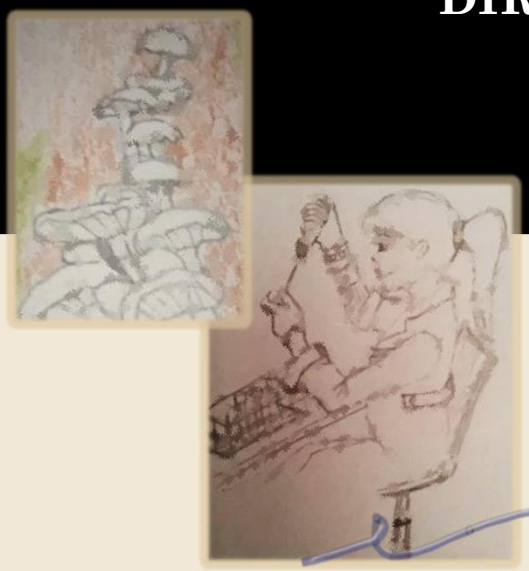

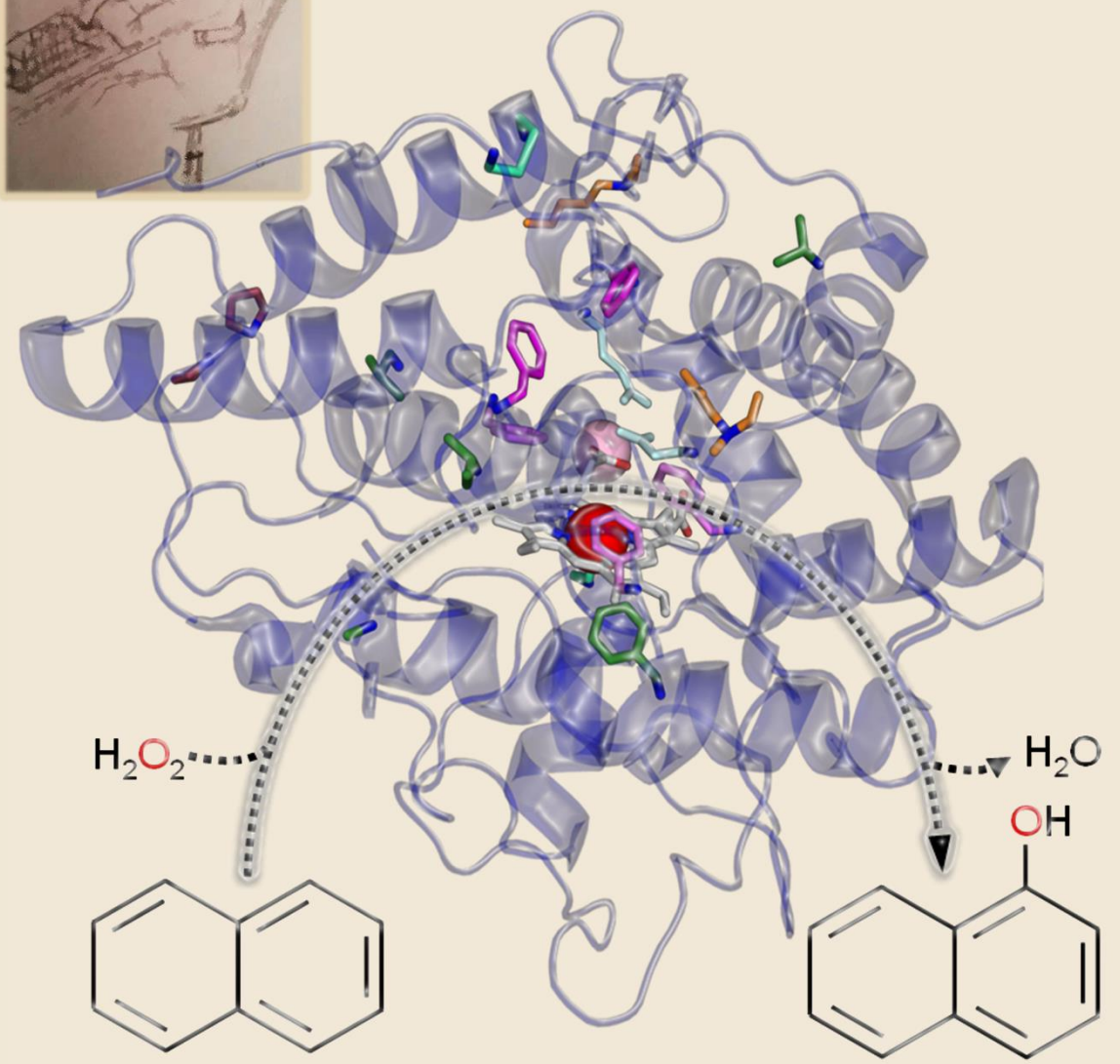

TESIS DOCTORAL

PATRICIA MOLINA ESPEJA

UNIVERSIDAD AUTÓNOMA DE MADRID

DEPARTAMENTO DE BIOLOGÍA MOLECULAR

PATRICIA MOLINA ESPEJA

DISEÑO DE LA PEROXIGENASA INESPECÍFICA DE *Agrocybe aegerita* MEDIANTE EVOLUCIÓN DIRIGIDA: EXPRESIÓN FUNCIONAL EN LEVADURAS Y SÍNTESIS DE 1-NAFTOL

MEMORIA

Para optar al grado de Doctora en Bioquímica, Biología Molecular, Biomedicina y Biotecnología (Biociencias Moleculares)

DIRECTOR

Dr. Miguel Alcalde

Instituto de Catálisis y Petroleoquímica

Consejo Superior de Investigaciones Científicas, Madrid

TUTORA:

Dra. María Fernández Lobato

Universidad Autónoma De Madrid

Facultad de Ciencias, Departamento de Biología Molecular

Madrid, 2016

Miguel Alcalde Galeote, Dr. en Ciencias Biológicas, Investigador Científico del CSIC

CERTIFICA: Que el presente trabajo "Diseño de la peroxigenasa inespecífica de *Agrocybe aegerita* mediante evolución dirigida: expresión funcional en levaduras y síntesis de 1-naftol" constituye la Memoria que presenta la Licenciada en Biología por la Universidad de Salamanca, Patricia Molina Espeja, para optar al grado de Doctora, y que ha sido realizada bajo su dirección en el Departamento de Biocatálisis y Petroleoquímica del CSIC, Campus de Excelencia Internacional UAM + CSIC, Madrid.

Y para que conste, firma el presente certificado en Madrid,

Dr. Miguel Alcalde Galeote

A mis padres

A Diego

"No matter how cold the winter, there's a springtime ahead"

"Do the evolution"

Eddie Vedder - PJ

AGRADECIMIENTOS

Enfrentarse a los agradecimientos de una Tesis Doctoral es tan fácil como complicado. Mucho que agradecer, pero difícil de expresar. Mucho se puede decir, pero hay cosas que se saben por sí mismas. A buen entendedor, pocas palabras bastan.

Quiero dar las gracias a aquellas instituciones que han posibilitado este trabajo, tanto a proyectos de la Unión Europea (PEROXICATS: FP7-KBBE-2010-4-26537 e INDOX: FP7-KBBE-2013-7-613549) como Nacionales (Evofacel: BIO2010-19697). Asimismo agradecer la dedicación de COST-Action (CM1303: Systems Biocatalysis) en su esfuerzo por formar jóvenes investigadores, al CSIC y la UAM.

A mi Director de Tesis, el Dr. Miguel Alcalde, que me dio esta oportunidad; gracias por enseñarme que se puede trabajar duro sin dejar de disfrutar, por empujarme a seguir mejorando día a día y por confiar en mí.

A mi Tutora de Tesis, la Dr. María Fernández Lobato, por estar año tras año tutelando este trabajo y por sus valiosas palabras de ánimo.

A los Dres. Francisco Plou y Antonio Ballesteros, con los que siempre he podido contar para todo lo que necesitase. Trabajar con personas así es una fuente de inspiración y de motivación; sin duda, grandes ejemplos a seguir.

A la Dra. Julia Sanz y a Mercedes Ramírez (IQFR-CSIC), que han cristalizado la proteína más bonita del mundo y nos han ayudado a comprenderla. Al Dr. Ángel Martínez (CIB-CSIC), por aportar muy valiosas ideas tanto en este proyecto como en tantos otros y por su enorme dedicación a la ciencia. A los Dres. Ana Gutiérrez y José Carlos del Río (IRNAS-CSIC), Víctor Guallar (ICREA, Barcelona), Fátima Lucas (BSC, Barcelona), Roland Ludwig, Su Ma (BOKU, Viena), José Manuel Sánchez Ruiz, Valeria Risso (Universidad de Granada) y Marina Cañellas (BSC, Barcelona) por su colaboración; todos ellos han ayudado a que esta Tesis se complete aportando cada uno el trabajo en el que tan expertos son. Muchas gracias a la Dr. Susana Camarero (CIB-CSIC), que me enseñó lo que era este mundo cuando apenas había salido de la universidad; sin aquella experiencia no habría llegado hasta aquí. Y claramente he de agradecer a los Dres. Martin Hofrichter y René Ullrich, así como a todo su

grupo (IHI-Universidad de Dresden) por compartir esta enzima y por el exhaustivo trabajo que han llevado a cabo desde que la descubrieron.

También tengo que agradecer a mis compañeros de grupo por el tiempo que hemos compartido (y compartiremos); hemos pasado todo tipo de situaciones a lo largo de estos casi 5 años: buenas, menos buenas, también dramas varios y muchas alegrías… ¡hasta nos hemos vuelto deportistas! Quiero agradecer a Eva, por su paciencia infinita y por su dedicación. A David, por las miles de horas compartidas en el labo y los ánimos en momentos complicados. A Paloma, por su sonrisa diaria y permanente; suerte es poder tener grandes amigos, amigos como ella. A Javi, dispuesto a ayudar y escuchar siempre. Siempre. A Xavi, que aunque costó hacerle uno de los nuestros, me hace muy feliz que lo sea. A Isa, que me asombra cada día con su maravillosa filosofía. A Berni, por tantas y tantas risas, y por el calendario, sin duda. A Pati, porque en ella veo una fuerza de voluntad que contagia. A Diana, Ivan y Luci (¡y Mateo!), porque entre todos hacéis que trabajar aquí sea un gustazo. Y a Bárbara, Barbi (¡y Hugo!), que con uno de sus abrazos te quita mil males. Gracias a Pamela, Paolo, Noa y muchos otros que han formado y forman parte de esta familia. En fin, a todos, gracias.

Al Dr. Manolo Ferrer y su grupo, por innumerables veces en la que nos habéis salvado un experimento y por toda vuestra ayuda. A la Dr. Mónica Martínez, ¡Moni!, otro gran ejemplo de lo que ayuda sonreir.

Por supuesto, mil gracias a mis padres, Julia y José Luis. Obviamente, nada de esto habría sido posible sin su apoyo. Aunque haya momentos difíciles, hay cosas que, por suerte, nunca cambian. A mis hermanos, Cristina y Antonino (¡sé lo que estáis pensando!), porque de ellos aprendo más de lo que me gusta reconocer. A mis pequeñitas (tus pequeñitas, Cris), Itzel y Aroa, que ocupan poco, pero son muy grandes. Verlas crecer me fascina. Y también gracias a mis abuelos, los que conocí y al que no, por los buenos ratos, y los buenos recuerdos.

A Inma, Quino, Sara y Guiller, porque sin apenas conocerme, me acogieron como uno más; a Hugo y Dani, a los que también he visto crecer, otra experiencia maravillosa. A ellos les agradezco todo el cariño con el que siempre me han tratado. Todos son, además, un gran ejemplo de unidad y fortaleza.

A la kuadrilla de riojanos más dispar, divertida y acogedora quiero darle las gracias por los grandes momentos que he podido compartir con ellos. Claro que sí, ¡MCD!

Hay, además, un grupo de personas en Soria que me han acompañado durante unos cuantos años. Mis mocitas saladas, que han estado conmigo ya mucho tiempo y de todo hemos pasado ¡Lo que yo les quiero! Gracias, gracias, por aguantar mis malos momentos, por todos los San Juanes, pasados y futuros, por las tardes de Herradores, los viajes, los eventos y todo lo que hemos pasado juntas. Muchos nombres van en este párrafo, pero hay dos que han de quedar marcados. Amaya: por su alegría y su bondad. Gabri: por su sonrisa y su fortaleza.

Quiero agradecer a Miriam e Irene, que fueron de las primeras personas que conocí al llegar a Madrid, por estar ahí en esos momentos de gran cambio para mí y por continuar estándolo.

Y mis años de universidad en tierras charras los pasé con tres chicas increíbles: María, Leti y Tamara. Sin olvidar a Chispa, ¡claro! Esos años siempre son especiales, pero con ellas fueron irrepetibles. Hits como: "no sé cómo se apaga" o "esconde a Chispa que viene la Feli" nunca dejarán de hacerme sonreír.

Y también mis años universitarios me trajeron a Diego. A él he de agradecer cada día que ha pasado conmigo desde hace casi 12 años. Todos y cada uno de ellos. Me ha acompañado a lo largo de este proceso, me acompañó antes y estoy deseando vivir lo que nos queda por llegar. Gracias por estar a mi lado.

ÍNDICE

Estructura general……...I

Índice de contenidos……..……II

Índice de figuras ……..……..……..IV

Índice de tablas……...……...…VI

Abreviaturas……..……VII

ESTRUCTURA GENERAL

La presente Memoria de Tesis Doctoral se organiza en los siguientes capítulos:

1. Introducción y objetivos

2. Publicación: "Directed evolution of unspecific peroxygenase from *Agrocybe aegerita*". En este capítulo se detalla el proceso de evolución molecular dirigida de la UPO para su expresión funcional en *Saccharomyces cerevisiae*. El objetivo fue obtener una variante expresada en cantidades apropiadas, en forma soluble y extracelular, activa y estable para su uso en futuros experimentos de ingeniería genética.

3. Publicación: "Mutagenic Organized Recombination Process by Homologous *IN vivo* Grouping (MORPHING) for directed enzyme evolution". Este capítulo describe una nueva técnica de creación de diversidad genética para experimentos de evolución dirigida enfocada que se empleó para evolucionar la secuencia señal de la UPO.

4. Publicación: "Tandem-yeast expression system for engineering and producing unspecific peroxygenase". En este capítulo se describe el clonaje, expresión y sobre-producción en biorreactor del mutante de secreción (del capítulo 2) en *Pichia pastoris*.

5. Publicación: "Synthesis of 1-naphthol by a natural peroxygenase engineered by directed evolution". Este capítulo detalla el diseño de la UPO para la síntesis eficiente de 1-naftol a través de herramientas evolutivas y computacionales.

6. Resumen de resultados y discusión

7. Conclusiones

8. Referencias bibliográficas

9. Anexos

Los capítulos correspondientes a publicaciones (2-5) se han mantenido en inglés, el idioma en el que fueron publicados. Todos ellos constan de introducción, materiales y métodos/sección experimental, resultados y discusión y finalmente conclusiones. Además, los capítulos 2 y 5 incluyen material suplementario.

ÍNDICE DE CONTENIDOS

1. INTRODUCCIÓN Y OBJETIVOS 1

1.1. La peroxigenasa inespecífica (UPO) 3

1.1.1. Descubrimiento, clasificación y distribución 3

1.1.2. Características generales de la *Aae*UPO1 7

1.1.3. Actividades de la *Aae*UPO1 8

1.1.4. Estructura y mecanismo 15

1.1.5. Aplicaciones y ventajas de la UPO 19

1.1.6. Problemática asociada a la expresión funcional heteróloga de UPOs 23

1.2. Evolución molecular dirigida 24

1.2.1. Evolución dirigida de oxidorreductasas fúngicas en *Saccharomyces cerevisiae* 26

1.3. Objetivos 29

2. DIRECTED EVOLUTION OF UNSPECIFIC PEROXYGENASE FROM *Agrocybe aegerita* 31

2.1. Introduction 34

2.2. Materials and methods 36

2.3. Results and discussion 40

2.4. Conclusions 55

2.5. Supplemental experimental procedures/figures and tables 56

3. MUTAGENIC ORGANIZED RECOMBINATION PROCESS BY HOMOLOGOUS *IN VIVO* GROUPING (MORPHING) FOR DIRECTED ENZYME EVOLUTION 69

3.1. Introduction 72

3.2. Materials and methods 74

3.3. Results and discussion 84

3.4. Conclusions 94

3.5. Supplemental material 96

4. TANDEM-YEAST EXPRESSION SYSTEM FOR ENGINEERING AND PRODUCING UNSPECIFIC PEROXYGENASE 99

4.1. Introduction 102

4.2. Materials and methods 103

4.3. Results and discussion 107

4.4. Conclusions 110

5. SYNTHESIS OF 1-NAPHTHOL BY A NATURAL PEROXYGENASE ENGINEERED BY DIRECTED EVOLUTION 113
5.1. Introduction 116
5.2. Results and discussion 118
5.3. Conclusions 128
5.4. Experimental section 128
5.5. Supplemental material 136
6. RESUMEN DE RESULTADOS Y DISCUSIÓN 143
6.1. Evolución dirigida de la UPO de *A. aegerita* (*Aae*UPO1) para su expresión funcional en levaduras 145
6.1.1. Preparación de la plataforma evolutiva en *S. cerevisiae* 145
6.1.2. Tácticas evolutivas 147
6.1.3. Caracterización bioquímica 149
6.1.4. Análisis mutacional 152
6.1.5. Sobreproducción en *P. pastoris*: sistema de expresión en tándem 154
6.2. Evolución dirigida de la *Aae*UPO1 para la síntesis de 1-naftol 155
6.2.1. Diseño del método HTS y tácticas evolutivas 156
6.2.2. Caracterización bioquímica y computacional 158
6.3. Perspectivas 159
7. CONCLUSIONES 161
8. REFERENCIAS BIBLIOGRÁFICAS 165
9. ANEXOS 187
9.1. Anexo I 189
9.2. Anexo II 191

INDICE DE FIGURAS

Figura 1.1. Comparación entre P450s y UPOs 6
Figura 1.2. Reacciones de oxigenación catalizadas por *Aae*UPO1 11
Figura 1.3. Actividad peroxidasa de la UPO 14
Figura 1.4. Estructura de la *Aae*UPO1 16
Figura 1.5. Detalle del bolsillo catalítico de la *Aae*UPO1 18
Figura 1.6. Ciclo catalítico de la UPO 20
Figura 1.7. Esquema general de un ciclo de evolución dirigida 25
Figure 2.1. Route for the directed evolution of UPO1 toward functional expression and improved activity 43
Figure 2.2. Biochemical characterization 47
Figure 2.3. Breakdown of specific activity and functional expression 49
Figure 2.4. Activity and stability in organic cosolvents 52
Figure 2.5. Mutations in evolved UPO1 54
Figure S2.1. Molecular mass and degrees of glycosylation of $_{wt}$UPO1 and the PaDa-I mutant 64
Figure S2.2. Structural model of PaDa-I 65
Figure 3.1. General approach for MORPHING 85
Figure 3.2. Overview of Versatile Peroxidase from *Pleurotus eryngii* 86
Figure 3.3. Structural alignment for oxidative stability 87
Figure 3.4. Mutagenic landscapes of the distal His environment 88
Figure 3.5. Mutational loads, PCR conditions and selected variants used for MORPHING of the distal His environment 90
Figure 3.6. (A) Apparent $t_{1/2}$ *vs* H_2O_2 for the R4 parental type, 5A9 mutant (P141A), 1C12 mutant (T45A) and 3G10 mutant (E40K) in the presence of 3,000 equivalents of H_2O_2. (B) T_{50} profiles (kinetic thermostability) of VP variants 92
Figure 3.7. Mutagenic landscapes for MORPHING of the signal peptide of UPO using ABTS (A) and NBD (B) in colorimetric assays 92
Figure S3.1. VP MORPHING 96
Figure S3.2. Selected areas of VP subjected to MORPHING 97
Figure S3.3. Combinatorial saturation mutagenesis landscapes at positions 262 and 265 of VP 97
Figure 4.1. (A) 6-12% SDS-PAGE gel stained with ProtoBlue™ (C), (D) and (E) pH activity profiles for UPO_{sac} and UPO_{pic} with ABTS, DMP and NBD 110
Figure 5.1. Dual screening assay for naphthalene transformation by UPO 119

Figure 5.2. Naphthalene conversion by evolved UPOs 121
Figure 5.3. (A) Turnover rates for 1-naphthol oxidation (B) Activities of W24F site-directed variants 123
Figure 5.4. Mutations in the evolved UPO 124
Figure 5.5. G241D induced conformational changes 126
Figure 5.6. (A) Distances between C1/C2 naphthalene carbons and the heme catalytic oxygen. (B) Variation of naphthalene's center of mass (COM) to heme oxygen (compound I) vs naphthalene's COM to CZ atom in R189 in PaDa-I and JaWa along PELE simulations 127
Figure S5.1. Directed evolution of *Aae*UPO1 136
Figure S5.2. Biochemical characteristics of UPO variants 137
Figure S5.3. Mass spectrometry analysis of the reaction products (A) PaDa-I or (B) JaWa 138
Figure S5.4. Protein modeling of (A) PaDa-I and (B) JaWa based on the *Aae*UPO1 crystal structure (PDB accession number 2YOR) 139
Figure S5.5. (A) QM/MM spin density distribution on Trp24 and Tyr47 in *Aae*UPO1 when including both residues in the quantum region. (B) Variation of the 241 residue dihedral along PELE simulations 140
Figure S5.6. B-factors for evolved UPOs 141
Figura 6.1. Árbol evolutivo de la *Aae*UPO1 148
Figura 6.2. MORPHING en el péptido señal de la UPO1 150
Figura 6.3. Estructura cristalográfica de PaDa-I. (A) Detalle de la mutación F311L. (B) Detalle de superficie 153
Figura 6.4. Reacción de transformación de naftaleno en naftol..... 156

INDICE DE TABLAS

Tabla 1.1. Clasificación EC-IUBMB 1.11 4

Table 2.1. Biochemical features of wild type and evolved UPO 44

Table 2.2. Kinetic parameters of wild type, recombinant and evolved UPO variants 50

Table S2.1. Strategies and mutations obtained along the directed UPO1 evolution 66

Table S2.2. Mutations in mature PaDa-I variant 67

Table S2.3. Primers used in the directed UPO evolution study 67

Table S3.1. Oligos used for VP and UPO MORPHING 98

Table 4.1. Biochemical and spectroscopy features of evolved UPO expressed in *S. cerevisiae* (UPO_{sac}) and *P. pastoris* (UPO_{pic}) 109

Table 4.2. Kinetic parameters of evolved UPO expressed in *S. cerevisiae* (UPO_{sac}) and *P. pastoris* (UPO_{pic}) 111

Table 5.1. Biochemical features of PaDa-I and JaWa variants 120

Table 5.2. Kinetic constants for the PaDa-I and JaWa variants 122

ABREVIATURAS

AAO - aril-alcohol oxidasa

ABTS - [2,2'-azino-bis(3-ethylbenzothiazoline-6-sulfonic acid)]

ACN - acetonitrilo

APO - aromatic peroxygenase, peroxigenasa aromática

***Aae*UPO** - unspecific peroxygenase (peroxigenasa inespecífica) from *Agrocybe aegerita,*

ABTS - ácido 2,2'-azino-bis(3-etilbenzotiazolin)-6-sulfónico

CLERY - Combinatorial Libraries Enhanced by Recombination in Yeast

cDNA - ácido desoxirribonucleico complemetario o copia

CPO - Cloroperoxidasa de *Caldariomyces fumago*

Da - dalton

DMP - 2,6-dimetoxifenol

DMSO - dimetilsulfóxido

DNA - ácido desoxirribonucleico

dNTPs - desoxinucleotido trifosfato

DSC - differential scanning calorimetry, calorimetría diferencial de barrido

DyP - peroxidasa decolorante de tinte

E. coli - *Escherichia coli*

***ep*PCR** - error prone polymerase chain reaction, reacción en cadena de la polimerasa con tendencia a error

FACS - Fluorescence-Activated Cell Sorting

FDCA - ácido 2,5-furandicarboxílico

GC-MS - gas chromatography/mass spectrometry

HDM - human drug metabolites, metabolitos de fármacos humanos

HPLC - high liquid performance chromatography

HRPL - high redox potential laccase, lacasa de alto potencial redox

HTP - heme-thiolate peroxidase, peroxidasa hemo-tiolada

HTS - high-throughput screening

IAN - incremento de actividad sobre naftaleno

IAT - incremento de actividad total; TAI - total activity improvement

IvAM - *In vivo* Assembly of Mutant libraries with different mutational spectra

IVOE - *In vivo* Overlap Extension

LC/MS - liquid chromatography/mass spectroscometry

LiP - Lignina peroxidasa

MALDI-TOF - matrix-assisted laser desorption/ionization-time of flight

MnP - manganeso peroxidasa

MORPHING - Mutagenic Organized Recombination Process by Homologous *IN vivo* Grouping

MPO - mieloperoxidasa

***Mro*UPO** - unspecific peroxygenase (peroxigenasa inespecífica) from *Marasmius rotula*

MtL - lacasa de *Myceliophthora thermophila*

NAD(P)H - Nicotinamida Adenina Dinucleótido (Fosfato)

NBD - 5-nitro-1,3-benzodioxol

NC-IUBMB - nomenclature committee of the international union of biochemistry and molecular biology

OD - optical density; DO - densidad óptica

PACE - Phage-Assisted Continuous Evolution

PAH - polycyclic aromatic hydrocarbon, hidrocarburo aromático policíclico

PcL - lacasa del hongo *Pycnoporus cinnabarinus*

PELE - Protein Energy Landscape Exploration

pI - punto isoeléctrico

PM1L - lacasa del hongo PM1

P. pastoris - *Pichia pastoris*

ProSAR - Protein Sequence-Activity Relationships

PVDF - polyvinylidene difluoride membranes

QM/MM - quantum mechanics/molecular mechanics

RA/IA - relative activity/ initial activity ratio, ratio entre actividad relativa y actividad inicial

RND - ratio actividad naftaleno/actividad DMP

r*Cci*UPO - recombinant unspecific peroxygenase (peroxigenasa inespecífica) from *Coprinopsis cinerea*

RE - retículo endoplasmático

RNA - ácido ribonucleico

rNOVO - recombinant unspecific peroxygenase from a mold

RPM - revoluciones por minuto

Rz - valor Reinheitszahl

SC - synthetic complete (medio mínimo selectivo)

S. cerevisiae - *Saccharomyces cerevisiae*

SDS-PAGE - sodium dodecil sulfate-polyacrylamide gel electrophoresis

SeSaM - Sequence Saturation Mutagenesis

SRP - signal recognition particle, partícula de reconocimiento de la señal

StEP - Staggered Extension Process

TOM - toluene *ortho*-monooxygenase, tolueno orto-monooxigenasa

TTN - total turnover number, número de recambio total

UPO - unspecific peroxygenase, peroxigenasa inespecífica

VA - alcohol veratrílico

VP - peroxidasa versátil

wtUPO - wild type unspecific peroxygenase, peroxigenasa inespecífica silvestre

RESUMEN

La peroxigenasa inespecífica (UPO, del inglés *unspecific peroxygenase*, también denominada peroxigenasa aromática) es una peroxidasa hemo-tiolada con actividad mono(per)oxigenasa para la oxifuncionalización selectiva de enlaces C-H. La UPO comparte con las P450 monooxigenasas gran parte de sus capacidades catalíticas sin requerir flavoproteínas auxiliares ni cofactores redox de alto coste. Activada mediante H_2O_2, esta enzima soluble, extracelular y altamente estable, presenta un prometedor futuro en una amplia variedad de transformaciones aplicables en procesos de síntesis orgánica. Desafortunadamente, el hecho de no disponer de un organismo de expresión heteróloga que posibilite su expresión funcional ha impedido su diseño a lo largo de los últimos 10 años.

En la presente Tesis Doctoral, se ha sometido la UPO de la seta comestible *Agrocybe aegerita* (*Aae*UPO1) a un exhaustivo proceso de evolución molecular dirigida con dos propósitos: conseguir expresión funcional en levaduras y diseñar un biocatalizador eficiente para la transformación de naftaleno en 1-naftol, uno de los compuestos agroquímicos más relevantes en la actualidad.

Para promover la expresión funcional en *Saccharomyces cerevisiae*, se fusionaron varios péptidos señal nativos y evolucionados con la secuencia de la proteína madura de la UPO, además de optimizar y validar un proceso de cribado de alta capacidad (*high-throughput screening* - HTS) colorimétrico dual. Con estos medios se llevaron a cabo 5 ciclos de evolución dirigida en los que se combinaron técnicas clásicas de creación de diversidad genética (p.ej. PCR mutagénica, *in vivo* DNA *shuffling* o mutagénesis dirigida) con un método de evolución enfocada diseñado específicamente para introducir mutaciones aleatorias -con tasa de error controlada- y eventos de recombinación en zonas delimitadas (MORPHING). Aplicando esta metodología, se evolucionó el péptido señal para promover la exocitosis de la UPO en la levadura. La variante final del proceso (PaDa-I), acumuló 4 mutaciones en el péptido señal que aumentaron la secreción y 5 más en la proteína madura, que incrementaron la secreción, los parámetros cinéticos y la estabilidad. Se alcanzaron unas mejoras en la

actividad total de ~3,000 veces y unos niveles de secreción de 8 mg/L en *S. cerevisiae*. Para discernir entre las mejoras en secreción y actividad específica, se diseñó una construcción con el péptido señal evolucionado y la UPO madura nativa. Cuando se clonó PaDa-I en *Pichia pastoris*, se obtuvo expresión funcional y tanto los niveles de secreción como las principales propiedades bioquímicas se mantuvieron. La producción de UPO en biorreactor alcanzó valores cercanos a los 217 mg/L sin necesidad de optimizar el proceso.

PaDa-I fue sometido a nuevos ciclos de evolución con el objetivo de que funcionase como monooxigenasa eficiente y selectiva en la transformación de naftaleno a 1-naftol. Se diseñó un ensayo dual de *screening* colorimétrico para proteger la actividad peroxigenasa y reducir su actividad peroxidasa no deseada. La variante final, JaWa, mostró TTN (*total turnover number,* número de recambio total) de 50.000 con elevada regioselectividad (97% de 1-naftol) y actividad peroxidasa reducida. Las dos nuevas mutaciones introducidas en la proteína madura fueron analizadas por modelado computacional (PELE y QM/MM) desvelando notables cambios conformacionales que permitieron una acomodación más apropiada del sustrato.

Como principales conclusiones de esta Tesis, se ha diseñado: i) una plataforma para realizar ingeniería de proteínas de la UPO mediante evolución dirigida y métodos semi-racionales, ii) un sistema de expresión en tándem en levaduras con el cual producir elevadas cantidades de nuevas variantes UPO y iii) una UPO mutante con actividad peroxidasa reducida para diversas aplicaciones potenciales en síntesis orgánica.

SUMMARY

Unspecific peroxygenase (UPO, also known as aromatic peroxygenase) is a heme-thiolate peroxidase with mono(per)oxygenase activity for the selective oxyfunctionalization of C-H bonds. UPO shares most of the catalytic attributes of P450 monooxygenases, but unlike the latter, it neither requires the presence of expensive redox cofactors nor auxiliary flavoproteins. Fueled by catalytic concentrations of H_2O_2, this soluble, extracellular and strongly stable enzyme is a potential biocatalyst for dozens of transformations of great interest in organic synthesis. Unfortunately, the lack of suitable heterologous hosts for its functional expression has precluded its engineering over the past 10 years.

In this Thesis, the UPO from the edible mushroom *Agrocybe aegerita* has been subjected to an exhaustive directed evolution campaign in order to: i) achieve functionally expression in yeasts and ii) design an efficient biocatalyst for the transformation of naphthalene into 1-napthol, an important agrochemical.

To foster functional expression in *Saccharomyces cerevisiae*, several evolved and native signal peptides were fused to the mature UPO, a colorimetric high-throughput screening assay was validated, and 5 generations of directed evolution were performed. In terms of library creation, we combined classical directed evolution approaches *(i.e.* mutagenic PCR, *in vivo* DNA shuffling, mutational recovery) with an ad hoc method for the introduction of mutational loads and recombination events in defined regions (MORPHING). The latter allowed us to evolve the signal peptide for the successful exocytosis of UPO in yeast. The final variant of the process (PaDa-I) accumulated 4 mutations in the signal sequence (for secretion) plus 5 mutations in the mature protein that improved secretion, kinetics and stability. Accordingly, an improvement of ~3,000-fold in total activity was achieved yielding secretion levels of 8 mg/L in *S. cerevisiae*. The breakdown in secretion and activity was assessed by fusing the evolved signal peptide to the native mature UPO gene. When PaDa-I was cloned and functionally expressed in *Pichia pastoris*, the secretion levels together with the main biochemical properties were maintained while the enzyme production

in bioreactor boosted up to 217 mg/L without further optimizing process engineering.

PaDa-I was further evolved to work as an efficient and selective monooxygenase for the transformation of naphthalene into 1-naphthol. A specific dual-screening assay was designed to protect the peroxygenase activity while reducing an unwanted peroxidase activity. The final mutant (JaWa) reported total turnover numbers of 50,000 with high regioselectivity (97% for 1-naphthol) and reduced peroxidase activity. The two extra mutations introduced into the mature protein were analyzed by computational modelling (PELE and QM/MM) unveiling noticeable conformational changes for a more proper accommodation of the substrate.

Concluding the whole study, we have developed: i) a platform to engineer UPO by directed evolution and semi-rational approaches, ii) a tandem-yeast expression system whereby new UPO variants can be produced in large amounts and iii) an efficient UPO mutant with reduced peroxidase activity and potential applications in organic synthesis.

1. INTRODUCCIÓN

Y OBJETIVOS

1

1.1. LA PEROXIGENASA INESPECÍFICA (UPO)

1.1.1. Descubrimiento, clasificación y distribución

El empleo de enzimas como catalizadores en procesos de síntesis orgánica es de indudable interés tecnológico ya que son moléculas capaces de trabajar en condiciones respetuosas con el entorno, a temperatura ambiente, en solución acuosa y presión atmosférica al tiempo que ofrecen especificidades y selectividades difíciles de alcanzar con los métodos químicos tradicionales. En efecto, las enzimas son modelos energéticos altamente eficientes que pueden acelerar las reacciones químicas varios órdenes de magnitud y, en algunos casos, realizan de manera exquisita transformaciones regio- y quimio-selectivas que derivan en valiosos productos de química fina, fármacos y *building blocks*.

Liderando un nuevo grupo de enzimas con gran potencial en síntesis orgánica se encuentra la UPO (*Unspecific Peroxygenase*, reconocida inicialmente como una inusual lignina peroxidasa alcalina, posteriormente como una haloperoxidasa, también ha sido frecuentemente denominada APO -*Aromatic Peroxygenase*-), la primera peroxigenasa natural descrita con la capacidad de realizar oxifuncionalizaciones selectivas de una amplia variedad de compuestos tanto alifáticos como aromáticos. Fue descubierta por primera vez en el basidiomiceto *Agrocybe aegerita* (sin. *A. cylindracea*, popularmente seta de chopo) (Ullrich et al., 2004), un agarical comestible que produce cierta podredumbre blanca y vive principalmente en los troncos de olmos y chopos de zonas templadas/cálidas, con una amplia distribución en el área mediterránea, Norte América y Asia (Hofrichter et al., 2015). Debido a su extenso espectro de sustratos y diversidad catalítica, el Comité de Nomenclatura de la Unión Internacional de Bioquímica y Biología Molecular (NC-IUBMB) le asignó en el año 2011 una nueva clasificación (EC 1.11.2.1), junto con la designación definitiva de "*Unspecific Peroxygenase*". Así, la UPO quedó ubicada dentro de la sub-subclase Peroxigenasa (EC 1.11.2), junto con la mieloperoxidasa de mamíferos (EC 1.11.2.2), la peroxigenasa de semilla de plantas (EC 1.11.2.3), la peroxigenasa de ácidos grasos (EC 1.11.2.4) y la peroxigenasa 3-metil-L-

tirosina de la bacteria *Streptomyces lavendulae* (EC 1.11.2.5) (**Tabla 1.1**). Todas estas sub-subclases tienen como denominador común la capacidad de insertar un átomo de oxígeno procedente del H_2O_2 en diferentes sustratos (actividad peroxigenasa), si bien la UPO es la más destacada por su amplia distribución en hongos y su enorme versatilidad en reacciones de transferencia de oxígeno.

Tabla 1.1. Clasificación EC-IUBMB 1.11.

EC 1 Oxidorreductasas	**EC 1.11 Peróxido como aceptor**	**EC 1.11.1 Peroxidasas**	EC 1.11.1.10 Cloroperoxidasa (CPO)
			EC 1.11.1.13 Manganeso peroxidasa (MnP)
			EC 1.11.1.14 Lignina peroxidasa (LiP)
			EC 1.11.1.16 Peroxidasa versátil (VP)
			EC 1.11.1.19 Peroxidasa decolorante de tinte (DyP)
		EC 1.11.2 Peroxigenasas	**EC 1.11.2.1 Peroxigenasa inespecífica (UPO)**
			EC 1.11.2.2 Mieloperoxidasa (MPO)
			EC 1.11.2.3 Peroxigenasa de semilla de plantas
			EC 1.11.2.4 Peroxigenasa de ácidos grasos
			EC 1.11.2.5 Peroxigenasa 3-metil-L-tirosina

Peroxidasas hemo-tioladas

Tras el descubrimiento y exhaustiva caracterización de la UPO de *A. aegerita* (*Aae*UPO1) se identificaron y caracterizaron 2 nuevas UPOs producidas por *Coprinus* (*Coprinellus*) *radians* (*Cra*UPO) y *Marasmius rotula* (*Mro*UPO), con un 59 y 33% de identidad de secuencia con *Aae*UPO1, respectivamente (Anh et al., 2007; Gröbe et al., 2011; Poraj-Kobielska, 2013). Otros hongos como *A. parasitica, A. chaxingu, A. alnetorum, Agaricus bisporus, Auricularia auricula-judae, Coprinopsis verticillata,*

Coprinus sp. DSM 14545 y *Mycena galopus* son también productores de UPOs y su caracterización está actualmente en proceso (Hofrichter et al., 2015). Además, recientemente el gen de una UPO procedente del genoma de *Coprinopsis cinerea* (putativa, r*Cci*UPO) (Babot et al., 2013) y de un moho sin determinar (rNOVO) (Peter et al., 2014), han sido expresadas heterólogamente en *Aspergillus oryzae* por la empresa Novozymes. Búsquedas en bases genómicas han detectado más de 1.000 secuencias putativas UPO en distintos tipos de hongos, perteneciendo en el 95% de los casos a basidiomicetos y ascomicetos, pero no a levaduras (Hofrichter et al., 2010; Hofrichter et al., 2014). De estos datos se sustrae el hecho de que las UPOs son un grupo de enzimas con una vasta distribución en hongos, catalogándose todas ellas dentro de 2 grandes grupos: las "UPO cortas" (grupo I presente en todo el filo de los hongos, con un tamaño proteico de ~26 kDa y representado por *Mro*UPO) y las "UPO largas" (grupo II únicamente localizado en basidiomicetos y ascomicetos, con un tamaño proteico de ~44 kDa, en el que se ubican tanto la *Aae*UPO1 como la *Cra*UPO) (Pecyna et al., 2009; Hofrichter et al., 2015). Las UPO largas y cortas se diferencian, aparte de en su tamaño y distribución, en que las primeras presentan un puente disulfuro interno y un residuo de arginina como estabilizador de carga en el sitio activo, mientras que las cortas carecen de puentes disulfuro y el estabilizador de carga es un residuo de histidina.

El descubrimiento de las UPOs ha permitido relacionar las citocromo P450 monooxigenasas (EC 1.14) con la cloroperoxidasa de *Caldariomyces fumago* (CPO, EC 1.11.1.10) (Ullrich y Hofrichter, 2005). El denominador común de P450s, CPO y UPOs es que todas ellas son enzimas hemo-tioladas (con un residuo de Cys como ligando axial del grupo hemo en su lado proximal) y presentan un potencial biotecnológico en reacciones de transferencia de oxígeno muy reconocido, lo que augura un prometedor futuro para las UPOs por su mayor selectividad en muchos procesos y menores requerimientos. En efecto, la UPO cataliza reacciones de oxifuncionalización de gran importancia en síntesis orgánica que hasta ahora eran terreno exclusivo de las P450s y en menor medida de la CPO.

Sin embargo, la UPO es una enzima soluble, estable y altamente activa que tan sólo necesita H_2O_2 para trabajar (*i.e.* el peróxido actúa tanto como donador de oxígeno como aceptor final de electrones), siendo independiente de flavoproteínas auxiliares y costosos cofactores redox (NAD(P)H), necesarios para la catálisis en las P450s. Estas últimas, además, suelen encontrarse asociadas a membranas celulares y a procesos de desacoplamiento oxidativo: los electrones que suministra el NAD(P)H no siempre se usan para oxigenar el sustrato, sino que pueden seguir otras rutas (han sido propuestas 3 vías distintas) derivando en la formación de especies reactivas de oxígeno (H_2O_2 y $O_2^{\cdot-}$) (Grinkova et al., 2013). Esto reduce de manera considerable el rendimiento catalítico, desviando equivalentes de reductores hacia la producción de moléculas improductivas (**Fig. 1.1**). Por último, las P450s son enzimas poco estables, al contrario que la UPO, lo que numerosas veces lleva asociado la pérdida su grupo hemo como consecuencia de cambios conformacionales bajo condiciones desfavorables (Sakaki, 2012). En lo referente a la CPO, al igual que la UPO, emplea el H_2O_2 como co-oxidante y donador de oxígeno, sin embargo su espectro de sustratos funcionalizables es más limitado, ya que no es capaz

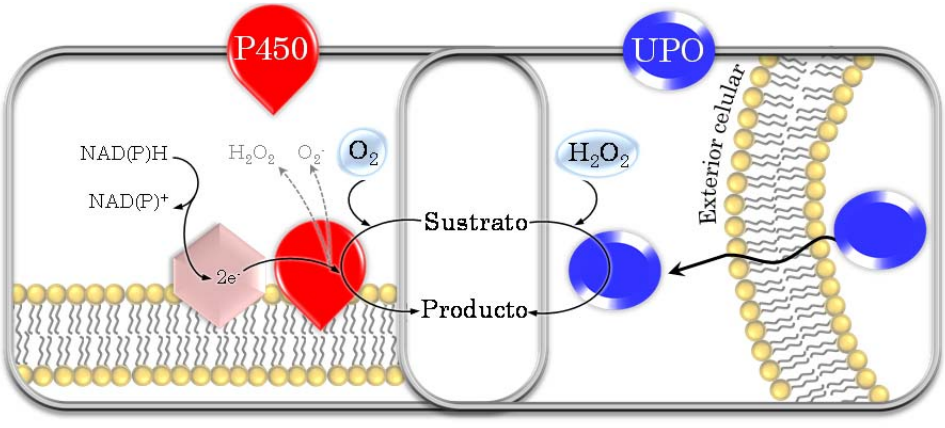

Figura 1.1. Comparación entre P450s y UPOs. Las P450s (izquierda, rojo) son proteínas asociadas a membrana, con baja estabilidad, que requieren la presencia otras proteínas auxiliares (flavoproteínas, hexágono rosa) para el suministro de electrones procedentes de NAD(P)H. Parte de esos electrones acaban formando especies oxigenadas improductivas, de manera que no se emplean para oxigenar el sustrato; esto supone una disminución del rendimiento. Al contrario que las P450s, la UPO (derecha, azul) es soluble, extracelular, estable e independiente de NAD(P)H y proteínas auxiliares; su único requerimiento es H_2O_2 que funciona como donador de oxígeno y aceptor final de electrones. Aunque las UPO no presentan los fenómenos de desacoplamiento oxidativo mencionados para las P450s, su actividad lateral peroxidasa puede resultar problemática.

de oxigenar carbonos de anillos aromáticos/alicíclicos o n-alcanos, altamente inertes desde un punto de vista químico, facultad que sí presenta la UPO. Por el contrario, la CPO tiene mayor potencial en reacciones de halogenación donde la UPO se limita fundamentalmente a brominaciones de sustratos activados, mientras que la CPO lleva a cabo clorinaciones, brominaciones e incluso iodinaciones (pero no fluorinaciones) (Hofrichter y Ullrich, 2006; Hofrichter y Ullrich, 2013). Aunque la CPO carece de homología con las P450s, sí comparte un 27% de identidad de secuencia con la *Aae*UPO1 y hasta un 35% en su extremo N-terminal (Ullrich et al., 2004; Pecyna et al., 2009). Debido a su relación filogenética y estructural, la UPO y la CPO se ubican dentro del grupo de peroxidasas hemo-tioladas (HTP, de sus siglas en inglés) en contraste con las hemo-peroxidasas convencionales (**Tabla 1.1**).

Aún no se tiene completa certeza de la función que desempeña la UPO en la naturaleza. Se han propuesto varias posibilidades, como su papel en la síntesis de metabolitos halogenados/hidroxilados (p.ej. antibióticos) (Hofrichter y Ullrich, 2006). Otra posible función es su implicación en la degradación del humus y de la lignina; en particular, se ha comprobado que la *Aae*UPO1 es capaz de llevar a cabo O-desmetilaciones y roturas en modelos no fenólicos de lignina (Kinne et al., 2011). Esto indica que estaría interviniendo en la degradación de la biomasa lignocelulósica en fases tardías de descomposición, donde los fragmentos son ya de pequeño tamaño. En otros estudios se postula la posibilidad de que esté involucrada en detoxificación de una manera general, ya sea de fitoalexinas vegetales, toxinas microbianas o xenobióticos, pudiendo actuar a modo de "hígado extracelular" (Piontek et al., 2013; Hofrichter et al., 2015).

1.1.2. Características generales de la *Aae*UPO1

El cDNA de la *Aae*UPO1 (el punto de partida de esta Tesis Doctoral) codifica 371 aminoácidos de los cuales 43 constituyen el péptido señal y 328 pertenecen a la proteína madura. Tras su descubrimiento y caracterización molecular (Ullrich et al., 2004; Pecyna et al. 2009), estudios recientes de

transcriptómica indican la presencia de 15 nuevas secuencias UPO en *A. aegerita* (12 largas y 3 cortas) (Hofrichter et al., 2015). La *Aae*UPO1 es una proteína extracelular de 46 kDa con un grado de glicosilación del 22% (presenta 6 sitios de N-glicosilación: Asn11, Asn141, Asn161, Asn182, Asn286 y Asn295, en los que se anclan hasta 8 residuos de manosa) (Piontek et al., 2013). Probablemente, esta fuerte glicosilación contribuya a su elevada estabilidad frente a diferentes factores como la temperatura o la presencia de disolventes orgánicos (p.ej. muestra una ligera activación -109%- tras 2 horas de incubación en 60% (v/v) de acetona) (Peter et al., 2011). Su punto isoeléctrico (pI) oscila entre 4,9 y 5,7, indicando la presencia de diferentes iso(glico)formas. En cuanto a sus características espectroscópicas, revelan un máximo de absorbancia a 420 nm, perteneciente a la banda Soret representativa de hemo-proteínas, y 2 hombros correspondientes a las bandas de transferencia de carga, CT1 (572 nm) y CT2 (540 nm) (Ullrich et al., 2004). Este perfil es casi idéntico al de las de las P450s en estado de reposo (Abs_{max} = 416-420 nm), pero distinto al de la CPO (Abs_{max} = 401 nm). Sin embargo, al observar el espectro UV-Vis del complejo UPO-CO (estado reducido, obtenido mediante adición de hidrosulfito sódico y tratado con CO durante 5 min), la banda Soret muestra un desplazamiento con un máximo a 445 nm. Este comportamiento también se observa en las P450s y en la CPO, lo cual es indicativo de la existencia del característico grupo hemo-tiolado (Lewis, 2001; Ullrich y Hofrichter, 2005).

1.1.3. Actividades de la *Aae*UPO1

En términos generales, la UPO puede catalizar reacciones de peroxigenación (inserción de un átomo de oxígeno, actividad peroxigenasa o mono(per)oxigenasa) (**Fig 1.2**) o de peroxidación (con la sustracción de un electrón, actividad peroxidasa o peroxidativa) (**Fig.1.3**). También es importante destacar que posee cierta actividad catalasa (ruptura de H_2O_2 en oxígeno y agua). Sin lugar a dudas, las reacciones de transferencia de oxígeno (*i.e.* conocidas como oxidaciones de 2 electrones), en las que la enzima toma un átomo de oxígeno del H_2O_2 para insertarlo en el sustrato,

son las que más interés biotecnológico suscitan. De hecho, se han descrito hasta el momento más de 300 compuestos susceptibles de ser peroxigenados por la UPO, y este número puede seguir creciendo en los años venideros. Entre las reacciones catalizadas por la UPO mediante la actividad peroxigenasa se incluyen hidroxilaciones aromáticas, alquílicas y alifáticas, epoxidaciones de olefinas aromáticas y alifáticas, ruptura de éteres, N-desalquilaciones, sulfoxidaciones, N-oxidaciones, y brominaciones (**Fig. 1.2**).

En particular, una de las primeras reacciones descritas en la *Aae*UPO1 fueron las halogenaciones. Se consideran reacciones de transferencia de oxígeno ya que en primera instancia se forma un hipohalito (OX^-) a partir del cual se transfiere el haluro a una molécula de sustrato (Ullrich y Hofrichter, 2005; Hofrichter et al., 2015) (**Fig. 1.2.1**). La *Aae*UPO1 presenta una fuerte actividad de bromination, convirtiendo fenoles en presencia de KBr en 4 y 2-bromofenol con una relación 4:1. Sin embargo su capacidad de clorinación es residual (unas 10.000 veces más baja que la bromination) dando lugar únicamente a trazas de 2-clorofenol. Asimismo, su actividad de iodinación es unas 200 veces inferior a la de la CPO.

En ausencia de haluros, la UPO cataliza la inserción de oxígeno sobre compuestos tanto aromáticos como alifáticos de diversa naturaleza. Así, oxida una amplia variedad de alcoholes aromáticos (p.ej. bencílico, vainillílico, veratrílico, anisílico) a los correspondientes aldehídos y adicionalmente a sus ácidos benzoicos (**Fig. 1.2.2**). La oxidación de todos ellos tiene lugar mediante la hidroxilación del carbono bencílico para dar lugar al correspondiente *gem*-diol (hidrato de aldehído) que se encuentra en equilibrio con el aldehído y que puede ser adicionalmente oxidado por la UPO dando finalmente lugar al ácido. Como se mencionó en el capítulo 1.1.1, la *Aae*UPO1 originariamente fue descrita como una lignina peroxidasa (LiP) alcalina porque era capaz de llevar a cabo la oxidación del alcohol veratrílico (VA, sustrato característico de actividad LiP) a veratraldehído a pH básico. La LiP sustrae un electrón del anillo aromático del VA dando lugar a la formación de un radical catiónico arílico, el cual

sufre desprotonación bencílica para formar el aldehído; sin embargo, la UPO hidroxila el carbono bencílico generando un alcohol geminal que representa la forma hidratada del veratraldehído (**Fig. 1.2.2**). En efecto, estudios empleando $H_2{}^{18}O_2$ (*i.e.* con el oxígeno del peróxido marcado radioactivamente) han establecido sin lugar a discusión que la fuente de oxígeno introducida en numerosas oxidaciones catalizadas por la UPO, incluyendo las hidroxilaciones de anillos aromáticos, la sulfoxidación de dibenzotiofeno, la N-oxidación de derivados de piridina, la ruptura de éteres para producir aldehídos y cetonas o la oxigenación del carbono bencílico del tolueno y nitrotolueno entre otros compuestos, procede del propio peróxido (Ullrich et al., 2008; Kluge et al., 2009; Aranda et al., 2009; Kinne et al., 2009b; Kinne et al., 2010; Karich et al. 2013). En el caso particular del tolueno, puede ser oxifuncionalizado tanto en el carbono bencílico como en el anillo aromático, liberando distintos productos, de los cuales el mayoritario es el alcohol bencílico (Ullrich y Hofrichter, 2005), siendo éste a su vez sustrato de la UPO, como se ha explicado arriba (**Fig. 1.2.2**). Como productos minoritarios de oxigenación del anillo aromático aparecen el *o*-cresol y *p*-cresol así como la metil-*p*-benzoquinona. Es importante señalar que los derivados de benceno con cadenas laterales más largas que las del tolueno son exclusivamente atacados en el carbono bencílico (no sufren hidroxilación aromática). Así, por ejemplo el etil benceno es hidroxilado para dar lugar al (R)-1-feniletanol con un exceso enantiomérico del 95-99%.

También numerosos hidrocarburos aromáticos policíclicos (PAHs) como el naftaleno, el antraceno, el fenantreno o el pireno son hidroxilados en distintas posiciones. En el caso del naftaleno se produce mayoritariamente 1-naftol a través de un epóxido intermediario (Kluge et al. 2007; Kluge et al. 2009) (**Fig. 1.2.2**), mientras que para los otros 3 compuestos se detectan entre 4 y 12 productos distintos (Aranda et al. 2010). Compuestos aromáticos heterocíclicos como el fluoreno resultan hidroxilados mayoritariamente en carbonos de los anillos bencénicos (**Fig. 1.2.3**). Sin embargo, los PAHs de alto peso molecular (con más de 5 anillos) no son sustratos para la UPO. Por otro lado, los arenos con sustituyentes como el 1-metil-naftaleno son hidroxilados prioritariamente

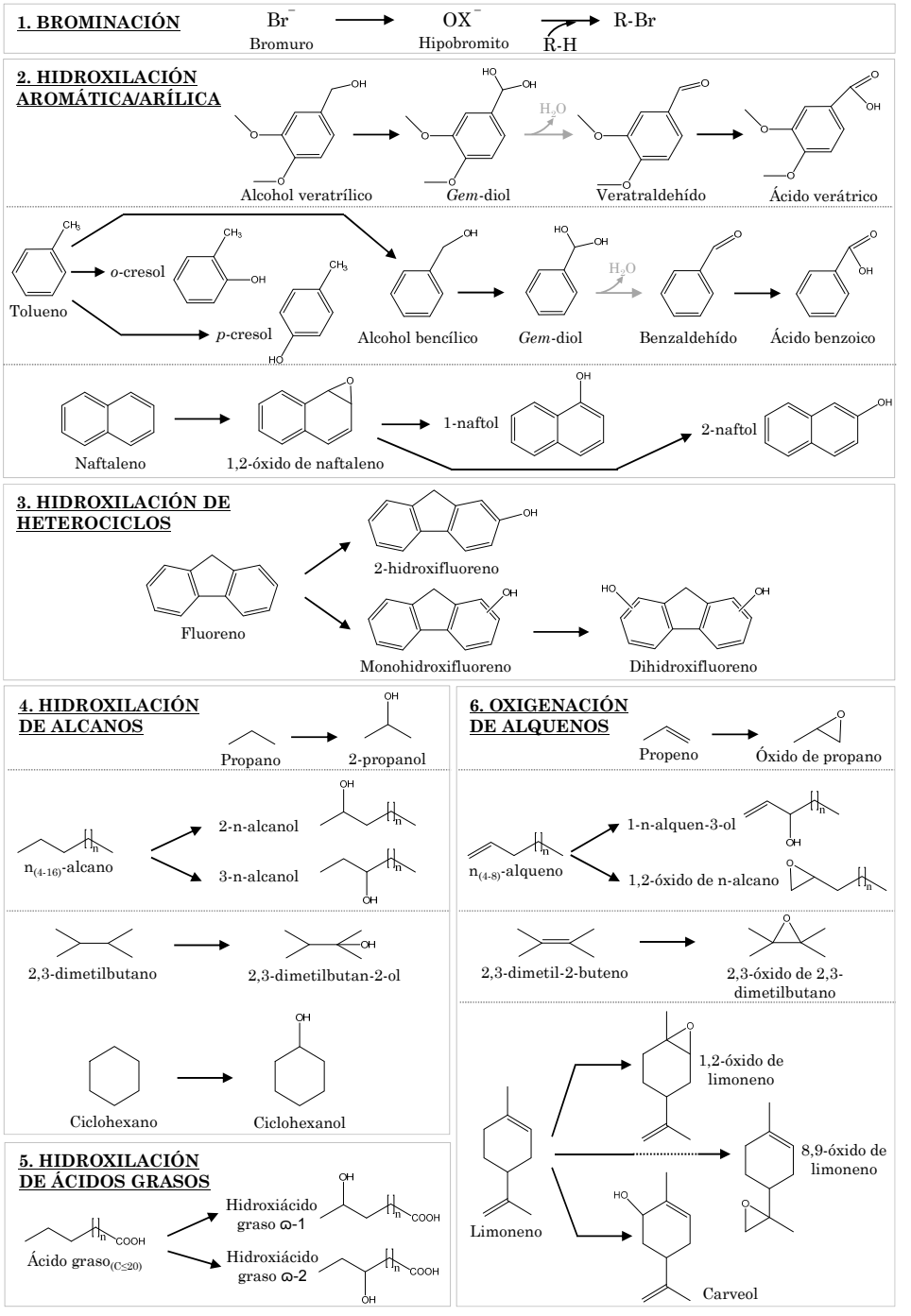

Figura 1.2. Reacciones de oxigenación catalizadas por *Aae*UPO1. En el caso de los productos aromáticos, se omiten las posibles reacciones de oxidación de un electrón. Pasos independientes de la actividad enzimática se marcan en gris.

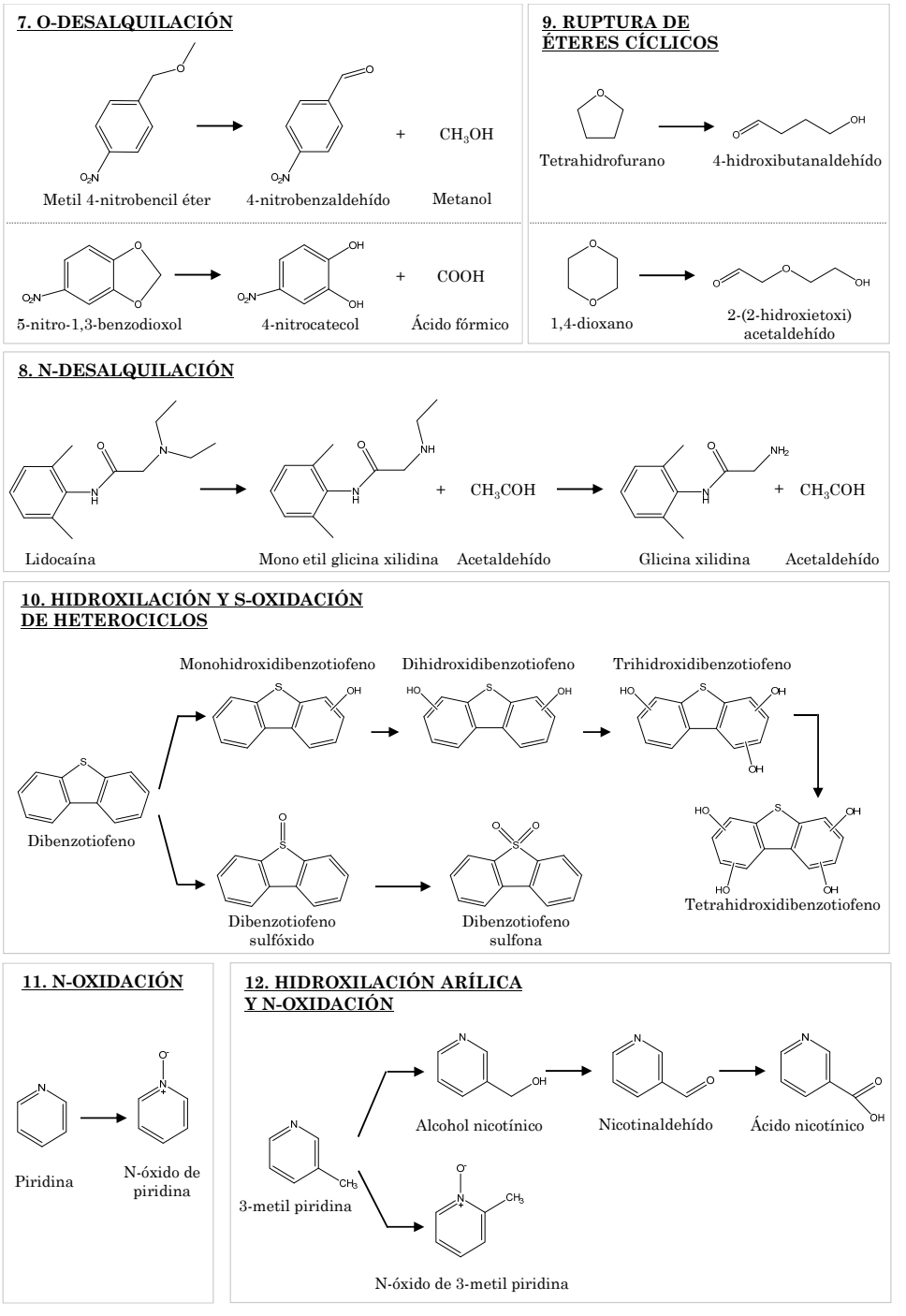

Figura 1.2. Continuación.

en los enlaces C-H del anillo aromático, mientras que el 2-metil-naftaleno es oxifuncionalizado en carbonos aromáticos y la cadena lateral por igual (Aranda et al., 2010).

Los compuestos alifáticos lineales, ramificados y cíclicos son susceptibles de ser oxigenados por la *Aae*UPO1. Así, alcanos lineales de 3 a 16C, ácidos grasos de hasta 20C y alcanos cíclicos (p.ej. ciclohexano) son mayoritariamente monohidroxilados (**Fig. 1.2.4**). En los casos de ácidos grasos, las hidroxilaciones tienen lugar fundamentalmente en posiciones sub-terminales ω-1 y ω-2 y muy minoritariamente en posición ω terminal mientras que para alcanos lineales no se ha descrito hidroxilación terminal (Gutiérrez et al. 2011) (**Fig. 1.2.5**). En el caso de los alcanos ramificados (hasta el 2,2,3,3-tetrametilbutano, que ya no es sustrato de la *Aae*UPO1) se obtienen uno o 2 compuestos hidroxilados por acción de la UPO (Gutiérrez et al., 2011; Peter et al., 2011; Peter et al., 2013). Asimismo, la UPO es capaz de epoxidar/hidroxilar cadenas hidrocarbonadas insaturadas lineales, ramificadas y cíclicas (olefinas como el propeno, el 2,3-dimetil-2-buteno, o el limoneno) (Peter et al., 2013), siendo mejor transformados estos 2 últimos tipos de alquenos que los primeros y sin mostrar una tendencia clara (**Fig. 1.2.6**).

La UPO presenta además la capacidad de O- y N-desalquilar compuestos como el metil 4-nitrobencil éter o la lidocaína (amina), respectivamente (**Fig. 1.2.7, 1.2.8**). Para ello, se forma un hemiacetal/hemiaminal intermediario inestable y consecuentemente se libera bien un alcohol/fenol o bien una amina primaria/secundaria, además de un aldehído en ambos casos (Kinne et al., 2009b; Poraj-Kobielska, 2011; Hofrichter et al., 2015). La UPO también puede realizar la oxigenación de éteres cíclicos promoviendo su ruptura como es el caso de la transformación de tetrahidrofurano a 4-hidroxibutanaldehído (**Fig. 1.2.9**). Además, compuestos heterocíclicos que presenten átomos de azufre o nitrógeno en su estructura pueden ser susceptibles de ser atacados por la UPO. En este caso, el heteroátomo es oxigenado. Por ejemplo, la *Aae*UPO1 transforma el dibenzotiofeno en el correspondiente sulfóxido así como a la sulfona derivada, a pesar de que es la hidroxilación del anillo bencénico la reacción

favorecida (Aranda et al., 2009) (**Fig. 1.2.10**). En el caso de piridina y sus derivados, se forma el N-óxido en exclusividad, excepto en las metil piridinas, que también se produce oxifuncionalización del grupo alquílico (Ullrich et al., 2008) (**Fig. 1.2.11, 1.2.12**).

Por otro lado, además de las reacciones de transferencia de oxígeno, la UPO cataliza oxidaciones de un electrón a través de su actividad peroxidativa. De esta manera, la UPO es capaz de sustraer un electrón a sustratos clásicos de peroxidasas, como diversos compuestos fenólicos (p.ej. DMP (2,6-dimetoxifenol) o el ABTS (ácido 2,2'-azino-bis(3-etilbenzotiazolin)-6-sulfónico) (Ullrich et al., 2004) (**Fig. 1.3**). Esta actividad puede resultar muy inapropiada cuando se desea un control preciso de la reacción de transferencia de oxígeno sobre sustratos aromáticos (p.ej. para la síntesis de naftol, flavonoides hidroxilados o metabolitos humanos de diversos fármacos) ya que los productos fenólicos resultantes son a su vez sustratos de la actividad peroxidativa de la UPO, dando lugar a un *pool* de radicales fenoxilo que pueden acoplarse promoviendo polimerizaciones no enzimáticas. Con el fin de limitar la actividad peroxidasa no deseada, la

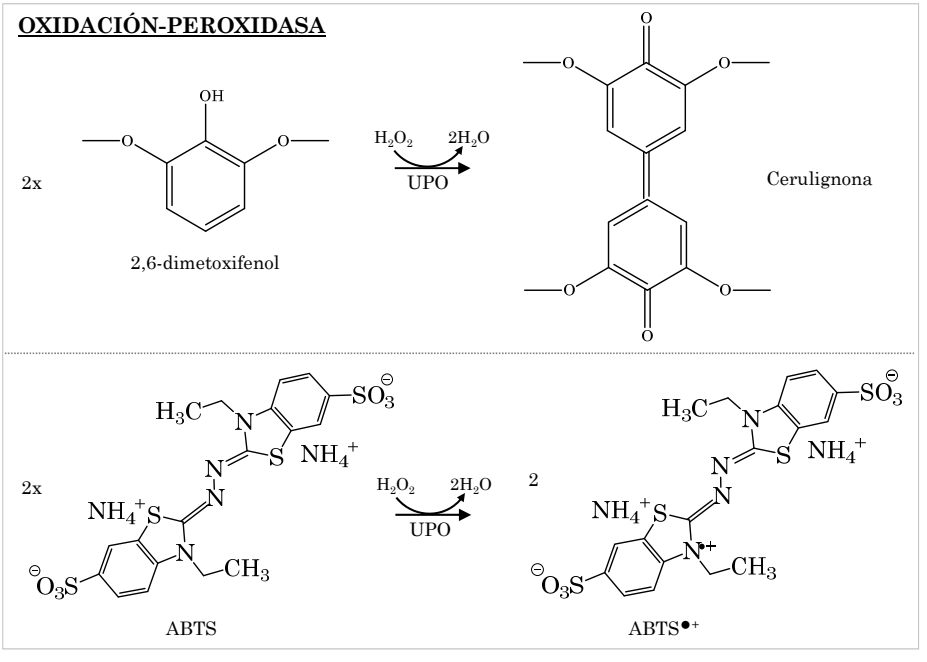

Figura 1.3. Actividad peroxidasa de la UPO.

única solución planteada hasta el momento en numerosos estudios consiste en la adición a la mezcla de reacción de un compuesto capaz de eliminar radicales libres (*radical scavenger*) como el antioxidante ácido ascórbico (Hofrichter et al., 2015). De esta forma, se reducen los radicales fenoxilo generados por la actividad peroxidasa mientras que el ascórbico es oxidado al radical ascorbilo que finalmente disproporciona en ácido dehidroascórbico y ácido ascórbico. Indudablemente, la manera más apropiada para prescindir de dicha actividad implica el diseño de la UPO con el fin de convertirla en una peroxigenasa autosuficiente e independiente de procesos peroxidativos. En base a estudios previos con otras peroxidasas ligninolíticas, se presupone que la actividad peroxidativa de la UPO puede estar localizada fuera del canal de acceso al hemo o a lo sumo en la entrada del mismo. En particular, existe la hipótesis de la oxidación peroxidativa mediada por un residuo catalítico superficial (posiblemente un Trp o una Tyr) que, tras ser activado a través de una ruta de transferencia electrónica de largo recorrido hacia el hemo (como ocurre en la LiP o en la VP), se encargue en su forma de radical catiónico de la oxidación de compuestos fenólicos. Sin embargo, este extremo no ha podido ser confirmado experimentalmente por falta de herramientas de ingeniería para la UPO.

1.1.4. Estructura y mecanismo

La estructura cristalográfica de la *Aae*UPO1 nativa fue publicada recientemente con una resolución de ~2 Å (Piontek et al., 2013). Su estructura secundaria se organiza en 10 hélices α y 5 láminas ß, éstas últimas formadas por muy pocos residuos (**Fig. 1.4**). En su centro activo se localiza un grupo hemo (protoporfirina IX), cuyo átomo de hierro se encuentra hexacoordinado por los cuatro nitrógenos del macrociclo tetrapirrolíco, la quinta posición ocupada por el azufre de una cisteína (Cys36) que actúa como ligando proximal (axial, por debajo del plano del hemo), lo cual la define como una proteína hemo-tiolada y la sexta posición por una molécula de agua (ligando distal) (**Fig. 1.5.A**). El ligando axial también es una Cys en la CPO y en las P450s, pero no en otras hemo-

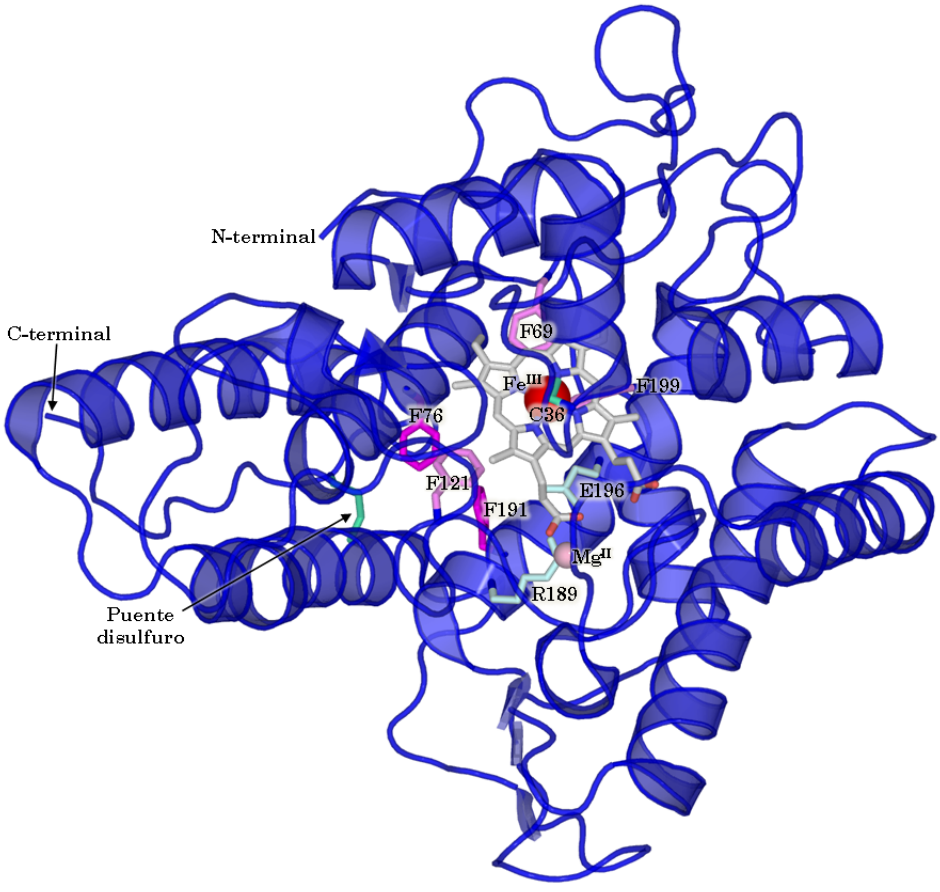

Figura 1.4. Estructura de la *Aae*UPO1 (PDB: 2YOR). Se indican sus 10 hélices α y 5 láminas ß, el puente disulfuro cercano al extremo C-terminal y la Cys36 axial se indican en verde, el Mg^{II} estructural en salmón, el par ácido-base (E196-R189) en azul claro y el grupo hemo con el Fe^{III} en rojo.

proteínas, como las peroxidasas clásicas (His, His+Asp, Tyr, Tyr+Arg son los posibles aminoácidos que se pueden encontrar en dicha posición) (Rydberg et al., 2004). Se cree que la Cys axial es determinante para la actividad de transferencia de oxígeno. El extremo N-terminal de la estructura resuelta carece de los 3 primeros residuos debido a una supuesta proteólisis entre la Gly3 y la Leu4. El extremo C-terminal está estabilizado mediante un puente disulfuro entre las cisteínas 278 y 319. Posee también un Mg^{II} estructural coordinado con 2 moléculas de agua, un propionato del grupo hemo y 3 átomos de oxígeno pertenecientes a 3 residuos (Glu122, Gly123 y Ser126) (Piontek et al., 2013) (**Fig. 1.5.B**). La entrada del sustrato al bolsillo catalítico se realiza a través de un canal de acceso de forma cónica (con diámetro externo e interno de 10 y 8,5 Å, respectivamente) y una longitud de 17 Å. Dicho canal es sumamente hidrofóbico, con 10

residuos aromáticos (9 Phe y 1 Tyr) que guían al sustrato al centro activo. De entre ellos, cabe destacar 3 fenilalaninas que actúan orientando el sustrato (Phe69, Phe121 y Phe199) y otras 2 que delimitan la entrada del mismo por el canal (Phe76, Phe191) (Piontek et al., 2013) (**Fig 1.5.C, D**). Cuenta también con un par ácido-base implicado en la catálisis (ver abajo), formado por el Glu196 y la Arg189. En su estructura también se halla un sitio de unión a haluros cerca de la entrada al bolsillo catalítico.

Para determinar la manera en la que la UPO lleva a cabo la catálisis, ha sido necesario revisar conocimientos previos de los ciclos catalíticos de las hemo-peroxidasas y las P450s (Dunford, 1999; Ortiz de Montellano y De Voss, 2005). Ya que combina las diferentes actividades catalíticas de estas enzimas, se presupone que la UPO oxigena enlaces C-H de una manera similar a como lo hacen las P450s a través de su ruta *bypass* del peróxido (ruta mono(per)oxigenasa), así como oxida fenoles (ruta peroxidasa) de manera similar a las hemo-peroxidasas. Teniendo en cuenta esta información, se ha propuesto el siguiente mecanismo de acción (Peter et al., 2011; Wang et al., 2012b; Wang et al., 2013; Hofrichter et al., 2015) (**Fig. 1.6**):

No se conoce con exactitud si el sustrato (R-H) se une inicialmente a la enzima en su estado de reposo, o una vez ésta ha sido activada por H_2O_2 (en Compuesto I). En cualquiera de los 2 casos, primeramente es necesario que la molécula de H_2O que actúa como sexto ligando (distal) del Fe^{III} del hemo en el estado en reposo (Fe^{III}-H_2O) sea reemplazada por una molécula de H_2O_2 para formar el Compuesto 0. Este complejo per-oxo sufre una reorganización electrónica finalizando con la escisión heterolítica del H_2O_2 unido para dar lugar al Compuesto I (intermediario oxo-ferril radical catiónico, Fe^{IV}=$O^{\bullet+}$). Tanto en la formación del Compuesto 0 como en la ruptura heterolítica del peróxido interviene directamente el Glu196 desprotonado. A partir de aquí, el mecanismo de acción depende de la naturaleza del sustrato, y puede seguir la ruta mono(per)oxigenasa (transferencia de oxígeno mediante 2 electrones) o la ruta peroxidasa (oxidación dependiente de la sustracción de un electrón).

En la ruta mono(per)oxigenasa, el Compuesto I abstrae un protón y un electrón al sustrato, dando lugar al Compuesto II (A) protonado (complejo ferril hidróxido, Fe^{IV}-OH) y al radical del sustrato (R•, situado en el sitio activo). A continuación, el oxígeno es transferido al sustrato, dando lugar a un complejo enzima-producto oxigenado/hidroxilado. Finalmente, el complejo se disocia liberando el producto oxigenado/hidroxilado y devolviendo a la enzima al estado de reposo.

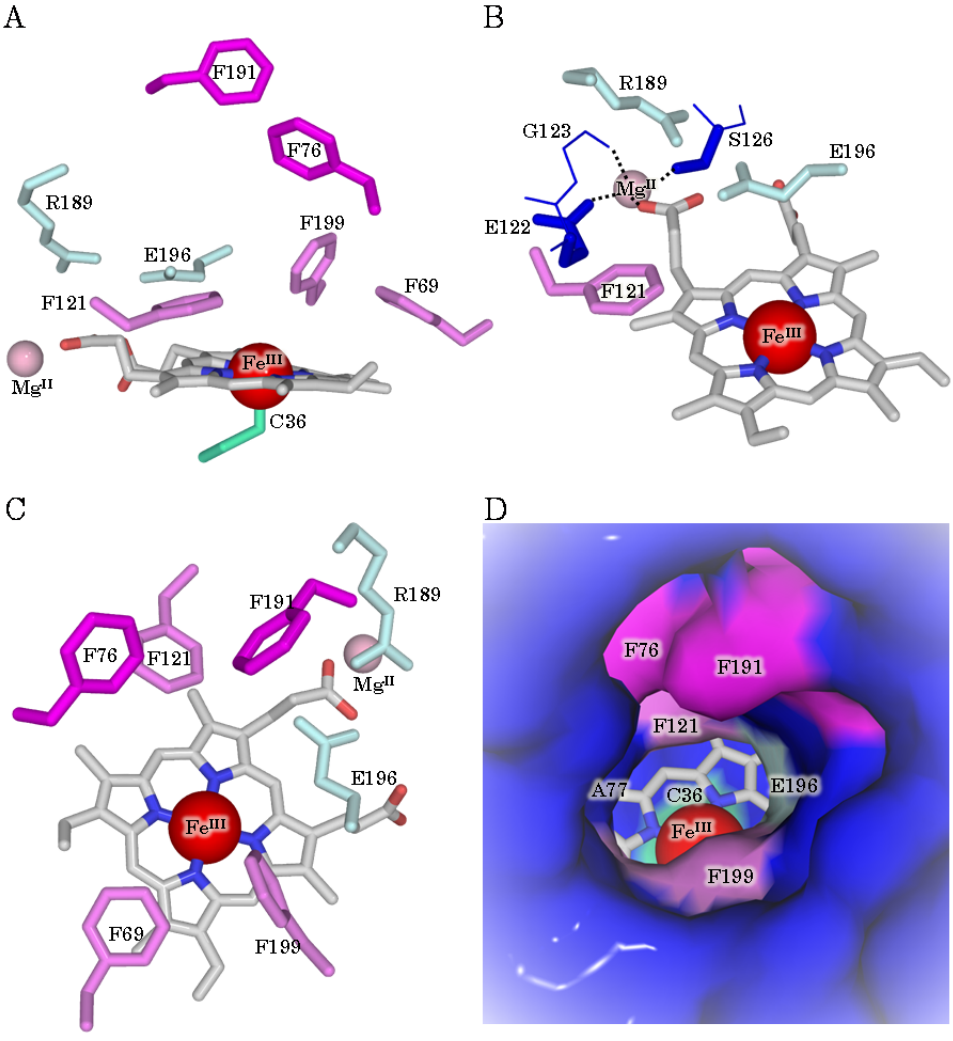

Figura 1.5. Detalle del bolsillo catalítico de la *Aae*UPO1. (A) Se observa el residuo axial Cys36 en verde, el Mg^{II} estructural en salmón, el Fe^{III} en rojo, el par ácido base Arg189-Glu196 en azul claro, las Phe que delimitan la entrada de sustratos en rosa oscuro y las tres Phe que orientan el sustrato en rosa claro. (B) Detalle de la coordinación del Mg^{II}. (C) y (D) Vista de la entrada al canal del hemo sin y con superficie, respectivamente.

En la ruta peroxidasa, el Compuesto I abstrae un electrón al sustrato, formando el Compuesto II (B) (Fe^{IV}=O) y liberando un producto radical. El Compuesto II (B) es reducido por una nueva molécula de sustrato, que cede un electrón produciendo el radical del sustrato correspondiente y restituyendo el estado de reposo de la enzima (Fe^{III}-H_2O).

Una de las desventajas de la UPO es que, como peroxidasa que es, puede sufrir la llamada inactivación por suicidio. En ocasiones, el Compuesto II junto con una molécula de H_2O_2 da lugar al Compuesto III (Fe^{III}-$O_2^{\bullet-}$). En esta configuración, la enzima no es capaz de volver al estado de reposo y pierde su integridad, ya sea mediante blanqueamiento del grupo hemo o por daño oxidativo causado por el ataque de radicales libres (Valderrama et al., 2002). A pesar de que la UPO sufre este efecto, es capaz de soportar una elevada concentración de H_2O_2 antes de inactivarse (probablemente debido a un mecanismo de protección mediado por su actividad catalasa), al contrario que la mayoría de las peroxidasas conocidas que se inactivan bajo concentraciones catalíticas de H_2O_2 (Ullrich et al., 2004).

1.1.5. Aplicaciones y ventajas de la UPO

Las oxifuncionalizaciones selectivas de enlaces C-H pertenecen al grupo de reacciones más deseadas en síntesis orgánica. En este sentido, las P450s han sido durante años las enzimas más estudiadas para estos fines habiendo sido sometidas a exhaustivos trabajos de ingeniería genética para tratar de adecuar sus propiedades a diversos procesos industriales (Jung et al., 2011; McIntosh et al., 2014; Roibana y Reetz, 2015). En particular, muchos de los esfuerzos realizados en la aplicación de P450s se concentran en potenciar la ruta bypass del peróxido (*peroxide shunt pathway*) como solución al problema asociado del suministro y/o regeneración del costoso cofactor redox; mediante esta ruta, la enzima hace uso de H_2O_2 en lugar de O_2 y NA(D)PH para reacciones de transferencia de oxígeno (Joo et al., 1999; Cirino y Arnold, 2002). Sin embargo, la eficiencia de esta ruta es todavía muy baja y especialmente, la estabilidad operacional de las enzimas

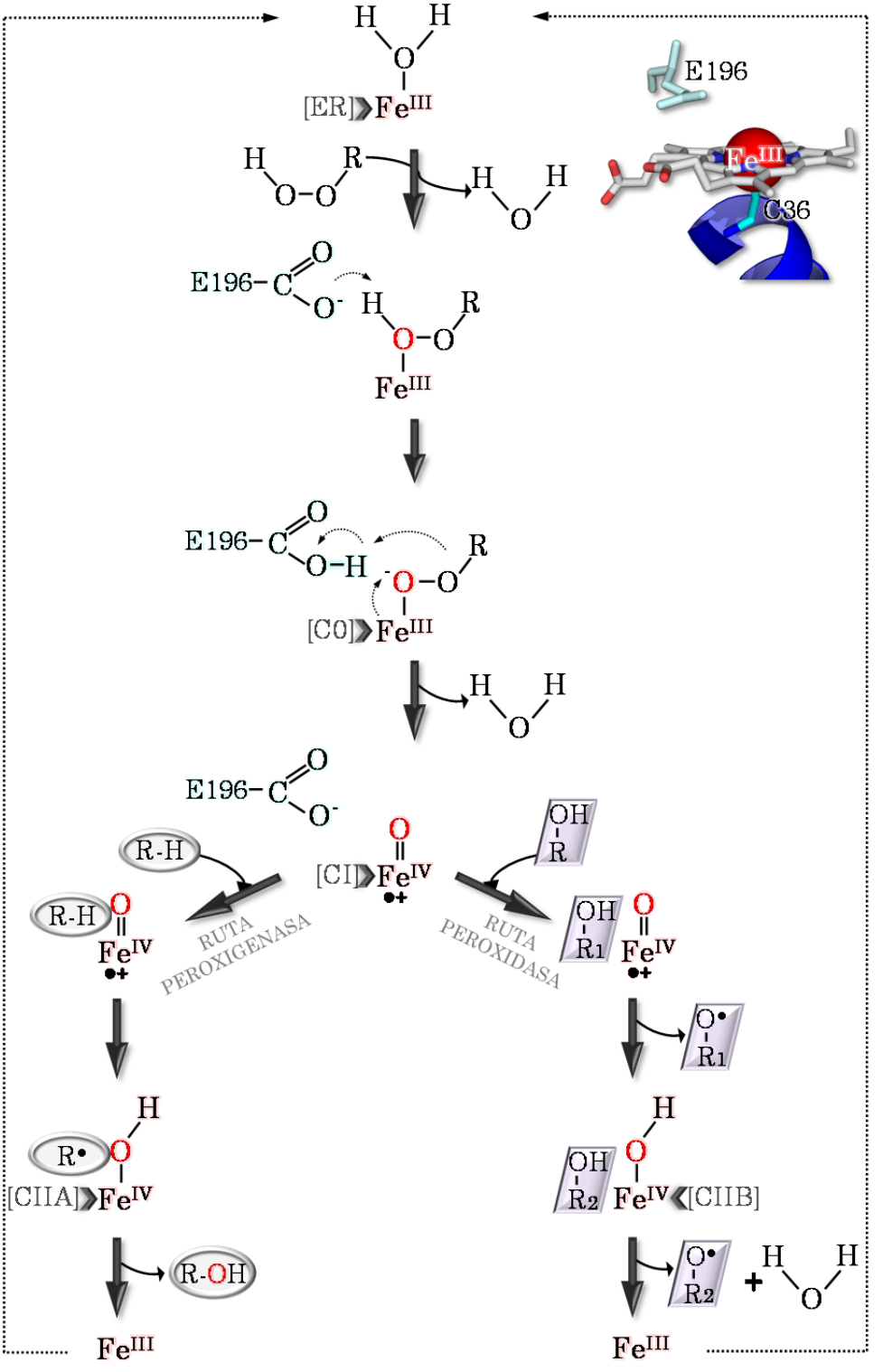

Figura 1.6. Ciclo catalítico de la UPO. Se muestran sus dos rutas oxidativas (mono(per)oxigenasa y peroxidasa).

diseñadas es crítica (Shoji y Watanabe, 2014). El descubrimiento y estudio de la UPO en el comienzo del siglo XXI ha supuesto una alternativa natural a las P450s, ya que ofrece selectividades equivalentes o incluso superiores (p.ej. en el caso de la hidroxilación de alcanos) para numerosos procesos al tiempo que presentan estabilidades superiores, independencia de dominios reductores (son enzimas solubles) y cofactores redox… en definitiva, sus requisitos son mínimos. Por ello, se prevé que la UPO paulatinamente releve a las P450s en una gran cantidad de procesos de síntesis orgánica de interés biotecnológico e industrial.

Una posible aplicación de la UPO se encuentra en la industria farmacéutica. Se ha demostrado la capacidad de esta enzima para producir tanto fármacos como intermediarios metabólicos de fármacos ("*human drug metabolites"*, HDM) (Poraj-Kobielska et al., 2011). En el hígado humano, las P450s metabolizan de manera natural los fármacos en complejos HDM de los cuales es necesario obtener información toxicológica; desafortunadamente, su síntesis por vía química resulta harto complicada. Así, se podría hacer uso de la UPO para producirlos de manera más sencilla y económica. Algunos ejemplos interesantes son la hidroxilación de flavonoides (sustancias antioxidantes como p.ej. apigenina) (Barková et al., 2011), de vitaminas (Lucas et al., 2016), de medicamentos ß bloqueantes (propranolol) (Kinne et al., 2009a), anti-inflamatorios (diclofenaco, ibuprofeno) o analgésicos-antipiréticos (acetanilida, precursor del paracetamol) (Poraj-Kobielska et al., 2011).

Otra aplicación interesante es la síntesis orgánica del alquenol cíclico limoneno, la ciclohexanona o los ácidos grasos hidroxilados que encuentran usos en cosmética, perfumería, alimentación, productos de limpieza, disolventes, polímeros (p.ej. plásticos como el tereftalato de polietileno, PET) u otros materiales (p.ej. el nylon), por poner algunos ejemplos (Gutiérrez et al., 2011; Peter et al., 2013; Peter et al., 2014). En este sentido, muy recientemente, se ha logrado la preparación del ácido 2,5-furandicarboxílico (FDCA) a partir de furfurales empleando una reacción en cascada con aril-alcohol oxidasa (AAO) y UPO. El FDCA es un importante *building block* para la industria de polímeros (Carro et al., 2015).

Otro caso de clara aplicación es la funcionalización de alcanos alifáticos en alcoholes, sin duda alguna todavía un reto muy presente de la química contemporánea. A pesar de los esfuerzos en diseñar P450s eficientes (p.ej. en la transformación de propano en propanol) (Lewis y Arnold, 2009), éstas siguen arrastrando problemas asociados a su escasa estabilidad operacional por lo que sus números de recambio totales en procesos escalados no son competitivos frente a los obtenidos por catálisis química. Esta última alternativa, por el contrario presenta problemas derivados de sus bajos rendimientos, pobres selectividades y condiciones energéticas desfavorables (altas temperaturas, presiones). Otro caso práctico donde la UPO aporta soluciones frente a los problemas arriba mencionados para las P450s es en la transformación de olefinas, tanto aromáticas como alifáticas, en sus correspondientes epóxidos. Éstos son intermediaros quirales de gran importancia en síntesis química debido a su elevada versatilidad. Su uso en aplicaciones para la producción de cosméticos, surfactantes, esterilizantes industriales o fumigantes permite su ubicación dentro de los más apreciados *building blocks*. La síntesis de epóxidos (particularmente en forma enantiopura) ha supuesto un importante esfuerzo de investigación durante décadas, sin embargo los principales problemas derivados de su preparación mediante catálisis química se traducen en pobres eficiencias catalíticas, particularmente para la epoxidación de *trans*-olefinas y unos elevados costes de producción que pueden ser resueltos con el uso de la UPO (Jacobsen, 1993).

También la UPO puede encontrar un prometedor futuro en el desarrollo de biosensores para la detección de compuestos aromáticos (Peng et al., 2010), así como en procesos de biorremediación enzimática (p.ej. transformación/hidrofilización de PAHs) (Kluge et al., 2009). No menor importancia tiene la funcionalización de hidrocarburos aromáticos en productos de alto valor añadido (p.ej. benceno en fenol) (Karich et al., 2013) o naftaleno en naftol (Kluge et al., 2009). En particular, la transformación de naftaleno por la UPO (objeto de estudio en la presente Tesis Doctoral), permite obtener un producto muy versátil para diversas industrias. El 1-naftol es un intermediario en procedimientos de síntesis orgánica, siendo

muy cotizado (su producción mundial supera las 40.000 toneladas al año). Se emplea como precursor para la preparación de tintes, aparece en formulaciones de herbicidas e insecticidas y es precursor de ciertos fármacos (Booth, 2012; Jegannathan y Nielsen, 2013). Para abastecer la demanda actual de este areno, se emplean procesos químicos contaminantes y de elevado consumo energético; además, hacen uso de catalizadores inorgánicos (p.ej. ácido sulfónico, platino, cromo, cobalto) con bajos números de recambio y reducida regioselectividad (Kudo et al., 1976; Schuster y Seid, 1979; Calinescu et al., 1994a, b y c; Molander et al., 2014). Estas razones hacen que la producción enzimática del 1-naftol sea un interesante objetivo.

Si bien la UPO nativa puede emplearse en la síntesis de los productos mencionados en esta sección, su ingeniería resulta fundamental para mejorar sus prestaciones en dichos procesos. Así, entre los grandes retos que se plantean para su futuro diseño se incluyen modelar sus selectividades en función del producto deseado (p.ej. para la hidroxilación terminal de alcanos o ácidos grasos), incrementar sus números de recambio, reducir su actividad peroxidasa lateral que puede generar subproductos no deseados, incrementar su estabilidad oxidativa o aumentar su actividad en presencia de co-disolventes. Para ello, se hace indispensable la expresión heteróloga y funcional de la enzima, así como el diseño de una plataforma de evolución dirigida con la que esculpir sus funciones.

1.1.6. Problemática asociada a la expresión funcional heteróloga de UPOs

Hasta la fecha, el no disponer de un vehículo para la expresión heteróloga funcional de la *Aae*UPO1 ha impedido realizar estudios estructura-función, así como trabajos de evolución dirigida mediante los cuales mejorar sus propiedades para su futura aplicación. Las dificultades asociadas a la expresión funcional de HTPs en hospedadores heterólogos no es algo nuevo; en efecto, y a pesar de que la CPO fue descubierta hace más de 50 años (Shaw y Hager, 1959a y b) no hay prácticamente estudios de la

mejora de esta enzima mediante evolución dirigida. Ello sin duda se debe a la falta de hospedadores heterólogos adecuados. Aunque se ha descrito la expresión de la enzima recombinante en *Aspergillus niger*, alcanzando valores de 10 mg/L (Conesa et al., 2001; Buchhaupt et al., 2011), dichos experimentos de expresión heteróloga no han podido ser reproducidos (Dra. M. Ayala, Universidad Autónoma de México, comunicación personal), por lo que la búsqueda de un sistema heterólogo apropiado para la CPO sigue siendo fundamental. El único ejemplo destacado de evolución dirigida de la CPO hizo uso de esferoplastos del microorganismo nativo, *C. fumago*, tanto para la mejora general de ciertas actividades de la enzima, como para reducir el efecto de inactivación que pueden generar las olefinas primarias en la enzima (Rai et al., 2000; Rai et al., 2001). En este sentido, el hacer uso de herramientas de evolución molecular dirigida para la expresión funcional de los complejos genes de HTPs es una alternativa sumamente útil y ampliamente versátil, como se describe en el siguiente apartado.

1.2. EVOLUCIÓN MOLECULAR DIRIGIDA

La evolución dirigida es una poderosa herramienta de diseño molecular que permite adaptar enzimas u otras moléculas a diferentes ambientes tecnológicos, que abarcan desde procesos industriales a aplicaciones medioambientales o biomédicas (Molina-Espeja et al., 2016). La evolución dirigida aplica una presión selectiva controlada por el científico a través de la cual RNA, proteínas, rutas metabólicas, circuitos genéticos o incluso células completas pueden ser evolucionados de manera iterativa con la finalidad de modelar propiedades a la carta para fines diferentes a los que se plantean en la naturaleza (Lutz, 2010; Dalby, 2011; Renata et al., 2015). Un ciclo convencional de evolución dirigida comprende 3 etapas esenciales: i) la generación de diversidad mediante mutagénesis aleatoria y/o recombinación del DNA de los genes parentales; ii) el clonaje y la expresión funcional de la librería de mutantes en hospedadores heterólogos apropiados; y iii) la selección o *screening* de las características de interés (**Fig. 1.7**), (Shivange et al., 2009; Tee y Wong, 2013; Packer y Liu, 2015; Maté et al., 2016).

Comúnmente, las librerías de mutantes se suelen examinar mediante un enfoque adaptativo (donde se busca la acumulación de mutaciones beneficiosas y la recombinación de las mismas en el curso del proceso evolutivo) (Bloom y Arnold, 2009). En muchos casos, el incremento gradual de la presión selectiva es sumamente efectivo para mejorar determinados atributos (adaptación a nuevos sustratos o frente a factores externos, como la temperatura o la presencia de inhibidores). Nuevas tendencias emergentes incluyen el empleo de la deriva genética neutral mediante la acumulación de mutaciones fenotípicamente irrelevantes para

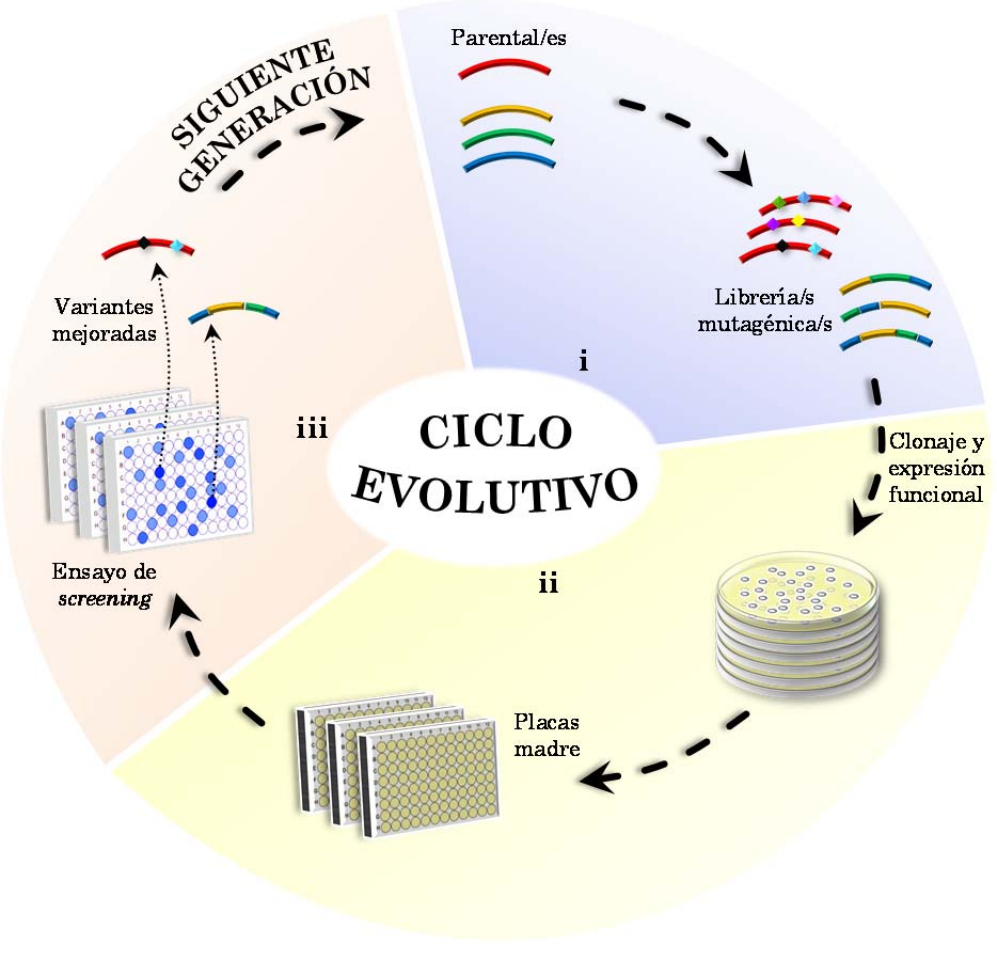

Figura 1.7. Esquema general de un ciclo de evolución dirigida.

la función natural de la enzima pero que pueden abrir nuevas vías adaptativas (Gupta y Tawfik, 2008; Tracewell y Arnold, 2009; Romero y Arnold, 2009).

Desde un punto de vista general, la evolución dirigida ha liderado el desarrollo de la biología sintética, estableciendo fuertes vínculos con la ingeniería metabólica y la biología de sistemas. Mientras surgen nuevas estrategias para la creación de diversidad genética (*i.e.* permutación circular, librerías ancestrales) que pueden ser combinadas con las herramientas tradicionales de evolución adaptativa (*i.e.* PCR mutagénica y recombinación), el diseño de métodos de *screening* de alta capacidad (*high-throughput screening*, HTS) o incluso ultra-HTS ayuda sobremanera a facilitar la exploración del espacio de secuencia proteica (Benner et al., 2007; Yu y Lutz, 2011). Muy recientemente, la conexión establecida entre la evolución dirigida y los nuevos algoritmos computacionales (p.ej. en el diseño de enzimas *de novo*) está permitiendo alcanzar metas que se sitúan más allá de los límites establecidos por la naturaleza (Verma et al., 2012; Kiss et al., 2013; Kries et al., 2013; Damborsky y Brezovsky, 2014). De esta manera, el empleo de la evolución dirigida para adaptar enzimas a ambientes artificiales, generar promiscuidad catalítica para reacciones no encontradas en la naturaleza, insertar aminoácidos no naturales en proteínas o crear moléculas de DNA artificiales es ya realidad biotecnológica (Molina-Espeja et al., 2016).

1.2.1 Evolución dirigida de oxidorreductasas fúngicas en *Saccharomyces cerevisiae*

Es importante enfatizar que desde sus comienzos, la evolución dirigida se ha empleado exhaustivamente para mejorar características inherentes de muchas enzimas: desde su expresión funcional, actividad, selectividad, ampliar el rango de sustratos o incrementar sus estabilidades para su aplicación industrial en diversos procesos de síntesis orgánica, producción de combustibles, *commodities*, biomateriales o procesos de biorremediación, por nombrar algunos ejemplos (Bornscheuer et al., 2012).

En este sentido, prácticamente la totalidad de ligninasas (oxidorreductasas ligninolíticas involucradas en la degradación de la lignina, típicamente secretadas por hongos de podredumbre blanca, y representadas por lacasas, peroxidasas de alto potencial redox y enzimas suministradoras de H_2O_2) diseñadas por evolución dirigida, han requerido de un previo ajuste para su expresión funcional (García-Ruiz et al., 2014; Alcalde, 2015). En efecto, las ligninasas naturales conocidas hasta la fecha apenas se expresan de manera funcional en hospedadores apropiados para la evolución molecular (clásicamente bacterias o levaduras). Durante las etapas de maduración, los polipéptidos ligninolíticos sufren variadas modificaciones postraduccionales (principalmente glicosilaciones, procesamientos de los extremos N- y C- terminales), que si bien transcurren con facilidad en el hongo nativo, son muy complicados de lograr en un hospedador heterólogo. De hecho, la práctica totalidad de experimentos orientados a expresar esta familia de genes en la bacteria *Escherichia coli* han conducido a plegamientos incorrectos y a la formación de cuerpos de inclusión. Probablemente, las diferencias en el uso de codones, la falta de chaperonas específicas y la ausencia de una maquinaria más sofisticada para los complejos procesados postraduccionales, impiden el correcto plegamiento de estas enzimas. Por el contrario, la fisiología de la levadura *S. cerevisiae* se encuentra mucho más próxima a la del hongo nativo, aunque la expresión funcional de estos genes tampoco es una tarea sencilla. Esto es debido fundamentalmente a que la ruta secretora de la levadura presenta diferencias sustanciales en lo referente a proteasas y/o peptidasas de secuencia señal. También influye el tiempo de residencia en el aparato de Golgi que conlleva en muchos casos hiperglicosilaciones que pueden ralentizar la ruta exportadora, ejerciendo en algunas ocasiones incluso un efecto tóxico sobre el hospedador. Por todo ello, la evolución dirigida se ha empleado como un eficaz "purgante molecular" que facilita la secreción de diferentes ligninasas en levaduras para su posterior diseño hacia nuevos fines (Gonzalez-Perez et al., 2012; Alcalde, 2015). Algunos ejemplos recientes incluyen:

i) La evolución de la lacasa de *Myceliophthora thermophila* (MtL): esta enzima se evolucionó para secreción en levadura (alcanzando ~18 mg/L) (Bulter et al., 2003). El mutante resultante se sometió a nuevas campañas evolutivas para aumentar su actividad en co-disolventes (Zumarraga et al., 2007), desplazar su perfil de pH en intervalo alcalino (Torres-Salas et al., 2013), así como su aplicación para la síntesis de tintes hetero-poliméricos (material no publicado).

ii) La evolución de la peroxidasa versátil (VP) de *Pleurotus eryngii*: la VP se expresó funcionalmente en levadura mediante evolución dirigida (~21 mg/L) y también se aumentó su termoestabilidad (Garcia-Ruiz et al., 2012); posteriormente se evolucionó para incrementar su estabilidad oxidativa (Gonzalez-Perez et al., 2014a) y más recientemente se ha hecho activa a pH alcalinos (material no publicado).

iii) La evolución dirigida de la lacasa del basidiomiceto PM1 (PM1L): inicialmente se evolucionó para secreción en levadura (~8 mg/L) (Mate et al., 2010) de manera paralela con la lacasa de *Pycnoporus cinnabarinus* (~2 mg/L) (Camarero et al., 2012); ambos mutantes se combinaron ulteriormente para crear lacasas quiméricas (Pardo et al., 2012). Más recientemente, la variante de PM1L fue evolucionada para ser activa en sangre y plasma humanos (Mate et al., 2013b) así como para aumentar su potencial redox (material no publicado).

iv) La evolución dirigida de la aril-alcohol oxidasa de *Pleurotus eryngii*: se sometió a evolución dirigida para secreción en *S. cerevisiae* (~2 mg/L) (Viña-Gonzalez et al., 2015) y más recientemente para la oxidación de alcoholes secundarios (material no publicado).

En muchos de estos casos (p.ej. PM1L, AAO, VP), tras el proceso evolutivo se ha incorporado un sistema de sobreproducción en *Pichia pastoris* que permite obtener cantidades elevadas del mutante diseñado en *S. cerevisiae* (Mate et al., 2013c y material no publicado). Tanto *S. cerevisiae* como *P. pastoris* son dos levaduras que, *a priori*, forman un tándem apropiado de ingeniería/sobreproducción. El hecho de que la maquinaria exportadora de ambas levaduras sea similar facilita la expresión de una

misma proteína sin variar notablemente sus atributos. Así, mientras *S. cerevisiae* resulta más conveniente a la hora de llevar a cabo modificaciones genéticas por evolución dirigida (debido a su elevada tasa de recombinación homóloga, alta eficiencia de transformación y disponibilidad de un amplio repertorio de vectores episomales), *P. pastoris* es capaz de alcanzar una densidad celular en biorreactor ~16 veces mayor que la levadura cervecera, de manera que la producción de la enzima puede verse disparada (Cereghino y Cregg, 2000).

1.3. OBJETIVOS

La *Aae*UPO1 se considera el relevo natural de las P450s para oxifuncionalizaciones de interés capital en síntesis orgánica, incluyendo la síntesis del agroquímico 1-naftol. A pesar de que han transcurrido más de 10 años desde el descubrimiento de esta versátil HTP, no se había logrado todavía su expresión funcional heteróloga en ningún hospedador conocido, paso que limitaba su ingeniería hacia nuevos procesos y su estudio estructura-función.

Los objetivos planteados en la presente Tesis Doctoral fueron:

- La utilización de herramientas de evolución dirigida para expresar funcionalmente la *Aae*UPO1 en *S. cerevisiae* con unos niveles que resultaran adecuados para detectar cómodamente cualquiera de sus actividades. Para ello, se hizo necesario el diseño de ensayos de *screening* específicos de actividad UPO y de métodos variados de creación de diversidad, así como la caracterización detallada de la variante final obtenida.
- La clonación, expresión y sobreproducción de la variante de secreción en biorreactor en *P. pastoris*, así como su caracterización para ser comparada con su homóloga en *S. cerevisiae*.
- Empleando como punto de partida el mutante de secreción, se propuso su diseño mediante evolución dirigida hacia la síntesis regioselectiva de 1-naftol. Como estrategia evolutiva se decidió promover la actividad peroxigenasa responsable de la síntesis de 1-

naftol a partir de naftaleno y reducir la actividad peroxidasa, que disminuye el rendimiento en la obtención del producto final. El mutante de este proceso fue sometido a un exhaustivo estudio en la reacción de interés así como a un minucioso análisis computacional mediante simulaciones moleculares.

DIRECTED EVOLUTION OF UNSPECIFIC PEROXYGENASE FROM *Agrocybe aegerita*

2

DIRECTED EVOLUTION OF UNSPECIFIC PEROXYGENASE FROM *Agrocybe aegerita*

Patricia Molina-Espeja, Eva Garcia-Ruiz, David Gonzalez-Perez, René Ullrich, Martin Hofrichter, Miguel Alcalde

Applied and Environmental Microbiology, 2014, Volume 80, Number 11, pages: 3496–3507.

http://dx.doi.org/10.1128/AEM.00490-14

Unspecific peroxygenase (UPO) represents a new type of heme-thiolate enzyme with self-sufficient mono(per)oxygenase activity and many potential applications in organic synthesis. With a view to taking advantage of these properties, we subjected the Agrocybe aegerita UPO1-encoding gene to directed evolution in Saccharomyces cerevisiae. To promote functional expression, several different signal peptides were fused to the mature protein, and the resulting products were tested. Over 9,000 clones were screened using an ad hoc dual-colorimetric assay that assessed both peroxidative and oxygen transfer activities. After 5 generations of directed evolution combined with hybrid approaches, 9 mutations were introduced that resulted in a 3,250-fold total activity improvement with no alteration in protein stability. A breakdown between secretion and catalytic activity was performed by replacing the native signal peptide of the original parental type with that of the evolved mutant; the evolved leader increased functional expression 27-fold, whereas an 18-fold improvement in the k_{cat}/K_m value for oxygen transfer activity was obtained. The evolved UPO1 was active and highly stable in the presence of organic cosolvents. Mutations in the hydrophobic core of the signal peptide contributed to enhance functional expression up to 8 mg/liter, while catalytic efficiencies for peroxidative and oxygen transfer reactions were increased by several mutations in the vicinity of the heme access channel. Overall, the directed-evolution platform described is a valuable point of departure for the development of customized UPOs with improved features and for the study of structure-function relationships.

2.1. INTRODUCTION

The unspecific peroxygenase (UPO) (EC 1.11.2.1; also known as aromatic peroxygenase [APO]) is secreted by the edible mushroom *Agrocybe aegerita*, and it belongs to a new type of peroxide using enzymes that are of considerable interest due to their wide range of potential biotechnological applications (Hofrichter and Ullrich, 2006). UPO is a compact protein with a thiolate axial ligand of the pivotal Fe^{3+} that governs the heme domain. Accordingly, UPO is classified as a member of the heme-thiolate peroxidase (HTP) superfamily, along with chloroperoxidase (CPO) from the ascomycete *Leptoxyphium fumago*, even though CPO is not capable of epoxidizing aromatic rings or hydroxylating alkanes like UPO (Hofrichter et al., 2010).

The diversity of enzymes in the HTP superfamily is conferred by 2 distinct clusters ("long" and "short" UPOs) that are included in basidiomycetes, ascomycetes, and other fungal sequences. UPO-type genes and proteins have been isolated and characterized in *Coprinellus radians*, *Marasmius rotula*, and *Coprinopsis cinerea* (Anh et al., 2007; Gröbe et al., 2011; Babot et al., 2016). Indeed, to date, over 1,000 UPO-like genes have been identified in genetic databases and in basidiomycete genome sequencing, indicating an ancient origin and a widespread distribution of UPO in nature (Floudas et al., 2012; Hofrichter et al., 2015). With over 300 identified substrates, UPOs exhibit considerable promiscuity in oxidation reactions, making them potentially attractive industrial biocatalysts. The versatile peroxide-dependent monooxygenase activity of UPO, which is based on a 2-electron oxygenation mechanism (*i.e.*, peroxygenase activity), is of particular significance, as selective oxyfunctionalizations are among the most important reactions in organic synthesis (Torres Pazmino et al., 2010). The array of oxygen transfer reactions catalyzed by UPO includes bromide oxidation, sulfoxidation, N-oxidation, aromatic peroxygenation, double-bond epoxidation, hydroxylation of aliphatic compounds, and ether cleavage (Hofrichter et al., 2010). Fueled by catalytic amounts of H_2O_2, UPO acts as a self-sufficient monooxygenase through a complex catalytic mechanism that joins the reactive intermediates of heme-peroxidases and P450s (the "peroxide shunt" pathway) (Hofrichter et al., 2015). Moreover, a UPO oxoiron(IV) protoporphyrin

radical cation intermediate (UPO compound I) was recently described and proposed as the main active oxygen species involved in the mono(per)oxygenase activity of UPO (Wang et al., 2012b; Wang et al., 2013). Thus, UPO may be considered to be the missing link between P450 monooxygenases and heme-peroxidases (Hofrichter et al., 2015).

Despite much biotechnological interest in this enzyme, no protein-engineering studies have attempted to adapt its unique features to the requirements of specific biotransformation processes in industrial settings. Moreover, endeavors to gain a better understanding of UPO's complex mechanism of action are hindered by the absence of tools with which to design mutants. Indeed, the successful adaptation of UPO has been hampered by many of the same bottlenecks that have precluded the engineering of CPO for decades, including several obstacles that prevent successful functional expression of HTPs in heterologous hosts (*e.g.,* different codon usage, cumbersome posttranslational modifications, and heme-thiolate prosthetic group attachments) (Conesa et al., 2001; Shaw and Beckwith, 1960).

Escherichia coli and *Saccharomyces cerevisiae* are the most attractive heterologous hosts in which directed evolution can be performed (Pourmir and Johannes, 2012). *S. cerevisiae* is a particularly versatile vehicle for the functional expression and directed evolution of fungal genes involved in lignin modification (including laccases and peroxidases), and it has been used in the directed evolution of versatile peroxidases (VP) for functional expression and stabilization, whereby medium-redox-potential laccases have been engineered to confer high secretion levels and activity on organic cosolvents (Bulter et al., 2003; Garcia-Ruiz et al., 2012; Zumarraga et al., 2007). More recently, this host has been used in the design of high-redox-potential laccases (HRPLs) that are active in human blood and to develop chimeric laccases with combined properties (Camarero et al., 2012; Mate et al., 2010; Mate et al., 2013b; Pardo et al., 2012). The number of protocols developed for the generation of DNA diversity in yeast is steadily increasing, and as such, the *in vivo* homologous recombination machinery of the host can be used to enrich mutant libraries (Gonzalez-Perez et al., 2012; Pirakitikulr et al., 2010; Shao et al., 2009). These

strategies have helped to extend the study of *S. cerevisiae* into the fields of synthetic biology and metabolic engineering, highlighting a wide range of potential applications ranging from biofuel production to novel green processes (Da Silva and Srikrishnan, 2012; Hong and Nielsen, 2012; Krivoruchko et al., 2011).

Here, for the first time, we describe the use of directed evolution to produce a soluble, active, and highly stable form of UPO in *S. cerevisiae*. Several fusion genes were tested to increase initial secretion levels, which were then further optimized by iterative rounds of random mutagenesis, DNA recombination, and semi-rational strategies. The enzyme's substrate promiscuity was maintained by simultaneously performing a dual high-throughput screening (HTS) assay to efficiently explore mutant libraries without altering protein stability. The final mutant produced was comprehensively characterized and exhibited markedly improved kinetic properties, secretion, and stability over a range of temperatures, as well as in the presence of high concentrations of cosolvents.

2.2. MATERIALS AND METHODS

Laboratory evolution: general aspects. The original parental n-UPO1 and the α-UPO1, α*-UPO1, n*-UPO1 and n*-3F10 fusion genes were constructed as described in the supplemental material. After each round of directed evolution, the PCR products were loaded onto a preparative agarose gel and then purified using the Zymoclean Gel DNA Recovery kit (Zymo Research). The recovered DNA fragments were cloned under the control of the GAL1 promoter of the pJRoC30 expression shuttle vector, using BamHI and XhoI to linearize the plasmid and remove the parent gene. The linearized vector was loaded onto a low-melting-point preparative agarose gel and purified as described above. The mutational loads, recombination strategies, library sizes, and general conditions for each cycle of evolution are described in **Table S2.1** in the supplemental material. All the primers used in this study are listed in **Table S2.3** in the supplemental material.

First generation. Four libraries were devised, using n-UPO1 and α-UPO1 as the parental types. For each parent, 2 different mutagenic PCR strategies were used: *Taq* DNA polymerase (Sigma) in the presence of $MnCl_2$ (1 to 3 mutations/1,000 bp) and the Genemorph II kit (4 to 9 mutations/1,000 bp) (Stratagene; Mutazyme II). The PCR for *Taq*/$MnCl_2$ was performed in a final volume of 50 µl containing 3% dimethyl sulfoxide (DMSO), 90 nM RMLN, 90 nM RMLC, 0.3 mM deoxynucleoside triphosphates (dNTPs) (0.075 mM each), 0.01 mM $MnCl_2$, 1.5 mM $MgCl_2$, 0.05 U/µl *Taq* DNA polymerase, and 0.1 ng/µl of the corresponding template. The PCRs for Mutazyme II were carried out in a final volume of 50 µl containing 3% DMSO, 0.37 µM RMLN, 0.37 µM RMLC, 0.8 mM dNTPs (0.2 mM each), 0.05 U/µl Mutazyme II, and 300 ng of the corresponding initial target template (2,800 ng of pJR-n-upo1 and 2,566 ng of pJR-α-upo1). Error-prone PCR was performed on a gradient thermocycler (Mycycler; Bio-Rad) using the following parameters: 95°C for 2 min (1 cycle); 94°C for 45 s, 53°C for 45 s, and 74°C for 3 min (28 cycles); and 74°C for 10 min (1 cycle). The PCR products (200 ng) were mixed with the linearized plasmid (100 ng) and transformed into competent *S. cerevisiae* cells using the Yeast Transformation kit (Sigma). To promote *in vivo* ligation, ~50-bp overhangs homologous to the linear vector were designed. Transformed cells were plated on synthetic complete (SC) drop-out plates and incubated for 3 days at 30°C. Colonies containing the whole autonomously replicating vector were selected and subjected to the dual HTS assay and additional rescreening, as described in the supplemental material.

Second generation. The best mutants obtained from the first generation (1A11 and 3C2) were submitted to error-prone PCR (*Taq*/$MnCl_2$ and Mutazyme II), as well as *in vivo* DNA shuffling. The mutagenic rates, the PCR conditions, and the thermal-cycling program employed were the same as those described for the first generation. The mutated PCR products were mixed with the linearized vector (at a 4:1 ratio of PCR products to linearized plasmid) and transformed into competent *S. cerevisiae* cells in order to promote *in vivo* DNA shuffling.

Third generation. The best mutant from the second round of evolution (mutant 12C12) was subjected to 2 different processes.

(i) *In vivo* assembly of mutant libraries. A recombined mutant library was built by *in vivo* assembly of mutant libraries constructed with different mutational spectra (IvAM) (Zumarraga et al., 2008). *Taq*/$MnCl_2$ and Mutazyme II libraries were mixed in equimolar amounts and transformed into competent *S. cerevisiae* cells along with the linearized vector, as described above (at an 8:1 ratio of mutant library to vector).

(ii) Focused domain mutagenesis at the signal peptide. The 12C12 signal sequence was independently subjected to random mutagenesis by MORPHING (mutagenic organized recombination process by homologous *in vivo* grouping) (Gonzalez-Perez et al., 2014b). Mutagenic PCR was prepared in a final volume of 50 µl containing 3% DMSO, 90 nM RMLN, 90 nM Morphing psn apo1 rev, 0.3 mM dNTPs (0.075 mM each), 0.1 mM $MnCl_2$, 1.5 mM $MgCl_2$, 0.05 U/µl *Taq* polymerase DNA, and 0.92 ng/µl template. The amplification parameters were 95°C for 2 min (1 cycle); 94°C for 45 s, 50°C for 45 s, and 74°C for 30 s (28 cycles); and 74°C for 10 min (1 cycle). The remaining portion of the whole UPO1 gene was amplified by high-fidelity PCR in a final volume of 50 µl containing 3% DMSO, 0.5 µM Morphing psn apo1 dir, 0.5 µM RMLC, 1 mM dNTPs (0.25 mM each), 0.02 U/µl iProof DNA polymerase, and 0.2 ng/µl template. High-fidelity PCR was carried out on a gradient thermocycler using the following parameters: 98°C for 30 s (1 cycle); 98°C for 10 s, 55°C for 25 s, and 72°C for 45 s (28 cycles); and 72°C for 10 min (1 cycle). The whole gene was *in vivo* reassembled and recombined by transforming the different PCR products into *S. cerevisiae* competent cells, a process facilitated by ~50-bp overhangs flanking each recombination area. The DNA transformation mixture was composed of linearized plasmid (100 ng) mixed with the mutagenized leader (200 ng) and the mature nonmutagenized protein (200 ng).

Fourth generation. (i) Error-prone PCR and *in vivo* DNA shuffling. Mutagenic PCRs were performed separately with mutants I13D3, M5D2, and M4D8. The mutated PCR products were mixed with the linearized

vector (at a PCR product/linearized plasmid ratio of 6:1) and transformed into competent *S. cerevisiae* cells to promote *in vivo* DNA shuffling.

(ii) Site-directed mutagenesis. The I13D3 mutant from the third generation was used as a template to introduce F[12]Y, A[14]V and R[15]G mutations (positions in the signal peptide are indicated in brackets) using *in vivo* overlap extension (IVOE) (Alcalde, 2010). Two high-fidelity PCRs were performed in a final volume of 50 µl containing (i) 3% DMSO, 0.5 µM RMLN, 0.5 µM PSN*R, 1 mM dNTPs (0.25 mM each), 0.02 U/µl iProof DNA polymerase, and 0.2 ng/µl template or (ii) 3% DMSO, 0.5 µM PSN*F, 0.5 µM RMLC, 1 mM dNTPs (0.25 mM each), 0.02 U/µl iProof DNA polymerase, and 0.2 ng/µl template. The following PCR parameters were used for each reaction: (i) 98°C for 30 s (1 cycle), 98°C for 10 s, 47°C for 25 s, 72°C for 15 s (28 cycles), and 72°C for 10 min (1 cycle); (ii) 98°C for 30 s (1 cycle), 98°C for 10 s, 52°C for 25 s, 72°C for 40 s (28 cycles), and 72°C for 10 min (1 cycle). Both PCR products (200 ng each) were mixed with the linearized vector (100 ng) and transformed into *S. cerevisiae* for *in vivo* gene each segment were created to maximize the efficiency of *in vivo* DNA splicing between fragments.

Fifth generation. The V57A mutation from 22A10 was introduced into 2A12 by mutational recovery through IVOE. Two high-fidelity PCRs were performed in a final volume of 50 µl containing (i) 3% DMSO, 0.5 µM RMLN, 0.5 µM 2A12*REV, 1mM dNTPs (0.25mMeach), 0.02 U/µl iProof DNA polymerase, and 0.2 ng/µl template or (ii) 3% DMSO, 0.5 µM 2A12*DIR, 0.5 µM RMLC, 1mM dNTPs (0.25mMeach), 0.02 U/µl iProof DNA polymerase, and 0.2 ng/µl DNA template. The following PCR parameters were used for each reaction: (i) 98°C for 30 s (1 cycle), 98°C for 10 s, 47°C for 25 s, 72°C for 15 s (28 cycles), and 72°C for 10 min (1 cycle); (ii) 98°C for 30 s (1 cycle), 98°C for 10 s, 52°C for 25 s, 72°C for 35 s (28 cycles), and 72°C for 10 min (1 cycle). Both PCR products (200 ng each) were mixed with the linearized vector (100 ng) and transformed into *S. cerevisiae* for *in vivo* gene reassembly and cloning as described above.

High-throughput screening: peroxidative and peroxygenase activities were screened with the help of a dual HT assay based on the oxidation of ABTS [2,2'-azino-bis(3-ethylbenzothiazoline-6-sulfonic acid)] and the hydroxylation of

5-nitro-1,3-benzodioxole (NBD) (which is in turn spontaneously cleaved to form the chromophore 4-nitrocatechol), as indicated in the supplemental material. Three consecutive rescreenings were carried out to rule out the selection of false positives, which included a thermostability assay for the estimation of T_{50} (the temperature at which the enzyme retains 50% of its initial activity after 10 min of incubation) values.

Purification and biochemical characterization. n*-UPO1, the PaDa-I mutant, and $_{wt}$UPO1 were produced, purified, and biochemically characterized as described in the supplemental material.

2.3. RESULTS AND DISCUSSION

Point of departure: construction of fusion genes and design of the HTS assay. The starting point of this study was the cDNA (*upo1* gene) coding for the unspecific peroxygenase from *A. aegerita* (accession no. FM872457) (Pecyna et al., 2009; Ullrich et al., 2004). This gene encodes a protein of 328 amino acids plus a 43 amino acid signal peptide that directs secretion in *A. aegerita*. To achieve sufficient expression in the heterologous host in order to begin directed evolution, several constructs were prepared that contained the native signal sequence (n-UPO1), the α-factor prepro-leader from *S. cerevisiae* (α-UPO1), and the evolved α-factor prepro-leader (α*-UPO1). The evolved α-factor prepro-leader (α*) was previously engineered in association with an HRPL, achieving functional levels of expression after 8 rounds of laboratory evolution (Mate et al., 2010). The α* construct contained V10D-N23K-A87K mutations that boosted the expression of other HRPL genes (Camarero et al., 2012; Pardo et al., 2012; Mate et al., 2011) and that may also enhance UPO1 secretion. The secretion of each of the fusion genes was determined in 96-well plate microfermentations (mU ABTS/liter): n-UPO1, 149; α-UPO1, 74; α*-UPO1, negligible. While the use of evolved α-factor prepro-leaders as universal peptides for heterologous expression has been proposed (Rakestraw et al., 2009), this approach appears to work only when signal sequences are switched between protein templates with a high degree of sequence identity (as in the case of HRPLs), indicating that they cannot be used in other, less related systems.

Several substrates were tested to develop a screening assay for directed UPO evolution. They included benzyl alcohol, veratryl alcohol, NBD, 2,6-dimethoxyphenol (DMP), ABTS, and *p*-nitrophenoxy carboxylic acid (*p*NCA). Given the low levels of UPO1 secretion in microtiter plates, only the ABTS oxidation assay was reliable and stable, with good signal response and a low level of interference in culture broth. This assay was adjusted for the appropriate substrate concentrations (0.3 and 2 mM ABTS and H_2O_2, respectively) and the optimum pH (4.4). After improving secretion levels (from the second round of evolution onward), a peroxygenase (oxygen transfer) assay using NBD as the substrate was also incorporated into the screening protocol to maintain or even improve mono(per)oxygenase activity. UPO converts NBD into 4-nitrocatechol (yellow) via an initial hydroxylation and the subsequent spontaneous release of formic acid. 4-Nitrocatechol can be deprotonated at basic pH values to produce a strong red color (Poraj-Kobielska et al., 2012). The microfermentation conditions were optimized to minimize interference during screening, evaluating several heme sources (α-aminolevulinic acid, hemine, and hemoglobin), the concentration of $MgSO_4$ (a source of structural Mg^{2+}), and the effect of ethanol on membrane permeability, as well as a range of temperatures, stirring rates, and periods of incubation (see the supplemental material for details). The heme source chosen for UPO expression (hemoglobin) generated unwanted background activity during screening, and it was removed from the expression medium in the last rounds of evolution, as secretion was sufficiently high in its absence. Moreover, the coefficient of variance of the assays was reduced by up to 12% in the final cycles of evolution due to the stronger activity displayed by the variants. Three consecutive rescreenings were performed to rule out the presence of false positives. To protect UPO stability during the course of the evolution, the T_{50} was estimated for each mutant studied during the third rescreening.

Directed evolution. The total activity of UPO1 was improved ~3,250-fold with respect to the parental type after 5 generations (9,000 clones screened) of directed evolution. Moreover, expression levels of ~8 mg/liter were achieved with activity values of 6,500 U ABTS/liter and 1,300 U NBD/liter. A combination of several error-prone PCR strategies with *in vivo* DNA recombination protocols,

focused domain mutagenesis on the signal peptide, and mutational recovery was performed. In the first generation, both the n-UPO1 and α-UPO1 fusion genes were used as starting points to enhance expression by subjecting the complete constructs to random mutagenesis and recombination. Accordingly, 4 mutant libraries were designed using different DNA polymerases and mutational loads, 2 for each construct. Mutants selected after several consecutive rescreenings were derived exclusively from n-UPO1 libraries. The 2 best variants from this round were 1A11 (L67F) and 3C2 (I248V-F311L), with 13- and 9-fold improvements in total activity compared to n-UPO1, respectively (**Fig. 2.1**; see **Table S2.1** in the supplemental material).

The mutations of 1A11 and 3C2 were sufficiently distant (L67F of 1A11 was located at a distance of 181 residues from I248V in the 3C2 mutant) to permit a suitable crossover event to take place in the next cycle of evolution via the yeast *in vivo* recombination machinery. Accordingly, in the second generation, these 2 variants were subjected to random mutagenesis and *in vivo* DNA shuffling. As planned, all variants selected from this round combined L67F-I248V-F311L, and they included some extra point mutations in either the mature protein or the signal peptide. The mutant best secreted in this generation (12C12) contained the aforementioned L67F-I248V-F311L mutations, as well as A[21]D in the signal peptide. At this stage of evolution, the NBD assay could be incorporated into the screening protocol to measure oxygen transfer activity, thanks to the high levels of secretion observed for the 12C12 mutant. The use of the dual screening assay based on the NBD/ABTS ratio allowed mutant hits to be selected without jeopardizing activity and variants with improved NBD/ABTS ratios to be identified (see below).

In the third generation, a dual approach was taken. First, mutant libraries with different mutational spectra were assembled *in vivo* by IvAM (Zumarraga et al., 2008), using the 12C12 mutant (including its signal peptide) as a template (**Fig. 2.1a**). In addition, the signal peptide of 12C12 was subjected

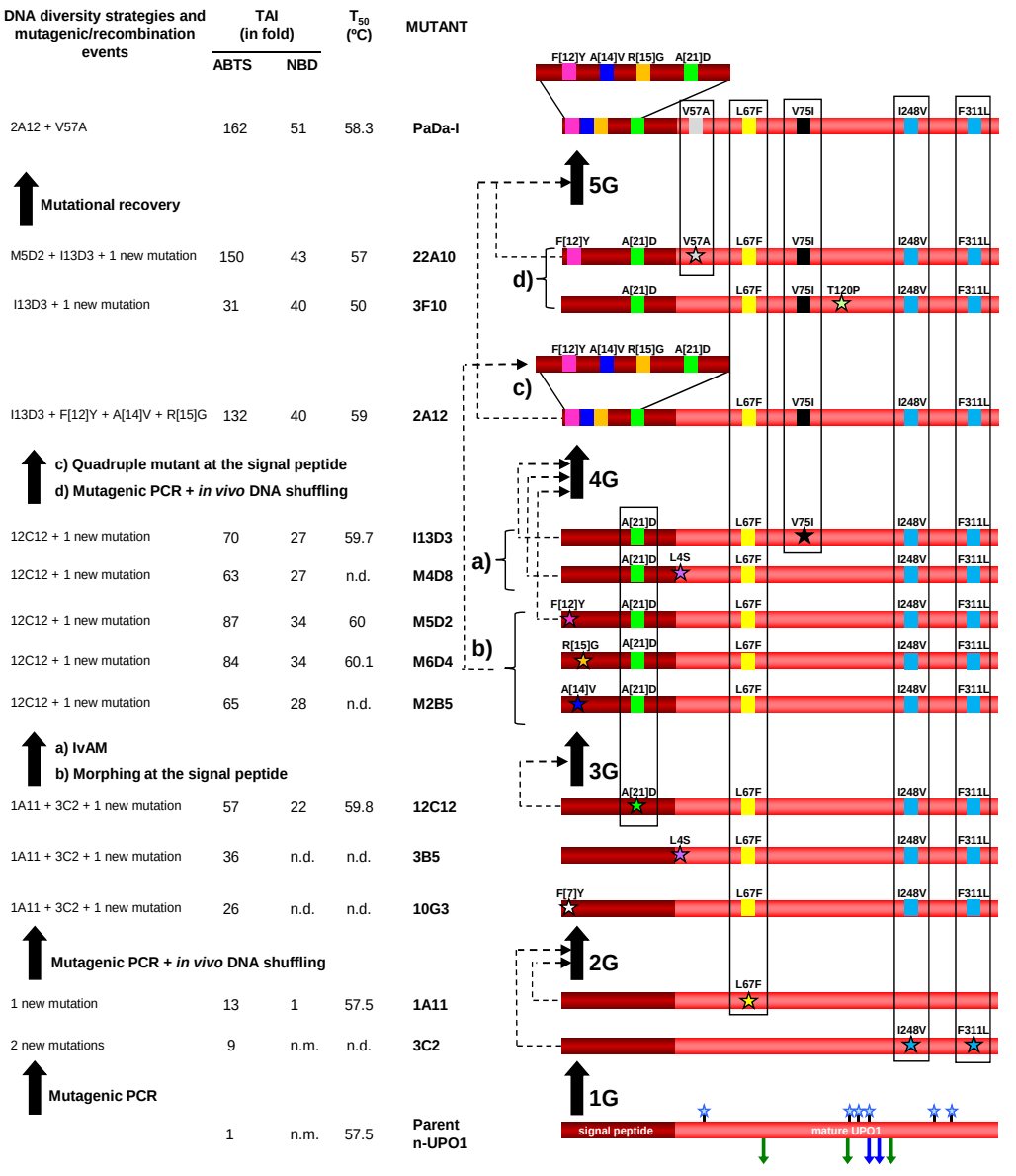

Fig. 2.1. Route for the directed evolution of UPO1 toward functional expression and improved activity. New mutations are depicted as stars and accumulated mutations as squares. Mutations in the mature PaDa-I mutant and their origins are boxed. The signal peptide is represented in dark red and the mature protein in red. In the parental n-UPO1, the glycosylation sites (Asn11, Asn141, Asn161, Asn182, Asn286 and Asn295) are represented as blue stars, the Phe triad (Phe69, Phe121, and Phe199) involved in the binding of aromatic substrates is marked with green arrows, and the acid-base pair for peroxide cleavage (Glu196 and Arg189) is indicated with blue arrows. TAI represents the improvement in UPO1 activity detected in *S. cerevisiae* microcultures for each mutant compared with the parental n-UPO1. Thermostability (T_{50}) was estimated from culture supernatants (**Fig. 2.2B**). The breakdown of the TAI into specific activity and expression is shown in **Fig. 2.3**. The dashed arrows indicate the parental types used for each round of evolution. In the 3rd generation, "a" indicates the offspring obtained by IvAM of 12C12 and "b" indicates the offspring obtained by MORPHING in the signal peptide of 12C12. In the 4th generation, "c" indicates the triple mutant at the signal peptide constructed using I13D3 as a template and "d" the offspring obtained by mutagenic PCR and shuffling of parents I13D3, M5D2, and M4D8. n.d., not determined; n.m., not measurable. (See also **Table S2.1** in the supplemental material).

to focal mutagenesis by MORPHING (Gonzalez-Perez et al., 2014b) in an attempt to enrich the signal peptide in mutations that favor secretion (**Fig. 2.1b**). Library landscapes revealed a higher tolerance for mutations in the leader than in the whole UPO1 gene. This is consistent with the observation that mutations in the leader affect only secretion whereas mutations at the whole-gene level may also modify catalytic properties. The most promising mutant from the IvAM library, I13D3, contained the new V75I mutation, and it displayed a 70-fold total activity improvement with respect to n-UPO1. By focusing mutational loads in the signal peptide, 3 beneficial mutations were introduced between positions 12 and 15 in 3 independent mutant winners.

Table 2.1. Biochemical features of the wild type and evolved UPOs.

	Value	
Biochemical and spectroscopy features [h]	$_{wt}$UPO1 [e]	PaDa-I mutant [f]
MW (Da) [a]	46,000	52,000
MW (Da) [b]	ND [g]	51,100
MW (Da) [c]	35,942	35,914
Glycosylation degree (%)	22	30
Thermal stability, T_{50} (ºC) [d]	53	55
pI	4.9-5.7	5.5
Optimum pH for ABTS	4.0	4.0
Optimum pH for DMP	7.0	6.0
Optimum pH for NBD	6.5	6.0
R_Z, (A_{418}/A_{280})	2.4	1.8
Soret region (nm)	420	418
CT1 (nm)	572	570
CT2 (nm)	540	537

[a] Estimated by SDS-PAGE. [b] Estimated by MALDI-TOF mass spectrometry. [c] Estimated from amino acid composition. [d] Estimated from purified variants. [e] $_{wt}$UPO1, UPO1 wild type expressed in *A. aegerita*. [f] PaDa-I mutant, the ultimate variant of the whole evolution process in *S. cerevisiae* (containing the evolved signal peptide [n*] plus the evolved UPO1) (see **Fig. S2.1** in the supplemental material). [g] ND, not determined. [h] CT1 and CT2, charge transference bands 1 and 2, respectively.

Mutations F[12]Y, A[14]V and R[15]G in the leader were so close to one another that the likelihood of recombination by *in vitro* or *in vivo* methods was very low. Thus, for the fourth generation, we constructed a triple mutant by site-directed mutagenesis using the I13D3 mutant as a template (**Fig. 2.1c**). The resulting mutant (2A12) contained 4 beneficial mutations, F[12]Y-A[14]V-R[15]G-A[21]D, in the signal sequence, and it showed markedly improved secretion. In addition, a new round of random mutagenesis and recombination was also performed using I13D3, M5D2 and M4D8 as templates. Although M4D8 was not the best variant in generation 3, it was chosen as the parent due to the mutational redundancy observed at position 4, as this substitution also appeared in the 3B5 mutant from generation 2. From this set of experiments, we identified the 22A10 mutant, generated by a recombination event between M5D2 and I13D3 and containing the new mutation V57A (**Fig. 2.1d**). Finally, the V57A mutation was introduced into 2A12 by mutational recovery, giving rise to the final mutant, PaDa-I.

Biochemical characterization. Wild type UPO1, produced homologously by *A. aegerita* ($_{wt}$UPO1), and the PaDa-I mutant secreted in *S. cerevisiae* were purified to homogeneity (Reinheitszahl value [Rz] [A_{418}/A_{280}], ~2) and characterized biochemically (**Table 2.1**; see **Fig. S2.1** in the supplemental material). The average molecular mass measured by matrix-assisted laser desorption ionization-time of flight mass spectrometry (MALDI-TOF MS) was 51,100 Da for PaDa-I (*i.e.*, 5,000 Da higher than that of $_{wt}$UPO1), and the contribution of glycosylation deduced by deglycosylation gels was around 22% for the wild type and 30% for the mutant (see **Fig. S2.1** in the supplemental material). *S. cerevisiae* tends to hyperglycosylate foreign proteins up to levels of ~50%, conferring on them increased stability and protection against proteolytic degradation. The glycosylation of $_{wt}$UPO1 observed was exclusively dependent on 6 predicted N-glycosylation sites (O-glycosylation sites are not described for the enzyme), associated with up to 8 moieties of the high-mannose type (Pecyna et al., 2009; Piontek et al., 2013). None of the amino acid substitutions in PaDa-I introduced new glycosylation motifs, and thus, the higher sugar content in the mutant may be due to an increased Golgi residence time that leads to the addition of more mannose moieties, as described in other directed evolution

studies in yeast (Bulter et al., 2003; Camarero et al., 2012). The PaDa-I and $_{wt}$UPO1 proteins had similar spectroscopic characteristics in the Fe^{3+} resting state, with both enzymes showing a maximum in the Soret region of around 418 nm and 2 Q bands at 570 and 540 nm (**Fig. 2.2A**).

The very weak expression of the parental n-UPO1 in *S. cerevisiae* (~0.007 mg/liter) hampered its purification to homogeneity. To overcome this impediment, we constructed a fusion gene in which the native signal peptide of n-UPO1 was replaced by that obtained after 5 cycles of directed evolution in yeast (n*, containing F[12]Y A[14]V R[15]G A[21]D mutations). Larger amounts of native UPO1 were produced in *S. cerevisiae* from the n*-UPO1 fusion gene, which was then purified to homogeneity. This approach allowed us to make an accurate breakdown of the total activity improvement (TAI) in terms of both specific activity and heterologous functional expression (**Fig. 2.3**). The product of the n*-UPO1 fusion gene showed biochemical characteristics similar to those of the PaDa-I mutant in terms of molecular mass, the degree of glycosylation, and thermal stability. After large scale fermentation, the PaDa-I protein showed a 3,250-fold TAI compared to the parental n-UPO1 (6,500 U ABTS/liter for PaDa-I versus 2 U ABTS/liter for n-UPO1), an improvement that was 20-fold greater than that obtained in microtiter plates, where stirring conditions and oxygen availability were limiting. The product of n*-UPO1 showed a 27-fold TAI with respect to n-UPO1, reflecting the potency of the evolved signal peptide in promoting UPO1 secretion. The breakdown of the TAI value revealed a 1,114-fold increase in functional expression and a 3.6-fold increase in peroxidative activity (using ABTS) with respect to the parental type. Bearing in mind that n* enhanced functional expression 27-fold, there was a further ~41-fold improvement in functional expression conferred by mutations in the mature UPO1. Secretion levels were significantly enhanced, from 0.007 mg/liter to 8 mg/liter, *i.e.*, to levels similar to those obtained in the original fungus *A. aegerita* (Ullrich et al., 2004).

The pH profiles for peroxidative (with ABTS and DMP) and peroxygenase (with NBD) activities revealed similar shapes and optimum pH values for $_{wt}$UPO1, n*-UPO1, and PaDaI (~4.0, 5.0, and 6.0 for ABTS, DMP, and

NBD, respectively) (**Fig. 2.2C** and **D** and **Table 2.1**). Kinetic constants for peroxidative and peroxygenase activities were assayed using several compounds, along with aryl alcohols with different redox potentials (**Table 2.2**). The k_{cat} for n*-UPO1 expressed in yeast was ~5-fold lower than that of $_{wt}$UPO1, although they showed similar substrate affinities, with the exception of the K_m for H_2O_2 (2-fold lower in n*-UPO1). General differences in protein folding in the heterologous host, particularly those affecting posttranslational modifications (*e.g.*, hyperglycosylation), may affect the activity of the recombinant enzyme. These results are consistent with those reported for lignin-modifying enzymes heterologously expressed in yeast, in which a decrease in the k_{cat} of up to 10-fold was observed (Mate et al., 2013a). Both PaDa-I and $_{wt}$UPO1 showed very similar

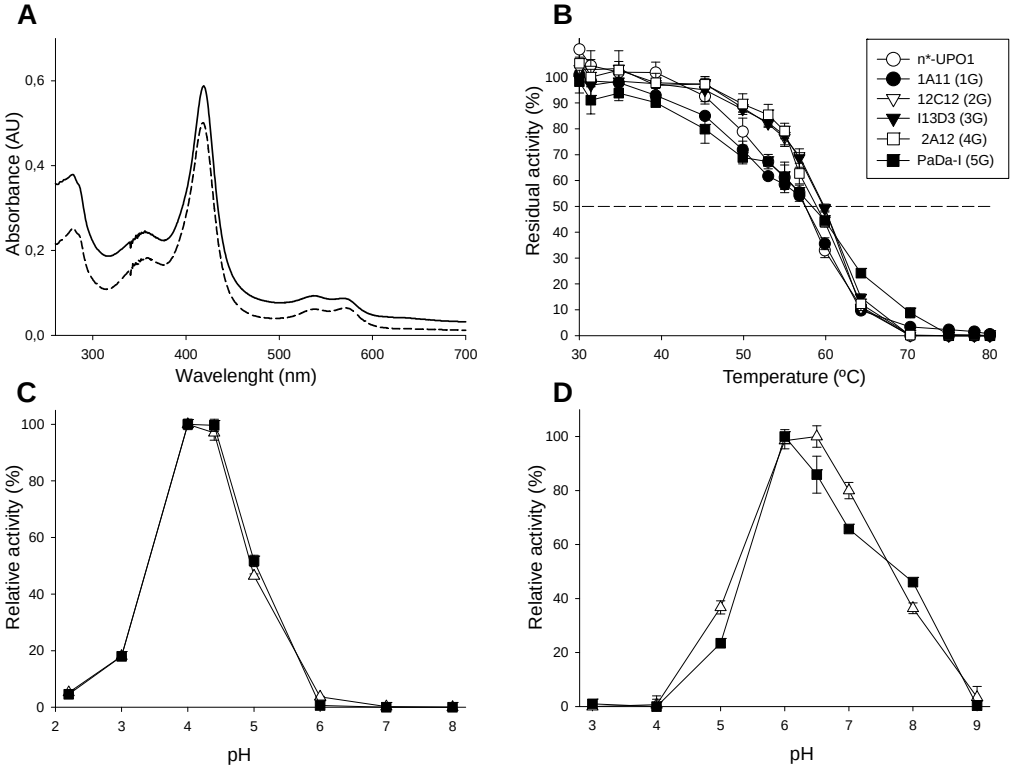

Fig. 2.2. Biochemical characterization. (A) Spectroscopic characteristics of $_{wt}$UPO1 (dashed line) and the PaDa-I mutant (solid line). AU, arbitrary units. (B) Thermostability (T_{50}) of PaDa-I and different parental types. Each point represents the mean and standard deviation of 3 independent experiments. 1G to 5G, 1st generation to 5th generation. (C and D) pH activity profiles for $_{wt}$UPO1 (triangles) and PaDa-I (squares). Activities were measured in 100 mM citrate/phosphate/borate buffer at different pH values with 2mM H_2O_2 and 0.3mM ABTS (C) or with 1mM H_2O_2 and 1mM NBD (D). UPO1 activity was normalized to the optimum activity value, and each point represents the mean and standard deviation of 3 independent experiments.

catalytic efficiencies for all the substrates tested, indicating marked improvements in the activity of UPO1 after each round of evolution. Indeed, a notable improvement in the k_{cat} value was detected when n*-UPO1 was compared with PaDa-I (with increases of 10-, 9-, 8- and 7-fold for NBD, ABTS, veratryl alcohol, and benzyl alcohol, respectively) and these increases accounted for an overall increase in catalytic efficiency: the 18-fold improvement in the k_{cat}/K_m value for NBD hydroxylation comparing n*-UPO1 and PaDa-I was 2.2 times greater than that of $_{wt}$UPO1 (*i.e.*, 700 and 320 mM^{-1} s^{-1} for PaDa-I and $_{wt}$UPO1, respectively). Thus, the dual screening assay used during *in vitro* evolution helped to conserve and even improve both peroxidative and mono(per)oxygenase activities.

Many of the aromatic substrates and oxyfunctionalized compounds converted by UPO are further oxidized by the enzyme, generating a pool of products of various complexities. Accordingly, for certain applications, the removal of UPO's peroxidative activity (1-electron oxidation) may be considered a biotechnological priority. Using the HTS assay, we attempted to uncouple the peroxidation and monooxygenase activities. Taking the NBD/ABTS ratio as a discriminatory factor, the 3F10 variant (T120P mutation) identified in the fourth generation showed a dramatic decrease in peroxidative activity (a 4-fold decrease in the TAI for ABTS, from 132- to 31-fold) while conserving its peroxygenase activity (with similar TAIs for NBD and the parental 2A12) (**Fig. 2.1**). The signal peptide was switched in the 3F10 variant, as described for the n*-UPO1 construct (see the supplemental material) and the corresponding n*-3F10 construct was produced on a larger scale and compared with both $_{wt}$UPO1 and n*-UPO1. The NBD/ABTS ratios (expressed as percentages) were 19%, 20% and 61% for $_{wt}$UPO1, n*-UPO1 and n*3F10, respectively. During the preliminary characterization of this variant, we detected a dramatic decrease in the thermostability produced by the beneficial but destabilizing T120P mutation (with a 7°C decrease in T_{50}), which precluded its purification and further analysis. Although monooxygenase activity is a clear target for directed UPO evolution, our results indicate that the line between peroxidation and mono(per)oxygenase activity in UPO is very fine and that its catalytic mechanisms are strongly implicated in protein stability (Wang et al., 2013). This

problem may be overcome by including iterative rounds of neutral genetic drift in order to introduce stabilizing mutations into the 3F10 mutant before further evolving its monooxygenase activity (Goldsmith and Tawfik, 2013).

Kinetic thermostability was conserved over the course of evolution, with T_{50} values in the 57 to 59°C range for all the offspring of the mutants used as parental types in each round of directed evolution (**Fig. 2.1** and **2.2B**). This effect was due to the screening assay used during evolution, in which destabilizing mutations were excluded from the evolutionary pathway.

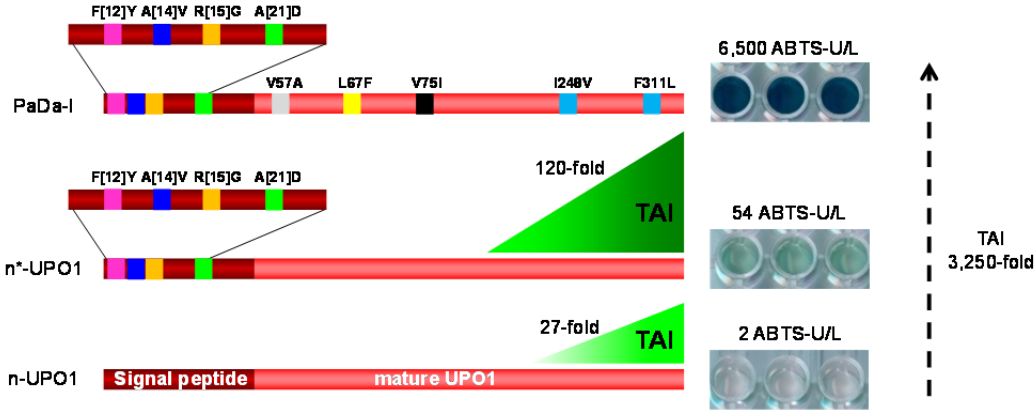

	U/L (crude extract)	U/mg	Secretion levels (mg/L)	Improvement breakdown		
				Total activity improvement: TAI (fold increase)[b]	Specific activity (fold)	Expression (fold)
n-UPO1	2	n.m.	0.007[a]	1	1	1
n*-UPO1	54	233	0.2	27	1	27
PaDa-I mutant	6,500	828	7.8	3,250	3.6	1,114

[a]Secretion levels for n-UPO1 were calculated assuming the same specific activity as n*-UPO1. [b]Total activities (U/L) and TAI values (in fold) are calculated from large scale fermentation experiments. Activities were assessed in 100 sodium citrate/phosphate pH 4.4 containing 0.3 mM ABTS and 2 mM H_2O_2.

Fig. 2.3. Breakdown of specific activity and functional expression. A fusion gene containing the evolved signal peptide (n*) attached to the native mature UPO1 was engineered. The n-UPO1, n*-UPO1 and PaDa-I variants were produced on a large scale, and their TAIs were measured. n*-UPO1 and PaDa-I were purified, and their specific activities were calculated. n* enhanced functional expression ~27-fold, whereas mutations in mature PaDa-I resulted in an ~120-fold increase in total activity. The 3,250-fold increase in the total activity of PaDa-I was broken down as a 3.6-fold improvement in specific activity and a 1,114-fold improvement in functional expression.

The presence of organic cosolvents is required for many of the transformations mediated by UPO. The activity and stability of $_{wt}$UPO and the PaDa-I mutant were evaluated in the presence of high concentrations of cosolvents with different polarities (with a logP [octanol-water partition coefficient] ranging from -0.23 to -1.3) and chemical characteristics (**Fig. 2.4A** and **B**). Regardless of the enzyme tested, activity was reduced drastically in the presence of increasing concentrations of cosolvents in the following order: ethanol > DMSO > acetonitrile (ACN) ~ methanol > acetone. Activities in cosolvents were estimated by measuring the concentration of cosolvent at which the enzyme shows 50% of the corresponding activity in buffer (C_{50}). The strongest activity was observed in acetone (C_{50}, 10 to 12%) and the weakest in ethanol and DMSO (C_{50}, ~2%). In terms of stability in cosolvents, both enzymes were very stable at concentrations as high as 50% (vol/vol), with a half-life of

Table 2.2. Kinetic parameters of wild type, recombinant and evolved UPO variants.

Substrate	Kinetics constants	Value [a]		
		$_{wt}$UPO1	n*-UPO1	PaDa-I
ABTS	K_m (mM)	0.025 ± 0.002	0.027 ± 0.005	0.048 ± 0.004
	k_{cat} (s^{-1})	221 ± 6	45.0 ± 2.7	395 ± 13
	k_{cat}/K_m (mM^{-1} s^{-1})	8,800 ± 692	1,600 ± 37	8,200 ± 598
NBD	K_m (mM)	0.684 ± 0.207	0.782 ± 0.352	0.483 ± 0.095
	k_{cat} (s^{-1})	219 ± 25	31.7 ± 6.1	338 ± 22
	k_{cat}/K_m (mM^{-1} s^{-1})	320 ± 64	38.0 ± 11	700 ± 99
Benzyl alcohol	K_m (mM)	1.90 ± 0.11	1.10 ± 0.23	2.47 ± 0.32
	k_{cat} (s^{-1})	329 ± 7	44.8 ± 3.1	307 ± 15
	k_{cat}/K_m (mM^{-1} s^{-1})	174 ± 7	41.0 ± 6.3	124 ± 11
Veratryl alcohol	K_m (mM)	5.20 ± 0.31	5.30 ± 0.82	7.9 ± 0.7
	k_{cat} (s^{-1})	88 ± 2	15.2 ± 1.1	121 ± 5
	k_{cat}/K_m (mM^{-1} s^{-1})	17 ± 0.7	2.9 ± 0.25	15 ± 0.9
H_2O_2	K_m (mM)	1.37 ± 0.16	0.69 ± 0.20	0.49 ± 0.06
	k_{cat} (s^{-1})	290 ± 15	40.9 ± 3.8	238 ± 8
	k_{cat}/K_m (mM^{-1} s^{-1})	211 ± 15	59.0 ± 12.3	500 ± 42

[a] ABTS kinetic constants for UPO1 were estimated in 100 mM sodium citrate/phosphate pH 4.4, containing 2 mM H_2O_2 and those for the rest of the substrates in 100 mM potassium phosphate, pH 7.0, containing 2 mM H_2O_2 (benzyl and veratryl alcohols) or 1 mM H_2O_2 (NBD). H_2O_2 kinetic constants were estimated using benzyl alcohol as reducing substrate at the corresponding saturated conditions. $_{wt}$UPO1, UPO1 wild type expressed in *A. aegerita*; n*-UPO, native UPO1 fused to the evolved signal peptide for secretion in *S. cerevisiae*; PaDa-I mutant, ultimate variant of the whole evolution process *in S. cerevisiae* (containing the evolved signal peptide plus the evolved UPO1).

over 48 h and some hyperactivation (**Fig. 2.4C** and **D**). Under more extreme conditions (concentrations ranging from 60 to 90%), cosolvents exerted detrimental effects in the following order: DMSO > ethanol > methanol > acetone ~ ACN. Interestingly, PaDa-I was very stable, retaining ~25% and ~55% of its activity at concentrations of up to 90% (vol/vol) methanol and ethanol, respectively, when the stability of $_{wt}$UPO1 was negligible (**Fig. 2.4E** and **F**). The combined effects of hyperglycosylation together with the introduction of stabilizing mutations appear to underlie this resistance.

Mutation analysis. PaDa-I harbored 9 beneficial mutations (no silent mutations were introduced during evolution), 4 in the signal peptide and 5 in the mature protein. Five of the mutations (2 in the mature protein and 3 in the signal peptide) favored codon usage, which might support secretion (see **Table S2.1** in the supplemental material). The 4 mutations in the signal peptide were located in the hydrophobic core of the leader, and 3 of them (underlined) were nearly consecutive: F[12]Y-A[14]V-R[15]G-A[21]D. Substitutions at positions 12 and 21 enhanced the polarity of this region, while those at positions 14 and 15 had the opposite effect. Overall, these 4 mutations enhanced secretion by up to 27-fold, as seen in the n*-UPO1 fusion gene (**Fig. 2.3**). Subtle differences in the adjustment between the signal recognition particle (SRP) and the evolved signal peptide may benefit secretion, bearing in mind that the SRP strongly interacts with the hydrophobic region of the leader. It has been reported that SRP binding to the signal peptide pauses translation at different stages, depending on the nature of the leader (Nothwehr and Gordon, 1990). In our mutant, this arrest of translation could facilitate proper recognition by the signal peptidase before cleavage and translocation of the nascent UPO polypeptide to the endoplasmic reticulum (Romanos et al., 1992).

Mutations in the mature UPO1 were mapped onto the recently solved crystal structure of UPO1 (Piontek et al., 2013). UPO1 is mostly formed by helical substructures composed of 1 halide binding site, 1 Mg^{2+} binding site, and the heme-thiolate domain, with Arg189 and Glu196 forming the acid-base pair for compound I formation. The funnel-shaped access channel to the substrate binding pocket is 8.5 Å in diameter and mainly covered with aromatic residues.

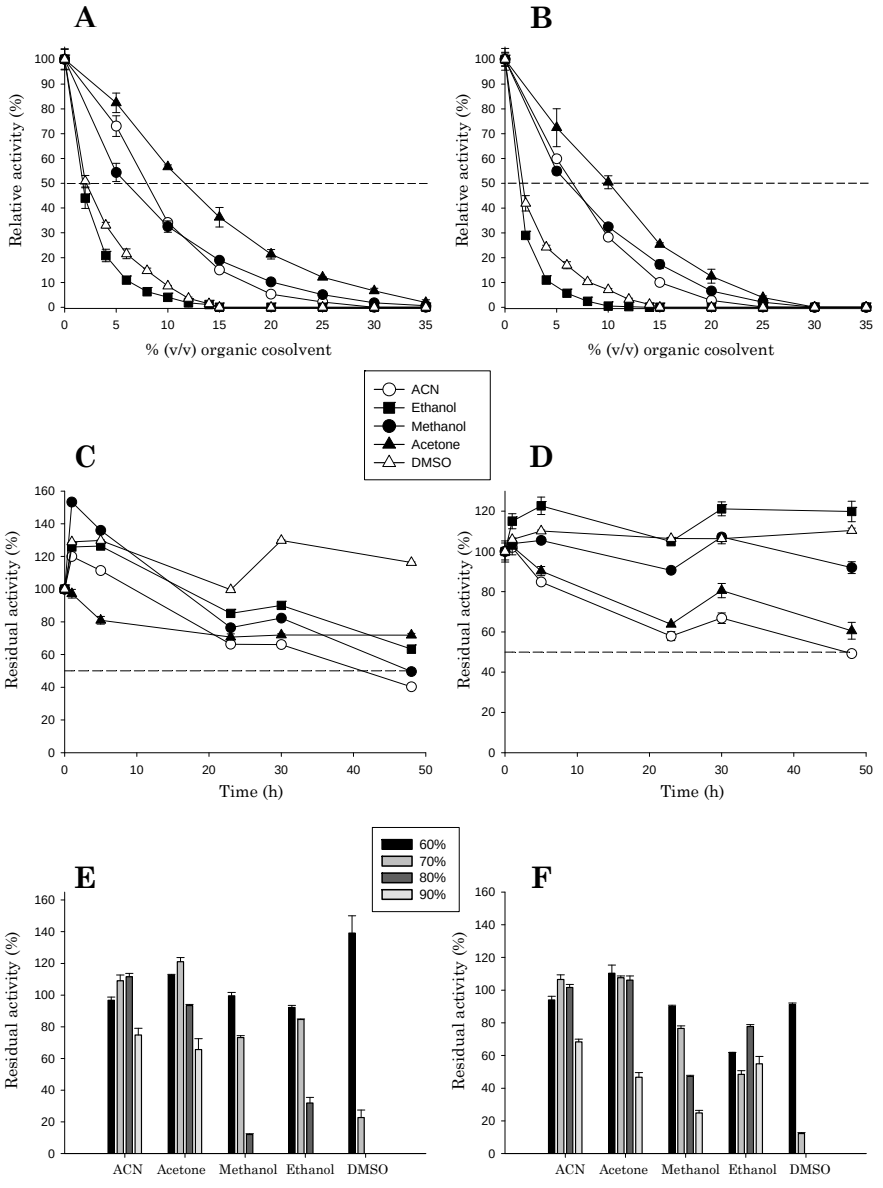

Fig. 2.4. Activity and stability in organic cosolvents. (A and B) The relative activities of $_{wt}$UPO1 (A) and the PaDa-I mutant (B) in organic cosolvents were assessed with 2 mM H_2O_2 and 0.3mM ABTS in 100mM sodium phosphate/citrate buffer (pH 4.4) containing the corresponding concentration of cosolvent. (C and D) The stabilities of $_{wt}$UPO1 (C) and the PaDa-I mutant (D) after incubation for 48 h in 50% organic cosolvents were assessed by incubating enzyme samples in 100 mM potassium phosphate buffer (pH 7.0) containing 50% (vol/vol) organic cosolvent in screw-cap vials. After 48 h, aliquots were removed and analyzed in an activity assay with 2mM H_2O_2 and 0.3m MABTS in 100mM sodium phosphate/citrate buffer (pH 4.4). (E and F) The stabilities of $_{wt}$UPO1 (E) and the PaDa-I mutant (F) at high concentrations of organic cosolvents were assessed after 5 h of incubation in increasing concentrations of cosolvents and incubating enzyme samples at 20°C in 100 mM potassium phosphate buffer (pH 7.0) containing increasing concentrations (vol/vol) of organic cosolvent (60 to 90%). After 5 h, aliquots were removed and analyzed in the activity assay, as described for panels C and D. Residual activities were expressed as percentages of the original activity at the corresponding concentration of organic cosolvent. The error bars indicate standard deviations.

This binding pocket is controlled by a Phe triad (Phe69, Phe121, and Phe199), which is essential for the orientation of (aromatic) substrates. All mutations were conservative in terms of polarity and charge, *i.e.*, nonpolar substitutions (V57A, L67F, V75I, I248V and F311L), leading to few apparent changes in terms of H bond or salt bridge formation/interruption (see **Table S2.2** in the supplemental material). In fact, mutations were located in hydrophobic environments, in some cases far from the catalytic site (see **Fig. S2.2** in the supplemental material). At this point, it is important to note that our aim was to improve total activity while conserving enzyme stability. Thus, we can only speculate as to whether a less rigid directed evolution approach would have unmasked other, less conservative substitutions at the cost of threatening protein stability (Bloom et al., 2006). The 41-fold enhancement in secretion induced by these mutations may be due to tighter folding during the earliest posttranslational stages, which ultimately favors protein stability and secretion. The V57A mutation lies in a helix at the surface of the protein next to the N terminus (**Fig. 2.5A** and **B**). According to our model, the replacement of Val57 with a less bulky residue may compress this region between adjacent prolines (at positions 5 and 6 of the N terminus) and thereby increase the protein's robustness. The L67F mutation is located in the vicinity of the catalytic pocket, very close to Phe69 of the Phe triad involved in binding aromatic substrates. This mutation may be partially responsible for the kinetic enhancements observed, since after substitution, the aromatic ring of Phe67 is oriented toward the active site (**Fig. 2.5C** and **D**). The V75I mutation is produced by the replacement of a hydrophobic residue with another, slightly larger hydrophobic residue, which may establish new hydrophobic contacts with surrounding residues, thereby favoring protein stability (**Fig. 2.5A** and **B**). Finally, the I248V and F311L mutations are positioned in the surroundings of the heme channel. The I248V mutation is produced by the replacement of Ile248 at the entrance of the channel to the heme cavity with a Val residue, which could favor the access of bulkier substrates (**Fig. 2.5E** and **F**). The F311L mutation is located in front of the heme channel, with Phe76 in between. The replacement of Phe with Leu enlarges the cavity, which may in turn have beneficial effects on kinetics (**Fig. 2.5A** and **B**).

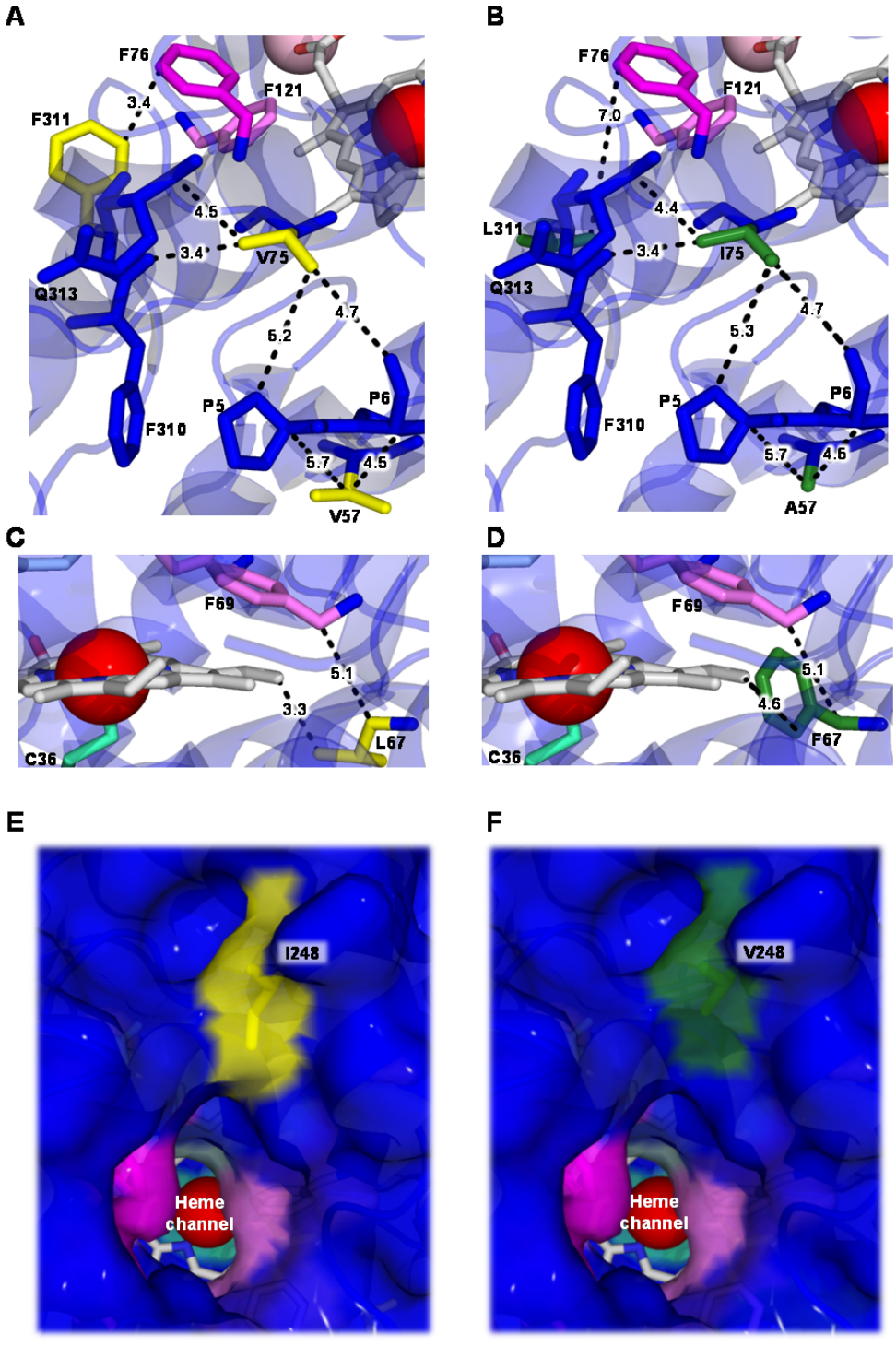

Fig. 2.5. Mutations in evolved UPO1. A molecular model using as the template the *A. aegerita* crystal structure (PDB code 2YOR) was prepared to map the mutations. Shown are details of the 5 mutations (green) in the PaDa-I mutant (B, D and F) compared with the corresponding residues (yellow) in the native UPO1 (A, C and E). The dashed lines indicate distances (in Å) from the surrounding residues. Phe residues delimiting the active site are highlighted in pink and the Cys36 axial ligand in light blue. The Fe^{3+} of heme is shown as a red sphere and the structural Mg^{2+} as a pink sphere (See also **Table S2.2** in the supplemental material and **Fig. S2.2** in the supplemental material).

2.4. CONCLUSIONS

Since its discovery 10 years ago, the potential use of UPO in applications ranging from chemical processes (including some relevant industrial transformations, such as alkane hydroxylation and olefin epoxidation) to the preparation of O- and N-dealkylated human drug metabolites, as well as bioremediation (polycyclic aromatic hydrocarbon [PAH] oxidation) and biosensor development, has been studied exhaustively (Aranda et al., 2010; Barkova et al., 2011; Gutierrez et al., 2011; Kinne et al., 2010; Kinne et al., 2009a; Kluge et al., 2012; Peng et al., 2010; Peter et al., 2013; Poraj-Kobielska et al., 2013; Poraj-Kobielska et al., 2011). For decades, regio- and enantioselective oxyfunctionalization has been a "forbidden territory" for most biocatalysts, except for P450 monooxygenases. However, unlike the latter, UPO is soluble and requires neither expensive cofactors (NAD[P]H) nor auxiliary flavoproteins. Despite these advantages, the lack of suitable directed evolution platforms with which to enhance UPO's catalytic properties has limited the exploitation of this versatile biocatalyst. The directed evolution process presented here describes for the first time an attractive pathway through which ad hoc UPO variants can be tailored for use in several industrial reactions, such as alkane hydroxylation and the transformation of benzene into phenol and naphthalene into naphthol (Karich et al., 2013; Kluge et al., 2009).

The evolved UPO1 variant from this study is very active and stable over a wide temperature range, as well as in the presence of a variety of cosolvent types. Easily secreted by yeast, this mutant and any future evolved variants could be translated to other expression systems for overproduction. Preliminary trials in the methylotrophic yeast *Pichia pastoris* indicate that the evolved enzyme is overproduced 5-fold thanks to the increased density in the host (unpublished data). Future goals for UPO engineering include the conversion of the enzyme into an enantioselective self-sufficient mono(per)oxygenase by quenching its peroxidative activity, the improvement of its activity in the presence of cosolvents, and the enhancement of its oxidative/operational stability in the presence of peroxides. The future combination of directed evolution (including neutral genetic drift) and rational/hybrid design should provide a

wealth of information that will help us to better understand the complex mechanism of action as UPO becomes an efficient oxyfunctionalization biocatalyst.

ACKNOWLEDGMENTS

This work was supported by European Commission Projects (Peroxicats-FP7-KBBE-2010-4-26537 and Indox-FP7-KBBE-2013-7-613549) and the National Project (Evofacel) (BIO2010-19697).

2.5 SUPPLEMENTAL EXPERIMENTAL PROCEDURES

Reagents and enzymes. ABTS (2,2'-azino-bis(3-ethylbenzothiazoline-6-sulfonic acid)), DMP (2,6-dimethoxyphenol), veratryl alcohol, benzyl alcohol, hemoglobin from bovine blood, *Taq* DNA polymerase for random mutagenesis and the *Saccharomyces cerevisiae* transformation kit were purchased from Sigma-Aldrich (Madrid, Spain). NBD (5-nitro-1,3-benzodioxole) was acquired from TCI America (USA). The cDNA of *upo1* (clone C1A-2) from *Agrocybe aegerita* was provided by Dr. Martin Hofrichter (Pecyna et al. 2009). The *Escherichia coli* XL2-Blue competent cells and the Genemorph II Random Mutagenesis kit (Mutazyme II) were obtained from Stratagene (La Jolla, CA, USA). The uracil independent and ampicillin resistance shuttle vector pJRoC30 was from the California Institute of Technology (CALTECH, USA). The protease deficient *S. cerevisiae* strain BJ5465 was obtained from LGCPromochem (Barcelona, Spain) and the pGAPZαA vector containing α-factor prepro-leader was from Invitrogen. The Zymoprep Yeast Plasmid Miniprep kit and Zymoclean Gel DNA Recovery kit were from Zymo Research (Orange, CA, USA). The NucleoSpin Plasmid kit was purchased from Macherey-Nagel (Germany) and the restriction enzymes BamHI, XhoI, EcoRI and NotI were from New England Biolabs (Hertfordshire, UK). The high-fidelity polymerase iProof was acquired from Bio-Rad (USA). The oligonucleotides were synthesized by Isogen Life Science (Barcelona, Spain). All chemicals were reagent-grade purity.

Culture media. Sterile minimal medium contained 100 mL 6.7% filtered yeast nitrogen base, 100 mL 19.2 g/L filtered yeast synthetic drop-out medium supplement without uracil, 100 mL filtered 20% raffinose, 700 mL *dd*H_2O and 1 mL 25 g/L filtered chloramphenicol. SC drop-out plates contained 100 mL 6.7% filtered yeast nitrogen base, 100 mL 19.2 g/L filtered yeast synthetic drop-out medium supplement without uracil, 20 g autoclaved bacto agar, 100 mL 20% filtered glucose, 1 mL 25 g/L filtered chloramphenicol and *dd*H_2O to 1,000 mL. Sterile expression medium contained 720 mL autoclaved YP, 67 mL 1 M filtered KH_2PO_4 pH 6.0 buffer, 111 mL 20% filtered galactose, 22 mL filtered $MgSO_4$ 0.1 M, 31.6 mL absolute ethanol, 1 mL 25 g/L filtered chloramphenicol and *dd*H_2O to 1,000 mL. From 1st to 3rd generation, 2.75 mL of filtered hemoglobin 20 g/L were added. For large scale cultures, the expression medium was supplemented with 300mg/L of filtered hemoglobin. YP medium contained 10 g yeast extract, 20 g peptone and *dd*H_2O to 650 mL. YPD solution contained 10 g yeast extract, 20 g peptone, 100 mL 20% sterile glucose, 1 mL 25 g/L chloramphenicol and *dd*H_2O to 1,000 mL. Luria-Bertani (LB) medium was prepared with 5 g yeast extract, 10 g peptone, 10 g NaCl, 100 mg ampicillin and *dd*H_2O to 1,000 mL.

Constructions of fusion genes. The gene used as starting point was the cDNA of *upo1* (clone C1A-2) from *A. aegerita*, cloned in the pSTBlue-1 plasmid. Four UPO1 constructs (α-UPO1, α*-UPO1, n*-UPO1 and n*-3F10) were engineered to switch signal peptides in the shuttle vector pJRoC30. The pSTBlue1-upo1 vector was used as a template to amplify the original *upo1* gene (containing native signal peptide *upo*1, n-upo1). PCR reactions were performed in a final volume of 50 µL containing 3 % DMSO, 0.5 µM psn-apo1 N, 0.5 µM apo1 C (2), 1 mM dNTPs (0.25 mM each), 0.02 U/µL of iProof DNA polymerase, and 0.2 ng/µL pSTBlue1-upo1. The thermal cycling programme was: 98ºC for 30 s (1 cycle), 98ºC 10 s, 52ºC for 25 s, 72ºC for 1 min (28 cycles) and 72ºC for 10 min (1 cycle). The n-upo1 product was digested with BamHI and NotI, and ligated by the T4 DNA ligase to the pJRoC30 plasmid linearized with the same restriction enzymes, giving rise to pJR-n-upo1.

pJR-α-upo1 and pJR-α*-upo1: both fusions were obtained by *in vivo* overlap extension (IVOE) (Alcalde, 2010). Firstly, the sequence corresponding to the mature protein of the *upo1* gene was amplified from pSTBlue1-upo1 with the primers apo-dir and aporev-RMLC. The α-factor prepro-leader and the evolved (α*) factor prepro-leader were amplified from templates pJR-α-PM1 and pJR- α*-OB1, respectively (Maté et al., 2010) using primers RMLN and alphaaporev. PCR reactions were performed in a final volume of 50 µL containing 3 % DMSO, 0.5 µM primer N, 0.5 µM primer C, 1 mM dNTPs (0.25 mM each), 0.02 U/µL of iProof DNA polymerase, and 0.2 ng/µL of template. The thermal cycling programme was: 98ºC for 30 s (1 cycle), 98ºC 10 s, 49ºC for 25 s (α-factors) / 48ºC for 25 s (*upo1*), 72ºC for 30 s (α-factors) /1 min (*upo1*) (28 cycles) and 72ºC for 10 min (1 cycle). The amplified PCR fragments were purified as detailed in Experimental Procedures (Chapter 2.2) and transformed in *S. cerevisiae* with the pJRoC30 linearized plasmid (BamHI and XhoI) for *in vivo* cloning.

n*-UPO1 and n*3F10: the evolved signal peptide (n*) was amplified from 2A12 mutant using primers RMLN and Morph psn apo1 rev. The UPO1 native mature sequence was amplified from n-upo1 whereas the mature 3F10 mutant was amplified from its own template. For the mature sequence amplifications the primers used were Morphpsnapo1dir and RMLC. PCR experiments were performed in a final volume of 50 µL containing 3 % DMSO, 0.5 µM primer N, 0.5 µM primer C, 1 mM dNTPs (0.25 mM each), 0.02 U/µL of iProof DNA polymerase, and 0.2 ng/µL of template. Two different thermal cycling programmes were employed: i) 98ºC for 30 s (1 cycle), 98ºC 10 s, 47ºC for 25 s, 72ºC for 10 s (28 cycles), 72ºC for 10 min (1 cycle) to amplify the n*; ii) 98ºC for 30 s (1 cycle), 98ºC 10 s, 52ºC for 25 s, 72ºC for 40 s (28 cycles), 72ºC for 10 min (1 cycle) to amplify the mature protein sequences. The amplified PCR fragments were purified as detailed in Experimental Procedures (Chapter 2.2). Cloning was performed *in vivo* by transforming the corresponding PCR fragments along with the linearized gene using a ratio signal sequence: mature protein: linearized plasmid of 2: 2: 1.

High-throughput dual-screening assay. Individual clones were picked and inoculated in sterile 96-well plates (Greiner Bio-One GmbH, Germany) containing 50 µL of minimal medium per well. In each plate, column number 6 was inoculated with the corresponding parent type, and one well (H1-control) was inoculated with untransformed *S. cerevisiae* cells. Plates were sealed to prevent evaporation and incubated at 30°C, 220 RPM and 80% relative humidity in a humidity shaker (Minitron- INFORS, Biogen, Spain). After 48 h, 160 µL of expression medium were added to each well, and the plates were incubated for 48 h. The plates (master plates) were centrifuged (Eppendorf 5810R centrifuge, Germany) for 10 min at 3,500 RPM at 4°C. 20 µL of supernatant were transferred from the master plate to two replica plates by a robot (Liquid Handler Quadra 96-320, Tomtec, Hamden, CT, USA). 180 µL of reaction mixture with ABTS or NBD were added to each replica plate. ABTS reaction mixture contained 100 mM sodium phosphate/citrate buffer at pH 3.5 (from 1st to 3rd generation) or at pH 4.4 (for generations 4 and 5), 0.3 mM ABTS and 1 mM H_2O_2 (from 1st to 3rd generation) or 2 mM H_2O_2 (for generations 4 and 5). Reaction mixture with NBD contained 100 mM potassium phosphate buffer pH 7.0, 1 mM NBD, 15% acetonitrile (ACN) and 1 mM H_2O_2. Plates were stirred briefly and the initial absorptions at 418 nm ($\varepsilon_{ABTS^{\bullet+}}$ = 36,000 M^{-1} cm^{-1}) and 425 nm (ε_{NBD} = 9,700 M^{-1} cm^{-1}) were recorded in the plate reader (SPECTRAMax Plus 384, Molecular Devices, Sunnyvale, CA). The plates were incubated at room temperature until a green (ABTS) or yellow (NBD) color developed, and the absorption was measured again. The values were normalized against the parental type in the corresponding plate. To rule out false positives, two rescreenings were carried out. Finally a third rescreening was performed in order to assess kinetic stability.

First rescreening. Aliquots of 5 µL of the best ~50 clones of the screening were transferred to new sterile 96-well plates with 50 µL of minimal medium per well. Columns 1 and 12 plus rows A and H were not used to prevent the appearance of false positives. After 24 h of incubation at 30°C and 220 RPM, 5 µL were transferred to the adjacent wells and further incubated for 24 h. Finally, 160 µL of expression medium were added and plates were incubated for 48 h. Accordingly, every single mutant was grown in 4 wells. Parental type was

subjected to the same procedure (lane D, wells 7-11). Plates were assessed using the same HTS protocol of the screening described above.

Second rescreening. An aliquot from the wells with the best ~10 clones of first rescreening was inoculated in 3 mL of YPD and incubated at 30°C and 220 RPM for 24 h. Plasmids from these cultures were extracted with Zymoprep Yeast Plasmid Miniprep kit. Due to the impurity of the zymoprep product and the low concentration of extracted DNA, the shuttle vectors were transformed into super-competent *E. coli* cells XL2-Blue and plated onto LB-amp plates. Single colonies were picked and used to inoculate 5 mL LB-amp media and were grown overnight at 37°C and 250 RPM. Plasmids were then extracted by NucleoSpin Plasmid kit and competent *S.cerevisiae* cells were transformed with these plasmids and with the parental type. Five colonies of every single mutant were picked and rescreened as described above.

Third rescreening: thermostability assay. A single colony from the *S. cerevisiae* clone containing the corresponding mutant gene was selected from an SC drop-out plate, inoculated in 3 mL of minimal medium and incubated for 48 h at 30ºC and 220 RPM (Minitron- INFORS, Biogen, Spain). An aliquot of the cells was removed and inoculated in a final volume of 5 mL of minimal medium (optical density, OD_{600} = 0.25). The cells were incubated for two complete growth phases (6 to 8 h). Thereafter, 9 ml of expression medium was inoculated with the 1 mL preculture in a 100 mL flask (OD_{600} = 0.1). After incubating for 72 h at 25ºC and 220 RPM (UPO activity was maximal; OD_{600} = 25-30), the cells were separated by centrifugation for 10 min at 4,500 RPM (4ºC) and the supernatant was double-filtered (using both glass membrane and a nitrocellulose membrane of 0.45 µm pore size). Appropriate dilutions of supernatants were prepared in such a way that aliquots of 20 µL gave rise to a linear response in kinetic mode. 50 µL supernatant were used for each point in a gradient scale ranging from 30 to 80°C. This gradient profile was achieved using a thermocycler (Mycycler, Bio-Rad, USA). After 10 min of incubation, samples were removed and chilled out on ice for 10 min. After that, samples of 20 µL were removed and incubated at room temperature for 5 min. Finally, samples were subjected to the same ABTS colorimetric assay described above for the screening (100 mM sodium

phosphate/citrate buffer pH 4.4, 0.3 mM ABTS and 2 mM H_2O_2). Thermostability values were calculated from the ratio between the residual activities incubated at different temperature points and the initial activity at room temperature. The T_{50} value was determined by the transition midpoint of the inactivation curve of the protein as a function of temperature, which in our case was defined as the temperature at which the enzyme lost 50% of its activity following an incubation of 10 minutes.

Production and purification. $_{wt}$UPO1 was produced and purified as described elsewhere (Ullrich et al., 2009). Production of recombinant UPO variants in *S. cerevisiae*: a single colony from the *S. cerevisiae* clone containing the parental or mutant *upo1* gene was picked from a SC drop-out plate, inoculated in minimal medium (20 mL) and incubated for 48 h at 30ºC and 220 RPM. An aliquot of cells was removed and used to inoculate minimal medium (100 mL) in a 500 mL (at a OD_{600} of 0.25). The cells completed two growth phases (6-8 h) and then expression medium (900 mL) was inoculated with the pre-culture (100 mL) (OD_{600} of 0.1). After incubating for 72 h at 25ºC and 220 RPM (maximal UPO activity; OD_{600} = 25-30), the cells were recovered by centrifugation at 4,500 RPM (4ºC) and the supernatant was double-filtered (using both glass membrane and a nitrocellulose membrane of 0.45 µm pore size). Purification of recombinant UPO variants: recombinant UPO purification was achieved by cationic exchange chromatography and anion exchange chromatography (ÄKTA purifier, GE Healthcare). The crude extract was first submitted to a fractional precipitation with ammonium sulfate (55%, first cut) and after removing the pellet, the supernatant was again precipitated with ammonium sulfate (85%, second cut). The final pellet was re-suspended in buffer sodium phosphate/citrate 10 mM at pH 4.3 (buffer A), and the sample was filtered and loaded on to a strong cation-exchange column (HiTrap SP FF GE Healthcare) pre-equilibrated with buffer A. The proteins were eluted with a linear gradient from 0 to 25% of buffer A within 55 mL of NaCl and from 25 to 100% within 5mL at a flow rate of 1 mL/min. Fractions with UPO activity *vs* ABTS were harvested, concentrated, dialyzed against buffer Bis Tris 10 mM at pH 6.5 (buffer B) and loaded onto a 10 µm high resolution anion-exchange Biosuite Q column (Waters) pre-equilibrated with buffer B. The proteins were

eluted with a linear gradient from 0 to 15% within 40 mL of NaCl and from 15 to 100% within 5mL at a flow rate of 1 mL/min. The fractions with UPO activity *vs* ABTS were pooled, dialyzed against buffer potassium phosphate 50 mM at pH 7.0 and stored at 4ºC. The Reinheitszahl values (Rz A_{418}/A_{280}) achieved were around 2. Throughout the purification protocol, the fractions were analysed by SDS/PAGE on 12% gels and the proteins were stained with colloidal Coomassie Blue (Bio-Rad). The concentrations of all crude protein extracts were determined using the Bio-Rad protein reagent and BSA as standard. One unit of ABTS-activity was defined as the amount of enzyme that oxidizes 1 µmol of ABTS per min in 100 mM sodium phosphate/citrate buffer pH 4.4 containing 2 mM H_2O_2.

MALDI-TOF-MS analysis and pI determination. The MALDI-TOF-MS experiments were performed on an Autoflex III MALDI-TOF-TOF instrument with a smartbeam laser (Bruker Daltonics). The spectra were acquired using a laser power just above the ionization threshold, and the samples were analysed in the positive-ion detection and delayed extraction linear mode. Typically, 1,000 laser shots were summed into a single mass spectrum. External calibration was performed, using the BSA from Bruker, covering the range 15,000-70,000 Da. Purified UPOs (8 µg each) were subjected to two-dimensional electrophoresis gel in order to determine the pI. These determinations were carried out at the Proteomic and Genomic Services from CIB (CSIC, Spain).

Steady-state kinetic constants. ABTS kinetic constants for UPO1 were estimated in 100 mM sodium phosphate/citrate pH 4.4 containing 2 mM H_2O_2; for the rest of the substrates in 100 mM potassium phosphate pH 7.0 containing 2 mM H_2O_2 (benzyl and veratryl alcohols) or 1 mM H_2O_2 (NBD). H_2O_2 kinetic constants were estimated using benzyl alcohol as reducing substrate at the corresponding saturated conditions. Reactions were performed by triplicate and substrates oxidations were followed by measuring the absorption at 418 nm for ABTS, ε_{418} = 36,000 M^{-1} cm^{-1}; DMP, ε_{469} = 27,500 M^{-1} cm^{-1}; NBD, $\varepsilon_{42\,5}$= 9,700 M^{-1} cm^{-1}; veratryl alcohol, ε_{310} = 9,300 M^{-1} cm^{-1} and benzyl alcohol, ε_{280} = 1,400 M^{-1} cm^{-1}. To calculate the values of K_m and k_{cat}, the average V_{max} was represented versus substrate concentration and fitted to a single rectangular

hyperbola function in SigmaPlot 10.0, where parameter a was equaled to k_{cat} and parameter b was equaled to K_m.

pH activity profiles. Appropriate dilutions of enzyme samples were prepared in such a way that aliquots of 20 µL gave rise to a linear response in kinetic mode. The optimum pH activity was determined using 100 mM sodium phosphate/citrate buffer at different pH values for ABTS (0.3 mM ABTS and 2 mM H_2O_2), NBD (1 mM NBD, 15% acetonitrile and 1 mM H_2O_2) and DMP (1 mM DMP and 2 mM H_2O_2). The activities were measured in triplicate mode and the relative activity (in percent) is based on the maximum activity for each variant in the assay.

DNA sequencing. Plasmid-containing variant *upo1* genes were sequenced by using an ABI 3730 DNA Analyzer/Applied Biosystems Automatic Sequencer from Secugen (Spain). The primers used were: RMLN; apo1secdir; apo1secrev and RMLC.

Protein modeling. The structure of wild type UPO1 (purified from *A. aegerita* culture) at a resolution of 2.1 Å (protein Data Bank Europe [PDB] accession number 2YOR) was used as a template to generate a molecular model where the new found mutations were mapped. The resulting model was analyzed with PyMOL Molecular Visualization System (http://pymol.org).

SUPPLEMENTAL FIGURES AND TABLES

A

PaDa-I mutant	Total activity (U/mL)	[Protein] (mg/mL)	Specific activity (U/mg)	Purification factor
Culture broth	3.4	0.14	25	1
55-85% $(NH_4)_2SO_4$	320	1.92	167	6.7
Cation exchange SP Sepharose	133	0.35	381	15.2
Anion exchange MonoQ	174	0.21	828	33.1

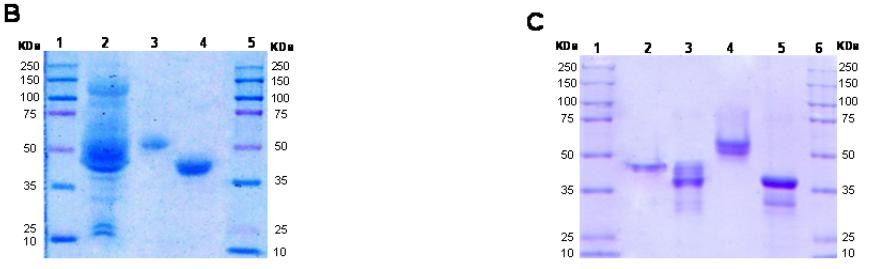

Fig. S2.1. Molecular mass and degrees of glycosylation of $_{wt}$UPO1 and the PaDa-I mutant. (**A**) Purification table for PaDa-I. (**B**) SDS-PAGE (PVDF membrane). Lanes: 1 and 5, protein markers; 2, PaDa-I culture broth; 3, purified PaDa-I; 4, purified $_{wt}$UPO1. (**C**) Deglycosylation/SDS-PAGE with PNGase F. Lanes: 1 and 6, protein markers; 2, $_{wt}$UPO1; 3, deglycosylated $_{wt}$UPO1; 4, PaDa-I mutant; 5, deglycosylated PaDa-I mutant. See also **Table 2.1**.

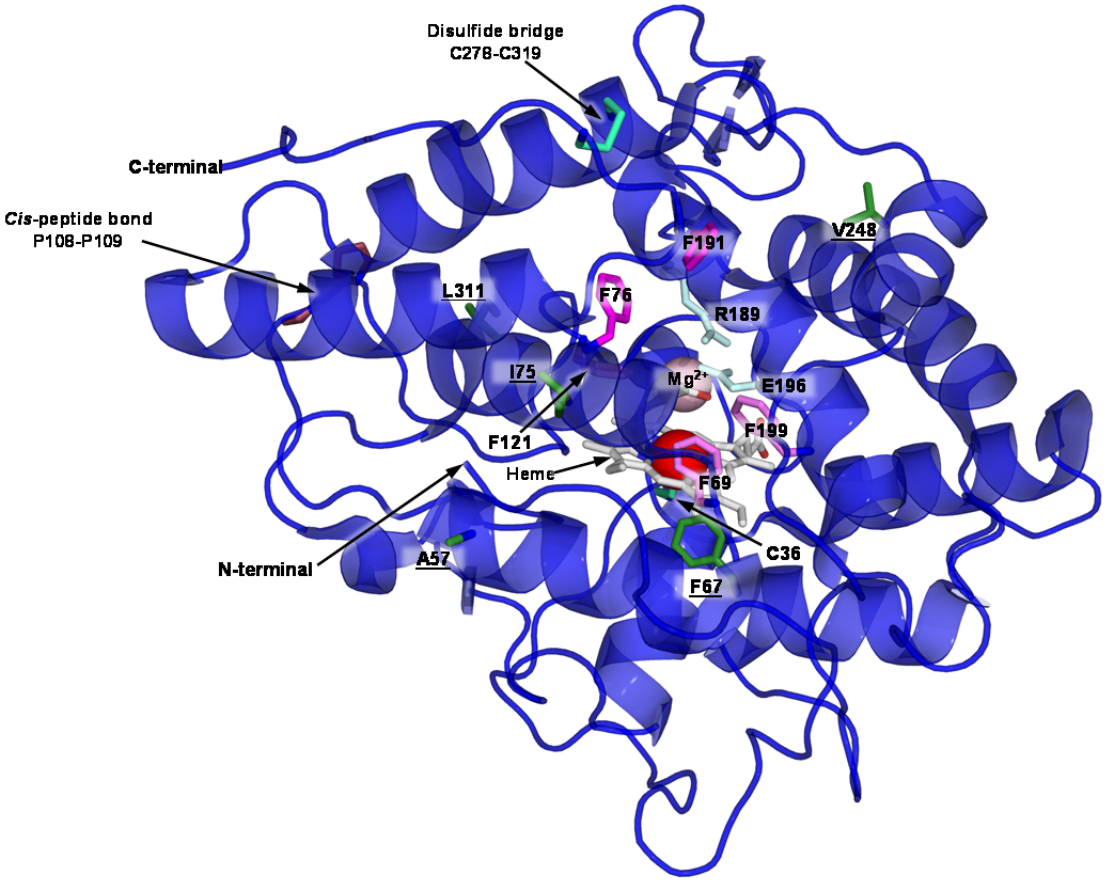

Fig. S2.2. Structural model of PaDa-I. Mutations V57A, L67F, V75I, I248V and F311L are shown in green and underlined. The heme group is shown in CPK coloring, Fe^{3+} in red and the structural Mg^{2+} in salmon. The model shows the Cys36 axial heme ligand, the disulfide bridge formed between Cys278 and Cys319, and the *cis*-peptide bond between P108 and P109. The catalytic pocket contains 5 Phe residues that mediate the adjustment of the substrates (Phe 69, Phe 76, Phe 121, Phe 191 and Phe 199: in pink) and two catalytic residues (R189 and E196: light cyan). See also **Fig. 2.5**, **Table S2.2.**

Table S2.1. Strategies and mutations obtained along the directed UPO1 evolution.

	Parental type	Generation of diversity	Mutational rate (mutations/1,000bp)	Library size (nº clones)	Total clones	Selected mutants	Improvements referred to n-UPO1 parent (ABTS screening)*	New mutations	Suggested recombination events	Codon usage (%) parental/mutant
1stG	n-UPO1	*Taq*/$MnCl_2$	Low (1-3)	522	2,088	1A11 (n-UPO1, Mutaz)	13 (pH 3.5; 1mM H_2O_2)	L67F ($_{199}$CTC/**T**TC$_{201}$); H251H ($_{751}$CA**T**/CA**C**$_{753}$)		4/47 60/40
		Mutazyme II	Medium (4-9)	522		3C2 (n-UPO1, Mutaz)	9 (pH 3.5; 1mM H_2O_2)	I248V ($_{742}$**A**TA/**G**TA$_{744}$); F311L ($_{931}$TT**C**/TT**A**$_{933}$)		20/16 47/27
	α-UPO1	*Taq*/$MnCl_2$	Low (1-3)	522						
		Mutazyme II	Medium (4-9)	522						
2ndG	1A11, 3C2	*Taq*/$MnCl_2$+ *in vivo* DNA shuffling	Low (1-3) (*Taq*)	1,044	2,088					
		Mutazyme II + *in vivo* DNA shuffling	Medium (4-9) (Mutazyme II)	1,044		12C12 (Mutaz)	57 (pH 3.5; 1mM H_2O_2)	A[21]D ($_{61}$G**C**C/G**A**C$_{63}$)	L67F(1A11) with I248V and F311L (3C2)	28/38
3rdG	12C12	IvAM	Low (1-3) and medium (4-9)	2,088	2,610	I13D3	70 (pH 3.5; 1mM H_2O_2)	V75I ($_{223}$**G**TC/**A**TC$_{225}$)		24/30
		MORPHING at the leader	Low (1-3 per segment, 129bp)	522		M6D4	84 (pH 3.5; 1mM H_2O_2)	R[15]G ($_{43}$**A**GG/**G**GG$_{45}$)		17/9
						M2B5	65 (pH 3.5; 1mM H_2O_2)	A[14]V ($_{40}$G**C**G/G**T**G$_{42}$)		8/15
						M5D2	87 (pH 3.5; 1mM H_2O_2)	F[12]Y ($_{34}$T**T**C/T**A**C$_{36}$)		47/50
						M4D8	63 (pH 3.5; 1mM H_2O_2)	L4S ($_{10}$T**T**A/T**C**A$_{12}$)		27/19
4thG	I13D3, M5D2 and M4D8	*Taq*/$MnCl_2$ + *in vivo* DNA shuffling	Low (1-3)	2,088	2,262	22A10	150 (pH 4.4; 2mM H_2O_2)	V57A ($_{169}$G**T**G/G**C**G$_{171}$)	F[12]Y and A[21]D (M5D2) with L67F, V75I, I248V, F311L (I13D3)	15/8
						3F10	31 (pH 4.4; 2mM H_2O_2)	T120P ($_{358}$**A**CC/**C**CC$_{360}$)		25/13
	M5D2, M2B5, M6D4 and I13D3	Site-directed mutagenesis (iProof)	0	174		2A12	132 (pH 4.4; 2mM H_2O_2)	F[12]Y; A[14]V; R[15]G		
5thG	2A12 and 22A10	Site-directed mutagenesis (iProof)	0	87	87	**PaDa-I**	162 (pH 4.4; 2mM H_2O_2)	V57A		

*From 1st to 3rd generation, screening was carried out in the presence of hemoglobin as external heme supply that produced a strong background due to interactions with ABTS assay. To reduce the unwanted signal, reaction mixture was set at lower [H_2O_2] (1 mM) and pH (3.5) than that of the optimum for UPO1. In generations 4 and 5, UPO1 mutants were produced without hemoglobin allowing the use of optimum reaction conditions (2mM H_2O_2, pH 4.4). See also **Fig. 2.1**.

Table S2.2. Mutations in mature PaDa-I variant. See also **Fig. 2.5**, **S2.2**.

Mutation	Secondary structure motif	Relative position	Distance to heme-Fe (Å)	H bonding surrounding residues	
				Before mutation	After mutation
V57A	Alpha helix	Surface (in front of N-terminal)	15.7	N61 (x2)	N61 (x2)
L67F	Alpha helix	Near heme domain (close to F69)	8.1	V63	V63
V75I	Alpha helix	Surface (close to F76)	12.1	N71, Y79	N71, Y79
I248V	Alpha helix	Surface (next to F191, access to the heme channel)	17.2	V244	V244
F311L	Alpha helix	Near C-terminal	14.0	N307, G314	N307, G314

Table S2.3. Primers used in the directed UPO evolution study.

Primer name	Sequence (5' → 3')
RMLN	CCTCTATACTTTAACGTCAAGG
RMLC	GCTTACATTCACGCCCTCCC
psn-apo1 N	*CGGGATCCATGAAATATTTTCCCCTGTTCCCAACCTTG
apo1 C (2)	*AAGGAAAAAAGCGGCCGCTCAATCTCGCCCGTATGGGAAG
apo-dir	GAGCCAGGATTACCTCCTG
apo-rev	**AACTAATTACATGATGCGGCCCTCTAGATGCATGCTCGATCAATCTCGCCCGTATGG
alpha-aporev	**GCAGAGCTATTCTCGAGAGGACCAGGAGGTAATCCTGGCTCGCTTCAGCCTCTCTTTCTC
Morph psn apo1 rev	CAGAGCTATTCTCGAGAGGA
Morph psn apo1 dir	GAGCCAGGATTACCTCCTGG
apo1secdir	GAAGGCGACGCCAGTATGACC
apo1secrev	GGTCATACTGGCGTCGCCTTC
PSN*R	GTCAGGAAAAGCAACGACCCCCACTGCGTAGACCAAGGTTGGGAACAGG
PSN*F	***CCTGTTCCCAACCTTGGTCTACGCAGTGGGGGTCGTTGCTTTTCCTGAC
2A12*REV	GAACCGCGTTTATTATTTGCGCCGGGGTTGCAACGCCATTTC
2A12*DIR	***GAAATGGCGTTGCAACCCCGGCGCAAATAATAAACGCGGTTC

*The target sequences for BamHI (psn-apo1 N) and NotI (apo1 C (2)) are underlined.
** Overhangs for *in vivo* cloning are underlined.
*** The changed nucleotides are underlined.

MUTAGENIC ORGANIZED RECOMBINATION PROCESS BY HOMOLOGOUS *IN VIVO* GROUPING (MORPHING) FOR DIRECTED ENZYME EVOLUTION

3

MUTAGENIC ORGANIZED RECOMBINATION PROCESS BY HOMOLOGOUS *IN VIVO* GROUPING (MORPHING) FOR DIRECTED ENZYME EVOLUTION

David Gonzalez-Perez, Patricia Molina-Espeja, Eva Garcia-Ruiz, Miguel Alcalde

PLoS ONE, 2014, Volume 9, Issue 3: e90919.

http://dx.doi.org/10.1371/journal.pone.0090919

Approaches that depend on directed evolution require reliable methods to generate DNA diversity so that mutant libraries can focus on specific target regions. We took advantage of the high frequency of homologous DNA recombination in Saccharomyces cerevisiae to develop a strategy for domain mutagenesis aimed at introducing and in vivo recombining random mutations in defined segments of DNA. Mutagenic Organized Recombination Process by Homologous IN vivo Grouping (MORPHING) is a one-pot random mutagenic method for short protein regions that harnesses the in vivo recombination apparatus of yeast. Using this approach, libraries can be prepared with different mutational loads in DNA segments of less than 30 amino acids so that they can be assembled into the remaining unaltered DNA regions in vivo with high-fidelity. As a proof of concept, we present two eukaryotic-ligninolytic enzyme case studies: i) the enhancement of the oxidative stability of a H_2O_2-sensitive versatile peroxidase by independent evolution of three distinct protein segments (Leu28-Gly57, Leu149-Ala174 and Ile199-Leu268) and ii) the heterologous functional expression of an unspecific peroxygenase by exclusive evolution of its native 43-residue signal sequence.

3.1. INTRODUCTION

In the past two decades directed evolution strategies have had a huge impact on protein engineering and synthetic biology (Bershtein and Tawfik, 2008; Bloom and Arnold, 2009; Cobb et al., 2012; Romero and Arnold, 2009; Tracewell and Arnold, 2009). Combining directed evolution with new computational and hybrid approaches has allowed researchers to design "smart" mutant libraries to address bottlenecks in enzyme functionality, helping to maintain the balance between activity and stability, or even creating novel catalytic activities (Lutz, 2010; Wong et al., 2007). The use of non-adaptive evolution involving neutral genetic drift has been added to this arsenal of techniques to create polymorphic populations with the aim of enhancing protein robustness and substrate promiscuity (Gupta and Tawfik, 2008; Peisajovich and Tawfik, 2007; Bloom et al., 2007a; Bloom et al., 2007b).

Although the majority of the vast protein sequence space is probably non-functional, with 20^n possible permutations (if we exclude the introduction of non-natural amino acids), it is still far from being fully explored (Voloshchuk and Montclare, 2010). Advances in the field involve the use of ultrahigh-throughput screening methods and the construction of focused mutant libraries to restrict the sequence space (Dalby, 2011; Goldsmith and Tawfik, 2013). Most of the available methods used to create targeted libraries are based on computational studies that identify a limited number of positions for saturation mutagenesis, combinatorial and/or iterative (Shivange et al., 2009; Reetz et al., 2005; Reetz and Carballeira, 2007). A more recent approach is to introduce ancestral consensum mutations that have been identified by phylogenetic analysis and ancestral inference in extant enzymes (Alcolombri et al., 2011). Despite the wide array of focused evolution methods, there remains a need for consistent domain mutagenesis/recombination strategies targeting specific protein subsets for random mutagenesis and recombination, while conserving the remaining protein regions. Although this kind of focused-indiscriminate approach has received little attention in the literature (Hidalgo et al., 2008; Herman and Tawfik 2007), it can effectively unmask structural determinants of

specific enzymatic attributes, which can then be optimized using the aforementioned methods.

Escherichia coli is by far the most common host in directed evolution experiments of prokaryotic proteins. However, broad differences with eukaryotic cells (missing chaperones, different codon usage, lack of posttranslational modifications) preclude the use of this bacteria to engineer eukaryotic enzymes which mostly end up in misfolding and inclusion bodies formation. Alternatively, *Saccharomyces cerevisiae* is the model organism of choice for *in vitro* evolution of eukaryotic genes, permitting the development of comprehensive synthetic biology and metabolic engineering studies, particularly when dealing with the production of fuels and chemicals (Hong and Nielsen, 2012; Krivoruchko et al., 2011; Nevoigt, 2008; Da Silva and Srikrishnan, 2012). In recent years, a range of methods have been described in this yeast to construct mutant libraries with different mutational bias, to integrate multiple DNA fragments for creating combinatorial libraries or to assemble expression cassettes that generate fully autonomous artificial pathways (Alcalde, 2010; Ostrov et al., 2013; Zumarraga et al., 2008; Shao et al., 2009). The high frequency of homologous DNA recombination in *S. cerevisiae* permits to simply shuffle foreign genes creating multiple crossover events, to repair linearized vectors for *in vivo* cloning or to promote the molecular evolution of multigenic phenotypes (Pompon and Nicolas, 1989; Wingler and Cornish, 2011; Gonzalez-Perez et al., 2012; Wang et al., 2012a; Finney-Manchester and Maheshri, 2013).

Here, we present a simple, rapid and reliable random domain mutagenesis/recombination method for short fragments that is based on the physiological properties of *S. cerevisiae*. Mutagenic Organized Recombination Process by Homologous *IN vivo* Grouping (MORPHING) randomly introduces mutations in specific protein segments using overlapping areas to favor *in vivo* splicing and recombination in yeast. The versatility of this method was evaluated in two case studies of ligninolytic oxidoreductases. First, we used MORPHING to enhance the oxidative stability of a versatile peroxidase (VP) from the basidiomycete *Pleurotus eryngii*. VP has three different catalytic sites for the oxidation of low-, medium- and high-redox potential compounds, which

makes the enzyme extremely fragile in the presence of catalytic concentrations of H_2O_2 (Ruiz-Dueñas et al., 2009). The second enzyme studied was the unspecific peroxygenase (UPO) from the edible mushroom *Agrocybe aegerita*, a heme-thiolate peroxidase with special catalytic capacity that includes oxygen transfer reactions (Hofrichter and Ullrich, 2006). Despite its importance in organic synthesis, heterologous functional expression and directed evolution of this enzyme has not yet been reported. We used MORPHING to exclusively target the native UPO signal peptide for evolution towards functional expression in yeast.

3.2. MATERIALS AND METHODS

VP from *Pleurotus eryngii* (the R4 mutant) was used as the parental type in the construction of the library. This R4 mutant was engineered for secretion by 4 rounds of directed evolution, resulting in expression levels of 22 mg/L (Garcia-Ruiz et al., 2012). The UPO1 variant (12C12) was generated by directed evolution in a previous study to functionally express the *upo1* gene (clone C1A-2) from *A. aegerita* (Pecyna et al., 2009) in *S. cerevisiae* (Molina-Espeja et al., 2014). ABTS (2,2'-azino-bis(3-ethylbenzothiazoline-6-sulfonic acid)), *Taq* polymerase, and the *S. cerevisiae* transformation kit were purchased from Sigma-Aldrich (Madrid, Spain). The iProof High-Fidelity DNA polymerase was purchased from Bio-Rad (USA). The Zymoprep Yeast Plasmid Miniprep Kit and Zymoclean Gel DNA Recovery Kit were obtained from Zymo Research (Orange, CA, USA), while NBD (5-nitro-1,3-benzodioxole) was purchased from TCI America (USA). The *Escherichia coli* XL2-Blue competent cells and the GeneMorph II Kit (Mutazyme II polymerase) were from Stratagene (La Jolla, CA, USA), and the uracil independent and ampicillin resistance pJRoC30 shuttle vector was obtained from the California Institute of Technology (CALTECH, USA). The protease-deficient *S. cerevisiae* strain BJ5465 (*a ura3-52 trp1 leu2Δ1 his3Δ200 pep4::HIS3 prb1Δ1.6R can1 GAL*) was obtained from LGCPromochem (Barcelona, Spain), the NucleoSpin Plasmid kit was purchased from Macherey-Nagel (Germany) and the restriction enzymes BamHI and XhoI from New England Biolabs (Hertfordshire, UK). All chemicals were of reagent-grade purity.

Culture media. Minimal medium (SC) contained 0.67% (w/v) sterile yeast nitrogen base, 1.92 g/L sterile yeast synthetic drop-out medium supplement without uracil, 2% (w/v) sterile D-raffinose and 25 mg/mL chloramphenicol. YP medium contained 10 g yeast extract, 20 g peptone and *dd*H_2O to 650 mL. Flask expression medium contained 720 mL YP, 67 mL 1 M KH_2PO_4 buffer (pH 6.0), 111 mL 20% (w/v) D-galactose, 25 g/L ethanol, 500 or 300 mg/L bovine hemoglobin (for VP and UPO, respectively), 1 mM $CaCl_2$ for VP or 2 mM $MgSO_4$ for UPO, 1 mL 25 g/L chloramphenicol and *dd*H_2O to 1,000 mL. Microplate expression medium contained 720 mL YP, 67 mL 1 M KH_2PO_4 buffer (pH 6.0), 111 mL 20% (w/v) D-galactose, 100 or 50 mg/L bovine hemoglobin (for VP and UPO, respectively), 2 mM $MgSO_4$ for UPO, 1 ml 25 g/L chloramphenicol and *dd*H_2O to 1,000 mL. YPD solution contained 1% (w/v) yeast extract, 2% (w/v) peptone, 2% (w/v) sterile D-glucose and 25 mg/mL chloramphenicol. SC drop-out plates contained 0.67% (w/v) sterile yeast nitrogen base, 1.92 g/L (w/v) sterile yeast synthetic drop-out medium supplement without uracil, 2% (w/v) bacto agar, 2% (w/ v) sterile D-glucose and 25 mg/mL chloramphenicol. Luria-Bertani (LB) medium was prepared with 1% (w/v) peptone, 0.5% (w/v) yeast extract, 1% (w/v) NaCl and 100 mg/mL ampicillin.

MORPHING protocol. All the PCR products generated were cleaned, concentrated and loaded onto a low-melting-point preparative agarose gel and purified using the Zymoclean Gel DNA Recovery Kit (Zymo Research). The PCR products were cloned by replacing the corresponding parental gene in pJRoC30. To remove the parental gene, the plasmid was linearized with BamHI and XhoI. The pJRoC30-R4 variant was used as a template to construct MORPHING libraries of VP, while the pJRoC30-12C12 was used as the template to construct MORPHING libraries of UPO signal peptide.

For VP MORPHING, the whole gene was fragmented into three different segments in individual PCR reactions. Each segment contained homologous overhangs of ~50 bp that overlapped one another to promote *in vivo* cloning in yeast. The targeted regions were subjected to random mutagenesis while the remaining segments were amplified by high-fidelity polymerases (**Fig. S3.1**). The distal His environment region was selected to tune mutational loads. Small

mutant libraries of around 500 clones were screened to optimize the mutagenic conditions. A similar protocol was followed for UPO MORPHING but in this case the UPO gene was split into two segments, one containing the signal peptide and the other the mature protein.

1. VP MORPHING. i) Mutagenic PCR of targeted regions: reaction mixtures were prepared in a final volume of 50 µL containing the following: DNA template (0.1 ng/µL or 0.92 ng/µL), 90 nM Forward primer, 90 nM Reverse primer (different forward (F) and reverse (R) primers were used to amplify each region; **Table S3.1**, **Fig. S3.1**), 0.3 mM dNTPs (0.075 mM each), 3% (v/v) dimethylsulfoxide (DMSO), 1.5 mM $MgCl_2$, increasing concentrations of $MnCl_2$ (0.01, 0.05, 0.1, 0.2, 0.4 mM) and 0.05 U/µL *Taq* polymerase. Error-prone PCRs were carried out on a gradient thermocycler (Mycycler, BioRad, USA) using the following conditions: 95°C for 2 min (1 cycle); 94°C for 45 s, 56°C for 45 s, 74°C for 45 s (28 cycles); and 74°C for 10 min (1 cycle). For the proximal His environment and Met environment, the final DNA template concentration was 0.92 ng/µL and the $MnCl_2$ concentration was set at 0.2 mM and 0.01 mM, independently for both targeted regions. **ii)** High-fidelity PCR in non-mutated segments: reaction mixtures were prepared in a final volume of 50 µL containing: DNA template (0.2 ng/µL), 0.5 mM Forward primer, 0.5 mM Reverse, (different forward (F) and reverse (R) primers were used to amplify each region; **Table S3.1**, **Fig. S3.1**), 0.8 mM dNTPs (0.2 mM each), 3% (v/v) dimethylsulfoxide (DMSO) and 0.02 U/µL iProof polymerase. High-fidelity PCRs were performed on a gradient thermocycler using the following conditions: 98°C for 30 s (1 cycle); 98°C for 10 s, 45 or 50°C for 30 s, 72°C for 1 min (28 cycles); and 72°C for 10 min (1 cycle). **iii)** Reassembly of the whole gene: the whole gene was reassembled *in vivo* and recombined by transformation into *S. cerevisiae* cells using the Yeast Transformation Kit. The DNA transformation mixture contained the linearized plasmid (200 ng) mixed with the targeted region, as well as the segments upstream and downstream of those regions (400 ng per segment). Transformed cells were plated on SC drop-out plates and incubated for 3 days at 30°C. Subsequently, the mutant libraries were subjected to the HTP-protocol for oxidative stability, as described below.

2. UPO MORPHING. i) Mutagenic PCR in signal peptide: reaction mixtures were prepared in a final volume of 50 µL containing the following: DNA template (0.92 ng/µL), 90 nM RMLN F primer, 90 nM MORPH SP R primer (**Table S3.1**), 0.3 mM dNTPs (0.075 mM each), 3% (v/v) dimethylsulfoxide (DMSO), 1.5 mM $MgCl_2$, 0.1 mM $MnCl_2$ and 0.05 U/µL *Taq* polymerase. Error-prone PCR was carried out on a gradient thermocycler using the following parameters: 95°C for 2 min (1 cycle); 94°C for 45 s, 50°C for 45 s, 74°C for 30 s (28 cycles); and 74°C for 10 min (1 cycle). **ii)** High-fidelity PCR of non-mutated segment: reaction mixtures were prepared in a final volume of 50 µL containing DNA template (0.2 ng/µL), 0.5 mM MORPH SP D primer, 0.5 mM RMLC R primer (**Table S3.1**), 1 mM dNTPs (0.25 mM each), 3% (v/v) dimethylsulfoxide (DMSO) and 0.02 U/µL iProof polymerase. High-fidelity PCR was carried out on the gradient thermocycler using the following conditions: 98°C for 30 s (1 cycle); 98°C for 10 s, 55°C for 25 s, 72°C for 45 s (28 cycles); and 72°C for 10 min (1 cycle). **iii)** Reassembly of the whole gene: the whole gene was reassembled *in vivo* and recombined by transformation into *S. cerevisiae* cells using the Yeast Transformation Kit. The DNA transformation mixture contained the linearized plasmid (100 ng) mixed with the targeted region, as well as the mature protein (200 ng per segment). Transformed cells were plated on SC drop-out plates and incubated for 3 days at 30°C. Subsequently, the mutant libraries were subjected to the HTP-protocol to assess activity as described below.

Directed evolution of whole UPO gene. The whole UPO gene including its signal peptide was subjected to one round of directed evolution by *In vivo* Assembly of Mutant libraries (IvAM) (Zumarraga et al., 2008).

1. Mutagenic PCR with *Taq* polymerase. Reaction mixtures were prepared in a final volume of 50 µL containing: DNA template (0.1 ng/µL), 90 nM RMLN F primer, 90 nM RMLC R primer (**Table S3.1**), 0.3 mM dNTPs (0.075 mM each), 3% (v/v) dimethylsulfoxide (DMSO), 1.5 mM $MgCl_2$, 0.01 mM $MnCl_2$ and 0.05 U/µL *Taq* polymerase. Error-prone PCR was carried out under the following conditions: 95°C for 2 min (1 cycle); 94°C for 45 s, 53°C for 45 s, 74°C for 3 min (28 cycles); and 74°C for 10 min (1 cycle).

2. Mutagenic PCR with Mutazyme II. Reaction mixtures were prepared in a final volume of 50 µL containing: DNA template (56 ng/µL), 0.37 mM RMLN F primer, 0.37 mM RMLC R primer (**Table S3.1**), 0.8 mM dNTPs (0.2 mM each), 3% (v/v) dimethylsulfoxide (DMSO) and 0.05 U/µL Mutazyme II. Error-prone PCR was carried out using the following parameters: 95°C for 2 min (1 cycle); 94°C for 45 s, 53°C for 45 s, 74°C for 3 min (28 cycles); and 74°C for 10 min (1 cycle).

3. *In vivo* recombination of mutant libraries in *S. cerevisiae*. *Taq* polymerase library and Mutazyme library were added in equimolar concentrations (200 ng each) to the linearized vector (100 ng). Transformed cells were plated on SC drop-out plates and incubated for 3 days at 30°C. Thereafter, the mutant libraries were subjected to the HTP-protocol to assay activity as described below.

Construction of the evolved signal peptide F12Y-A14V-R15G-A21D by site-directed mutagenesis and fusion to the native *upo* gene.

1. Construction of the evolved signal peptide (SP*) by site-directed mutagenesis. Reaction mixture was prepared in a final volume of 50 µL containing: DNA template (0.2 ng/µL), 0.5 mM Forward primer RMLN F, 0.5 mM Reverse primer SP* R (**Table S3.1**), 1 mM dNTPs (0.25 mM each), 3% (v/v) dimethylsulfoxide (DMSO) and 0.02 U/µL iProof polymerase. High-fidelity PCR1 was carried out on the gradient thermocycler under the following conditions: 98°C for 30 s (1 cycle); 98°C for 10 s, 47°C for 25 s, 72°C for 15 s (28 cycles); and 72°C for 10 min (1 cycle).

2. Construction of fusion gene (evolved signal peptide plus the native *upo*) by *In Vivo* Overlap Extension (IVOE). The native *upo* was amplified by high-fidelity PCR in a final volume of 50 µL containing: DNA template (0.2 ng/µL), 0.5 mM Forward primer SP* F, 0.5 mM Reverse primer RMLC R (**Table S3.1**), 1 mM dNTPs (0.25 mM each), 3% (v/v) dimethylsulfoxide (DMSO) and 0.02 U/µL iProof polymerase. High-fidelity PCR was carried out on the gradient thermocycler under the following conditions: 98°C for 30 s (1 cycle); 98°C for 10 s, 52°C for 25 s, 72°C for 40 s (28 cycles); and 72°C for 15 min (1

cycle). PCR fragments corresponding to the SP* and the native *upo* (200 ng each) were recombined together with the linearized vector (100 ng) by IVOE (Alcalde, 2010).

Combinatorial saturation mutagenesis experiments in VP. Reaction mixtures were prepared in a final volume of 50 µL containing: DNA template (0.2 ng/µL), 0.2 mM Forward primer, 0.2 mM Reverse primer (RMLN F/MET SAT R primers and MET SAT F/RMLC R for first PCR and second PCR, respectively, (**Table S3.1**)), 0.8 mM dNTPs (0.2 mM each), 3% (v/v) dimethylsulfoxide (DMSO) and 0.02 U/µL iProof polymerase. High-fidelity PCRs were carried out on the gradient thermocycler under the following conditions: 98°C for 30 s (1 cycle); 98°C for 10 s, 53°C for 30 s, 72°C for 1 min (28 cycles); and 72°C for 10 min (1 cycle). The whole gene was reassembled *in vivo* and recombined by transformation into *S. cerevisiae* cells using the Yeast Transformation Kit. The DNA transformation mixture was composed of the linearized plasmid (200 ng) mixed with the mutated fragments (400 ng per fragment). Transformed cells were plated on SC drop-out plates and incubated for 3 days at 30°C. Thereafter, the mutant libraries were subjected to the HTP-protocol described below.

High-throughput oxidative stability assay of VP. Individual clones were selected and cultured in sterile 96-well plates (Greiner Bio-One GmbH, Germany) containing 50 µL per well of SC minimal medium. In each plate, column number 6 was inoculated with the parental R4 mutant as an internal standard and well-H1 (containing minimal medium supplemented with uracil) was inoculated with untransformed *S. cerevisiae* as a negative control. Plates were wrapped in parafilm to prevent evaporation and incubated at 30°C, 225 RPM and 80% relative humidity in a humidity shaker (Minitron-INFORS, Biogen, Spain). After 48 h, 160 µL of expression medium was added to each well and the plates were incubated for a further 24 h. The plates (master plates) were centrifuged for 15 min at 3,000 RPM and 4°C (Eppendorf 5810R centrifuge, Germany) and the master plates were duplicated with the help of a robot (Liquid Handler Quadra 96- 320, Tomtec, Hamden, CT, USA) by transferring 20 µL of supernatant into two replica plates: the initial activity plate (IA plate) and the

residual activity plate (RA plate). Next, 180 µL of stability buffer (20 mM sodium tartrate buffer, pH 5.0: Buffer A) was added to the IA plates and 180 µL of incubation solution (Buffer A containing 0.3 mM H_2O_2) was added to the RA plates using a Multidrop robot (Multidrop Combi, ThermoFischer Scientific, Vantaa, Finland). Both plates were briefly stirred and incubated at room temperature for 60 min, such that the activity assessed in the RA plates was reduced by 2/3^{rds} with respect to the initial activity of the parental type. The supernatants (20 µL) were transferred from both RA and IA plates to new plates to measure the residual and initial activity values by adding ABTS in specific buffers: 180 µL of 100 mM sodium tartrate buffer (pH 3.5) containing 2 mM ABTS and 0.1 mM H_2O_2 to estimate of residual activity; and 180 µL of 100 mM sodium tartrate buffer (pH 3.5) containing 2 mM ABTS and 0.13 mM H_2O_2 to estimate the initial activity. The plates were stirred briefly and the absorption at 418 nm (ε_{ABTS} = 36,000 M^{-1} cm^{-1}) was recorded (end-point mode, t_0) on a plate reader (SPECTRAMax Plus 384, Molecular Devices, Sunnyvale, CA). The plates were then incubated at room temperature until a green color developed and the absorption was measured again (t_1). The relative activities were calculated from the difference between the absorption value after incubation and that of the initial measurement normalized to the parental type in the corresponding plate (Δt_1-t_0). Oxidative stability values were calculated as the ratio between residual activity and the initial activity values (RA/IA). To rule out false positives, two consecutive rescreenings were carried out. Moreover, a third rescreening was performed to determine the increase in the apparent half-life of each selected variant ($t_{1/2}$ H_2O_2, expressed in minutes) relative to the parental R4 in different molar ratios [H_2O_2]/[VP in supernatants].

First rescreening: aliquots of 5 µL of the best clones were removed from the master plates and used to inoculate 50 µL of minimal medium in new 96-well plates. Columns 1 and 12, and rows A and H, were not used to prevent the appearance of false positives. After incubating for 24 h at 30°C, 225 RPM, and 80% relative humidity, 5 µL was transferred to the adjacent wells and incubated for a further 24 h. Finally, 160 µL of expression medium was added and the plates were incubated for another 24 h. Accordingly, each mutant was grown in 4 wells. The parental types were subjected to the same procedure (row D, wells

7-11) and the plates were assessed using the same protocols as those used for the screening described above.

Second rescreening: an aliquot from the wells with the best clones in the first rescreening was inoculated in 3 mL of YPD and incubated at 30°C and 225 RPM for 24 h, recovering the plasmids from these cultures (Zymoprep Yeast Plasmid Miniprep Kit). As the product of the zymoprep was very impure and the concentration of DNA extracted very low, the zymoprep mixtures containing shuttle vectors were transformed into super-competent *E. coli* cells (XL2-Blue, Stratagene) and plated on LB/amp plates. Single colonies were picked and used to inoculate 5 mL LB/amp media, and they were grown overnight at 37°C and 225 RPM. The plasmids were then extracted (NucleoSpin Plasmid kit, Macherey-Nagel, Germany) and *S. cerevisiae* was transformed with plasmids from the best mutants as well as with the parental type. Five colonies for each mutant were selected and rescreened as described above.

Third rescreening (determination of $t_{1/2}$ H_2O_2): a single colony from the *S. cerevisiae* clone containing the parental R4, the new mutants and untransformed yeast were picked from a SC drop-out plate (SC supplemented with uracil for untransformed cells), used to inoculate 5 mL of minimal medium, and incubated for 48 h at 30°C and 225 RPM (Minitron-INFORS, Biogen, Spain). An aliquot of cells was removed and used to inoculate a final volume of 5 mL of minimal medium in a 50 mL falcon tube (optical density, OD_{600} = 0.3), and they were incubated until two growth phases had been completed (6-8 h, OD_{600} = 1). Thereafter, 9 mL of expression medium (500 mg/L bovine hemoglobin) was inoculated with 1 mL of this preculture in a 100 mL flask (OD_{600} = 0.1). After incubating for ~48 h at 30°C and 225 RPM (maximal VP activity; OD_{600} = 25-30), the cells were separated by centrifugation for 15 min at 3,000 RPM and 4°C (Eppendorf 5810R Centrifuge, Germany) and the supernatants were collected and stored at 4 °C. The protein concentration was estimated from supernatants using the Bio-Rad protein assay kit, (Bio-Rad, USA). VP apparent concentration was calculated as the difference between the total protein content of yeast expressing VP and that in its absence (from non-transformed yeast cells -lacking VP gene-). The parental R4 and the mutants (final concentration 0.1 mM) were

incubated at room temperature in 20 mM sodium tartrate buffer (pH 5.0) in the presence or absence of different concentrations of H_2O_2 (0.3, 0.6 mM). Aliquots (20 μL) were removed at different times and the residual/initial activities were measured in a final volume of 200 μL containing 100 mM sodium tartrate buffer (pH 3.5), 2 mM ABTS and 0.13 mM or 0.16 mM H_2O_2 (for samples incubated in the presence of 0.3 and 0.6 mM H_2O_2, respectively). The residual activity was determined relative to the corresponding mutant incubated in the absence of H_2O_2, taking into account the final concentration of H_2O_2 in each activity assay. Each point represents the mean of three independent experiments performed in triplicate. Increment in apparent half-lives ($\Delta t_{1/2}$ *vs* H_2O_2) were calculated for each mutant at given molar ratio VP (supernatants) : H_2O_2.

High-throughput screening assay for UPO secretion. Individual clones were selected and inoculated in sterile 96-well plates (Greiner Bio-One GmbH, Germany) containing 50 μL per well of SC minimal medium. In each plate, column number 6 was inoculated with the corresponding parental type, and one well (H1-control) was inoculated with untransformed *S. cerevisiae* cells in minimal medium containing uracil. The plates were wrapped in parafilm to prevent evaporation and incubated at 30°C, 225 RPM and 80% relative humidity in a humidity shaker. After 48 h, 160 μL of expression medium was added to each well and the plates were incubated for 48 h. The plates (master plates) were centrifuged (Eppendorf 5810R Centrifuge, Germany) for 15 min at 3,000 RPM and 4°C, and the supernatants (20 μL) were transferred from the master plate to two replica plates by a robot (Liquid Handler Quadra 96-320, Tomtec, Hamden, CT, USA), adding the reaction mixture (180 μL) together with ABTS or NBD to each replica plate. Both colorimetric assays were used for properly detecting secretion levels improvements regardless of the substrate used (ABTS is typically used for assessing peroxidative activity whereas NBD for peroxygenase activity). The reaction mixture with ABTS contained 100 mM sodium citrate/phosphate buffer (pH 4.4), 0.3 mM ABTS and 2 mM H_2O_2, while the reaction mixture with NBD contained 100 mM potassium phosphate buffer (pH 7.0), 1 mM NBD, 15% (v/v) acetonitrile and 1 mM H_2O_2. Plates were stirred briefly and the initial absorptions at 418 nm (ε_{ABTS} = 36,000 M^{-1} cm^{-1}) and 425 nm (ε_{NBD} = 9,700 M^{-1} cm^{-1}) were recorded on the plate reader (SPECTRAMax

Plus 384, Molecular Devices, Sunnyvale, CA). The plates were then incubated at room temperature until a green (ABTS) or yellow (NBD) color developed, and the absorption was measured again. The values were normalized against the parental type in the corresponding plate. To rule out false positives, two rescreenings were carried out as described above for VP.

Thermostability assay (T_{50}). Appropriate dilutions of the supernatants were prepared such that aliquots (20 µL) produced a linear response in kinetic mode. A gradient profile was constructed using a thermocycler (Mycycler, Bio-Rad, USA) for the selected mutants and the parental type, using 50 µL for each point in a gradient scale ranging from 30 to 80°C. After a 10 min incubation, samples were removed and chilled on ice for 10 min. Thereafter, 20 µL samples were removed and incubated for 5 min at room temperature. Finally, 180 µL of 100 mM sodium tartrate buffer (pH 3.5), 2 mM ABTS and 0.1 mM H_2O_2 was added to the samples to measure activities. The thermostability values were calculated as the ratio between the residual activity at different temperature points and the initial activity at room temperature. The T_{50} value was determined as the transition midpoint of the inactivation curve of the protein as a function of temperature, which in our case was defined as the temperature at which the enzyme lost 50% of its initial activity after a 10 min incubation.

DNA sequencing. Plasmids containing the VP/UPO variants were sequenced on an ABI 3730 DNA Analyzer-Applied Biosystems Automatic Sequencer at the Secugen (CIB, Madrid). The following primers were designed using Fast-PCR software (University of Helsinki, Finland): for VP: RMLN F; 3R-direct (5'-GTTCCATCATCGCGTTCG- 3'); 5F-reverse (5'-GGATTCCTTTCTTCTTGG-3') and RMLC R (**Table S1**). For UPO: RMLN F; upo1 sec direct (5'-GAAGGCGACGCCAGTATGACC-3'); upo1 sec reverse (5'-GGTCATACTGGCGTCGCCTTC-3'); and RMLC R (**Table S3.1**).

Protein and homology modeling. The crystal structure of VPL2 from *P. eryngii* at 2.8 Å resolution (1 Å = 0.1 nm, PDB ID: 3FJW) was used to generate a model to map the new mutations found with the help of the PyMOL Molecular Visualization System (Schrödinger). A homology model was generated by carrying out a structural alignment in PyMOL with the following crystal

structures (PDB IDs are indicated): 3FJW, native VP from *P. eryngii*; 1IYN, recombinant chloroplastic ascorbate peroxidase (ApX) from *N. tabacum* expressed in *E. coli*; 3M5Q, native manganese peroxidase (MnP) isozyme 1 from *P. chrysosporium*; 1H3J, native peroxidase from *C. cinerea* (CiP); and 1W4W, recombinant horseradish peroxidase C1A from horseradish (HRP) expressed in *E. coli*. IDENTITY and SIMILARITY percentages were obtained using SEQUENCE SIMILARITY AND IDENTITY Software (http://imed.med.ucm.es/Tools/sias.html).

3.3. RESULTS AND DISCUSSION

MORPHING is a method of generating DNA diversity based on the high frequency of homologous recombination of *S. cerevisiae*. In a single step, this approach allows us to assemble delimited randomly mutagenized regions with the remaining, unaltered fragments of a gene. Unlike most evolution methods focused in restricted areas, mutations are randomly generated and they do not depend on the engineering of a set of spiked/degenerate synthetic oligonucleotides. By MORPHING, small segments are targeted and subjected to error-prone PCR with defined mutational frequencies, while the remaining portions of the gene are amplified using high-fidelity polymerases (**Fig. 3.1**). Error-prone PCR methods have the drawback of codon bias although they can be modified by alternating between different polymerases in successive generations of evolution. Indeed, standard *Taq* polymerases (with a transition/transversion ratio [T_s/T_v] ranging from 2.9 to 0.8 (Wong et al., 2006), were employed in our mutagenic experiments, although mutational bias may be altered by combining this protocol with other well-known polymerases and mutational strategies (Zumarraga et al., 2008; Garcia-Ruiz et al., 2012; Cherry et al., 1999). The pool of mutated/conserved fragments and the linearized plasmid are subjected to *one-pot* repair and cloned *in vivo*, giving rise to a complete autonomously replicating plasmid upon transformation in yeast, without the need for additional PCR reactions or ligation/amplification steps. The number of crossover events (n+1, where n is the number of fragments) between segments is directly proportional to the number of segments assembled, allowing several regions to be studied alone or in a combinatorial manner. Depending on the distance between muta-

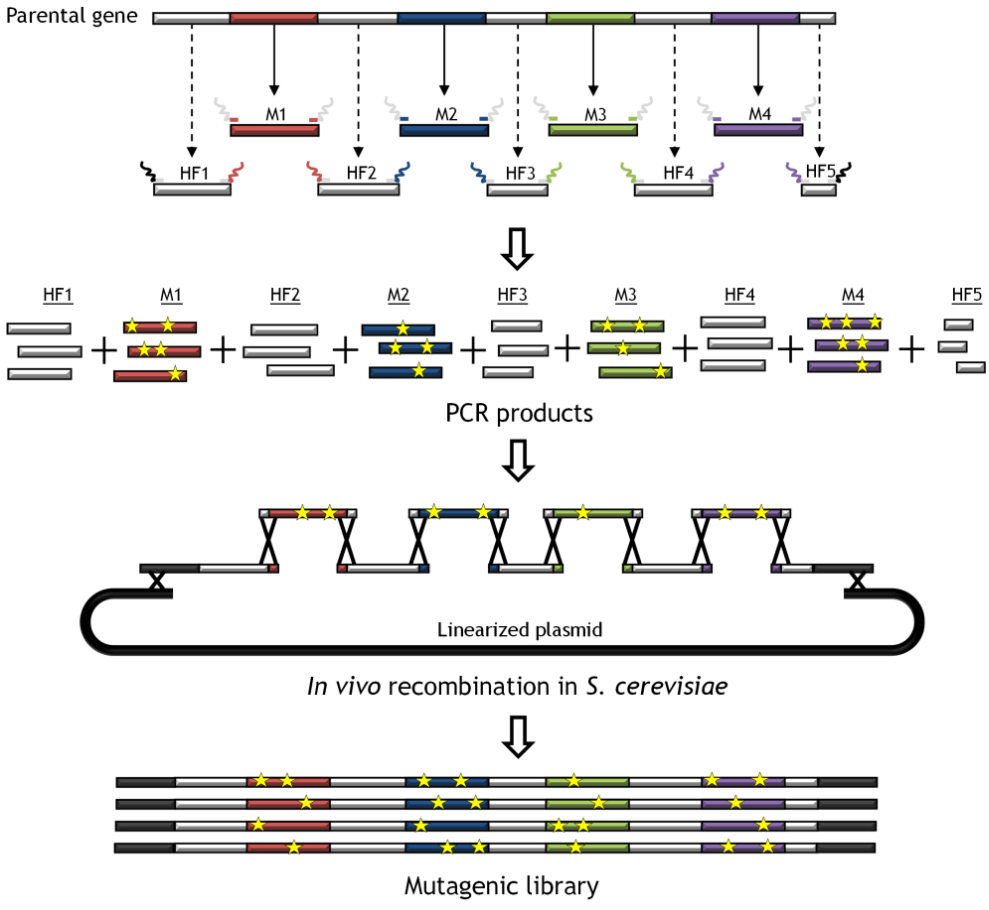

Fig. 3.1. General approach for MORPHING. Segments subjected to random mutagenesis (M1 to M4) are shown in color and the non-mutagenized high-fidelity amplified segments (HF1 to HF5) in light grey. After PCR, the pool of segments is co-transformed into *S. cerevisiae* along with the linearized vector. Overlapping areas of ~50 bp flanking each segment allow specific crossover events to occur between fragments (represented by crosses), giving rise to an autonomously repaired vector carrying a full version of the target gene with random mutations (yellow stars) only in the defined regions.

tions, crossover events can occur between the different mutations in the target fragment(s), mediated by the *S. cerevisiae* recombination machinery, fostering enrichment. The success of this method is facilitated by the high-fidelity DNA splicing of fragments through the small overhangs with overlapping sequences of ~50 bp that flank each segment. These overhangs ensure the *in vivo* reconstitution of the whole gene with random mutations only in the segments specifically targeted. Under these rules, up to six recombination events between fragments can be created without significantly affecting transformation efficiencies (~10^5 clones per transformation reaction can be obtained, which are good enough to screen mutant libraries).

Engineering oxidative stability. We first used this protocol to engineer oxidative stability in an evolved VP variant, the VP-R4 mutant generated in a previous directed evolution experiment to enhance its functional expression yeast and its stability (Garcia-Ruiz et al., 2012). The sensitivity of VP (EC 1.11.1.16) to peroxides is the highest reported for any peroxidase to date being strongly inhibited in the presence of catalytic concentrations of H_2O_2 due to a mechanism-based phenomenon known as suicide inactivation that is common to all peroxidases (Valderrama et al., 2002). The inherent fragility of VP is explained by its complex structure. With a redox potential of over +1.2 V, three different catalytic sites (the heme domain, a catalytic tryptophan located at the protein's surface and the Mn^{2+} binding site) and two access channels, the dense production and traffic of free radicals jeopardizes the enzyme's stability and function (Ruiz-Dueñas et al., 2009; Garcia-Ruiz et al., 2012) (**Fig. 3.2**).

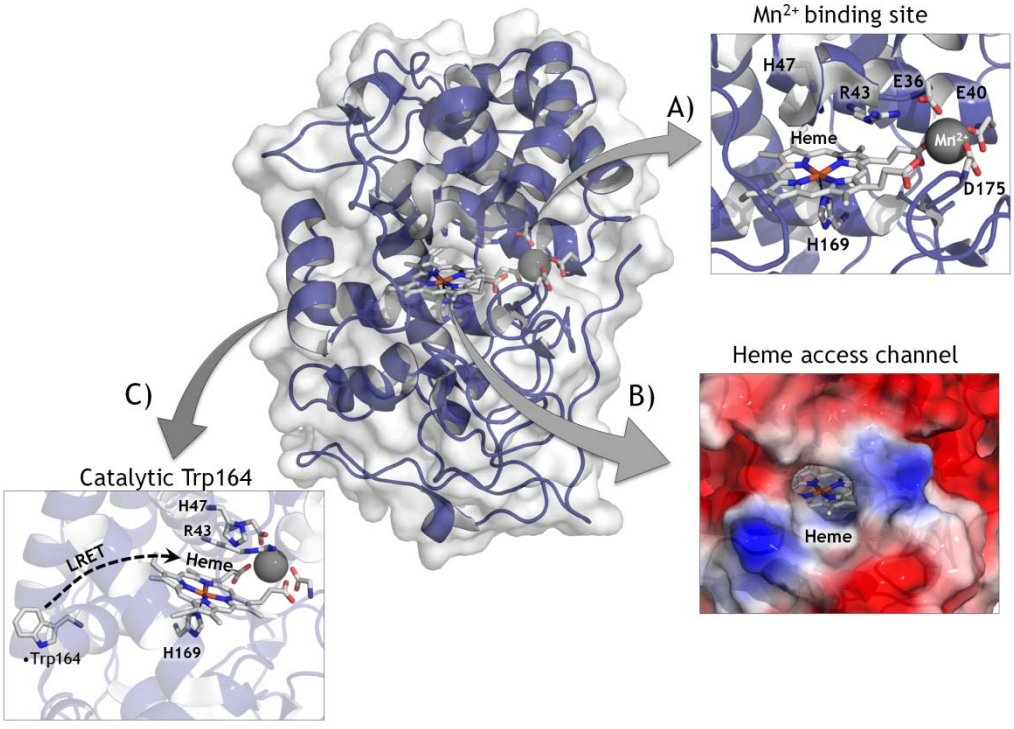

Fig. 3.2. Overview of Versatile Peroxidase from *Pleurotus eryngii* (PDB ID: 3FJW). Heme prostetic group and catalytic residues are shown as sticks in CPK color. The three catalytic sites are shown in detail. (A) The Mn^{2+} binding site (Mn^{2+}, black sphere), the distal and proximal His (His47 and His169) the Arg43 involved in H_2O_2 reduction and the coordinating triad (Glu36, Glu40, Asp175) are depicted. (B) Heme access channel represented as electrostatics surface with heme group (stick mode) at the bottom of channel. (C) Catalytic Trp164 (LRET; long range electron transfer).

To identify what are potentially the most H_2O_2-sensitive regions of the VP, we performed a multiple structural alignment using high- and medium-redox potential peroxidases with improved oxidative stability (Cherry et al., 1999; Miyazaki-Imamura et al., 2003; Ryan and O'Fagain, 2007; Kitajima et al., 2008) (**Fig. 3.3**). After careful examination of the model, three different regions (of 26, 30 and 69 amino acids each, excluding the recombination areas) in the vicinity of the heme group were targeted for random mutagenesis and recombination (**Fig. S3.1**, **S3.2**). The first region subjected to MORPHING was the distal His environment (L28-G57) that contains the H_2O_2 binding site within a helix that is highly conserved in all high-redox potential peroxidases. The second target region was the proximal His environment (L149-A174) located on the opposite side to the distal His, in the surroundings of the heme domain. The third region was the Met environment (I199-L268), containing three of the five

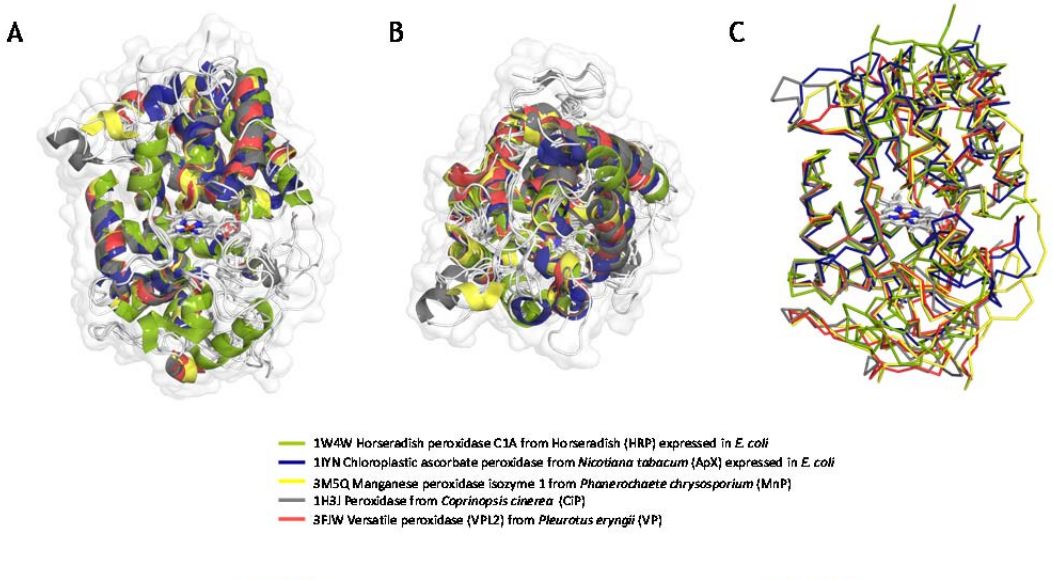

D

IDENTITY (%)

Enzyme	R4	CiP	MnP	HRP	ApX
R4	100	-	-	-	-
CiP	31.1	100	-	-	-
MnP	75.6	28.3	100	-	-
HRP	55.2	8.7	52.2	100	-
ApX	59.2	14.3	57.1	62.2	100

SIMILARITY (%)

Enzyme	R4	CiP	MnP	HRP	ApX
R4	100	-	-	-	-
CiP	37.9	100	-	-	-
MnP	80.2	33.8	100	-	-
HRP	59.5	13	56.7	100	-
ApX	63.4	18.8	61.6	66.3	100

Fig. 3.3. Structural alignment for oxidative stability. (A, B) Front and upper view (cartoon) with the protein surfaces shown in white. (C) Structural alignment in ribbon mode. The prosthetic heme group is highlighted in CPK colors. (D) Identities and similarities for each protein scaffold using the following PDB entries for the analysis: 1W4W, horseradish peroxidase C1A (HRP) expressed in *E. coli* (green); 1IYN, chloroplastic ascorbate peroxidase (ApX) from *Nicotiana tabacum* expressed in *E. coli* (blue); 3M5Q, manganese peroxidase isozyme 1 (MnP) from *Phanerochaete chrysosporium* (yellow); 1H3J, peroxidase from *Coprinopsis cinerea* CiP (gray); and 3FJW, Versatile peroxidase (VPL2) from *Pleurotus eryngii* (red).

putative oxidizable Met in the VP-R4 variant. Several mutational loads were assayed for each region to construct independent mutant libraries and then explore them for oxidative stability. Mutational loads were adjusted by modifying the PCR conditions in order to introduce 1 to 5 mutations per segment (including the crossover areas). The frequencies of mutation were estimated from different landscapes of mutant libraries (500 clones each), calculating the number of clones with <10% of the parental enzyme activity, and they were further verified by DNA sequencing of a random sample of mutants including active and non-active variants (**Fig. 3.4**). Overall, an average value of T_s of 65% (A↔G, 52%; T↔C, 13%) and T_v of 35% (T↔A, 17.4%; A↔C, 8.8%; G↔C, 8.8%) was observed in the libraries under study (*i.e.* T_s/T_v ratio ~1.8). Mutational frequencies of 0.5 nucleotide changes/100 bp were obtained with T_s G→A when $[MnCl_2] \leq 0.1$ mM, regardless of the DNA template concentration. In segments as short as 30 residues long (*e.g.,* the distal His environment: L28-G57), we obtained high mutational loads at $[MnCl_2] > 0.1$ mM (frequencies of ~3 mutations/100 bp). Among the high mutational variants, the 1E11 ($2T_s$, $3T_v$) and 2G4 ($3T_s$, $2T_v$) mutants incorporated 5 mutations each that inactivated the protein due to the highly conserved nature of this region (**Fig. 3.5**).

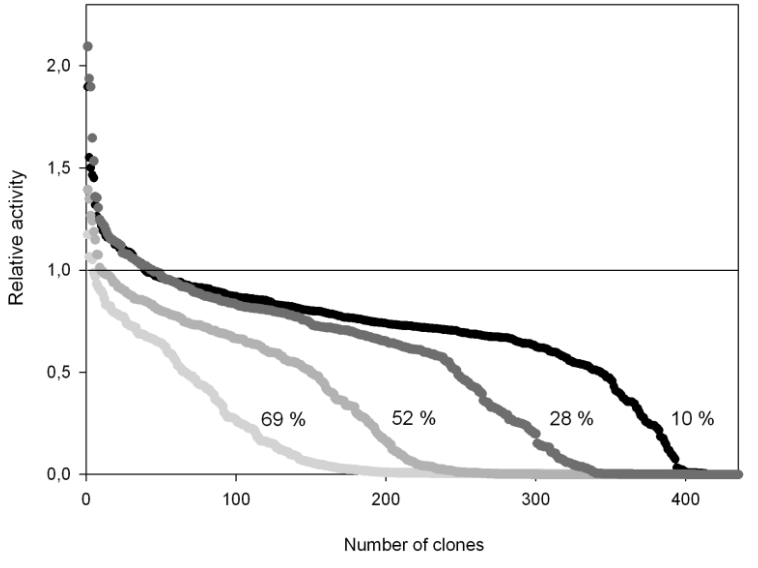

Fig. 3.4. Mutagenic landscapes of the distal His environment (L28-G57) generated using 0.92 ng/μL of DNA template, and 0.01 mM (black), 0.1 mM (dark gray), 0.2 mM (medium gray), 0.4 mM (light gray) of $MnCl_2$, respectively. The percentages indicate the number of clones having less than 10% of the parent enzyme's activity; the solid horizontal line indicating the parental activity in the assay.

After the initial screening and three consecutive rescreenings, several mutants with an improved increment in apparent half-life ($\Delta t_{1/2}$ *vs* H_2O_2) were identified. We found two beneficial mutations at the L28-G57 segment. The 3G10 variant showed a 2.1-fold improvement in stability *vs* H_2O_2, with a significant $\Delta t_{1/2}$ *vs* H_2O_2 of 18 min with respect to the parental type and a 5.5°C increase in the T_{50} (the temperature at which the enzyme retains 50% of its activity after a 10 min incubation, **Fig. 3.6**). Only one mutation, $_{GAG}$E40K$_{AAG}$, was found in 3G10 and the same mutation was introduced in 2F5 and 5D1 variants. This mutational redundancy highlights the role of this specific alteration in generating oxidative stability in VP and significantly, the highly stable CiP contains a Lys residue at the same position (Cherry et al., 1999) (**Fig. 3.5)**. In VP, E40 is one of three acidic residues that form the Mn^{2+} binding site (**Fig. 3.2**) and it is plausible that closing some of the protein inlets involved in the generation of free radicals may be beneficial for VP stability, albeit at the cost of compromising this catalytic site. The $_{ACT}$T45A$_{GCT}$ mutation was discovered in both the 1C12 and 2G8 mutants, the latter of which also contained the silent $_{GCT}$A61A$_{GCC}$ mutation (**Fig. 3.5**). While the T45A mutation did not alter thermostability (T_{50} = 59°C), it conferred a 1.3-fold improvement in stability and it was associated with a $\Delta t_{1/2}$ *vs* H_2O_2 of ~10 min with respect to the parental type (**Fig. 3.6**). The same amino acid (V53A according to CiP numbering) was introduced into the evolved CiP although without improving thermostability (Cherry et al., 1999) (**Fig. 3.5**). It is likely that the only effect of introducing an Ala at this position relates with the accessibility of H_2O_2 to the internal protein structure. The $_{CCT}$P141A$_{GCT}$ mutation in the 5A9 variant arose in the L149-A174 segment (proximal His environment). Situated at the heme entrance, Pro141 is a highly conserved residue in all fungal peroxidases. However, the P141A mutation resulted in a 1.4-fold improvement in oxidative stability, producing a $\Delta t_{1/2}$ *vs* H_2O_2 of ~5 min with respect to the parental type and no change in thermostability (**Fig. 3.6**). P141A is located in a strictly conserved region and according to our model, the substitution of Ala by Pro may widen the heme channel making easier the traffic of oxidized species and therefore limiting their harmful residence time in the inner protein structure. To further study the possible synergies between beneficial mutations E40K, T45A and P141A, a triple variant was constructed by site-directed mutagenesis

doubling the $\Delta t_{1/2}$ *vs* H_2O_2 to 45 min (data not shown). This mutant was the departure point to engineer an oxidative stable VP variant by successive rounds of *in vitro* evolution (unpublished material).

No mutants were discovered in the I199-L268 segment (the Met environment), suggesting that the three oxidizable methionines in this area are not involved in the oxidative stabilization of VP. This result was corroborated by subjecting Met262 and Met265 to combinatorial saturation mutagenesis and screening. No improved variants were identified in this way and ~95% of the clones were inactive in this mutagenic landscape, indicating that these residues are very sensitive and do not tolerate changes (**Fig. S3.3**). Similarly, Met152 in the proximal His environment was not mutated.

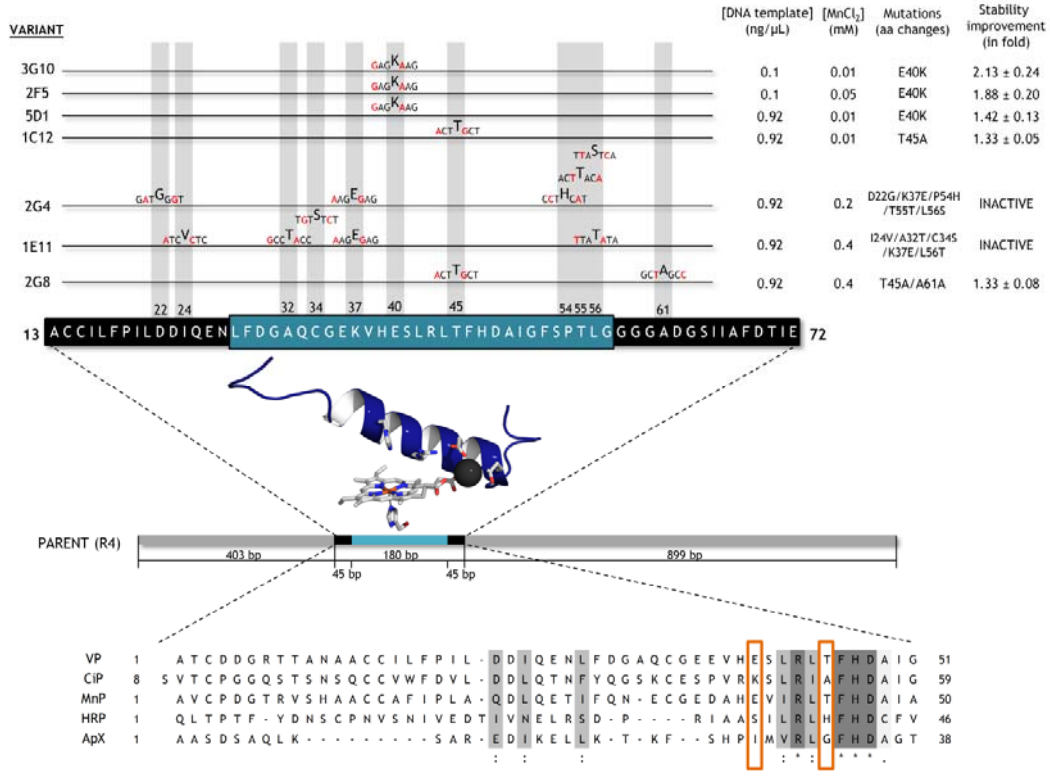

Fig. 3.5. Mutational loads, PCR conditions and selected variants used for MORPHING of the distal His environment. Point mutations are highlighted in red and the overhangs in black. Improvements in oxidative stability are indicated as the fold increase with respect to the parental type at a $[H_2O_2]$/[Enzyme] ratio of 3,000:1. Sequence alignments with stable peroxidase scaffolds are depicted, framing the mutations at positions 40 and 45 for VP and 53 and 48 for CiP, respectively. The MSA (multiple sequence alignment) was generated with T-coffee software: http://www.igs.cnrsmrs.fr/Tcoffee/tcoffee_cgi/index.cgi.

In this first enzyme case study, MORPHING effectively identified new structural determinants, such as the P141A mutation, that are important for oxidative stability. Significantly, the identification of the E40K and T45A mutations was in good agreement with previous findings (Cherry et al., 1999), thereby validating this approach. Although each mutated segment was analyzed independently by constructing small high-quality libraries with different mutational loads, it is also feasible that different combinations of mutated segments can be prepared using the yeast's recombination machinery.

Enhancing functional UPO expression. MORPHING was also used to assess whether the secretion levels of an unspecific peroxygenase (UPO) could be enhanced in *S. cerevisiae*. UPO (EC 1.11.2.1) is a new, potentially ligninolytic, peroxidase that has attracted much research attention due to its versatility and applicability in a variety of synthetic processes (Hofrichter and Ullrich, 2006; Hofrichter et al., 2010). Its peroxygenative (oxygen-transfer) activity is of particular importance as UPO can behave as a self-sufficient monooxygenase to mediate regio- and enantio-selective oxyfunctionalizations that are essential for organic synthesis. Among the array of oxygen transfer reactions catalyzed by UPO are brominations, sulphoxidations, N-oxidations, aromatic peroxygenations, alkyl hydroxylations, double bond epoxidations and ether cleavages. Like many other ligninolytic oxidoreductases, UPO is not readily expressed in heterologous hosts so that it can be tailored by directed evolution and therefore, we recently addressed this problem by subjecting the whole UPO gene to several rounds of random mutagenesis, recombination and screening in *S. cerevisiae* (Molina-Espeja et al., 2014). To further enhance the secretion of this protein, we used MORPHING to independently evolve the 43 amino acid UPO signal peptide in order to enrich the signal leader in beneficial mutations without altering the biochemical properties of the enzyme. To reliably compare the two directed evolution strategies, we exposed the signal peptide alone and the entire UPO gene (including its signal leader) to one round of directed evolution in two parallel experiments. Mutational rates for the leader library and the full-gene library were 0.5 and 0.1 nucleotide changes/100 bp, respectively. Both libraries were screened with the help of an ad hoc dual-colorimetric assay to estimate the enzymes peroxidase (with ABTS) and

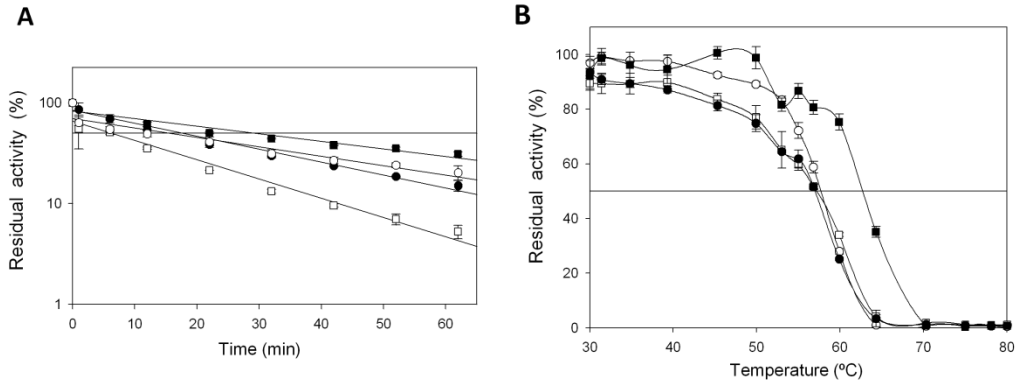

Fig. 3.6. (A) Apparent $t_{1/2}$ *vs* H_2O_2 for the R4 parental type, 5A9 mutant (P141A), 1C12 mutant (T45A) and 3G10 mutant (E40K) in the presence of 3,000 equivalents of H_2O_2. Horizontal line indicates 50% of residual activity. (B) T_{50} profiles (kinetic thermostability) of VP variants. White squares, R4 parental type; white circle, 5A9 mutant (P141A); black squares, 3G10 mutant (E40K); black circles, 1C12 mutant (T45A). Each point represents the mean and standard deviation of three independent experiments.

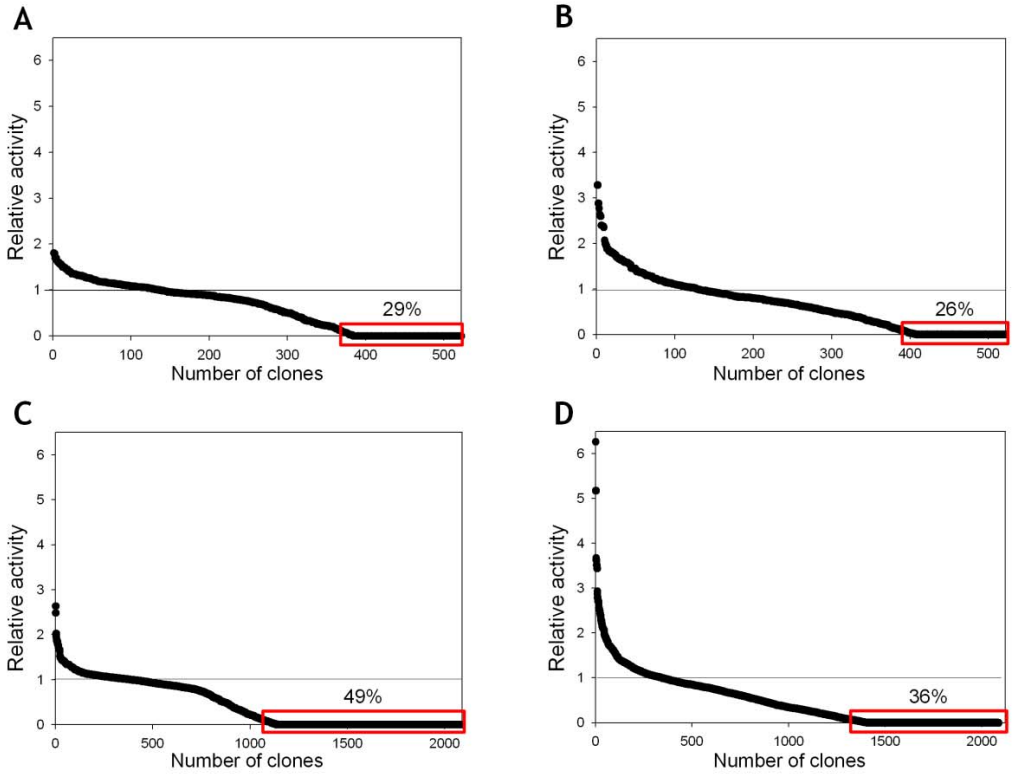

Fig. 3.7. Mutagenic landscapes for MORPHING of the signal peptide of UPO using ABTS (A) and NBD (B) in colorimetric assays. Directed evolution landscapes of the whole UPO gene obtained with ABTS (C) and NBD (D) assays. The activity of the clones is plotted in descending order. The solid horizontal line indicates the activity of the parental type in the assay.

peroxygenase (with NBD) activities. The mutagenic landscape generated by MORPHING revealed an increased tolerance to mutations in the signal peptide than in the whole UPO gene. Indeed, we found that when random mutagenesis of the leader and the whole UPO gene was compared, 30% and 49% of clones had <10% of parental enzyme activity on ABTS as a substrate, respectively (**Fig. 3.7**). These results are consistent with the fact that mutations in the leader sequence only affect secretion, whereas those in the whole UPO gene may also compromise the catalytic properties. While no variants carrying mutations in the leader were identified in the whole UPO gene after one round of evolution, several independent but almost consecutive mutations were observed in three independent beneficial variants after MORPHING of the leader sequence ($_{TTC}$F12Y$_{TAC}$, $_{GCG}$A14V$_{GTG}$ and $_{AGG}$R15G$_{GGG}$). Each of these mutations individually enhanced secretion by ~20% with respect to the parental type. Although MORPHING was useful to unmask these beneficial mutations for secretion, the eukaryotic machinery of *S. cerevisiae* was unable to join these positions by homologous recombination due to their proximity. Therefore, we constructed a signal peptide containing the full set of these mutations by conventional site-directed mutagenesis looking for a synergic effect in secretion levels. The evolved signal peptide also included the beneficial mutation $_{GCC}$A21D$_{GAC}$ (discovered in the earlier stages of evolution). Finally, the signal peptide of native UPO was replaced by the evolved signal peptide F12Y-A14V-R15G-A21D (see Materials and Methods for details), resulting in a 27-fold increase in total secretion compared to the native UPO fused to its original leader (~2 ±0.11 ABTS U/L and 54 ±5.7 ABTS U/L, respectively). F12Y-A14V-R15G-A21D mutations are located at the hydrophobic core of the leader and they may exert a beneficial effect on secretion by promoting a more suited interaction with the signal recognition particle during translocation to the endoplasmic reticulum.

This second case study demonstrates that the use of our focused mutagenesis method to direct the evolution of signal leaders is a suitable approach to promote heterologous functional expression of complex eukaryotic genes in yeast. Targeting mutational loads to leader sequences is a simple means of detecting mutations that are beneficial for secretion and that can be

subsequently combined in a single signal peptide to generate potential synergies along the *S. cerevisiae* secretory pathway.

3.4. CONCLUSIONS

The random domain mutagenesis/recombination method presented here is a reliable *one-pot* approach for the construction of focused mutant libraries of eukaryotic genes in *S. cerevisiae*. In general terms, MORPHING allows the researcher to focus exclusively on the random introduction of mutations and their recombination in restricted region/s, while protecting critical domains from mutagenesis. The selection of the target regions to be evolved is as important as the mutational loads chosen for each mutant library, which can be easily varied to enrich the target segments in beneficial mutations.

The two case studies presented here validate the versatility of our method by tackling two distinct problems. While MORPHING proved useful to explore limited targeted regions, allowing us to identify several structural determinants of H_2O_2 inhibition in VP that could be applied to other high redox-potential fungal peroxidases, it also effectively decoupled secretion and catalytic activity for functional UPO expression. This approach can also be used to explore other complex problems, such as to alter substrate specificity or enantio-selectivity by subjecting several segments of the same gene to random mutagenesis, promoting their *in vivo* assembly in one transformation step. Indeed, this strategy is currently being used by our group to evolve a fungal aryl alcohol oxidase for the selective oxidation of different alcohols. Apart from structure-function relationship studies, MORPHING can be also useful when structural information is absent, *e.g.*, for the evolution of leader peptides for secretion, for the modification of promoters, or in the evolution of unknown regions of biochemical relevance that have been revealed by conventional directed evolution.

Additional advantages of this method include the reduction of the sequence space to be explored (good results can be achieved with small libraries of 400-500 clones), the conservation of certain catalytic properties while improving other traits, and the discovery of new structural/catalytic

determinants that can be further optimized using focused saturation mutagenesis. The combination of MORPHING with classical directed evolution and semi-rational approaches, or with neutral genetic drift, may lead to the development of new adaptive pathways to engineer more robust eukaryotic enzymes in yeast (Gupta and Tawfik, 2008; Dalby, 2011; Goldsmith and Tawfik, 2013).

ACKNOWLEDGMENTS

The authors thank A. T. Martínez, F. J. García-Dueñas (Centro de Investigaciones Biológicas, CIB-CSIC, Madrid, Spain) and M. Hofrichter (International Graduate School of Zittau, IHIZ, Germany) for helpful discussions.

AUTHOR CONTRIBUTIONS

Conceived and designed the experiments: MA. Performed the experiments: DGP, PME, EGR. Analyzed the data: DGP, PME, EGR, MA. Contributed reagents/materials/analysis tools: PME, EGR, DGP. Wrote the paper: MA.

3.5. SUPPLEMENTAL MATERIAL

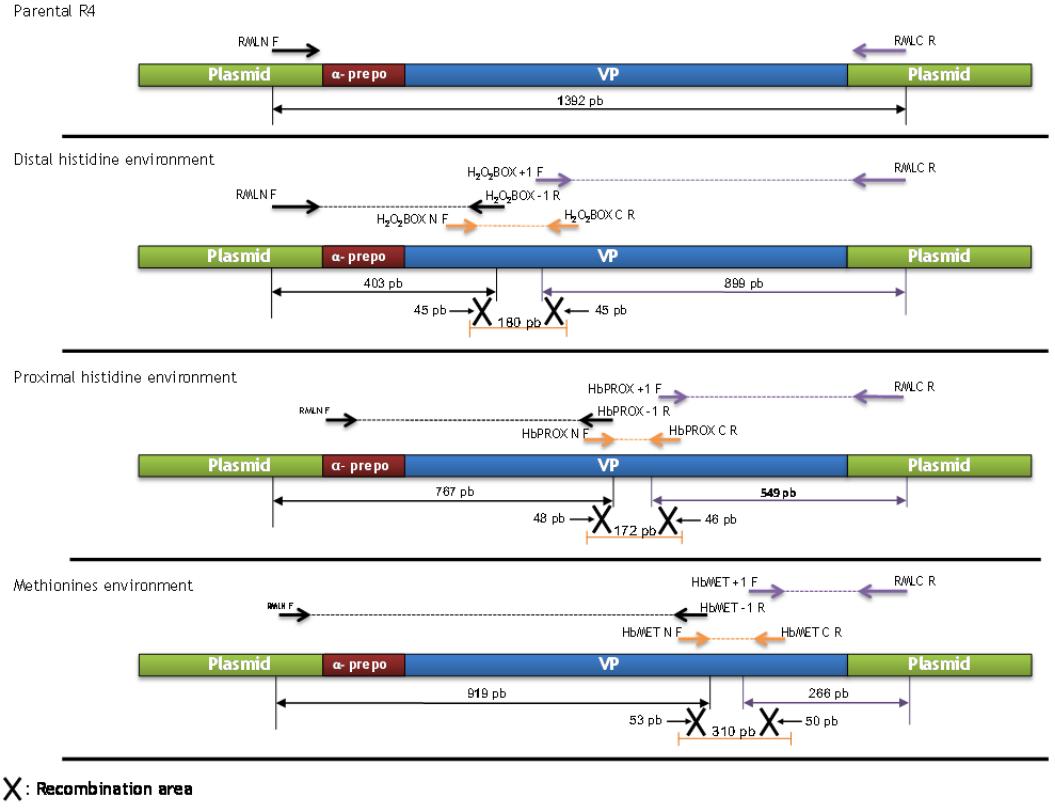

Fig. S3.1. VP MORPHING. Three different regions of VP were targeted for random mutagenesis and recombination (L28-G57, L149-A174 and I199-L268). The VP gene is shown in blue, the α-factor prepro-leader to promote secretion in yeast in red and the shuttle vector in green. The areas of crossover between the fragments are represented by crosses. The overlapping areas between segments were created by superimposing PCR reactions in defined regions (see also **Fig. S3.2** and **Table S3.1**).

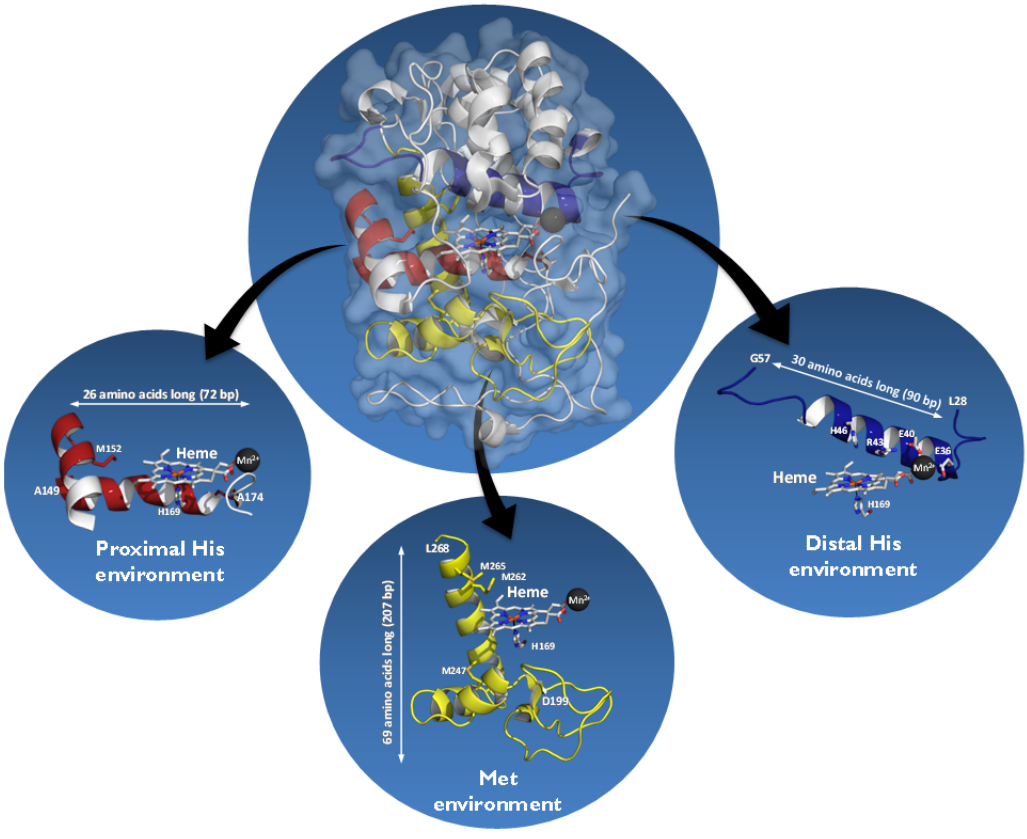

Fig. S3.2. Selected areas of VP subjected to MORPHING: proximal His environment (red), Met environment (yellow), and distal His environment (blue). The heme domain is depicted in stick mode and CPK colors. The amino acids delimiting mutated regions and the most relevant residues are highlighted (proximal and distal histidines; Mn^{2+} binding pocket with manganese represented as a grey sphere).

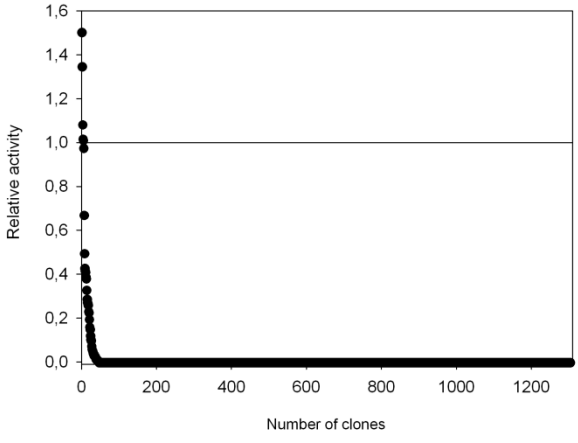

Fig. S3.3. Combinatorial saturation mutagenesis landscapes at positions 262 and 265 of VP. Clone activity is plotted in descending order. The solid horizontal line indicates the activity of the parental type in the assay.

Table S3.1 Oligos used for VP and UPO MORPHING.

Region	Primer name	Sequence	Tm (°C)	Base pair (bp)	Mutagenesis (*ep*PCR/HF-PCR)	PCR Product length (bp)	Overlapping areas (bp)
Distal His environment	RMLN F	5'-CCTCTATACTTTAACGTCAAGG-3'	51.1	22	NO	403	
	H_2O_2BOX -1 R	5'-GTTTTCTTGGATGTCATCGAGG-3'	50.5	21			→ 45
	H_2O_2BOX N F	5'-GCATGTTGCATTCTGTTCCCCATCCTC-3'	61.3	27	YES	180	
	H_2O_2BOX C R	5'-CTCAATGGTGTCGAACGCGATGATGG-3'	61.0	26			→ 45
	H_2O_2BOX +1 F	5'-GGAGGAGGAGCTGACGGTTC-3'	56.3	21	NO	899	
	RMLC R	5'-GGGAGGGCGTGAATGTAAGC-3'	55.9	20			
Proximal His environment	RMLN F	5'-CCTCTATACTTTAACGTCAAGG-3'	51.1	22	NO	767	
	HbPROX -1 R	5'-GAATGGAGTCAACAGAATCAAAAG-3'	52.3	24			→ 48
	HbPROX N F	5'-TCCCCGGACCACCTCGTG-3'	57.2	18	YES	172	
	HbPROX C R	5'-GGGTTGAATCGAATGGCATTCCAG-3'	57.4	24			→ 46
	HbPROX +1 F	5'-CGACAAGGTTGACCCATCGATTC-3'	57.1	23	NO	549	
	RMLC R	5'-GGGAGGGCGTGAATGTAAGC-3'	55.9	20			
Met environment	RMLN F	5'-CCTCTATACTTTAACGTCAAGG-3'	51.1	22	NO	919	
	HbMET -1 R	5'-GATGAAGAATTGAGAATCAAAAACTC-3'	51.7	26			→ 52
	HbMET N F	5'-CTGGAATGCCATTCGATTCAACCCCC-3'	61.1	26	YES	310	
	HbMET C R	5'-GGGGTGGGGATAACATCGGAACAGTC-3'	62.7	26			→ 50
	HbMET +1 F	5'-GGCCAAGACAAGACCAAATTGATTG-3'	56.0	25	NO	266	
	RMLC R	5'-GGGAGGGCGTGAATGTAAGC-3'	55.9	20			
CSM (M262/M265)	RMLN F	5'-CCTCTATACTTTAACGTCAAGG-3'	51.1	22			
	MET SAT R	5'-GGTCTTGTCTTGGCCAAGAAGAGC**SNN**CTT CGA**SNN**GGTAGCAGCGAAACGGTTCTGAATC-3'	76.1	61	NO	1,141	→ 49
	MET SAT F	5'-GATTCAGAACCGTTTCGCTGCTACC**NNS**TCG AAG**NNS**GCTCTTCTTGGCCAAGACAAGACC-3'	76.1	61	NO	312	
	RMLC R	5'-GGGAGGGCGTGAATGTAAGC-3'	55.9	20			
MORPHING UPOsp	RMLN F	5'-CCTCTATACTTTAACGTCAAGG-3'	51.1	22	YES	210	
	MORPH SP R	5'-CAGAGCTATTCTCGAGAGGA-3'	50.7	20			→ 40
	MORPH SP D	5'-GAGCCAGGATTACCTCCTGG-3'	57.7	20	NO	1,061	
	RMLC R	5'-GGGAGGGCGTGAATGTAAGC-3'	55.9	20			
IvAM	RMLN F	5'-CCTCTATACTTTAACGTCAAGG-3'	51.1	22	YES	1,231	
	RMLC R	5'-GGGAGGGCGTGAATGTAAGC-3'	55.9	20			
Evolved signal peptide and fusion gene	RMLN F	5'-CCTCTATACTTTAACGTCAAGG-3'	51.1	22			
	SP* R	5'-CCTGTTCCCAACCTTGGTCTACGC AGTGGGGGTCGTTGCTTTTCCTGAC-3'	74.6	49	NO	104	→ 49
	SP* F	5'-CCTGTTCCCAACCTTGGTCTACGC AGTGGGGGTCGTTGCTTTTCCTGAC-3'	74.6	49	NO	1,176	
	RMLC R	5'-GGGAGGGCGTGAATGTAAGC-3'	55.9	20			

The lengths of the PCR products and the overlapping areas are shown. NNS and SNN indicate NN(G/C) and (G/C)NN codons for the saturation mutagenesis libraries. CSM, combinatorial saturation mutagenesis; UPOsp, UPO signal peptide; IvAM, *In vivo* Assembly of Mutant libraries for the directed evolution of the whole UPO gene; epPCR, error-prone PCR; HF-PCR, high-fidelity PCR.

TANDEM-YEAST EXPRESSION SYSTEM FOR ENGINEERING AND PRODUCING UNSPECIFIC PEROXYGENASE

4

TANDEM-YEAST EXPRESSION SYSTEM FOR ENGINEERING AND PRODUCING UNSPECIFIC PEROXYGENASE

Patricia Molina-Espeja, Su Ma, Diana M. Mate, Roland Ludwig, Miguel Alcalde

Enzyme and Microbial Technology, 2015, Volumes 73-74, pages: 29-33.

http://dx.doi.org/10.1016/j.enzmictec.2015.03.004

Unspecific peroxygenase (UPO) is a highly efficient biocatalyst with a peroxide dependent monooxygenase activity and many biotechnological applications, but the absence of suitable heterologous expression systems has precluded its use in different industrial settings. Recently, the UPO from Agrocybe aegerita was evolved for secretion and activity in Saccharomyces cerevisiae (Molina-Espeja et al., 2014). In the current work, we describe a tandem-yeast expression system for UPO engineering and large scale production. By harnessing the directed evolution process in S. cerevisiae, the beneficial mutations for secretion enabled Pichia pastoris to express the evolved UPO under the control of the methanol inducible alcohol oxidase 1 promoter. Whilst secretion levels were found similar for both yeasts in flask fermentation (~8 mg/L), the recombinant UPO from P. pastoris showed a 27-fold enhanced production in fed-batch fermentation (217 mg/L). The P. pastoris UPO variant maintained similar biochemical properties of the S. cerevisiae counterpart in terms of catalytic constants, pH activity profiles and thermostability. Thus, this tandem-yeast expression system ensures the engineering of UPOs to use them in future industrial applications as well as large scale production.

4.1 INTRODUCTION

Fungal unspecific peroxygenases (EC 1.11.2.1, UPOs, also known as aromatic peroxygenases) are heme containing enzymes with a peroxide dependent monooxygenase activity (referred to as peroxygenase activity, assisted by a 2-electron oxygenation route) (Hofrichter and Ullrich, 2006).UPO was recently categorized within the fungal heme-thiolate peroxidase (HTP) superfamily along with chloroperoxidase (CPO) from *Leptoxyphium (Caldariomyces) fumago* (Hofrichter et al., 2010). In nature, the biological function of UPO is not well defined although it may be involved in lignin and humus transformation as well as in the detoxification of plant compounds. From a biotechnology viewpoint, UPO is being considered by many as the most gifted biocatalyst for the selective oxy-functionalization of organic compounds. Indeed, UPO has been comprehensively studied for different types of reactions including oxidation of aromatic and heterocyclic compounds, epoxidation of alkenes, hydroxylation of aliphatic compounds, O- and N-dealkylations and many more (over 300 compounds are currently recognized as UPO's substrates) (Hofrichter and Ullrich, 2014; Ullrich and Hofrichter, 2007). Notably, the selective introduction of oxygen functionalities has been profoundly studied for P450 monooxygenases, which are typically intracellular membrane-bound proteins with a strong dependency on the expensive electron donor NAD(P)H and auxiliary flavoproteins (Bernhardt, 2006). By contrast, UPO is soluble, extracellular and stable, being fueled by catalytic concentrations of H_2O_2. Despite these advantages, the heterologous UPO expression and genetic engineering remain as the main bottlenecks to meet the requirements for industrial applications of this enzyme. In 2004, the UPO secreted by the edible mushroom *Agrocybe aegerita* was first described (Ullrich et al., 2004; Pecyna et al., 2009). One decade later, we have evolved this enzyme for heterologous functional expression in *Saccharomyces cerevisiae* achieving similar secretion levels as those reported for the homologous host (Molina-Espeja et al., 2014). After five generations of directed evolution, the ultimate UPO mutant comprised 9 mutations that enhanced secretion by 1,114 folds whilst showing high stability in terms of temperature and the presence of co-solvents. The recombinant evolved UPO and its evolutionary platform in *S. cerevisiae* are a suitable point of

departure towards further engineering goals (from the synthesis of intermediates for agrochemicals, like 1-naphthol from naphthalene, to active pharmaceutical ingredients like the pain killer paracetamol). However, for such applications UPO expression must be scaled up. In the current work, we describe a compatible tandem-yeast expression system based on *S. cerevisiae* for directed evolution and *Pichia pastoris* for large scale fermentation whereby the UPO production and its adaptation to industrial applications can be readily accomplished.

4.2. MATERIALS AND METHODS

Strains and chemicals. The *P. pastoris* expression vector (pPICZα-B), the *P. pastoris* strain X-33, PTM1 trace salts and the antibiotic zeocin were purchased from Invitrogen (Carlsbad, CA, USA). The *Escherichia coli* strain XL2-Blue competent cells were obtained from Agilent Technologies (Santa Clara, CA, USA). Restriction endonucleases EcoRI, XbaI and PmeI, the DNA Ligation Kit, the Antarctic phosphatase and the PNGase F were purchased from New England Biolabs (Ipswich, MA, USA). iProof high-fidelity DNA Polymerase was purchased from Bio-Rad (Hercules, CA, USA). Oligonucleotide primers were acquired from Isogen Life Science (Barcelona, Spain). Zymoclean Gel DNA Recovery kit was from Zymo Research (Orange, CA, USA). NBD (5-nitro-1,3-benzodioxole) was from TCI America (Portland, OR, USA); ABTS (2,2'-azino-bis(3-ethylbenzothiazoline-6-sulfonic acid)), DMP (2,6-dimethoxyphenol), veratryl alcohol, benzyl alcohol and Antifoam 204 were purchased from Sigma-Aldrich (Saint Louis, MO, USA). All chemicals and media components were of the highest purity available.

UPO expression in *S. cerevisiae*. Evolved UPO expression in *S. cerevisiae* and purification were carried out as described elsewhere (Molina-Espeja et al., 2014).

UPO expression in *P. pastoris*. UPO construct for *P. pastoris*. The 1,113 bp DNA fragment containing the coding region of the evolved UPO gene in *S. cerevisiae* (PaDa-I mutant) (Molina-Espeja et al., 2014) was cloned into the expression vector pPICZ-B. The vector pJRoC30-PaDa-I, resulting from previous

directed evolution work (Molina-Espeja et al., 2014) was used to amplify the evolved UPO with the primers psnUPO1DIR2 (5'-ccg**gaattc** ATGAAATATTTTCCCCTGTTCCCAA-3') and UPO1REV2 (5'-gc**tctaga** TTATCAATCTCGCCCGTATGGGAAGAC-3'), which included targets for EcoRI and XbaI restriction enzymes, respectively (in bold; capital letters correspond to UPO sequence). PCR reactions were performed using a thermocycler (Mycycler, Bio-Rad, Hercules, CA, USA) in a final volume of 50 µl containing 0.25 µM of each primer, 100 ng template, 1 mM dNTPs (250 µM each), 3% dimethyl sulfoxide (DMSO) and 1 U of iProof polymerase. The PCR conditions were 98ºC for 30 s (1 cycle); 98ºC for 10 s, 55ºC for 27 s, 72ºC for 30 s (28 cycles); and 72ºC for 10 min (1 cycle). The pPICZ-B vector and the PCR product were digested with the restriction enzymes EcoRI and XbaI at 37ºC for 1 h. The linearized pPICZ-B vector 5' and 3' ends were dephosphorylated using Antarctic phosphatase (1 U per every 200 ng of linearized vector) at 37ºC for 1 h. The PCR product and the linearized vector were loaded onto a preparative agarose gel, purified using the Zymoclean Gel DNA Recovery kit and ligated with T4 DNA ligase at room temperature for 30 min. After transformation of the pPICZ-B-PaDa-I construct into chemically competent *E. coli* XL2-Blue cells, the plasmid was proliferated, linearized with the restriction enzyme PmeI at 37ºC for 1 h and transformed into electro-competent *P. pastoris* X-33 cells. Electro-competent *P. pastoris* cells were prepared and transformed with the construction as described elsewhere (Lin-Cereghino et al., 2005) using 200 ng of linearized vector and 50 µL of competent cells. Transformants were grown on YPD plates (10 g/L yeast extract, 20 g/L peptone, 4 g/L glucose and 15 g/L agar) containing 25 mg/L zeocin.

Deep well plate microfermentation screening. *P. pastoris* clones containing PaDa-I under the control of the AOX1 promoter (pPICZ-B-PaDa-I) were cultivated in 96-deep well plates with 300 µL of BMD1 medium per well (100 mM potassium phosphate buffer pH 6.0, 3.5 g/L yeast nitrogen base without amino acids, 400 µg/L biotin, 10 g/L glucose) at 25ºC, 300 RPM and 80% humidity for 2 days in a humidity shaker (Minitron, INFORS, Bottmingen, Switzerland). Then 300 µL of BMM2 were added per well (final concentrations per well: 100 mM potassium phosphate buffer pH 6.0, 3.5 g/L yeast nitrogen

base without amino acids, 400 μg/L biotin, 2% methanol, 3 mM $MgSO_4$ and 20 mg/L hemoglobin). Twelve hours later, 70 μL of BMM10 were added (final concentrations per well: 100 mM potassium phosphate buffer pH 6.0, 3.5 g/L yeast nitrogen base without amino acids, 400 μg/L biotin, 10% methanol), and this was repeated every 24 h during 3 days. After 147 h, the activity with ABTS was measured (reaction mixture contained 100 mM sodium phosphate/citrate buffer at pH 4.4, 0.3 mM ABTS and 2 mM H_2O_2).

Small scale flask fermentation. The two clones from microfermentations with the highest activity were grown in YPD/zeocin agar plates and inoculated in 5 mL of liquid YPD at 30 ºC and 250 RPM. When optical density at 600 nm (OD_{600}) ~1 (7-8 h) the culture was used to inoculate 20 mL of BMMY (100 mM potassium phosphate buffer pH 6.0, 3.5 g/L yeast nitrogen base without amino acids, 400 μg/L biotin, 0.5% methanol, 3 mM $MgSO_4$ and 300 mg/L hemoglobin) in 100 mL baffled shaken flasks. The cultures were incubated at 25ºC or 30ºC, with 300 mg/L hemoglobin or without hemoglobin and 250 RPM, and they were supplemented with 250 μL of methanol every 24 h. This was repeated during 3 days until reaching the maximum activities. The clone with the highest activity was selected to be grown in bioreactor.

Large scale fed-batch fermentation. The pPICZ-B-PaDa-I construct was large scale produced in *P. pastoris* using a 7-L glass vessel fermenter (MBR, Wetzikon, Switzerland) filled with basal salts medium (26.7 mL/L 85% phosphoric acid, 0.93 g/L $CaSO_4 \cdot 2H_2O$, 14.9 g/L $MgSO_4 \cdot 7H_2O$,18.2 g/L K_2SO_4, 4.13 g/L KOH; 40 g/L glycerol, initial volume: 4 L). After autoclaving, 4.35 mL/L PTM1 trace salts and 1 mL Antifoam 204 were added to the medium. Furthermore, the pH was adjusted to 5.0 with ammonium hydroxide solution (28%), keeping it at this value throughout the entire process. The fermentation was started by adding 0.4 L of *P. pastoris* preculture grown on YPD medium in several 1-L baffled shaken flasks at 150 RPM and 30ºC for 16 h. According to the Pichia Fermentation Process Guidelines of Invitrogen, the batch was run at 30ºC and 800 RPM. A 50% (w/v) glycerol feed containing 12 mL/L PTM1 trace salts was initiated when all the glycerol was consumed, keeping the dissolved oxygen (DO) concentration above 20%. At the end of the glycerol batch phase, methanol

(0.5%, v/v) was injected aseptically into the fermenter, and the glycerol feed faded out by a linear ramp 20-0 g L^{-1} h^{-1} over 2 h. Once the DO concentration spiked, the methanol feed was started. From this time on, the temperature was set to 25ºC. Samples were taken regularly and wet biomass, protein concentration and UPO activity were determined.

To compare UPO expression in bioreactor by *S. cerevisiae* and *P. pastoris*, a fed-batch cultivation of *S. cerevisiae* was additionally performed. To that purpose a single colony from the *S. cerevisiae* clone containing pJRoC30-PaDa-I was picked from a SC drop-out plate, inoculated in 20 mL minimal medium and incubated for 48 hat 25ºC and 160 RPM. The minimal medium contained 100 mL filtered yeast nitrogen base (67 g/L), 100 mL filtered yeast synthetic drop-out medium supplement without uracil (19.2 g/L), 100 mL filtered raffinose solution (200 g/L), 700 mL deionized water and 1 mL of filtered chloramphenicol solution (25 g/L). The inoculum 10% (v/v) was added into a 500 mL fermenter (Sixfors, Infors, Switzerland) containing 250 mL of expression medium, which consisted of 180 mL autoclaved YP medium (10 g/L yeast extract and 20 g/L casein peptone), 16.75 mL of filtered 1 M KH_2PO_4 pH6.0, 27.75 mL of filtered galactose (200 g/L), 5.5 mL of filtered 0.1 M $MgSO_4$, 7.9 mL absolute ethanol, 0.25 mL filtered chloramphenicol solution (25 g/L) and deionized water added to 250 mL. The yeast was cultivated at 25ºC and 600 RPM with an aeration rate of 0.1-0.2 vvm. The pH was adjusted to 6.0 with 4 M NaOH, keeping it at this value throughout the entire process. After 48 h the fed-batch (2.5 times concentrated expression medium) was started at a feed rate of 2 mL/h.

Purification of the UPO from *P. pastoris*. The culture broth of UPO mutant containing the *P. pastoris* cells was clarified by centrifugation at 6,000 × g for 50 min at 4ºC (Sorvall Evolution RC Super speed Centrifuge, Thermo Fisher Scientific, Waltham, MA, USA) and saturated ammonium sulfate solution was slowly added to give a 40% saturated solution at 4ºC. The suspension was again centrifuged at 6,000 × g for 50 min at 4ºC to discard precipitated protein. Then, the supernatant containing UPO activity was applied to a 750 mL Phenyl Sepharose FF column (GE Healthcare, Piscataway, NJ, USA) equilibrated with 20 mM Tris-HCl pH 7.0 containing ammonium sulfate (40% saturation).

Proteins were eluted within a linear gradient from 40% to 0% ammonium sulfate at a flow rate of 10 mL/min for 3 h. Fractions with UPO activity were pooled, diafiltrated and concentrated in 20 mM Tris-HCl pH 7.0 using a Vivaflow 50 cassette (10 kDa cut-off, Sartorius Stedim Biotech GmbH, Goettingen, Germany). The enzyme solution with a conductivity of 3 mS cm^{-1} was divided into two parts and consecutively loaded onto a 19-mL Q-source column, previously equilibrated with buffer 20 mM Tris-HCl 7.0 (buffer A). Proteins were eluted with a linear gradient of buffer B (20 mM Tris-HCl 7.0 containing 2 M NaCl) from 0% to 15% for 40 min and from 15% to100% in 5 min at 1 mL/min. Active fractions were pooled, diafiltrated against 50 mM potassium phosphate buffer at pH 7.0 and stored at 4ºC.

Enzyme characterization. Spectroscopic measurements, kinetic thermostability (T_{50} determination), pH activity profiles, MALDI-TOF analysis, pI determination, and kinetic parameters were performed as described previously (Molina-Espeja et al., 2014). For the N-terminal analysis, purified UPOs were resolved by SDS-PAGE and the proteins transferred to polyvinylidene difluoride (PVDF) membranes. The PVDF membranes were stained with Coomassie Brilliant Blue R-250, after which the enzyme bands were cut out and processed for N-terminal amino acid sequencing on a precise sequencer at the Core facilities of the Helmholtz Centre for Infection Research (HZI, Braunschweig, Germany).

4.3. RESULTS AND DISCUSSION

The secretion of the native UPO in *S. cerevisiae* was increased from 0.007 to 7.8 mg/L by means of directed evolution (Molina-Espeja et al., 2014). Even though this expression levels are high enough for future engineering works, another heterologous host is required to guarantee high expression in large scale fermentations. Ideally, the over-produced genetic product must keep the same properties as that of the enzyme evolved in *S. cerevisiae*. Among the possible candidates to develop the UPO tandem expression system, we chose the methylotrophic yeast *P. pastoris* since it shares with *S. cerevisiae* a similar processing of newly synthesized proteins allowing the different post-

translational steps to occur for a successful exocytosis. Indeed, *P. pastoris* has been exhaustively used for decades in large scale production of proteins rendering high cell titers in bioreactors under the control of strong promoters (Cereghino and Cregg, 2000). It is also worth noting that, with very few exceptions aside, *P. pastoris* is not a suitable host for directed evolution experiments due to its poor transformation efficiencies and the lack of proper episomal vectors (Gonzalez-Perez et al., 2012). The evolved UPO mutant from *S. cerevisiae* was the starting point for this study. Firstly, we cloned it into the expression vector pPICZ-B under the control of the methanol inducible alcohol oxidase 1 promoter (P_{AOX1}) for functional expression in *P. pastoris*. The evolved UPO harbors 9 substitutions (F12Y-A14V-R15G-A21D-V57A-L67F-V75I-I248V-F311L, mutations in the signal peptide are underlined) that furnished functional expression in *S. cerevisiae*. Bearing in mind that the native UPO cloned in *P. pastoris* showed almost undetectable expression levels (as it happens in *S. cerevisiae*, data not shown), it was reasonable to think that the beneficial mutations for secretion in *S. cerevisiae* also would boost expression levels in *P. pastoris*. To select the best transformants (*P. pastoris* can integrate from one to six copies of the foreign gene into the genome after plasmid linearization), several microfermentations were performed in 96-deep well plates. Transformants with activities values in the range of 30-40 U/L (using the ABTS-peroxidase activity assay) were selected for scale-up in 100-mL baffled flasks. Culture conditions were optimized in terms of heme supply and incubation temperature. After 72 h incubation at 30ºC using hemoglobin as heme source, clone 16 was selected (with 5,826 and 728 U/L of ABTS-peroxidase activity and NBD-peroxygenase activity, respectively). These activity values are quite close to that obtained when the evolved UPO was expressed in *S. cerevisiae* (6,500 and 1,000 U/L for ABTS and NBD, respectively) indicating that secretion levels (~8 mg/L) were maintained irrespective of the yeast used. In a bioreactor, clone 16 produced a volumetric activity of 232,000 U/L (ABTS) after 6 days, which corresponds to a production of 217 mg/L. The strong improvement of UPO production in fed-batch fermentation can be explained by the higher cell densities achieved (up to 106 g dry biomass/L; OD_{600} ~400) when compared with flask production (10 g dry biomass/L; OD_{600} ~30). As expected, UPO production

Table 4.1. Biochemical and spectroscopy features of evolved UPO expressed in *S. cerevisiae* (UPO_{sac}) and *P. pastoris* (UPO_{pic}).

Feature	UPO_{sac}	UPO_{pic}
MW (kDa)[1]	51.1	51.1
MW (kDa)[2]	35.9	35.9
Glycosylation degree (%)	30	30
N-terminal end	EPGLPPPGPL	EPGLPPPGPL
Thermal stability, T_{50} (ºC)	54.8	52.3
pI	5.5	5.5
Optimum pH for ABTS	4.0	4.0
Optimum pH for DMP	6.0	6.0
Optimum pH for NBD	6.0	6.0
*R*z, (A_{418}/A_{280})	1.8	2.4
Soret region (nm)	418	418
CT1 (nm)	570	570
CT2 (nm)	537	537

[1]Estimated by MALDI-TOF mass spectrometry. [2]Estimated from amino acid composition. *R*z, Reinheitszahl value; CT1 and CT2, charge transference bands 1 and 2, respectively.

in *S. cerevisiae* fed-batch fermentation (10,250 U/L, ABTS) was much lower due to the growth constrains (22.4 g dry biomass/L; OD_{600} ~48) generated by the ethanol toxic levels achieved during the fermentation (Cereghino and Cregg, 2000). The evolved UPO in *P. pastoris* (UPO_{pic}) was purified to homogeneity and compared with its counterpart from *S. cerevisiae* (UPO_{sac}). Both recombinant UPOs showed similar characteristics in terms of N-terminal end (the 43 amino acid long signal peptide was properly processed), molecular mass, glycosylation degrees, thermostability, optimum pH activity values, and spectroscopic properties (**Table 4.1**, **Fig. 4.1**). Kinetic parameters for peroxygenase and peroxidase activities were studied with several substrates along with aryl alcohols with distinct redox potentials showing similar catalytic efficiencies for both enzymes (**Table 4.2**). Taken together, we succeeded in transferring the evolved UPO from *S. cerevisiae* to *P. pastoris*, preserving all the biochemical properties whilst significantly increasing the production level.

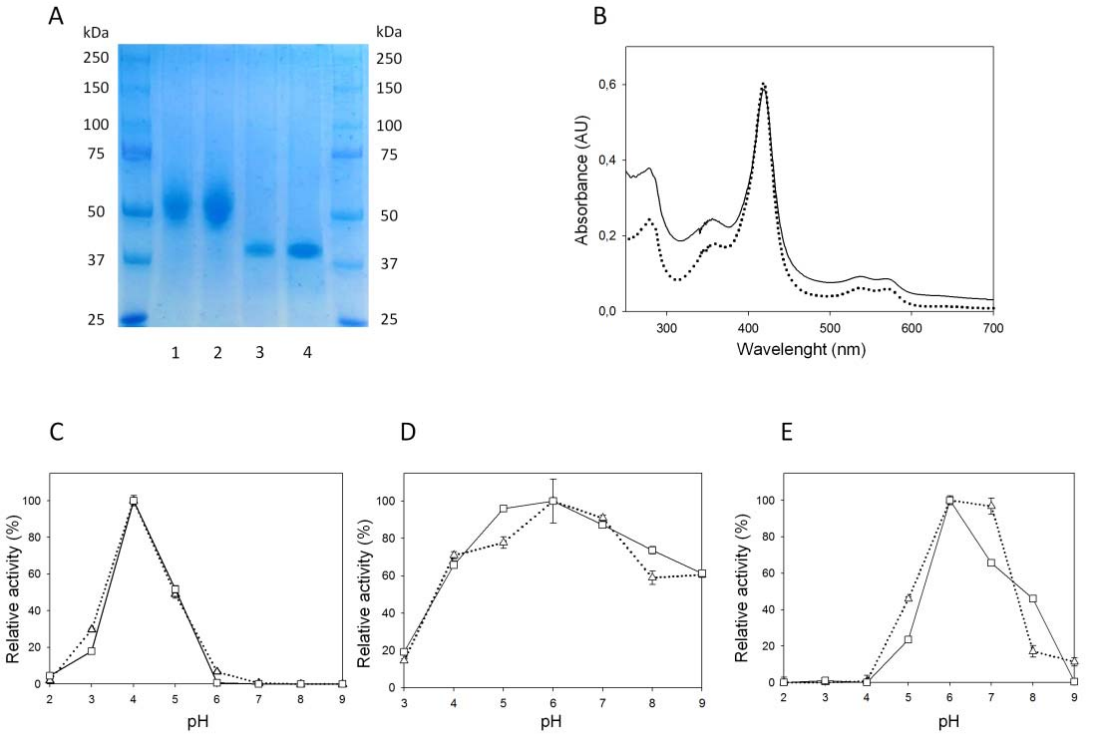

Fig. 4.1. (A) 6-12% SDS-PAGE gradient gel stained with ProtoBlue™ Safe (National Diagnostics, Atlanta, GA, USA). 1, UPO_{sac}; 2, UPO_{pic}; 3, UPO_{sac} after deglycosylation with PNGase F; 4, UPO_{pic} after deglycosylation with PNGase F. (B) Spectroscopic characteristics of UPO_{sac} (straight line) and UPO_{pic} (dotted line). (C), (D) and (E) pH activity profiles for UPO_{sac} (straight line, squares) and UPO_{pic} (dotted line, triangles) with ABTS, DMP and NBD, respectively. UPO activity was normalized to the optimum activity value and each point represents the mean and standard deviation of three independent experiments.

4.4. CONCLUSIONS

So far, only 3 UPO genes have been identified, homologously expressed and biochemically characterized in *Coprinellus radians, Marasmius rotula* and *Agrocybe aegerita* (Ullrich et al., 2004; Anh et al., 2007; Gröbe et al., 2011). The latter was used for the first case-study of directed UPO evolution to enhance its catalytic attributes while achieving heterologous expression in *S. cerevisiae* (Molina-Espeja et al., 2014). Here, this evolved UPO has been strongly over-produced in *P. pastoris* while conserving the evolved traits closing the biotechnological circle of protein engineering and enzyme production. Advances in computational genomics have permitted to identify over 1,000 UPO-like genes

Table 4.2. Kinetic parameters of evolved UPO expressed in *S. cerevisiae* (UPO_{sac}) and *P. pastoris* (UPO_{pic}).

Substrate	Kinetic constant	UPO_{sac}	UPO_{pic}
ABTS	K_m (mM)	0.048 ± 0.04	0.05 ± 0.0057
	k_{cat} (s^{-1})	395 ± 13	546 ± 19
	k_{cat}/K_m (s^{-1} mM^{-1})	8,200 ± 600	11,000 ± 2,175
NBD	K_m (mM)	0.483 ± 0.095	0.85 ± 0.26
	k_{cat} (s^{-1})	338 ± 22	498 ± 77
	k_{cat}/K_m (s^{-1} mM^{-1})	700 ± 99	590 ± 101
Benzyl alcohol	K_m (mM)	2.5 ± 0.3	2.8 ± 0.5
	k_{cat} (s^{-1})	307 ± 15	524 ± 35
	k_{cat}/K_m (s^{-1} mM^{-1})	124 ± 11	190 ± 20
Veratryl alcohol	K_m (mM)	7.9 ± 0.7	6.2 ± 1.1
	k_{cat} (s^{-1})	121 ± 5	203 ± 13
	k_{cat}/K_m (s^{-1} mM^{-1})	15 ± 1	32 ± 4
H_2O_2	K_m (mM)	0.49 ± 0.06	1.53 ± 0.08
	k_{cat} (s^{-1})	238 ± 8	676 ± 24
	k_{cat}/K_m (s^{-1} mM^{-1})	500 ± 42	442 ± 120

ABTS kinetic constants for UPO were estimated in 100 mM sodium phosphate/citrate pH 4.0 containing 2 mM H_2O_2; for the rest of the substrates in 100 mM potassium phosphate pH 7.0 containing 2 mM H_2O_2 (benzyl and veratryl alcohols) or 1 mM H_2O_2 (NBD). H_2O_2 kinetic constants were estimated using benzyl alcohol as reducing substrate at the corresponding saturated conditions.

in databases, many of them becoming possible candidates for future heterologous functional expression (Martinez et al., 2014). Indeed, without previous isolation and characterization, UPO genes from the genomes of *Coprinopsis cinerea* and from a soil mould were recently expressed in *Aspergillus oryzae* by Novozymes (Copenhagen, Denmark) supporting this approach (Babot et al., 2013; Peter et al., 2014). The use of compatible tandem expression systems for protein engineering in *S. cerevisiae* (paying special attention to directed evolution and hybrid approaches) and over-production (*e.g.* in *P. pastoris* or *A. oryzae*) is an efficient way to design potential enzymes for different biotechnological purposes as it has already been demonstrated with peroxidases, laccases and cellobiose dehydrogenases, among other examples (Cherry et al., 1999; Morawski et al., 2000; Mate et al., 2013c; Sygmund et al., 2013). In the upcoming years, we foresee the common use of tandem expression systems for

UPOs engineering and production aiming to convert these group of enzymes into highly efficient industrial biocatalysts.

AUTHOR CONTRIBUTION

Patricia Molina-Espeja carried out the directed UPO evolution, the production and the purification of the UPO_{sac} as well as the characterization of UPO_{pic} and UPO_{sac}. Su Ma produced UPO_{pic} and UPO_{sac} in fed-batch fermentation and carried out UPO_{pic} purification. Diana M. Mate was in charge of the cloning of the UPO_{pic} and the optimization of fermentation conditions previous to bioreactor. Roland Ludwig supervised the work for the production of UPO in the bioreactor and the purification of the variant. Miguel Alcalde conceived the project, supervised its development and wrote the manuscript.

ACKNOWLEDGEMENTS

The laboratory of M.A. gratefully acknowledges the financial support received from the EU (FP7-KBBE-2013-7-613549-INDOX,FP7-People-2013-ITN-607793, COST-Action CM1303 Systems Biocatalysis) and the Spanish Government (BIO2010-19697-EVOFACEL, BIO2013-43407-R-DEWRY and CAMBIOS-RTC-2014-1777-3 projects).

SYNTHESIS OF 1-NAPHTHOL BY A NATURAL PEROXYGENASE ENGINEERED BY DIRECTED EVOLUTION

5

SYNTHESIS OF 1-NAPHTHOL BY A NATURAL PEROXYGENASE ENGINEERED BY DIRECTED EVOLUTION

Patricia Molina-Espeja, Marina Cañellas, Francisco J. Plou, Martin Hofrichter, Fatima Lucas, Victor Guallar, Miguel Alcalde

ChemBioChem, 2016, En prensa.

http://dx.doi.org/10.1002/cbic.201500493

There is an increasing interest in enzymes that catalyze the hydroxylation of naphthalene under mild conditions and with minimal requirements. To address this challenge, an extracellular fungal aromatic peroxygenase with mono(per)oxygenase activity was engineered to convert naphthalene selectively into 1-naphthol. Mutant libraries constructed by random mutagenesis and DNA recombination were screened for peroxygenase activity on naphthalene together with quenching of the undesired peroxidative activity on 1-naphthol (one-electron oxidation). The resulting double mutant (G241D-R257K) obtained from this process was characterized biochemically and computationally. The conformational changes produced by directed evolution improved the substrate´s catalytic position. Powered exclusively by catalytic concentrations of H_2O_2, this soluble and stable biocatalyst has a total turnover number of 50 000, with high regioselectivity (97%) and reduced peroxidative activity.

5.1. INTRODUCTION

Currently, around 40 000 tons of 1-naphthol (naphthalene-1-ol) are generated each year to fulfill the need to produce herbicides, insecticides, pharmaceuticals and dye precursors (Booth, 2000; Jegannathan and Nielsen, 2013). The manufacturing process involves the use of hazardous chemical catalysts with low turnover numbers and poor regioselectivity, and it is associated with elevated energy consumption, high costs and the release of harmful waste products (Kudo et al., 1976; Schuster and Seid, 1979; Calinescu et al., 1994a, b y c). Oxygenases that perform regioselective oxyfunctionalization of aromatic rings would offer a greener alternative to production by standard chemical methods. Accordingly, the manufacture of 1-naphthol with the aid of enzymes should ideally take place in a *one-pot* process under mild conditions [room temperature, atmospheric pressure and essentially aqueous solution (with small amounts of organic co-solvents)], while reducing both the energy required and the noxious waste products that result from chemical synthesis (Beilen et al., 2003; Bühler and Schmid, 2004; Urlacher and Schmid, 2006; Ullrich and Hofrichter, 2007). To date, most studies of the biocatalytic synthesis of 1-naphthol have focused on monooxygenases. In particular, over the years P450 monooxygenases have been designed for different purposes, from the selective hydroxylation of alkanes (including terminal hydroxylation) to the unnatural olefin cyclopropanation by carbene transfer (Joo et al., 1999; Cirino and Arnold, 2003; Meinhold et al., 2006; Coelho et al., 2013). These enzymes can transform naphthalene into 1-naphthol either by harnessing the peroxide shunt pathway or through their natural NAD(P)H-dependent activity. More recently, directed evolution of toluene *ortho*-monooxygenase (TOM) with a whole-cell biocatalytic system was described (Canada et al., 2002; Rui et al., 2004; Garikipati et al., 2009). However, poor enzyme stability and reliance on expensive redox cofactors and reductase domains have so far precluded the practical application of these enzymes in specific industrial settings.

Over a decade ago, the first “true natural” aromatic peroxygenase was discovered (EC 1.11.2.1; also referred to as unspecific peroxygenase, UPO) (Ullrich et al., 2004). This enzyme was recently classified as a member of the

new heme-thiolate peroxidase superfamily (HTP), along with chloroperoxidase (CPO) from *Caldariomyces fumago*, even though CPO is not capable of transferring oxygen to aromatic rings or *n*-alkanes (Hofrichter et al., 2010). The properties of UPO resemble those of P450s in terms of the selective C-H oxyfunctionalization of organic compounds. However, UPO is an extracellular, highly active and stable enzyme, and it does not depend on expensive redox cofactors or auxiliary flavoproteins. UPO is "fueled" by stoichiometric concentrations of H_2O_2, which serves both as an enzyme co-oxidant (*i.e.* primary electron acceptor) and as a source of oxygen. Thus, with minimal requirements UPO is capable of performing diverse transformations of great complexity and relevance for organic synthesis, such as the hydroxylation of aromatic and aliphatic compounds, the epoxidation of olefins, the N- and S-oxidation of heterocycles or the cleavage of ethers, to name but a few (Hofrichter and Ullrich, 2014). Over 300 substrates (a number that is still growing) for UPO have already been reported; among these, naphthalene can be converted to 1-naphthol through an epoxide intermediate (as previously described for P450s). Apart from its natural mono(per)oxygenase activity through two-electron monooxygenation, similar to that in the P450 shunt pathway (confirmed by experiments with ^{18}O-labeled H_2O_2), UPO also displays peroxidative activity towards phenolic substrates and other compounds through a one-electron oxidation route (Kluge et al., 2009). This convergence of two such activities in the same protein could become a problem from the point of view of applications, because UPO hydroxylation products are always found along with varying amounts of oxidation byproducts. This is especially true for aromatic hydroxylation reactions in which the product(s) (phenolics) released by peroxygenase activity can serve as reducing substrate(s) of the peroxidative activity, the latter promoting the formation of phenoxyl radicals and quinones that can undergo undesired nonenzymatic polymerization and affect the overall production yields.

In this work we have employed directed evolution to tailor a UPO from the edible mushroom *Agrocybe aegerita* (*Aae*UPO1) for the efficient regioselective synthesis of 1-naphthol. Mutant libraries were constructed and expressed in yeast, yielding a final variant that was characterized comprehensively, and its use in the reaction to synthesize 1-naphthol was

studied in depth. To obtain a detailed atomic explanation of the effects of the mutations, we also performed ligand migration and quantum chemical simulations.

5.2. RESULTS AND DISCUSSION

Directed evolution approach

Our departure point was a UPO mutant (PaDa-I) that we had previously created by directed evolution in *Saccharomyces cerevisiae* (Molina-Espeja et al., 2014). PaDa-I harbors 9 mutations (F12Y-A14V-R15G-A21D-V57A-L67F-V75I-I248V-F311L: the mutations in the signal peptide are underlined) that enhance its functional expression in yeast (8 mg L^{-1} in *S. cerevisiae* and over 200 mg L^{-1} in *Pichia pastoris*) (Molina-Espeja et al., 2015). At the same time this mutant retains strong activity and stability, particularly in terms of temperature and the presence of co-solvents. Here, mutant libraries of UPO were constructed by random mutagenesis, staggered extension process (StEP) recombination and *in vivo* shuffling and were explored for 1-naphthol synthesis. A sensitive ad hoc dual assay was designed to cap the peroxidative activity on 1-naphthol while protecting the peroxygenase activity on naphthalene (**Fig. 5.1**).

After only two rounds of directed evolution (~4000 clones screened), we identified the double mutant G241D-R257K (termed JaWa) which displayed a twofold improvement in peroxygenase activity and half the peroxidative activity of the parent (**Fig. S5.1** in the Supporting Information).

Biochemical characterization

PaDa-I and JaWa variants were produced, purified to homogeneity (Reinheitszahl value *R*z [A_{418}/A_{280}] ~2] and characterized biochemically. The general spectral characteristics, molecular weight, N-terminal processing and degree of glycosylation were maintained for both the parent and the mutant enzymes (**Table 5.1**).

JaWa showed improved thermostability (with a 2ºC increase in the T_{50} value, defined as the temperature at which the enzyme retains 50% of its activity after a 10 min incubation) and strong stability in the presence of

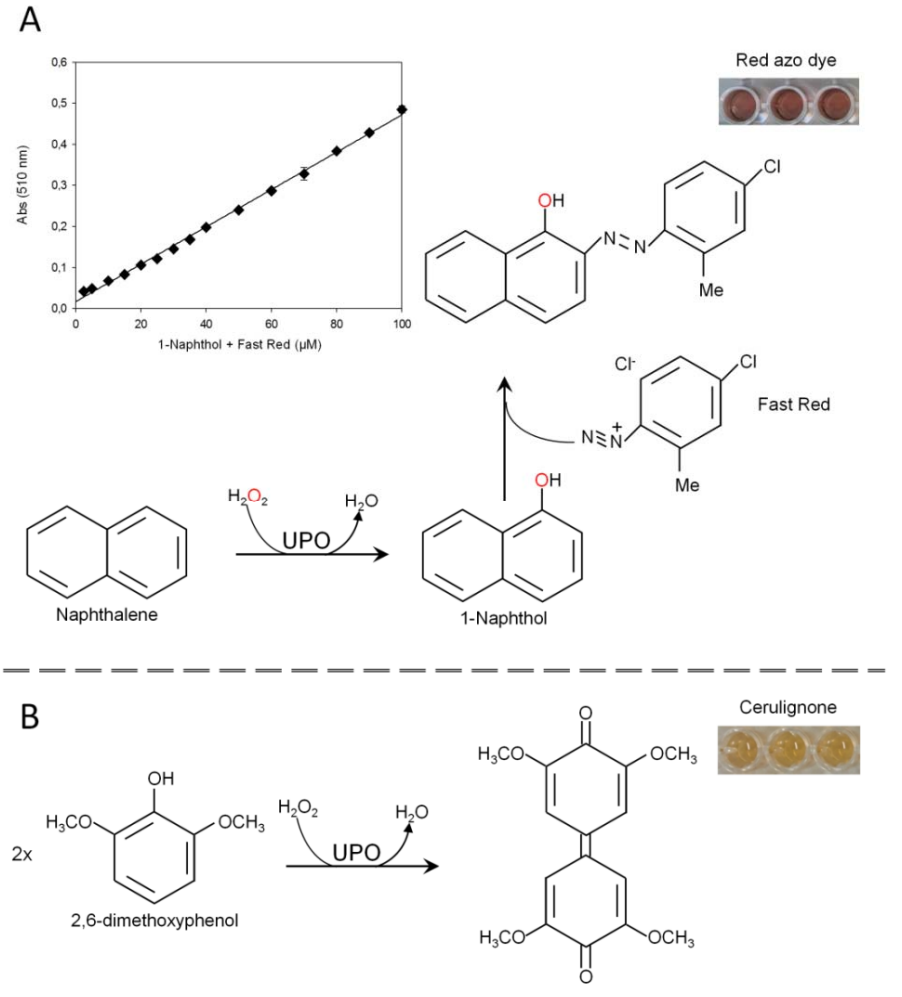

Fig. 5.1. Dual screening assay for naphthalene transformation by UPO. (A) For positive selection (peroxygenase activity), mutant libraries were screened with naphthalene such that the formation of the colorless 1-naphthol could be detected by use the Fast Red reagent (Zollinger, 2004). This compound couples specifically to 1-naphthol to form a red azo dye that can be readily measured at 510 nm (ε_{510} = 4 700 M^{-1} cm^{-1}), at which interference with the culture broth is minimal (the inset shows the linearity and the limit of detection of the assay). (B) For the negative criterion of the assay (peroxidative activity), we used a surrogate substrate (the aromatic 2,6-dimethoxyphenol, DMP) that can be oxidized by UPO to form the orange-colored cerulignone (ε_{469} = 27 500 M^{-1} cm^{-1}). The coefficient of variance for both assays was below 12%.

acetonitrile that is used to keep naphthalene in solution (solubility in pure water 31.7 mg L^{-1}, **Fig. S5.2**). Naphthalene transformation by JaWa and PaDa-I was analyzed by HPLC-PDA (photodiode array detector). Naphthalene oxygenation by *Aae*UPO1 occurs through an unstable naphthalene 1,2-oxide intermediate, which undergoes rapid hydrolysis at acid pH into naphthol (1- and 2-naphthol) (Kluge et al., 2009). Accordingly, we first measured the product distribution

Table 5.1. Biochemical features of PaDa-I and JaWa variants.

Biochemical and spectroscopy features	PaDa-I	JaWa
MW [Da][a]	52 000	52 000
MW [Da] [b]	51 100	51 100
MW [Da] [c]	35 914	35 944
Degree of glycosylation [%]	30	30
N-terminal end	EPGLPPPGPL	EPGLPPPGPL
Thermal stability, T_{50} [ºC][d]	57.6	59.7
pI	5.5	5.3
Optimum pH for ABTS	4.0	4.0
Optimum pH for DMP	6.0	6.0
Optimum pH for naphthalene	6.0	6.0
R_Z, (A_{418}/A_{280})	1.8	2.3
Soret region [nm]	418	418
CT1 [nm]	570	570
CT2 [nm]	537	537

[a]Estimated by SDS-PAGE. [b]Estimated by MALDI-TOF mass spectrometry. [c]Estimated from amino acid composition. [d]Estimated from culture supernatants.

after stopping a 15 min reaction with HCl. Both PaDa-I and JaWa showed similar regioselectivity (92% 1-naphthol, 8% 2-naphthol), whereas JaWa produced significantly more 1-naphthol (156% relative to PaDa-I) without any formation of the 1-naphthol oxidation product -1,4-naphthoquinone- being detectable (**Fig. 5.2A**). Similar behavior was observed when we followed the reaction for longer (270 min at pH 7.0 without stopping the reaction by adding HCl); this indicates that the chemical conversion of naphthalene 1,2-oxide into naphthols also occurs at neutral pH, although at lower rates. Moreover, traces of 1,4-naphthoquinone were detected (**Fig. 5.2B-D**). Whereas the formation of the epoxide intermediate by both enzymes reached a plateau at ~40 min (due to oxidative damage caused by H_2O_2), the regioselectivity was enhanced to 97% of 1-naphthol. This result is in good agreement with the loss of selectivity observed when HCl is used to stop the reaction due to the increased reactivity of the epoxide intermediate in an acid environment (Kluge et al., 2009). In terms of production yields, the differences between the mutants were even more pronounced (*i.e.* 0.14 and 0.32 mM 1-naphthol for PaDa-I and JaWa, respectively), whereas the products produced were similar when analyzed by

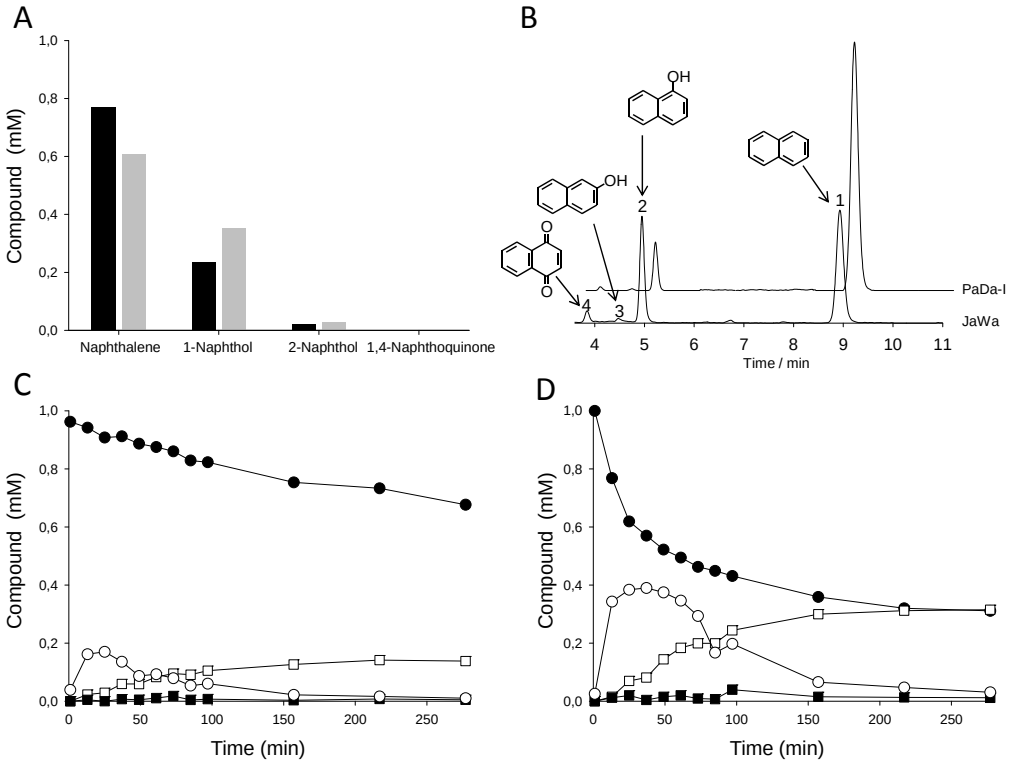

Fig. 5.2. Naphthalene conversion by evolved UPOs. (A) Product distribution after a 15 min reaction stopped with HCl (PaDa-I, black bars; JaWa, grey bars). Reactions were performed at room temperature and the reaction mixture contained 6.6 nM of purified enzyme, 1 mM naphthalene, 20% acetonitrile and 1 mM H_2O_2 in 100 mM potassium phosphate buffer pH 7.0 (1 mL final volume). After 15 min, the reaction was stopped with 20 µL of 37% HCl and the mixture was analyzed by HPLC-PDA. (B) HPLC elution profiles after a reaction time of 270 min: 1) naphthalene, 2) 1-naphthol, 3) 2-naphthol, 4) 1,4-naphthoquinone. (C) and (D) Time courses of the reactions over 270 min at pH 7.0 with PaDa-I and JaWa, respectively (without stopping of the reactions by adding HCl). ●: naphthalene; ○: naphthalene 1,2-oxide, □: 1-naphthol; ■: 2-naphthol. The total turnover numbers (TTNs, reported as µmol product/µmol enzyme) were estimated from the 1-naphthol concentration after 270 min.

mass spectrometry (**Fig. S5.3**). We calculated total turnover numbers (TTNs) of approximately 50 000 for JaWa as opposed to 20 000 for the PaDa-I parent. When the kinetic parameters of the peroxygenative and peroxidative activities of both enzymes were determined (**Table 5.2**), the k_{cat}/K_m value (catalytic efficiency) of JaWa for naphthalene hydroxylation was increased 1.5-fold, whereas the peroxidative activity was partially suppressed, with a dramatic three- to 12-fold decreases in catalytic efficiencies for the peroxidative substrates 2,6-DMP and ABTS (2,2'-azino-bis(3-ethylbenzothiazoline-6-sulfonic acid), respectively. Moreover, the k_{cat}/K_m value of H_2O_2 with benzyl alcohol as reducing substrate was also affected.

To ascertain how the decrease in the peroxidative activity affected the TTN for the hydroxylation of naphthalene, we measured the turnover rate [μmol product per μmol enzyme per min] for the conversion of 1-naphthol to 1,4-naphthoquinone by HPLC. Although the catalytic rate of PaDa-I for 1-naphthol was already low (200 min^{-1}), it dropped further to 92 min^{-1} in JaWa, with a ~1.5-fold reduction in the 1,4-naphthoquinone:1-naphthol molar ratio (**Fig. 5.3A**). This effect could also be visualized, because the polymeric products formed through the non-enzymatic coupling of the phenoxyl radicals produced by PaDa-I are colored (Joo et al., 1999) (inset in **Fig. 5.3A**).

Table 5.2. Kinetic constants for the PaDa-I and JaWa variants.

Substrate	Kinetic constants	PaDa-I	JaWa
ABTS	K_m (μM)	48.0 ± 4.5	181 ± 22
	k_{cat} (s^{-1})	395 ± 13	125 ± 5
	k_{cat}/K_m ($s^{-1}\,M^{-1}$)	$8.2 \times 10^6 \pm 6 \times 10^5$	$6.9 \times 10^5 \pm 6.3 \times 10^4$
DMP	K_m (μM)	126 ± 14	866 ± 108
	k_{cat} (s^{-1})	68 ± 2	142 ± 8
	k_{cat}/K_m ($s^{-1}\,M^{-1}$)	$5.4 \times 10^5 \pm 4.8 \times 10^4$	$1.6 \times 10^5 \pm 1.2 \times 10^4$
Naphthalene	K_m (μM)	578 ± 106	127 ± 27
	k_{cat} (s^{-1})	229 ± 17	78 ± 3
	k_{cat}/K_m ($s^{-1}\,M^{-1}$)	$4.0 \times 10^5 \pm 4.0 \times 10^4$	$6.2 \times 10^5 \pm 1.1 \times 10^5$
H_2O_2	K_m (μM)	486 ± 55	1,250 ± 300
	k_{cat} (s^{-1})	238 ± 8	447 ± 40
	k_{cat}/K_m ($s^{-1}\,M^{-1}$)	$5.0 \times 10^5 \pm 4.2 \times 10^4$	$3.6 \times 10^5 \pm 5.9 \times 10^4$

The kinetic constants for ABTS were measured in 100 mM sodium phosphate/citrate buffer pH 4.0 containing 2 mM H_2O_2, whereas the rest of the substrates were tested in 100 mM potassium phosphate pH 7.0 containing 2 mM H_2O_2 (DMP) or 1 mM H_2O_2. Varying amounts of naphthalene were added from stocks in acetonitrile to give a final co-solvent concentration of 20% v/v. For H_2O_2, benzyl alcohol was used as a reducing substrate at the corresponding saturated conditions.

It has been reported that UPO might resemble CPO in terms of the presence of different oxidation sites for peroxidative activity (Aranda et al., 2010). Thus, we examined the recent *Aae*UPO1 crystal structure to find a means to suppress alternative peroxidative pathways (Piontek et al., 2013). QM/MM calculations identified Trp24 as the most oxidizable surface residue (see computational analysis below); hence, we constructed site-directed variants by using the PaDa-I and JaWa variants as templates. The corresponding PaDa-I-W24F and JaWa-W24F mutants were compared: irrespective of the variant and the reducing substrate tested, the W24F mutation decreased the peroxidative

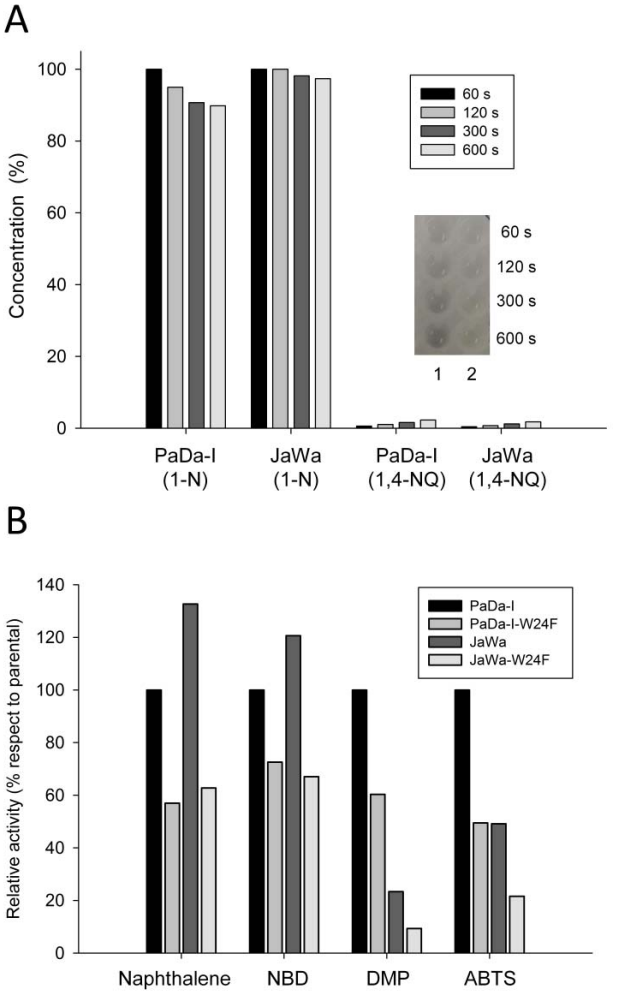

Fig. 5.3. (A) Turnover rates for 1-naphthol oxidation. Reactions (1 mL final volume) were carried out at room temperature and each mixture contained 1 mM 1-naphthol, 1mM H_2O_2, 20% acetonitrile and purified enzyme (40 nM) in 100 mM potassium phosphate pH 7.0. 1-N: 1-naphthol, 1,4-NQ: 1-4-naphthoquinone. The reactions were performed in triplicate and were stopped by addition of HCl (pH<1) after different times (60 to 600 s). Inset: colored polymeric products from 1,4-naphthoquinone; 1, PaDa-I. 2, JaWa. (B) Activities of W24F site-directed variants. The buffer used was 100 mM potassium phosphate pH 7.0, except for ABTS in which the buffer was 100 mM sodium phosphate/citrate pH 4.0. The substrate concentrations were: 0.5 mM naphthalene, 1 mM NBD, 3mM DMP and 0.3 mM ABTS. In all cases, 1 mM H_2O_2 and 15% acetonitrile were added to complete the reaction mixture. For naphthalene activity, a Fast Red assay was used (after 10 min of reaction, Fast Red was added at a final concentration of 0.5 mM and when a red color appeared and was stabilized, the absorbance was measured). The molar extinction coefficients are: ε_{510} = 4700 M^{-1} cm^{-1} for naphthalene+Fast Red, ε_{425} = 9700 M^{-1} cm^{-1} for NBD, ε469 = 27 500 M^{-1} cm^{-1} for DMP and ε_{418} = 36 000 M^{-1} cm^{-1} for ABTS.

activity by ~60% (**Fig. 5.3B**). However, this mutation also affected the peroxygenase activity, with a ~50% drop in the hydroxylation of naphthalene and the fission of 5-nitro-1,3-benzodioxole (NBD), thus suggesting that Trp24 might also play a role in the peroxygenase activity of UPO.

Computational analysis

The JaWa mutations were mapped in the *Aae*UPO1 structure with a characteristic binding pocket in which the hydrophobic Phe69-Phe121-Phe199 triad is involved in the correct orientation of aromatic compounds (**Figs. 5.4** and **S5.4**). The G241D mutation is located at the entrance of the heme access channel, whereas R257K is situated at the surface of the protein, far from any relevant catalytic sites. In order to improve our understanding of the atomic mechanistic details responsible for the observed differences between PaDa-I and JaWa variants, we turned to molecular modeling, using the PELE (protein energy landscape exploration) software (Madadkar-Sobhani and Guallar, 2013) and QM/MM methods (Guallar and Wallrapp, 2010) (see Supplementary **Movie**).

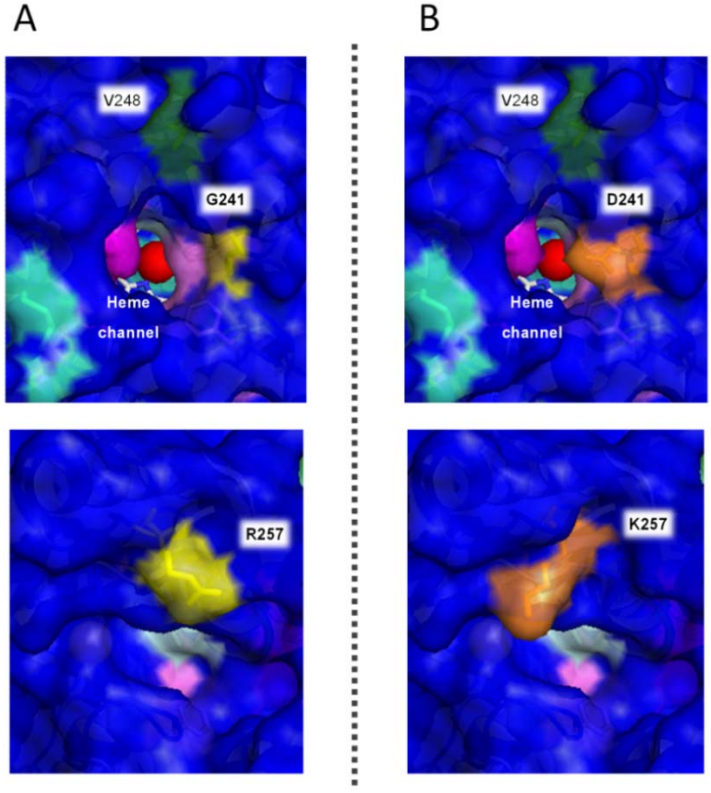

Fig. 5.4. Mutations in the evolved UPO. Protein modeling was based on the *Aae*UPO1 crystal structure (PDB accession number 2YOR). (A) PaDa-I. (B) JaWa. The G241D and R257K substitutions are depicted in yellow and orange. The V248 mutation (dark green) comes from previous directed evolution campaigns (Molina-Espeja et al., 2014). The Phe residues involved in accommodating substrates at the catalytic pocket are highlighted in pink, the Cys residues are in light green (C36 axial ligand and the C278-C319 disulfide bridge), the R189 component of the acid-base pair involved in the catalysis is tagged in light blue and the Fe^{3+} of heme is represented as a red sphere.

Peroxidative activity: global ligand migration exploration with PELE, aimed at identifying the most favorable binding sites, found the heme entrance, Trp24 and Tyr29 as the most favorable minima. Then, by the protocol previously employed to identify catalytically active surface residues in a dye-decolorizing peroxidase (Linde et al., 2015), QM/MM calculations were performed on wild type *Aae*UPO1. All potential surface oxidation sites (nine tyrosine residues and one tryptophan) were included in the quantum region, with one electron being removed and spin density computed. Furthermore, pairwise comparison was performed with the residues that showed a clear preference to be oxidized: Trp24 and Tyr47. Results showed Trp24 to be the most favorable site for peroxidative activity as described above (**Fig. S5.5A**).

Peroxygenase activity. To explain the effect of the two introduced mutations on k_{cat} and K_m, ligand exploration at the heme site was performed with PELE and use of the two *Aae*UPO1 variants: JaWa and PaDa-I. Additionally, QM/MM calculations were carried out to investigate the mutations' effect on naphthalene oxygenation.

1) Structural variations. Heme binding site PELE simulations with naphthalene show that in JaWa variant the G241D mutation induces a ~20º rotation in the aspartate backbone dihedral (**Fig. S5.5B**) leading to a shift on the loop where it is located. Along with this rotation we observed the disruption of the hydrogen bond between Thr198 and Gly241 (highly stable in PaDa-I: 86% residence time versus 0% in JaWa). These changes create space for the concomitant displacement of the α-helix that hosts the catalytic acid-base (Arg189-Glu196) pair (**Fig. 5.5**).

2) Naphthalene binding. The previously mentioned structural changes (induced by G241D), along with other minor variations in the protein's structure, caused a redistribution of the binding site occupation in JaWa mutant. Ideally, in order to facilitate epoxide intermediate formation, distances between C1 and C2 naphthalene carbon atoms and the heme catalytic oxygen should be below 3 Å for optimum reaction. As seen in **Fig. 5.6A**, analysis of naphthalene's binding site position along PELE simulations show an increased population of optimum catalytic orientations in JaWa (shorter naphthalene-heme distances).

This is in agreement with the 4.5-times decreased K_m for this variant (**Table 5.2**).

3) Hydroxylation of naphthalene. Mutation-induced structural variations have repercussions not only for naphthalene's binding site orientation, but also on its hydroxylation. The α-helix structural changes induce a new alternative position for Arg189, closer to the substrate (**Fig. 5.6B**). To compute the effect of this electrostatic environment change on naphthalene's oxidation we again turned to QM/MM calculations. Naphthalene ionization energies were computed for both PaDa-I and JaWa variants. The results show that the increase in the substrate's positive electrostatic environment increases naphthalene's ionization energy (from 213.55 kcal/mol in PaDa-I to 214.57 kcal/mol in JaWa), leading to a higher activation barrier, as shown in previous studies (Kumar et al., 2010; Ribeiro et al., 2015) and in agreement with the lower k_{cat} value for JaWa observed experimentally.

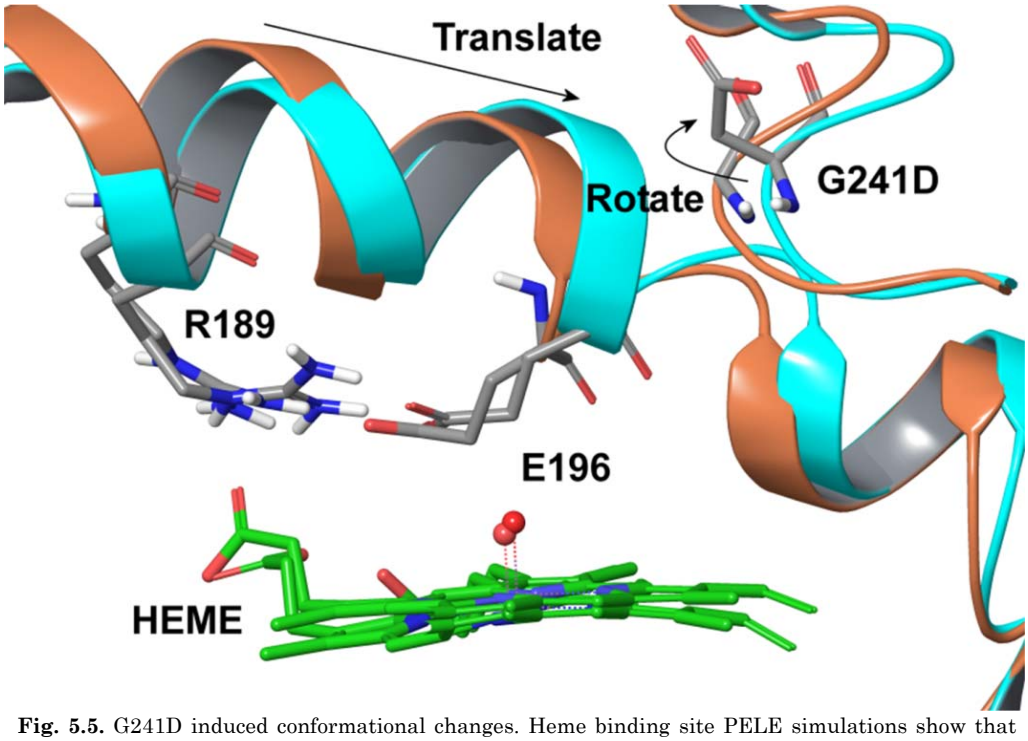

Fig. 5.5. G241D induced conformational changes. Heme binding site PELE simulations show that G241D leads to its backbone rotation, exposing Asp241 to the solvent and avoiding the hydrophobic protein environment. This rotation shifts the loop containing Asp241 and creates space for the displacement of the α-helix hosting the catalytic Arg189-Glu196 pair. JaWa shown in cyan and PaDa-I in orange, after α carbon superposition of the entire protein.

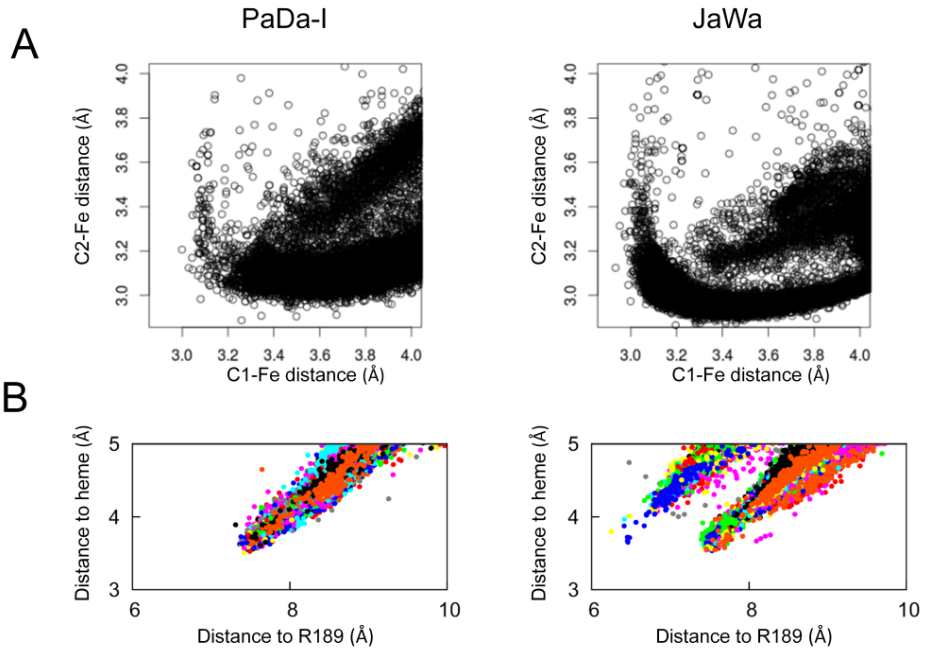

Fig. 5.6. (A) Distances between C1/C2 naphthalene carbons (hydroxylated carbons) and the heme catalytic oxygen showing a larger substrate population for optimum reactive distances (<3 Å) in JaWa. (B) Variation of naphthalene's center of mass (COM) to heme oxygen (compound I) *vs* naphthalene's COM to CZ atom in R189 in PaDa-I and JaWa along PELE simulations. Results show that in the case of JaWa the arginine side chain is in average closer to the substrate.

On the other hand, The R257K mutation was not expected to affect the hydroxylation of naphthalene but further PELE simulations with DMP as substrate show an additional access to the active heme site for this compound, not present in naphthalene simulations, that could affect both the K_m and k_{cat} for DMP. Moreover, it is known that some peroxidases have different inlets at the surface of the protein that serve for the one-electron oxidation of reducing substrates through a long-range electron transfer pathway towards the heme domain, as described here for W24F variants (Valderrama et al., 2002). The R257K substitution may affect some of these enzyme "circuits", possibly offering benefits in terms of improved thermostability through local rearrangements in secondary structures. Indeed, both the G241D and R257K mutations modified the local B factor profiles (**Fig. S5.6**).

5.3. CONCLUSIONS

To date, over 1000 UPO-like genes from fungi have been mined from genomic databases; this highlighs their widespread distribution in the fungal kingdom. Nevertheless, only three wild type UPOs have been biochemically characterized and published (from *Coprinellus radians*, *Marasmius rotula* and from the abovementioned *A. aegerita*). Some other UPOs have been identified (*e.g.,* from *Chaetomium* sp.) but they have not yet been characterized in detail (Hofrichter et al., 2015). More recently, UPO genes from the genomes of *Coprinopsis cinerea* and from a soil mold were expressed heterologously (Hofrichter and Ullrich, 2014). The *Aae*UPO1 engineered here shows the highest selectivity and TTN for the production of 1-naphthol so far reported in this enzyme superfamily. Readily secreted in an active, soluble and very stable form, this heterologous enzyme performs selective aromatic oxygenations in the absence of NAD(P)H cofactors and reductase domains. Its self-sufficient mono(per)oxygenase activity, along with a diminished peroxidative activity, make this UPO mutant a valuable biocatalyst for future synthetic applications.

5.4. EXPERIMENTAL SECTION

Reagents and enzymes: ABTS (2,2'-azino-bis(3-ethylbenzothiazoline-6-sulfonic acid)), DMP (2,6-dimethoxyphenol), benzyl alcohol, 1-naphthol, 2-naphthol, 1,4-naphthoquinone, Fast Red TR Salt hemi(zinc chloride) salt, *Taq* DNA polymerase and the Yeast Transformation kit were purchased from Sigma-Aldrich. NBD was acquired from TCI America (Portland, OR, USA) and naphthalene from Acros Organics. The Genemorph II Random Mutagenesis kit (Mutazyme II) was obtained from Agilent Technologies and the high-fidelity DNA polymerase iProof was acquired from Bio-Rad. The BamHI and XhoI restriction enzymes were purchased from New England Biolabs (Ipswich, MA, USA) and the protease deficient S. cerevisiae strain BJ5465 was from LGCPromochem (Barcelona, Spain). The Zymoprep Yeast Plasmid Miniprep kit and Zymoclean Gel DNA Recovery kit were from Zymo Research (Orange, CA, USA). The NucleoSpin Plasmid kit was purchased from Macherey-Nagel and the

oligonucleotides were synthesized by Isogen Life Science (Barcelona, Spain). All chemicals were reagent-grade purity.

Laboratory evolution: the parent PaDa-I was obtained as described elsewhere (Molina-Espeja et al., 2014). After each round of directed evolution, the PCR products were loaded onto a preparative agarose gel and purified by use of the Zymoclean Gel DNA Recovery kit. The recovered DNA fragments were cloned under the control of the GAL1 promoter of the pJRoC30 expression shuttle vector, with use of BamHI and XhoI to linearize the plasmid and to remove the parent gene. The linearized vector was loaded onto a low-melting-point preparative agarose gel and purified with the Zymoclean Gel DNA Recovery kit.

First generation: with use of PaDa-I as parent, error-prone PCR was carried out in a reaction mixture (50 μL final volume) containing dimethyl sulfoxide (DMSO, 3%), RMLN (5'-cctctatactttaacgtcaagg-3', 0.37 μM), RMLC (5'-gcttacattcacgccctccc-3', 0.37 μM), deoxynucleotide triphosphates (dNTPs, 0.8 μM, 0.2 μM each), Mutazyme II (Genemorph II kit, 0.05 U μL^{-1}) and the template (plasmid pJRoC30 containing PaDa-I, 2,822 ng, 300 ng of the target DNA). The mutagenic PCR was performed with a gradient thermocycler (Mycycler, Bio-Rad, USA) and use of the following cycles: 95°C for 2 min (1 cycle), 94°C for 45 s, 53°C for 45 s and 74°C for 3 min (28 cycles) and 74°C for 10 min (1 cycle). The PCR products (200 ng) were mixed with the linearized plasmid (100 ng) and transformed into competent *S. cerevisiae* cells for *in vivo* shuffling and cloning by using the Yeast Transformation kit. Transformed cells were plated on synthetic complete (SC) drop-out plates and incubated for 3 days at 30°C. Grown colonies were selected and subjected to the dual high-throughput screening (HTS) assay and additional rescreenings, as described below.

Second generation: the best mutants obtained from the first generation were used to perform mutagenic StEP (Zhao et al., 1998) combined with *in vivo* shuffling. The PCR reaction contained: DMSO (3%), RMLN (90 nM), RMLC (90 nM), 0.3 mM dNTPs (0.075 mM each), *Taq* DNA polymerase (0.05 U μL^{-1}) and the template (16 ng, pJRoC30 containing the four best mutants of the first generation). The PCR was performed with a gradient thermocycler and use the following cycles: 95°C for 5 min (1 cycle), 94°C for 30 s, 55°C for 20 s (90

cycles). The PCR products were mixed with the linearized vector (200 ng of each PCR product and 100 ng of linearized plasmid), transformed into competent *S. cerevisiae* cells and treated as for the first generation.

W24F site-directed variants: PCR reactions for each variant (PaDa-I and JaWa) were carried out with the primers: F24FOR (5'-ctcacccatttaagccgcttcgacctggcgatattcgtggac-3') and F24REV (5'-gtccacgaatatcgccaggtcgaagcggcttaaatgggtgag-3', mutated bases are underlined). The PCR reactions contained: 1) 50 µL final volume, DMSO (3%), RMLN (0.5 µM), F24REV (0.5 µM), dNTPs (1 mM, 0.25 mM each), high-fidelity DNA polymerase iProof (0.02 U μL^{-1}) and the templates (10 ng) and 2) 50 µL final volume, DMSO (3%), F24FOR (0.5 µM), RMLC (0.5 µM), dNTPs (1 mM, 0.25 mM each), high-fidelity DNA polymerase iProof 0.02 U μL^{-1} and the templates (10 ng). The thermocycler parameters were: 1) 98°C for 30 s (1 cycle), 98°C for 10 s, 47°C for 25 s, 72°C for 15 s (28 cycles) and 72°C for 10 min (1 cycle) or 2) 98°C for 30 s (1 cycle), 98°C for 10 s, 58°C for 25 s, 72°C for 45 s (35 cycles) and 72°C for 10 min (1 cycle). PCR products belonging to each template (200 ng each) were mixed with the linearized vector (100 ng) and transformed into *S. cerevisiae* for *in vivo* gene reassembly and cloning by IVOE (Alcalde, 2010).

High-throughput screening assay: individual clones were picked and inoculated in sterile 96-well plates (Greiner Bio-One GmbH, Germany), referred to as master plates, containing 200 µL of minimal expression medium per well [filtered yeast nitrogen base (100 mL, 6.7%), filtered yeast synthetic drop-out medium supplement without uracil (100 mL, 19.2 g L^{-1}), filtered potassium phosphate buffer (pH 6.0, 67 mL, 1 M), filtered galactose (111 mL, 20%), filtered $MgSO_4$ (22 mL, 0.1 M), absolute ethanol (31.6 mL), filtered chloramphenicol (1 mL, 25 g L^{-1}) and *dd*H_2O (to 1000 mL)]. In each plate, column 6 was inoculated with the corresponding parent and one well (H1-control) was inoculated with untransformed *S. cerevisiae* cells. The plates were sealed to prevent evaporation and incubated at 30°C, 220 RPM and 80% relative humidity in a shaker (Minitron, INFORS, Switzerland) for five days. The master plates were centrifuged (Eppendorf 5810R centrifuge, Germany) for 10 min at 2,500 *g* and 4°C. Aliquots of the supernatants (20 µL) were transferred from the master plates to two replica plates by using a liquid handler robotic station Freedom

EVO (Tecan, Switzerland). The reaction mixture (180 µL) with DMP or naphthalene was added to each replica plate with the help of a pipetting robot (Multidrop Combi Reagent Dispenser, Thermo Scientific). The DMP reaction mixture contained potassium phosphate buffer (pH 7.0, 100 mM), DMP (3 mM) and H_2O_2 (1 mM). At the same time, the same screening was carried out but with the addition of acetonitrile (10%) to assess possible changes in activity due to resistance to this organic co-solvent, needed to dissolve naphthalene. The reaction mixture with naphthalene contained potassium phosphate buffer (pH 7.0, 100 mM), naphthalene (0.5 mM), acetonitrile (10%) and H_2O_2 (1 mM). The plates were stirred briefly and the initial absorptions at 469 nm and 510 nm, for DMP and naphthalene, respectively, were recorded in the plate reader (SPECTRAMax Plus 384, Molecular Devices). After a reaction time of 10 min, Fast Red [Fast Red TR Salt hemi(zinc chloride) salt, 20 µL] was added to each well (final concentration of 0.5 mM) and the plates were incubated at room temperature until a red (naphthalene-Fast Red) or orange (DMP) color developed, then the absorption was measured again. The values were normalized against the parent in the corresponding plate. To rule out false positives, two rescreenings were carried out and a third rescreening was performed in order to assess the kinetic stability (the protocol for the rescreenings and the studies of kinetic stability - T_{50} - are described elsewhere) (Molina-Espeja et al., 2014).

Biochemical characterization: PaDa-I and JaWa variants were produced and purified as previously described (Molina-Espeja et al., 2014).

Steady-state kinetic constants: ABTS kinetic constants for UPO were estimated in sodium phosphate/citrate buffer (pH 4.0, 100 mM), containing H_2O_2 2 mM and for the rest of the substrates in potassium phosphate buffer (pH 7.0, 100 mM) containing H_2O_2 (2 mM, DMP) or H_2O_2 [1 mM, naphthalene, in acetonitrile (20%)-final concentration]. For H_2O_2, benzyl alcohol was used as a reducing substrate under the corresponding saturated conditions. Reactions were performed in triplicate and substrate oxidations were followed through spectrophotometric changes (ε_{418} = 36 000 M^{-1} cm^{-1} for ABTS, ε_{469} = 27,500 M^{-1} cm^{-1} for DMP, ε303 = 2,010 M^{-1} cm^{-1} for naphthalene, ε280 = 1,400 M^{-1} cm^{-1} for benzyl alcohol). Naphthalene kinetics were performed according to the protocol

described elsewhere (Kluge et al., 2007). To calculate the K_m and k_{cat} values, the average V_{max} was represented against substrate concentration and fitted to a single rectangular hyperbola function with the use of SigmaPlot 10.0, where parameter a was equal to k_{cat} and parameter b was equal to K_m.

HPLC analysis: the reaction mixtures were analyzed by reversed-phase chromatography (HPLC) with equipment consisting of a tertiary pump (Varian/Agilent Technologies) coupled to an autosampler (Merck Millipore) and an ACE C18 PFP (pentafluorophenyl, 15 cm x 4.6 mm) column at45 °C. Detection was performed with a PDA (Varian/Agilent Technologies, USA). The mobile phase was methanol (70%) and *dd*H_2O (30%, both with 0.1% acetic acid) at a flow rate of 0.8 mL min^{-1}. The reaction was quantified at 268 nm (from HPLC standards). For the 15 min reaction, the mixture contained purified enzyme (6.6 nM), naphthalene (1 mM), acetonitrile (20%) and H_2O_2 (1 mM) in potassium phosphate (pH 7.0, 100 mM, final volume of 1 mL). The reaction was started by the addition of the H_2O_2 and stopped by adding of HCl (20 µL, 37%); a sample (10 µL) was injected and analyzed. For the longer reactions, the conditions were as described above, but the reaction was not stopped with HCl. A sample (10 µL) was injected and analyzed at different times (1 to 270 min). To determine the kinetic values for 1-naphthol, the reaction was performed with the pure enzymes (40 nM), 1-naphthol (1 mM), acetonitrile (20%) and H_2O_2 (1 mM) in potassium phosphate (pH 7.0, 100 mM, final volume of 0.2 mL). Standard deviations were lower than 5% in all experiments.

MALDI–TOF-MS analysis and pI determination: experiments were performed with an Autoflex III MALDITOF-TOF instrument with a smartbeam laser (Bruker Daltonics). A laser power just above the ionization threshold was used in order to acquire the spectra and the samples were evaluated in the positive-ion detection mode. External calibration was performed, with the BSA from Bruker, covering the range 15 000-70 000 Da. To determine UPO's pI, purified enzyme (8 µg) was subjected to two-dimensional gel electrophoresis. These determinations were carried out at the Proteomic and Genomic Services at the CIB (CSIC, Spain).

LC/MS: a mass spectrometer with a hybrid Q-TOF mass analyzer (QSTAR, ABSciex, MA, USA) was used. The ionization source was electrospray (ESI) with methanol as the ionization phase and the inlet system was direct injection in a HPLC 1100 (Agilent Technologies, USA). The resolution of the assay was 9000 FWHM (full width at half maximum); the accuracy was 5-10 ppm and it was carried out in negative mode.

DNA sequencing: plasmid-containing variant *upo*1 genes were sequenced with an ABI 3730 DNA Analyzer/Applied Biosystems Automatic Sequencer by Secugen (Spain). The primers used were RMLN, apo1secdir (gaaggcgacgccagtatgacc), apo1secrev (ggtcatactggcgtcgccttc) and RMLC.

Computational analysis:

System preparation for molecular modeling. The structure of wild type UPO1 (purified from *A. aegerita* culture) at a resolution of 2.1 Å (PDB ID: 2YOR) was used as departure point for modeling of the PaDa-I and JaWa variants (Piontek et al., 2013). The wild type UPO1 crystal was used. Five different mutations (V57A-L67F-V75I-I248V-F311L) were introduced into model PaDa-I variant, with two additional mutations (G241D-R257K) for JaWa. Because the optimal pH for DMP and naphthalene activity is ~7, mutated structures (and the UPO1 crystal) were prepared accordingly with the aid of the Schrodinger's Protein Preparation Wizard and the H++ web server (Madhavi Sastry et al., 2013; Anandakrishnan et al., 2012). All acidic residues were deprotonated except Asp85. Histidines were δ-protonated, with the exceptions of His82 (ε-protonated) and His118 and His251 (double-protonated). To relax the systems after mutation and to investigate the mutations' possible effects on the protein structure, UPO1 variants were subjected to 5 ns molecular dynamics (MD) with Desmond (Desmond Molecular Dynamics System, version 2.2, 2009). Finally, the heme site was modeled as compound I after being fully optimized in the protein environment with quantum mechanics/molecular mechanics (QM/MM) and the use of QSite (Qsite, version 5.7, 2011). DMP and naphthalene molecules were also optimized with Jaguar (Jaguar, version 8.1, 2013) at the DFT/M06 level with the 6-31G** basis and PBF implicit solvent in order to obtain their electrostatic potential atomic charges.

Protein Energy Landscape Exploration (PELE) computational analysis. Once PaDa-I and JaWa structures were prepared and ligands optimized, heme binding site and global protein surface exploration were performed with PELE, a Monte Carlo algorithm capable of effectively sampling the protein-ligand conformational space (Madhavi Sastry et al., 2013). For the protein surface exploration, ligands were placed manually in 20 initial random positions on the protein's surface and the ligand allowed to explore freely. For each system, 160 independent 48 h simulations were performed. On the other hand, for the heme binding site exploration, the substrates were placed manually in identical positions at the entrance of the heme-access channel. From there, ligands were spawned inside the protein by PELE. Once the ligand's center of mass was within 5 Å of the heme catalytic oxygen, it was free to explore the active site cavity with 96 independent 48 h simulations.

QM/MM simulations. Hybrid quantum mechanics/molecular mechanics (QM/MM) calculations were carried out for two different purposes: to identify the most oxidizable surface residue in UPO1 protein, and to investigate the mutations' effect on naphthalene oxidation. For the first purpose, a QM/MM calculation was performed in wild type UPO1 by including all potential surface oxidation sites (nine tyrosine residues and one tryptophan) in the quantum region, subtracting one electron and computing the spin density. A subsequent QM/MM pairwise comparison was performed with residues that showed a clear preference for oxidation (Trp24 and Tyr47). Calculations were performed at the DFT M06-L(lacvp*)/OPLS level. On the other hand, to study the differences between PaDa-I and JaWa naphthalene oxygenation, five ionization energies of the substrate (located on the binding site of the variants) were computed. Energies were taken from single-point calculations by using the B97-D3(cc-pVTZ(-f)++) basis set. All QM/MM calculations were performed using Qsite.

ACKNOWLEDGEMENTS

We thank Paloma Santos Moriano (ICP, CSIC, Spain) for assistance with the HPLC and LC/MS analysis and Jesper Vind (Novozymes, Denmark) and Angel T. Martinez (CIB, CSIC, Spain) for helpful discussions. This work was supported by the European Commission projects Indox-FP7-KBBE-2013-7-613549 and Cost-Action CM1303-Systems Biocatalysis, and the National Projects Dewry [BIO201343407-R], Cambios [RTC-2014-1777-3] and OXYdesign [CTQ2013-48287-R].

5.5. SUPPLEMENTAL MATERIAL

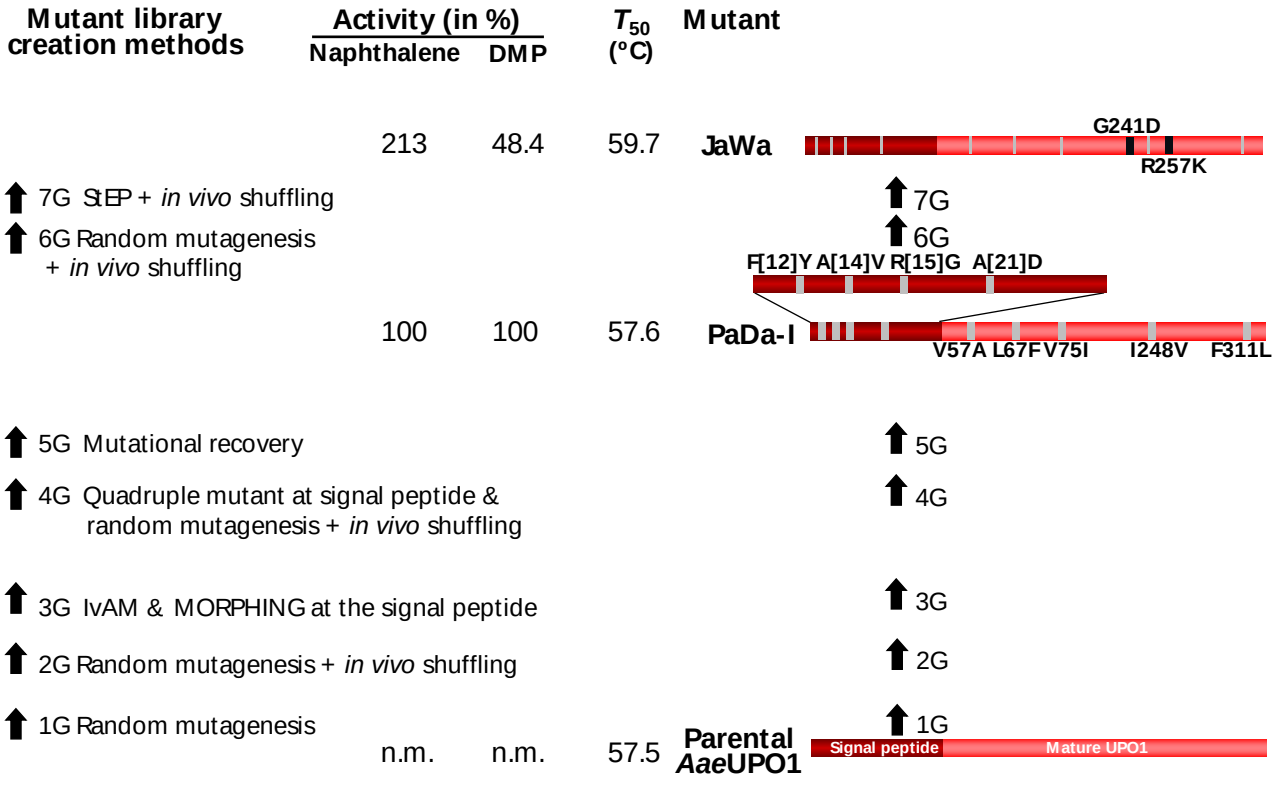

Fig. S5.1. Directed evolution of *Aae*UPO1. From rounds 1 to 5 the enzyme was improved for functional expression and activity (the accumulated mutations are shown as grey squares) (Molina-Espeja et al., 2014). Departing from the PaDa-I variant, two further rounds of evolution were performed to improve 1-naphthol synthesis (new mutations are shown as black squares). The signal peptide is represented in dark red and the mature protein in red. Thermostability (T_{50}) was estimated from the culture supernatants and the activity (given in %) was measured from *S. cerevisiae* microcultures in 96-well plates (second rescreening). n.m. not measurable.

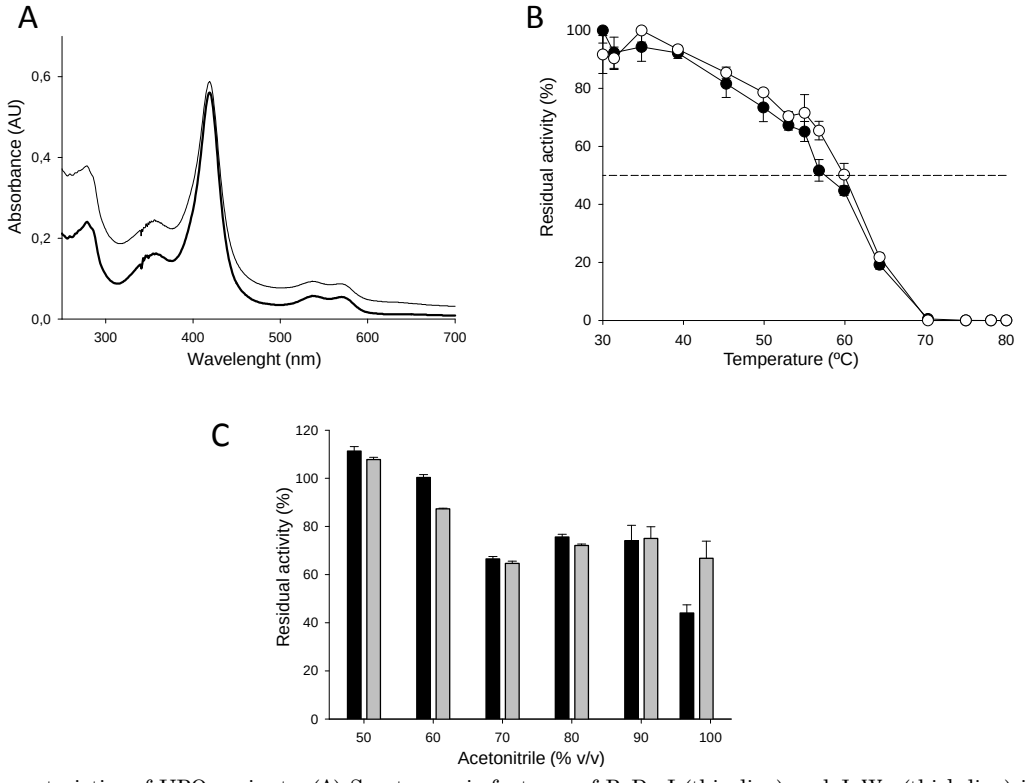

Fig. S5.2. Biochemical characteristics of UPO variants. (A) Spectroscopic features of PaDa-I (thin line) and JaWa (thick line) in the resting state. AU, arbitrary units. (B) Thermostability (T_{50}) of PaDa-I (black circles) and JaWa (white circles). Experiments were performed on fresh supernatants, and each point represents the mean and standard deviation of 3 different experiments. (C) Stability of PaDa-I (black bars) and JaWa (grey bars) at high concentrations of acetonitrile. Stability was assessed after a 5 h incubation at 20°C in potassium phosphate buffer (pH 7.0, 100 mM) containing increasing concentrations of acetonitrile (50 to 100%). At the end of the incubation, aliquots were removed and analyzed with the ABTS assay [H_2O_2 (2 mM) and ABTS (0.3 mM) in sodium phosphate/citrate buffer (pH 4.4, 100 mM)]. The error bars indicate the standard deviations.

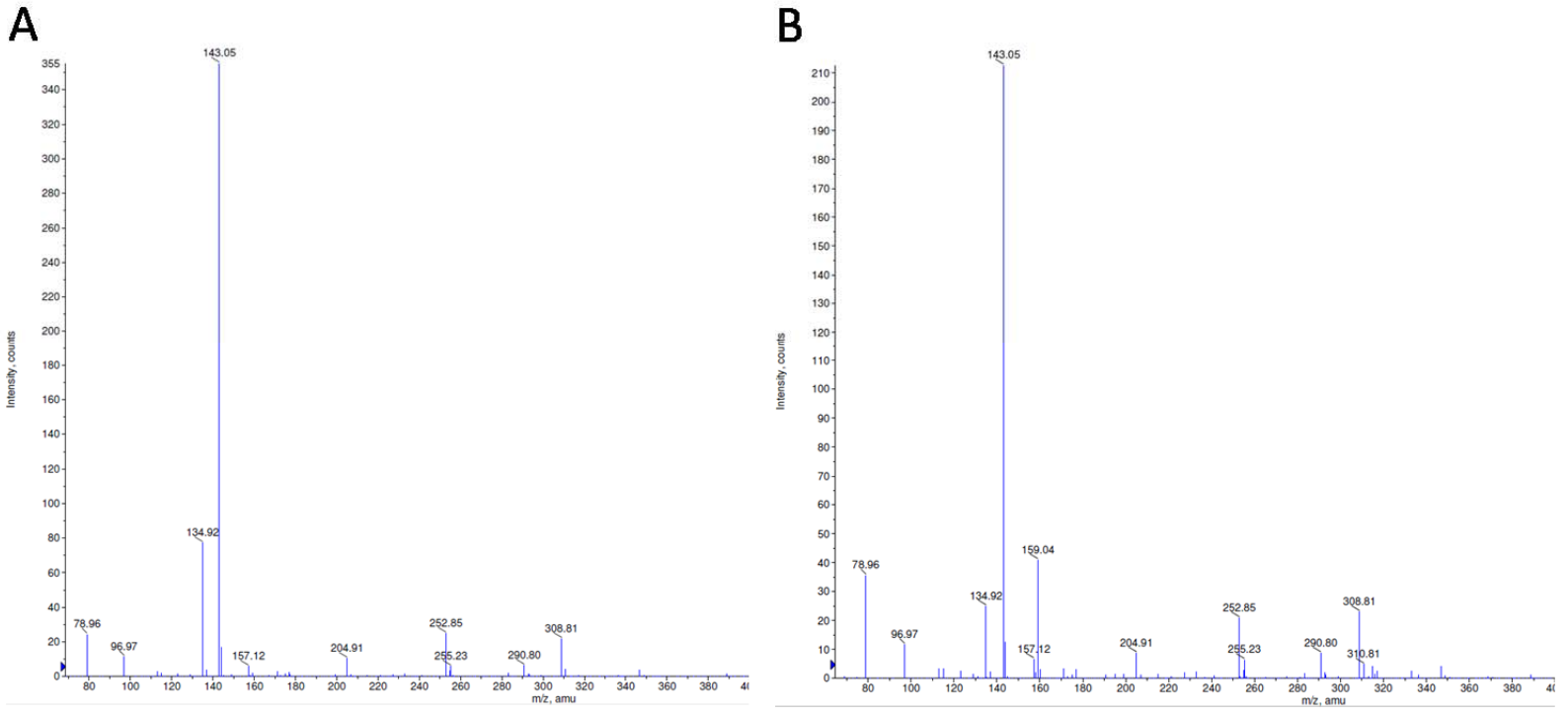

Fig. S5.3. Mass spectrometry analysis of the reaction products. The reactions mixtures with (A) PaDa-I or (B) JaWa contained purified enzyme (20 nM), naphthalene (1 mM), acetonitrile (20%) and H_2O_2 (1 mM) in potassium phosphate (pH 7.0, 100 mM). After 250 min, the reaction products were analyzed by electrospray ionization in negative mode (ESI-) with methanol as the ionization phase. The major peak represents naphthols (both 1-naphthol and 2-naphthol are equally charged upon ionization) with a $[M\text{-}H]^-$ value of 143.05 m/z. Minor peaks appeared to be identical for using PaDa-I or JaWa, which agrees with the m/z expected for the buffer used.

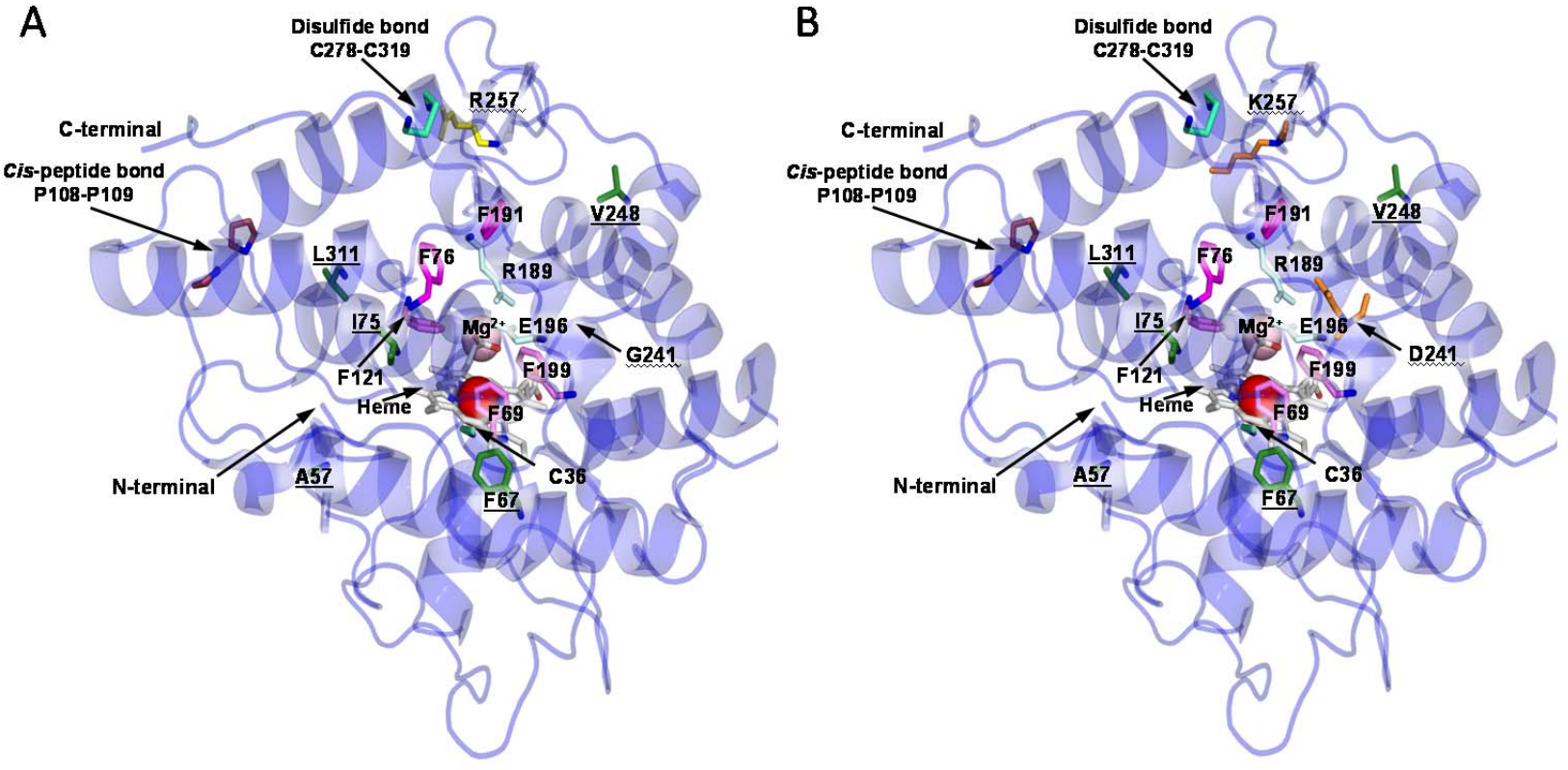

Fig. S5.4. Protein modeling of (A) PaDa-I and (B) JaWa with PyMOL Molecular Graphics System (Version 1.3 Schrödinger, LLC) based on the *Aae*UPO1 crystal structure (PDB ID: 2YOR). For PaDa-I: the new mutations relative to the native UPO are shown in dark green and underlined, and the residues in yellow and underlined in zigzag are those that are changed in JaWa. For JaWa: the new mutations are depicted in orange and underlined in zigzag. The heme is shown in CPK coloring; Fe^{3+} in red; structural Mg^{2+} in salmon; the Cys36 axial heme ligand and the disulfide bridge formed between Cys278 and Cys319 in light green; the *cis*-peptide bond between P108 and P109 is in brown; the 5 Phe residues that mediate the adjustment of the substrates, Phe69, Phe76, Phe121, Phe191 and Phe199, are in pink; and the two catalytic residues, R189 and E196, are in light cyan.

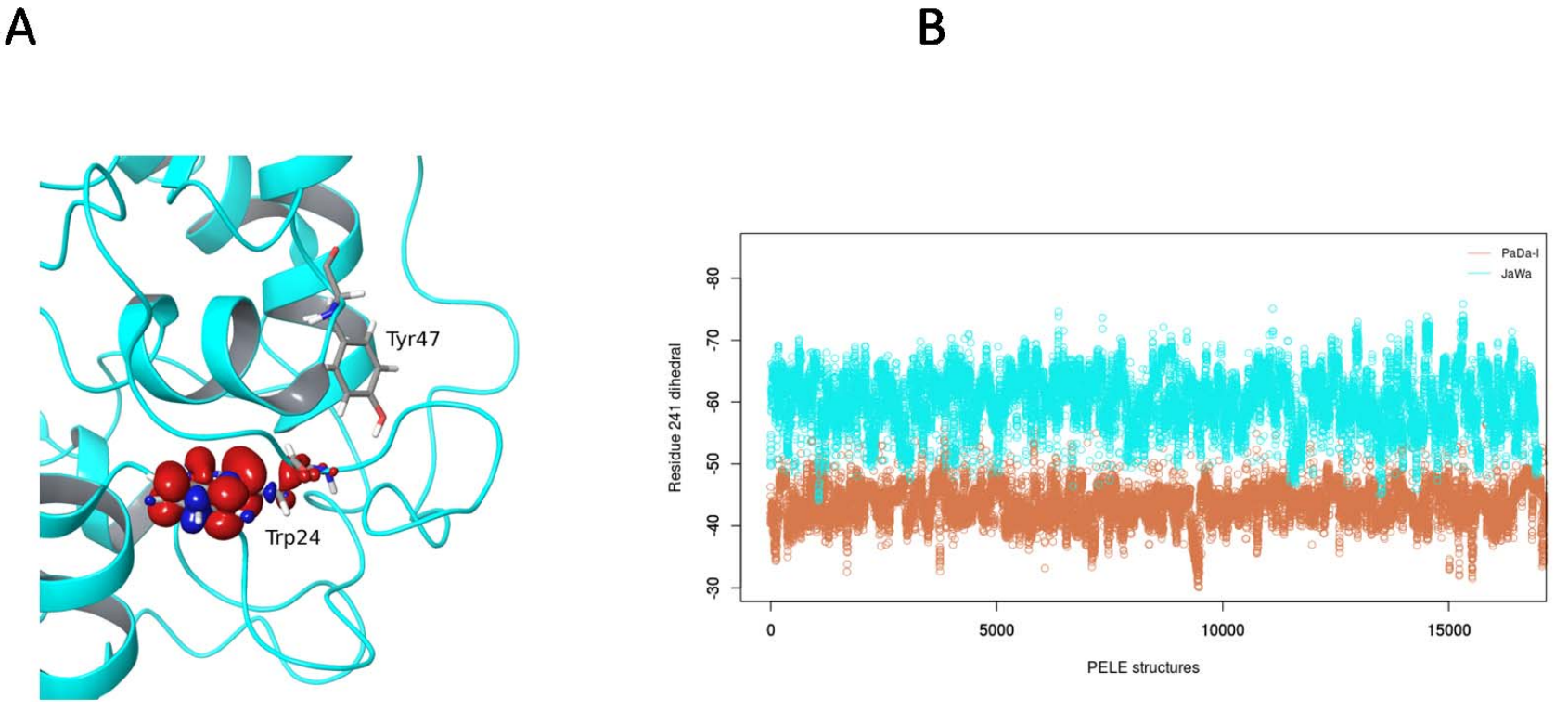

Fig. S5.5. (A) QM/MM spin density distribution on Trp24 and Tyr47 in *Aae*UPO1 when including both residues in the quantum region. (B) Variation of the 241 residue dihedral along PELE simulations. CB-CA-C-O dihedral was measured for JaWa (cyan) and HA3-CA-C-O for PaDa-I (orange). The average value for JaWa is -60.2° and -43.6° for PaDa-I.

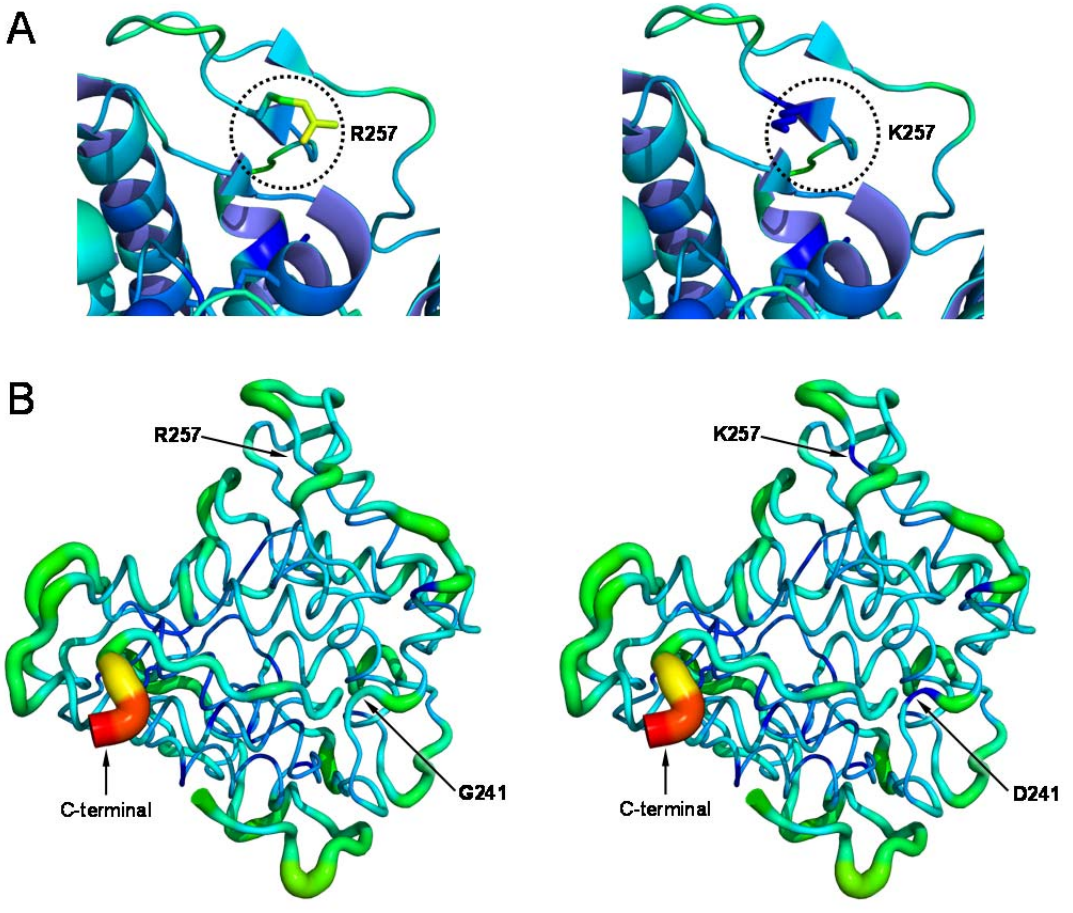

Fig. S5.6. B-factors for evolved UPOs. B-factor representation of the parental (PaDa-I, left) and JaWa variant (right), obtained using the PyMOL Molecular Graphics System (Version 1.3 Schrödinger, LLC). (A) Detail of the mutation at position 257, located at the surface. Flexibility increases in the following color code order: Blue<green<yellow<red. (B) Putty representation of the full UPO structure (the thicker the region, the more flexible it is).

RESUMEN DE RESULTADOS Y DISCUSIÓN

6

6.1. EVOLUCIÓN DIRIGIDA DE LA UPO DE *A. aegerita* (*Aae*UPO1) PARA SU EXPRESIÓN FUNCIONAL EN LEVADURAS

6.1.1. Preparación de la plataforma evolutiva en *S. cerevisiae*

El punto de partida de esta Tesis Doctoral fue el cDNA de la UPO1 de *A. aegerita* (*Aae*UPO1) (Pecyna et al., 2009). Dicha enzima fue descubierta en el año 2004 por el grupo del Prof. M. Hofrichter (Ullrich et al., 2004) y su gen aislado en 2009 (Pecyna et al., 2009). A pesar de contar con más de 30 estudios que evalúan sus actividades y potenciales aplicaciones, aún no se había logrado su expresión heteróloga, un paso fundamental para la ingeniería de sus propiedades, así como para trasladar su producción a mayor escala. En este punto, es importante subrayar que la expresión funcional heteróloga de oxidorreductasas fúngicas (especialmente ligninolíticas) es una ardua tarea que en muchas ocasiones requiere de un ajuste fino asociado a un laborioso proceso de evolución dirigida que permita adaptar el material foráneo a los requerimientos del hospedador (Garcia-Ruiz et al., 2014; Alcalde, 2015) (ver capítulo 1.2). Al contrario de lo que se ha descrito para otras peroxidasas ligninolíticas (LiP, MnP, VP) (Martinez et al., 2014), cuando se empleó *E. coli* como posible hospedador de la *Aae*UPO1 no se logró detectar actividad a partir de replegados *in vitro* de cuerpos de inclusión (comunicación personal del Prof. A.T. Martínez, CIB-CSIC). Cuando se intentó su expresión en hospedadores eucariotas (p.ej. *S. cerevisiae*, *P. pastoris*), sí observamos expresión funcional aunque las actividades resultantes fueron muy bajas (en el rango de mili-unidades/L). Para incrementar dicha expresión funcional en levaduras, en primer lugar se diseñaron 3 construcciones con la secuencia codificante de la proteína madura fusionada a 3 péptidos señal distintos. Se clonaron en *S. cerevisiae* y se sometieron a un *screening* de actividad con ABTS como sustrato. El clon con el péptido señal nativo de la UPO1 (n-UPO1) fue el que mayor actividad mostró, 149 mU/L. La evolución dirigida de péptidos señal puede ser importante cuando se hace frente a un proceso de ingeniería de proteínas con niveles de secreción extremadamente bajos (Rakestraw et al., 2009). Así, no sólo la proteína madura es la que ha de ser moldeada, sino que al incluir en la ecuación la secuencia líder, se añade un recurso muy potente que puede

incrementar sobremanera el proceso de expresión funcional y secreción. Se ha demostrado ampliamente la eficacia de esta estrategia en varios ejemplos anteriores con diversas enzimas ligninolíticas en nuestro laboratorio (Mate et al., 2010; Camarero et al., 2012; Viña et al., 2015). Por ello, se abordó la evolución dirigida conjunta del péptido señal y la proteína madura en el itinerario evolutivo de la n-UPO1 en *S. cerevisiae*, así como una evolución particularmente enfocada al péptido señal con el fin de concentrar las cargas mutacionales en dicha secuencia y promover aún más la secreción (ver abajo). En el proceso evolutivo se incorporó un ensayo de termoestabilidad cinética (basado en la determinación de la T_{50} a partir de sobrenadantes celulares) con la finalidad de conservar dicha propiedad y favorecer la "evolucionabilidad" (*i.e.* la tolerancia a la inclusión de futuras mutaciones beneficiosas pero potencialmente desestabilizantes) (Bloom et al., 2006). Como método principal de HTS se diseñó un ensayo colorimétrico dual para detectar la actividad peroxidasa y, especialmente, la actividad peroxigenasa de la enzima, ya que el objetivo final era disponer de una enzima equivalente a la UPO1 silvestre pero altamente manipulable con técnicas de ingeniería de proteínas. Tras probar diversos sustratos, finalmente la actividad peroxidasa fue evaluada con ABTS mientras que la actividad peroxigenasa se analizó con 5-nitro-1,3-benzodioxol (NBD). Este último compuesto sufre una desmetilación (O-desalquilación) por oxifuncionalización mediada por la UPO1, liberando un compuesto hidroxilado, el 4-nitrocatecol, y una molécula de ácido fórmico (ver **Fig. 1.2.7**) (Poraj-Kobielska et al., 2012; Hofrichter et al., 2015). Es importante destacar en este punto que la actividad peroxigenasa no pudo ser detectada en las primeras fases del estudio por la falta de niveles de secreción adecuados a partir de microfermentados (*i.e.* crecimiento celular en microplaca de 96 pocillos). Por ello, el ensayo con NBD tuvo que ser incorporado a partir del mutante 12C12 de la 2ª generación, lo cual garantizó la conservación de la actividad peroxigenasa.

Finalmente, las condiciones de microfermentación fueron optimizadas en lo referente a disponibilidad de oxígeno, temperatura de incubación y composición de medios de cultivo, lo que facilitó la creación de librerías de mutantes robustas y reproducibles.

6.1.2. Tácticas evolutivas

El proceso de evolución dirigida de la n-UPO1 se llevó a cabo mediante una combinación de estrategias de creación de diversidad *in vivo* e *in vitro* que permitió la selección y recombinación de mutaciones beneficiosas para la actividad y la secreción sin merma de la estabilidad enzimática. Entre las librerías diseñadas, es destacable el exitoso experimento de *in vivo shuffling* combinado con PCR mutágenica de la 2ª generación. Para ello se aprovechó la distancia entre las mutaciones de ambos clones parentales (3C2: I248V-F311L; 1A11: L67F) para promover los eventos de recombinación homóloga. Efectivamente, todos los clones seleccionados en esta generación incorporaron conjuntamente las 3 mutaciones (L67F-I248V-F311L) además de nuevas mutaciones en la secuencia líder o en la proteína madura (**Fig. 6.1**).

Otra táctica diseñada para la ocasión se basó en la evolución focalizada en la secuencia señal. En concreto, en la 3ª generación se puso a punto un método de mutagénesis aleatoria y recombinación por dominios (MORPHING: *Mutagenic Organized Recombination Process by Homologous IN vivo Grouping*, ver capítulo 3) que ofrece una gran versatilidad. Esta estrategia permite introducir mutaciones aleatorias y promover eventos de recombinación en regiones definidas por el investigador, manteniendo intactas las zonas de la secuencia que no se deseen variar. Esto se consigue amplificando las primeras mediante PCR mutagénica y las segundas mediante PCR de alta fidelidad. Con el diseño de secuencias homólogas y solapantes inter-región se posibilita que *S. cerevisiae* realice, en un único paso, el correcto ensamblado del gen completo y su clonaje con el vector de expresión (**Fig. 6.2**). Recientemente, nuestro grupo ha usado MORPHING para evolucionar la VP hacia resistencia a peróxidos (Gonzalez-Perez et al., 2014a y b), la AAO para la introducción de mutaciones consenso (Viña-Gonzalez et al., 2015), así como rubiscos bacterianas para funciones no definidas (material no publicado). Estos ejemplos son indicativos de la plasticidad de esta herramienta en la construcción de las conocidas como "*smart mutant libraries*" con las que se reduce notablemente la exploración del espacio de secuencia proteica (Sebestova et al., 2014). Los resultados de MORPHING en la secuencia señal de la UPO1 rindieron

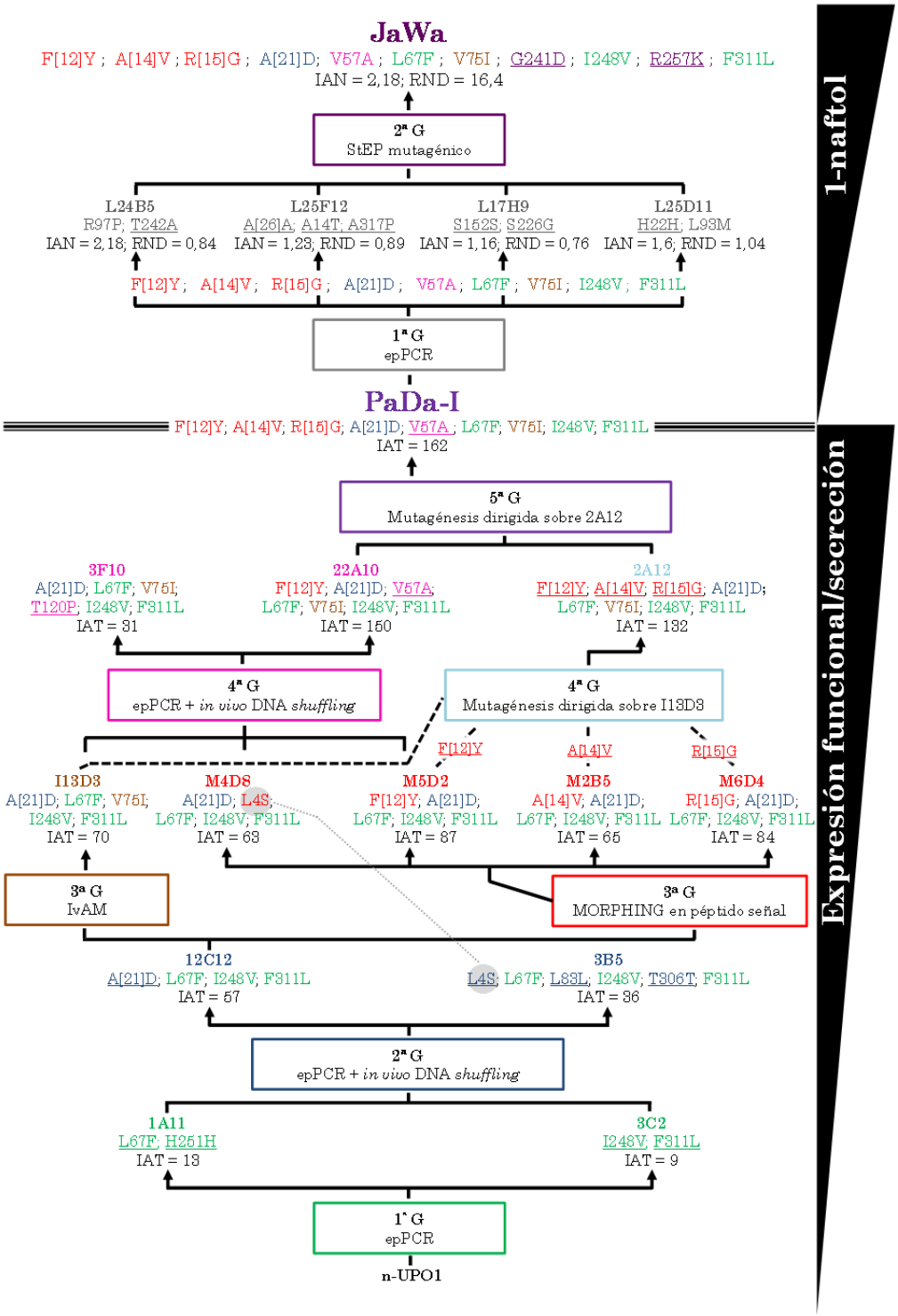

Figura 6.1. Árbol evolutivo de la *Aae*UPO1. Las nuevas mutaciones que aparecen en cada generación (G) se muestran subrayadas. IAT: incremento de actividad total, en veces (medido con ABTS en microplaca). IAN: incremento de actividad sobre naftaleno. RND: ratio actividad naftaleno/actividad DMP.

varios clones con mutaciones comprendidas entre las posiciones 12 y 15, que posteriormente se incluyeron en un único mutante mediante técnicas convencionales de mutagénesis dirigida. Etapas adicionales de mutagenésis aleatoria, *in vivo shuffling* y *mutational recovery* (mediante un análisis racional del árbol evolutivo artificial) dieron lugar al mutante final PaDa-I, con un total de 9 mutaciones (4 en la secuencia líder y 5 en la proteína madura) y unos elevados niveles de actividad y expresión funcional, tras explorar un total de 9.000 clones en 5 generaciones de evolución dirigida (**Fig. 6.1**).

6.1.3. Caracterización bioquímica

En el proceso evolutivo, se definió el incremento en actividad total como la actividad detectada a partir de sobrenadantes celulares, que de manera más precisa procede de multiplicar las mejoras en actividad específica y secreción.

Para desglosar dichas mejoras (ya que los niveles de expresión de n-UPO1 no permitían su purificación a homogeneidad), se construyó la fusión del péptido señal evolucionado de PaDa-I (n*) con la secuencia de la UPO1 madura nativa. Es importante señalar que dicha estrategia ya se había llevado a cabo por nuestro grupo con éxito durante la evolución dirigida de lacasas de alto potencial redox en levaduras (Camarero et al., 2012). El producto génico resultante n*-UPO1, así como n-UPO1 y PaDa-I fueron producidos y caracterizados bioquímicamente. Esta aproximación nos permitió deducir que las mutaciones en la secuencia señal aumentaron hasta 27 veces la secreción. Asimismo, las mutaciones en la proteína madura incrementaron tanto la actividad específica (~3,6 veces con ABTS como sustrato) como la expresión funcional (~41 veces). En suma, los niveles de expresión en levadura se fomentaron de ~0,007 mg/L a ~8 mg/L, encontrándose estos últimos dentro del mismo orden de valores alcanzados con el hongo original *A. aegerita* fermentado en biorreactor (cepa TM A1 = DSM22459, ~17 mg/L UPO1) (Ullrich et al., 2004; Hofrichter et al., 2015).

El análisis de las propiedades bioquímicas generales de la enzima evolucionada reveló características equivalentes a las de la enzima homóloga en lo referente al procesado correcto del extremo N-terminal, pI, perfiles de pH y

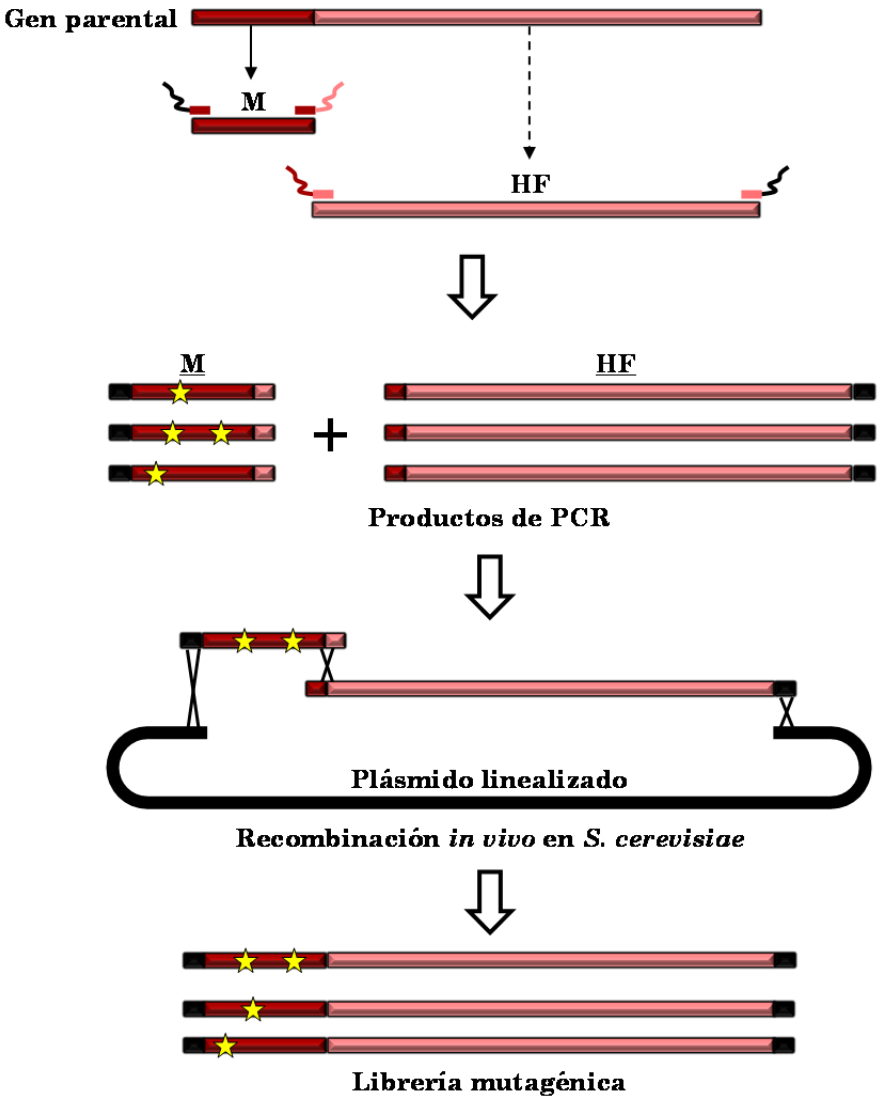

Fig 6.2. MORPHING en el péptido señal de la UPO1. El fragmento M corresponde al péptido señal (amplificado por PCR mutagénica, mutaciones representadas como estrellas amarillas) y el fragmento HF a la proteína madura (amplificada por PCR de alta fidelidad). Ambos fragmentos son co-transformados junto con el plásmido linealizado en *S. cerevisiae* para dar lugar al plásmido circular con la secuencia completa ensamblada gracias al uso de extremos solapantes.

características espectroscópicas. Sin embargo, el mutante PaDa-I mostró unos niveles de glicosilación ligeramente superiores a los del hongo, lo que es atribuible a la tendencia que muestra *S. cerevisiae* a hiperglicosilar los sitios de N-glicosilación en proteínas heterólogas (Shuster, 1991). Asimismo, el mutante evolucionado fue más estable en presencia de disolventes orgánicos, lo cual puede relacionarse con los niveles de glicosilación mencionados, así como con alguna de las mutaciones potencialmente estabilizantes. En lo referente a la

termoestabilidad, la selección precisa de variantes sin merma en sus valores de T_{50} permitió mantener prácticamente inalterada la termoestabilidad en el último mutante PaDa-I, a pesar de contener 5 mutaciones en la proteína madura. Para profundizar en este estudio, en colaboración con el Prof. J. M. Sánchez Ruiz y la Dra. V. A. Risso (departamento de Química Física, Universidad de Granada) se han realizado recientemente experimentos adicionales de calorimetría diferencial de barrido (DSC, del inglés), de los cuales se concluye que la estabilidad termodinámica es similar entre la enzima nativa homóloga y la variante PaDa-I (con valores de T_m -temperatura de desnaturalización- de 69 y 68°C, respectivamente-*scan rate* de 2°C min^{-1}). También se determinó que su desnaturalización es calorimétricamente irreversible (material no publicado). En lo referente a las constantes cinéticas de PaDa-I, se observó que mejoraron notablemente cuando se compararon con n*-UPO1 expresada en *S. cerevisiae*, y en particular, la eficiencia catalítica de la actividad peroxigenasa para NBD se incrementó 18 veces. Sin embargo, los parámetros cinéticos fueron equivalentes a los de la UPO1 expresada homólogamente en *A. aegerita*. En colaboración con la Dra. Ana Gutiérrez del Instituto de Recursos Naturales y Agrobiología de Sevilla (IRNAS-CSIC) se llevaron a cabo experimentos analíticos (GC-MS) de diversas reacciones tipo con comportamientos similares a la enzima homóloga y rendimientos mejorados en algunos casos (p.ej. en la oxidación de tetradecanol, material no publicado).

De todo este análisis se puede deducir que la UPO1 nativa en la levadura muestra actividades disminuidas respecto a su homóloga en *A. aegerita*, pero que fueron recuperadas tras 5 generaciones de mutación, recombinación y *screening*. Posiblemente, las diferencias halladas en los procesos de plegamiento y las modificaciones postraducionales (p.ej. glicosilación) entre los diferentes hospedadores puedan afectar de manera negativa a los valores cinéticos de la enzima heteróloga, como se ha descrito en estudios anteriores con otras oxidorreductasas ligninolíticas (Bulter et al., 2003; Mate et al., 2013a; Viña-Gonzalez et al., 2015).

En conclusión, el disponer del mutante PaDa-I supone tener al alcance una enzima recombinante con características equivalentes a la producida en la

naturaleza, pero con la ventaja de ser un vehículo idóneo para estudios evolutivos y/o de estructura función con los que lograr un potencial uso en diferentes procesos industriales y biotecnológicos.

6.1.4. Análisis mutacional

En lo referente a la capacidad de secreción mejorada, 2 de las mutaciones introducidas en el péptido señal, (F[12]Y y A[21]D), aumentaron la polaridad de la zona hidrofóbica de la secuencia líder, lo cual puede favorecer la formación del péptido naciente, así como su estabilidad en el medio celular. En efecto, se ha observado en estudios previos de evolución dirigida de lacasas fúngicas para expresión funcional en *S. cerevisiae*, que cambios similares (*i.e.* introducción de residuos más polares) en una región hidrofóbica resultaron beneficiosos para la secreción; esto parece estar relacionado con la interacción con la partícula de reconocimiento de señal, implicada en la translocación del polipéptido naciente al retículo endoplásmico (Mate et al., 2010; Camarero et al., 2012). Es más, el estudio de predicción de cortes peptídicos (PeptideCutter, ExPASy: http://www.expasy.org/) indica que la mutación A[21]D introduce un nuevo sitio de corte, lo que podría variar el procesamiento de la secuencia líder sin afectar a la secuencia de la proteína madura secretada (confirmado por análisis del extremo N-terminal).

La mayor parte de las mutaciones introducidas en la proteína madura fueron conservativas (cambios aminoacídicos con polaridades y cargas equivalentes), como consecuencia de la estrategia evolutiva escogida (*i.e.* no se hizo uso de un diseño enfocado mediante mutagénesis saturada, por lo que el perfil mutacional es sesgado y dependiente de las polimerasas empleadas; además, se priorizó la conservación de la estabilidad de la enzima sobre la inclusión de potenciales mutaciones beneficiosas pero desestabilizantes, como el caso de la variante 3F10 -con la mutación T120P que provoca una disminución de la actividad peroxidasa pero a expensas de la estabilidad-). De esta manera, la mayor parte de las mutaciones se localizan en zonas periféricas alejadas del centro activo, sin interacciones que parezcan relevantes para la catálisis. Aunque se puede teorizar acerca de los posibles efectos de estos cambios en la

actividad catalítica, la cristalización del mutante PaDa-I así como su estudio computacional son procesos necesarios para arrojar información relevante acerca de estas cuestiones. En este sentido, en colaboración con la Prof. J. Sanz, del IQFR (Instituto de Química Física Rocasolano, CSIC), se ha obtenido recientemente la estructura cristalográfica de PaDa-I con una elevada resolución (<1.5 Å) y un extremo N-terminal completo (los cristales procedentes de estudios previos sobre la *Aae*UPO1 nativa carecían de los 3 primeros residuos sugiriendo una posible escisión proteolítica EPG/LPP, algo que queda descartado para el mutante PaDa-I) (Piontek et al., 2013). Su análisis muestra que, como se propone en el capítulo 2, la mutación F311L hace que la entrada al bolsillo catalítico sea más amplia, modificando la posición de la Phe76, lo que puede incidir en mejoras catalíticas (**Fig. 6.3**). Además, se han obtenido datos de PaDa-I acomplejada con diferentes sustratos alojados en su bolsillo catalítico mediante *soaking* (naftaleno, alcohol veratrílico, alcohol bencílico, DMP, estireno, acetanilida y diclofenaco-material no publicado-). Se observa cómo los anillos aromáticos de todos ellos se acomodan en el mismo lugar y a distancia de Van der Waals del grupo hemo. Futuros avances en estos experimentos ayudarán a esclarecer los determinantes catalíticos de PaDa-I y a diseñar las próximas investigaciones.

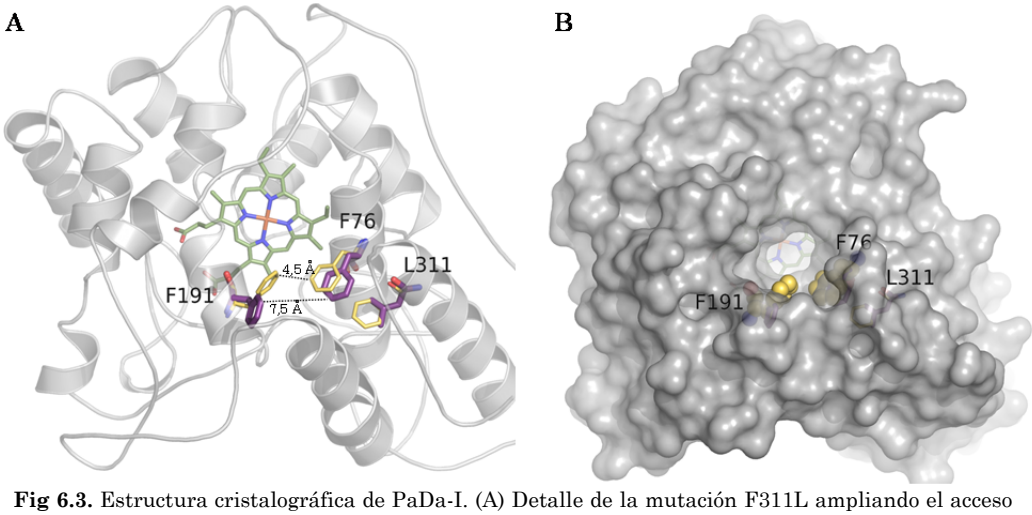

Fig 6.3. Estructura cristalográfica de PaDa-I. (A) Detalle de la mutación F311L ampliando el acceso al canal del hemo (los residuos se indican en amarillo y morado para *Aae*UPO1 y PaDa-I, respectivamente). (B) Detalle de superficie donde se aprecia el acceso al canal del hemo.

6.1.5. Sobreproducción en *P. pastoris*: sistema de expresión en tándem

En el trabajo de evolución dirigida descrito arriba, la secreción de la UPO1 (mutante PaDa-I) en *S. cerevisiae* alcanzó niveles de ~8 mg/L. Estos valores, aunque suficientes para llevar a cabo nuevas campañas evolutivas, son bajos a la hora de pensar en un proceso de producción a gran escala. Por esta razón, el empleo de un sistema de evolución/expresión en tándem puede resultar muy ventajoso. Para ello, es preciso disponer de otro hospedador heterólogo que sea capaz de expresar funcionalmente la variante en mayor cantidad sin que sus propiedades y características evolucionadas se vean alteradas. En nuestro caso, se seleccionó la levadura metilotrófica *P. pastoris*, capaz de lograr elevadas densidades celulares en biorreactor (hasta ~16 veces mayores que las de *S. cerevisiae*). Así, a partir de niveles de secreción similares, pueden obtenerse rendimientos más elevados de producción. Dada la similitud entre estos 2 hospedadores en términos de ruta secretora y modificaciones postraduccionales, la posibilidad de trasladar una enzima evolucionada en *S. cerevisiae* a *P. pastoris* (sin deteriorar las ventajas obtenidas con el proceso de ingeniería genética) resulta atractiva.

Para comprobar la aptitud de este sistema en tándem de evolución/producción, se clonó en *P. pastoris* el mutante PaDa-I y se determinó que los niveles de secreción en matraz son similares a los alcanzados en *S. cerevisiae*. Cuando se transfirió dicho clon a un biorreactor de 7 L, se consiguieron producciones de 217 mg/L, 27 veces superiores a los valores obtenidos en matraz debido a la mayor biomasa generada (*P. pastoris* pasó de 10 a 106 g de biomasa seca/L, para fermentación en matraz y biorreactor, respectivamente). Comparando las características del mutante PaDa-I producido en ambas levaduras (*i.e. S. cerevisiae* y *P. pastoris*) se concluyó que tanto las características espectroscópicas, como las bioquímicas y catalíticas resultaron similares, por lo que se garantizó la conservación de las propiedades evolucionadas tras la transferencia de hospedador.

Es importante reseñar que la mayor producción de peroxigenasa inespecífica lograda hasta la fecha se había descrito para la UPO de *M. rotula* expresada homólogamente en biorreactor (445 mg/L), mientras que *A. aegerita*

produce considerablemente menos cantidad (18 mg/L) (Hofrichter et al., 2015). En este sentido, los elevados niveles de producción en biorreactor obtenidos para el mutante PaDa-I en *P. pastoris* pueden ser aumentados mediante ingeniería del proceso. Efectivamente, en colaboración con la empresa Biópolis S.L. dentro del proyecto europeo INDOX (FP7-KBBE-2013-7-613549), se han realizado experimentos de escalado preliminar a biorreactor de 20 L con rendimientos en la producción de la variante PaDa-I de hasta ~1 g/L (resultados no publicados).

6.2. EVOLUCIÓN DIRIGIDA DE LA *Aae*UPO1 PARA LA SÍNTESIS DE 1-NAFTOL

Como se indica en el capítulo 1.1.5, la manufactura del 1-naftol en la actualidad mediante procesos químicos es altamente tóxica, de baja selectividad y eficiencia, además de conllevar elevados costes energéticos y medioambientales. Teniendo en cuenta el valor industrial de este compuesto, el uso de la biocatálisis como alternativa respetuosa con el medio ambiente para su síntesis puede resultar sumamente beneficioso. Así, se ha estudiado en profundidad el empleo de monooxigenasas capaces de insertar oxígeno de manera regioselectiva en anillos aromáticos. Por ejemplo, las P450s pueden transformar naftaleno en 1-naftol bien mediante la ruta *bypass* del peróxido o mediante su actividad NAD(P)H dependiente (Joo et al., 1999; Bernhardt, 2006). Más recientemente, también se ha descrito la evolución de la enzima tolueno *orto*-monooxigenasa (TOM) hacia la síntesis de 1-naftol y su uso en células completas (Canada et al., 2002; Rui et al., 2004). Desafortunadamente, la baja estabilidad de estas enzimas junto a los elevados requerimientos en lo que a cofactores redox de elevado coste (NAD(P)H) y dominios reductores asociados (flavoproteínas) se refiere, han supuesto un obstáculo para su uso práctico en este particular proceso industrial.

Como alternativa, la *Aae*UPO1 es la peroxigenasa inespecífica que mayor rendimiento de producción y regioselectividad en la transformación de naftaleno a 1-naftol muestra de todas las UPOs examinadas hasta la fecha (Dra. Lisbeth Kalum, Novozymes, comunicación personal). El disponer del sistema de expresión en tándem descrito anteriormente para el mutante PaDa-I supone una

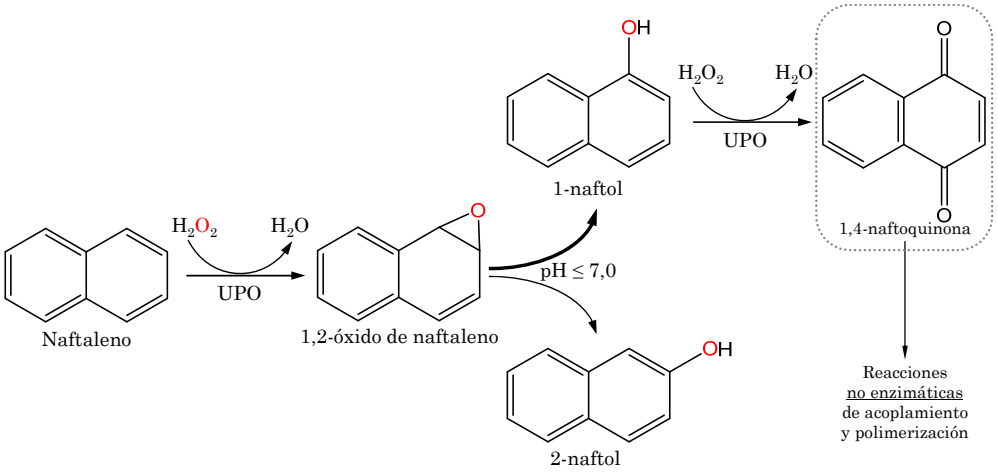

Figura 6.4. Reacción de transformación de naftaleno en naftol. A través de la actividad peroxigenasa de la UPO se forma el 1,2-óxido de naftaleno, un epóxido inestable, que deriva en 1-naftol (92-97%) y 2-naftol (3-8%). El 1-naftol actúa también como sustrato de la UPO, produciéndose 1,4-naftoquinona mediante su actividad peroxidasa. Las quinonas resultantes polimerizan por mecanismos no enzimáticos, dando lugar a precipitados visibles. El 2-naftol sufre mecanismos similares (no incluidos en la figura).

ventaja muy valiosa para diseñar y producir nuevas UPOs mutantes altamente eficientes. Así, la síntesis de 1-naftol podría ser optimizada mediante evolución dirigida a través de la mejora de su actividad peroxigenasa y la disminución de la actividad peroxidasa. Se decidió llevar a cabo esta táctica evolutiva porque la actividad peroxidasa puede resultar perjudicial en el proceso global de transformación de naftaleno en 1-naftol. En efecto, el anillo fenólico resultante de la hidroxilación del naftaleno por la UPO1 es susceptible de ser oxidado a través de la actividad peroxidasa de la enzima dando lugar a radicales fenoxilo y quinonas, que derivan en polimerizaciones no enzimáticas (**Fig. 6.4**) disminuyendo el rendimiento global y dificultando los procesos de purificación de productos.

6.2.1. Diseño del método HTS y tácticas evolutivas

Se puso a punto un método HTS dual para promover la actividad peroxigenasa (criterio de selección positiva) sobre naftaleno y reducir la actividad peroxidasa (criterio de selección negativa) sobre 1-naftol. Ambos compuestos absorben únicamente en la región UV. Se había descrito un protocolo espectrofotométrico de *screening* basado en la detección a 303 nm del máximo de absorción (con menor señal de fondo) para el 1-naftol (Kluge et al., 2007). Al

trasladar este ensayo a microfermentaciones de *S. cerevisiae*, surgieron problemas derivados de interferencias con los componentes del medio extracelular, que únicamente permitieron la selección de mutantes de secreción (resultados no publicados). Por este motivo, se decidió desarrollar un método colorimétrico reproducible y sensible que fuera específico de 1-naftol empleando el reactivo de Fast Red, un compuesto que se acopla al 1-naftol dando lugar a un colorante tipo azo (Zollinger, 2004). El protocolo fue validado para la evolución de PaDa-I en levadura (coeficientes de varianza inferiores al 12% y respuesta lineal en el intervalo de 2 a 100 μM) y se calculó un coeficiente de extinción molar (ε_{510}) de 4.700 M^{-1} cm^{-1}. En cuanto al ensayo de *screening* para actividad peroxidasa, lo más apropiado hubiera sido evaluar la ulterior transformación del 1-naftol producido por la UPO1 en 1,4-naftoquinona (*i.e.* el 1-naftol es producto mayoritario y nuevo sustrato de la enzima). Sin embargo, esta aproximación no fue posible ya que el nivel de secreción de UPO1 en microfermentaciones es muy limitado debido al escaso crecimiento celular de la levadura (con densidades ópticas ~1), por lo que la producción de 1-naftol en estas condiciones es muy baja, encontrándose fuera de los límites inferiores de detección del ensayo. Por este motivo, se decidió emplear un compuesto sustituto de tipo fenólico para el *screening* que fuera fácilmente oxidable y diera una respuesta en la zona visible, como el DMP (ε_{469} = 27.500 M^{-1} cm^{-1}). Dicho ensayo ya había sido validado con anterioridad para la evolución de ligninasas en levadura (Mate et al., 2010). Debido a la baja solubilidad del naftaleno y con el fin de garantizar la completa disolución del mismo, en la mezcla de reacción se requirió la inclusión de acetonitrilo a una concentración final del 10%. Así, el *screening* de la actividad peroxidasa tuvo que ser doble, tanto en presencia como en ausencia de acetonitrilo, con el fin de distinguir variantes de actividad de aquellas que mostraran mayor tolerancia al co-disolvente. Con este método HTS se llevaron a cabo 2 ciclos consecutivos de evolución dirigida empleando técnicas de PCR mutagénica, *in vivo shuffling* y StEP mutagénico. Tras explorar ~4.000 clones se identificó el mutante doble JaWa (G241D-R257K), que mostró una mejora de ~2 veces en su actividad peroxigenasa hacia naftaleno y una drástica reducción en su actividad peroxidasa (**Fig. 6.1**). Para tratar de disminuir aún más la actividad peroxidasa, se hicieron estudios computacionales (en colaboración con

el grupo del Prof. V. Guallar, del Barcelona Supercomputing Center -BSC-, y el asesoramiento de los Dr. J. Vind, Novozymes y A.T. Martinez, Centro de Investigaciones Biológicas, CIB-CSIC) sugiriendo el Trp24 superficial como posible residuo catalítico implicado en un mecanismo de oxidación de largo recorrido. Se crearon los correspondientes mutantes PaDa-I-W24F y JaWa-W24F consiguiendo una disminución manifiesta sobre la actividad peroxidasa, pero afectando negativamente la actividad peroxigenasa, por lo que finalmente dicha mutación fue descartada. Es importante reseñar que la disminución en la actividad peroxidasa de la UPO1 ha sido explorada adicionalmente, a parte de las estrategias comentadas en la presente Tesis (estudios computacionales y racionales para JaWa; evolución dirigida convencional para PaDa-I, ver mutante 3F10 en capítulo 2.3), mediante estudios de deriva genética sobre PaDa-I. En concreto, nuestro laboratorio ha diseñado recientemente librerías de *neutral genetic drift* o deriva genética neutral (Bloom et al., 2007b) combinadas con DNA *shuffling* para acumular mutaciones neutrales que permitan desbalancear las actividades subyacentes a la UPO1 al tiempo que revelen nuevas propiedades en cuanto a estabilidad o actividades latentes (Paret et al., 2015). En este proceso, se han descubierto nuevas sustituciones que disminuyen la actividad peroxidasa sin mermar la actividad peroxigenasa (material no publicado).

6.2.2. Caracterización bioquímica y computacional

El análisis de las propiedades bioquímicas generales mostró que JaWa poseía características equivalentes a las del tipo parental PaDa-I en lo referente al procesado correcto del extremo N-terminal, pI, perfiles de pH, glicosilación y rasgos espectroscópicos. La reacción de transformación de naftaleno en 1-naftol por JaWa fue estudiada en detalle mediante HPLC. El mutante JaWa se mostró altamente eficiente y selectivo en el proceso, con unos números de recambio totales (*total turnover numbers*, TTN) de ~50.000 (regioselectividad del 97% para 1-naftol), frente a los ~20.000 conseguidos para el tipo parental. Adicionalmente, se evaluó la velocidad de transformación de 1-naftol en 1,4-naftoquinona por HPLC observando una reducción a la mitad (hasta 92 min^{-1} para JaWa), lo que ratifica lo apropiado del diseño del método de *screening* con DMP como sustrato sustituto del 1-naftol. Los parámetros cinéticos confirmaron que mientras la

eficiencia catalítica para la transformación del naftaleno en 1-naftol aumentó 1,5 veces en JaWa, la actividad peroxidasa fue notablemente reducida (de 3 a 12 veces en función del sustrato reductor). En colaboración con el BSC, estudios computacionales adicionales empleando PELE (*protein energy landscape exploration*) y QM/MM (*quantum mechanics/molecular mechanics*) permitieron comprobar como la mutación G241D, localizada en el canal de acceso al hemo, fue determinante para la disposición del naftaleno en el centro activo. En efecto, las simulaciones mediante PELE muestran que dicha sustitución promueve un cambio conformacional que afecta a la α-hélice que contiene el par catalítico ácido-base (Glu196-Arg189) así como a la localización relativa del naftaleno, en consonancia con la reducción de 4,5 veces en la K_m. Por otro lado, la mutación R257K se sitúa en la superficie, lejos del centro activo. Las simulaciones computacionales parecen indicar que dicho cambio sí podría incidir en la oxidación de DMP (a través de un canal de acceso adicional al centro activo); sin embargo, no se hicieron simulaciones adicionales empleando 1-naftol como sustrato, por lo que no queda clara su función en la mejora global del proceso, si bien podría actuar como cambio estabilizante (presenta unos factores B mejorados) que favorecerían el empleo de la enzima en tiempos largos de reacción.

6.3. PERSPECTIVAS

A lo largo de la discusión se han expuesto las capacidades de los mutantes UPOs diseñados en la presente Tesis Doctoral mediante evolución dirigida. En lo referente a sus propiedades generales, PaDa-I es similar a la *Aae*UPO1 silvestre, pero preparada específicamente para ser utilizada como herramienta en procesos de ingeniería genética. Entre ellos, las posibilidades son tantas como potenciales aplicaciones tiene la enzima. Aunque la *Aae*UPO1 silvestre sea una de las enzimas más estudiadas y con mayor proyección en procesos de síntesis orgánica (actualmente se considera el relevo de las P450s) (Hofrichter y Ullrich, 2013), aún no se disponía de una plataforma que permitiera su modificación genética y adecuación a diferentes ámbitos biotecnológicos. El diseño del mutante PaDa-I, su futura trascendencia para estudios estructura-función, su amplia versatilidad como punto de partida para

otras rutas de evolución dirigida y su fácil sobreproducción en *P. pastoris* abren un enorme abanico de perspectivas. En efecto, con esta plataforma evolutiva se podrán diseñar y aplicar mutantes UPO "a la carta" para incontables procesos de síntesis orgánica, biorremediación o ingeniería metabólica, por citar algunas aplicaciones.

Como primer caso de estudio, se ha diseñado el mutante JaWa, con unos atributos muy interesantes para la síntesis selectiva de 1-naftol, que podrían trasladarse a otros procesos de interés donde se requieran oxifuncionalizaciones C-H exclusivas e independientes de actividad peroxidasa. De hecho, pruebas preliminares en nuestro laboratorio empleando el fármaco propranolol (ß bloqueante) como sustrato muestran que JaWa da lugar a mayor rendimiento en la transformación a 5-hidroxipropranolol que PaDa-I y también que la *Aae*UPO1 homóloga (material no publicado). Al igual que durante la oxifuncionalización del naftaleno, en este caso el producto hidroxilado es nuevamente tomado como sustrato y oxidado, reduciendo el rendimiento global de la reacción (Kinne et al., 2009a). JaWa soluciona este inconveniente, produciendo mayor cantidad de 5-hidroxipropranolol, sin merma en su actividad peroxigenasa (p.ej. con similares valores cinéticos que PaDa-I para los alcoholes veratrílico y bencílico) y sin la necesidad de añadir ningún *radical scavenger* (p.ej. ácido ascórbico). Este metabolito del propranolol es producido en el hígado humano, por lo que presenta un elevado valor para la industria farmacéutica y en estudios farmacocinéticos siendo un claro objetivo de nuevas campañas evolutivas por nuestro laboratorio.

Finalmente, el diseño de secretomas ligninolíticos en *S. cerevisiae* que facilite procesos de evolución conjunta supone una vía futura de investigación. En efecto, nuestro laboratorio ya ha preparado varias cepas secretoras de diferentes ligninasas (Gonzalez-Perez y Alcalde, 2014) entre las que recientemente hemos incluido levaduras con capacidad de co-expresar mutantes UPO y AAO (esta última como suministradora de H_2O_2) para su aplicación en procesos autosuficientes en reacciones en cascada al tiempo que se suaviza el proceso de inactivación suicida de la UPO por peróxido (material no publicado).

CONCLUSIONES

7

1. Se ha logrado la expresión funcional de la UPO1 de *A. aegerita* (*Aae*UPO1) en *S. cerevisiae* mediante evolución dirigida.

2. La táctica evolutiva comprendió la preparación de un sistema de *screening* dual para detectar actividad peroxidasa y peroxigenasa junto con la creación de diversidad genética mediante herramientas *in vitro* e *in vivo*.

3. Entre los métodos *in vivo* empleados, destacó el diseño de una nueva técnica de mutagénesis enfocada por dominios (MORPHING) que permitió concentrar las cargas mutacionales en la secuencia señal de la enzima para favorecer la secreción.

4. Tras 5 generaciones de evolución dirigida, se obtuvo la variante PaDa-I con un aumento en su actividad total de 3.250 veces, siendo una enzima fácilmente secretada (8 mg/L), activa y estable.

5. El mutante PaDa-I acumuló 9 mutaciones: las 4 mutaciones de su péptido señal (F12Y-A14V-R15G-A21D) aumentaron la secreción 27 veces, mientras que las mutaciones en la proteína madura (V57A-L67F-V75I-I248V-F311L) incrementaron tanto la secreción como los parámetros cinéticos, siendo estos últimos equivalentes a los de la enzima nativa expresada homólogamente en *A. aegerita*.

6. Se clonó y expresó la variante PaDa-I en *P. pastoris* con el objetivo de impulsar sus niveles de producción. Se alcanzaron hasta 217 mg/L de PaDa-I producido en *P. pastoris* en biorreactor, sin modificar las propiedades y capacidades de la variante mejorada. De esta manera, se ha preparado un efectivo sistema de expresión en levaduras en tándem para la evolución dirigida y producción de variantes de UPO1, muy apropiado para el desarrollo de futuras aplicaciones biotecnológicas.

7. La variante PaDa-I se optimizó para la síntesis de 1-naftol mediante evolución dirigida. En este abordaje, se aplicaron criterios de selección positivo y negativo para promover y reprimir las actividades peroxigenasa y peroxidasa de la enzima, respectivamente. Tras 2 generaciones de evolución, se identificó la

variante JaWa (G241D-R257K) con unos TTN de 50.000 y una regioselectividad del 97% para 1-naftol.

8. El análisis bioquímico y computacional de JaWa mostró que su rendimiento mejorado fue consecuencia de la reducción en su actividad peroxidasa así como de un acomodamiento más apropiado del naftaleno en el bolsillo hidrofóbico de la enzima debido a cambios conformacionales locales impulsados por las nuevas mutaciones.

9. La tecnología puesta a punto en esta Tesis Doctoral para la ingeniería de UPOs con propiedades mejoradas permitirá en un futuro próximo el diseño de nuevas variantes con aplicaciones sintéticas diversas, así como la realización de estudios estructura-función para profundizar en el conocimiento de este nuevo grupo de hemo-tiolato peroxigenasas.

REFERENCIAS BIBLIOGRÁFICAS

8

A

Alcalde M, 2010. Mutagenesis protocols in *Saccharomyces cerevisiae* by *in vivo* overlap extension. En: *In vitro* Mutagenesis Protocols, 3rd ed. Methods in Molecular Biology, 634: 3-15. Bramman J. ed., Totowa, New Jersey, Springer-Humana Press.
ISBN: 978-1-60761-651-1.
http://dx.doi.org/10.1007/978-1-60761-652-8_1

Alcalde M, 2015. Engineering the ligninolytic enzyme consortium. Trends in Biotechnology, 33: 155-162.
http://dx.doi.org/10.1016/j.tibtech.2014.12.007

Alcolombri U, Elias M y Tawfik DS, 2011. Directed evolution of sulfotransferases and paraoxonases by ancestral libraries. Journal of Molecular Biology, 411: 837-853.
http://dx.doi.org/10.1016/j.jmb.2011.06.037

Anandakrishnan R, Aguilar B y Onufriev AV, 2012. *H*++ 3.0: automating pK prediction and the preparation of biomolecular structures for atomistic molecular modeling and simulations. Nucleic Acids Research, 40: 537-541.
http://dx.doi.org/10.1093/nar/gks375

Anh DH, Ullrich R, Benndorf D, Svatoś A, Muck A y Hofrichter M, 2007. The Coprophilous Mushroom *Coprinus radians* Secretes a Haloperoxidase That Catalyzes Aromatic Peroxygenation. Applied and Environmental Microbiology, 73: 5477-5485.
http://dx.doi.org/10.1128/AEM.00026-07

Aranda E, Kinne M, Kluge M, Ullrich R y Hofrichter M, 2009. Conversion of dibenzothiophene by the mushrooms *Agrocybe aegerita* and *Coprinellus radians* and their extracellular peroxygenases. Applied Microbiology and Biotechnology, 82: 1057-1066.
http://dx.doi.org/10.1007/s00253-008-1778-6

Aranda E, Ullrich R y Hofrichter M, 2010. Conversion of polycyclic aromatic hydrocarbons, methyl naphthalenes and dibenzofuran by two fungal peroxygenases. Biodegradation, 21: 267-281.
http://dx.doi.org/10.1007/s10532-009-9299-2

B

Babot ED, del Río JC, Kalum L, Martínez AT y Gutiérrez A, 2013. Oxyfunctionalization of aliphatic compounds by a recombinant peroxygenase from *Coprinopsis cinerea*. Biotechnology and Bioengineering. 110: 2323-2332.
http://dx.doi.org/ 10.1002/bit.24904

Barková K, Kinne M, Ullrich R, Hennig L, Fuchs A, Hofrichter M, 2011. Regioselective hydroxylation of diverse flavonoids by an aromatic peroxygenase. Tetrahedron, 67: 4874-4878.
http://dx.doi.org/10.1016/j.tet.2011.05.008

Benner SA, Sassi SO y Gaucher EA, 2007. Molecular paleoscience: systems biology from the past. Advances in Enzymology and Related Areas of Molecular Biology, 75: 1-132.
http://dx.doi.org/10.1002/9780471224464.ch1

Bernhardt R, 2006. Cytochromes P450 as versatile biocatalysts. Journal of Biotechnology, 124: 128-45.
http://dx.doi.org/10.1016/j.jbiotec.2006.01.026

Bershtein S y Tawfik DS, 2008. Advances in laboratory evolution of enzymes. Current Opinion in Chemical Biology, 12: 151-158.
http://dx.doi.org/10.1016/j.cbpa.2008.01.027

Bloom JD, Labthavikul ST, Otey CR y Arnold FH, 2006. Protein stability promotes evolvability. Proceedings of the National Academy of Sciences of the United States of America, 103: 5869-5874.
http://dx.doi.org/10.1073/pnas.0510098103

Bloom JD, Lu Z, Chen D, Raval A, Venturelli OS and Arnold FH, 2007a. Evolution favors protein mutational robustness in sufficiently large populations. BMC Biology, 5: 29.
http://dx.doi.org/10.1186/1741-7007-5-29

Bloom JD, Romero PA, Lu Z y Arnold FH, 2007b. Neutral genetic drift can alter promiscuous protein functions, potentially aiding functional evolution. Biology Direct, 2:17.
http://dx.doi.org/10.1186/1745-6150-2-17

Bloom JD y Arnold FH. 2009. In the light of directed evolution: Pathways of adaptive protein evolution. Proceedings of the National Academy of Sciences, 106: 9995-10000.
http://dx.doi.org/10.1073/pnas.0901522106

Booth G, 2012. Naphthalene Derivatives, In: Ullmann's Encyclopedia of Industrial Chemistry. Wiley-VCH Verlag GmbH & Co. KGaA. Weinheim, Germany.
http://dx.doi.org/10.1002/14356007.a17_009

Bornscheuer UT, Huisman GW, Kazlauskas RJ, Lutz S, Moore JC y Robins K, 2012. Engineering the third wave of biocatalysis. Nature, 485: 185-194.
http://dx.doi.org/10.1038/nature11117

Buchhaupt M, Ehrich K, Huttmann S, Guder J y Schrader J, 2011. Over-expression of chloroperoxidase in *Caldariomyces fumago*. Biotechnology Letters, 33: 2225-2231. http://dx.doi.org/10.1007/s10529-011-0683-8

Bulter T, Alcalde M, Sieber V, Meinhold P, Schlachtbauer C y Arnold FH, 2003. Functional expression of a fungal laccase in *Saccharomyces cerevisiae* by directed evolution. Applied Environmental Microbiology, 69: 987-995. http://dx.doi.org/10.1128/AEM.69.2.987-995.2003

C

Calinescu I y Avram R, Revista de chemie 1994a, 45, 97-103.

Calinescu I, Avram R, Iovu H, Revista de chemie 1994b, 45, 299-305.

Calinescu I y Avram R, Revista de chemie 1994c, 45, 865-867.

Camarero S, Pardo I, Cañas AI, Molina P, Record E, Martínez AT, Martínez MJ y Alcalde M, 2012. Engineering Platforms for Directed Evolution of Laccase from *Pycnoporus cinnabarinus*. Applied and Environmental Microbiology, 78: 1370-1384. http://dx.doi.org/doi:10.1128/AEM.07530-11

Canada KA, Iwashita S, Shim H y Wood TK, 2002. Directed evolution of toluene ortho-monooxygenase for enhanced 1-naphthol synthesis and chlorinated ethene degradation. Jounal of Bacteriology, 184: 344-349. http://dx.doi.org/10.1128/JB.184.2.344-349.2002

Carro J, Ferreira P, Rodríguez L, Prieto A, Serrano A, Balcells B, Ardá A, Jiménez-Barbero J, Gutiérrez A, Ullrich R, Hofrichter M y Martínez AT, 2015. 5-hydroxymethylfurfural conversion by fungal aryl-alcohol oxidase and unspecific peroxygenase. FEBS Journal, 282: 3218-3229. http://dx.doi.org/10.1111/febs.13177

Cereghino JL y Cregg JM, 2000. Heterologous protein expression in the methylotrophic yeast *Pichia pastoris*. FEMS Microbiology Reviews 24: 45-66 http://dx.doi.org/10.1111/j.1574-6976.2000.tb00532.x

Cherry JR, Lamsa MH, Schneider P, Vind J y Svendsen A, Jones A y Pedersen AH, 1999. Directed evolution of a fungal peroxidase. Nature Biotechnology, 17: 379-384. http://dx.doi.org/10.1038/7939

Cirino PC y Arnold FH, 2002. Protein engineering of oxygenases for biocatalysis. Current Opinion in Chemical Biology, 6: 130-135

http://dx.doi.org/10.1016/S1367-5931(02)00305-8

Cirino PC, M. Mayer KM y Umeno D, 2003. Generating Mutant Libraries Using Error-Prone PCR. En: Methods in Molecular Biology, Directed Evolution Library Creation, 231: 3-9. Arnold FH y Georgiou ed., Totowa, New Jersey: Springer-Humana Press.
ISBN: 978-1-58829-285-8
http://dx.doi.org/10.1385/1-59259-395-X:3

Cobb RE, Si T y Zhao H, 2012. Directed evolution: an evolving and enabling synthetic biology tool. Current Opinion in Chemical Biology, 16: 285-291.
http://dx.doi.org/10.1016/j.cbpa.2012.05.186

Coelho PS, Brustad EM, Kannan A y Arnold FH, 2013. Olefin Cyclopropanation via Carbene Transfer Catalyzed by Engineered Cytochrome P450 Enzymes. Science, 339: 307-310.
http://dx.doi.org/10.1126/science.1231434

Conesa A, van de Velde F, van Rantwijk F, Sheldon RA, van den Hondel CAMJ y Punt PJ, 2001. Expression of the *Caldariomyces fumago* chloroperoxidase in *Aspergillus niger* and characterization of the recombinant enzyme. Journal of Biological Chemistry, 276: 17635-17640.
http://dx.doi.org/10.1074/jbc.M010571200

D

Damborsky J y Brezovsky J, 2014. Computational tools for designing and engineering enzymes. Current Opinion in Chemical Biology, 19: 8-16.
http://dx.doi.org/10.1016/j.cbpa.2013.12.003

Dalby PA, 2011. Strategy and success for the directed evolution of enzymes. Current Opinion in Structural Biology, 21: 473-480.
http://dx.doi.org/10.1016/j.sbi.2011.05.003

Da Silva NA y Srikrishnan S, 2012. Introduction and expression of genes for metabolic engineering applications in *Saccharomyces cerevisiae*. FEMS Yeast Research, 12: 197-214.
http://dx.doi.org/10.1111/j.1567-1364.2011.00769.x

Desmond Molecular Dynamics System, version 2.2, D. E. Shaw Research, New York, NY, 2009. Maestro-Desmond Interoperability Tools, version 2.2, Schrödinger, New York.

Dunford HB, 1999. Heme peroxidases. Wiley, New York.
ISBN: 0471242446, 9780471242444.

F

Finney-Manchester SP y Maheshri N, 2013. Harnessing mutagenic homologous recombination for targeted mutagenesis in vivo by TaGTEAM. Nucleic Acids Research, 41: e99.
http://dx.doi.org/10.1093/nar/gkt150

Floudas D, Binder M, Riley R, Barry K, Blanchette RA, Henrissat B, Martinez AT, Otillar R, Spatafora JW, Yadav JS, Aerts A, Benoit I, Boyd A, Carlson A, Copeland A, Coutinho PM, de Vries RP, Ferreria P, Findley K, Foster B, Gaskell J, Glotzer D, Gorecki P, Heitman J, Hesse C, Hori C, Igarashi K, Jurgens JA, Kallen N, Kersten P, Kohler A, Kues U, Arun Kumar TK, Kuo A, Labutti K, Larrondo LF, Lindquist E, Ling A, Lombard V, Lucas S, Lundell T, Martin R, McLaughlin DJ, Morgenstern I, Morin E, Murant C, Nagy LG, Nolan M, Ohm RA, Patyshakuliyeva A, Rokas A, Ruiz-Dueñas FJ, Sabat G, Salamov A, Samejima M, Schumtz J, Slot JC, St. John F, Stenlid J, Sun H, Sun S, Syed K, Tsang A, Wiebenga A, Young D, Pisabarro A, Eastwood DC, Martin F, Cullen D, Grigoriev IV y Hibbet DS, 2012. The paleozoic origin of enzymatic lignin decomposition reconstructed from 31 fungal genomes. Science, 336: 1715-1719.
http://dx.doi.org/10.1126/science.1221748

G

Garcia-Ruiz E, Gonzalez-Perez D, Ruiz-Dueñas FJ, Martínez AT y Alcalde M, 2012. Directed evolution of a temperature-, peroxide- and alkaline pH-tolerant versatile peroxidase. Biochemical Journal, 441: 487-498.
http://dx.doi.org/10.1042/BJ20111199

Garcia-Ruiz E, Mate DM, Gonzalez-Perez D, Molina-Espeja P, Camarero S, Martínez AT, Ballesteros AO y Alcalde M, 2014. Directed Evolution of Ligninolytic Oxidoreductases: from Functional Expression to Stabilization and Beyond. En: Cascade Biocatalysis: Integrating Stereoselective and Environmentally Friendly Reactions, 1-22, 1st ed. Riva S y Fessner WD eds. Wiley-VCH Verlag GmbH & Co. KGaA.
ISBN: 978-3-527-33522-0

Garikipati SVBJ, McIver AM y Peeples TL, 2009. Whole-cell biocatalysis for 1-naphthol production in liquid-liquid biphasic systems. Applied and Environmental Microbiology, 75: 6545-6552.
http://dx.doi.org/10.1128/AEM.00434-09

Goldsmith M y Tawfik DS, 2013. Enzyme engineering by targeted libraries. Methods in Enzymology, 523: 257-283.
http://dx.doi.org/10.1016/B978-0-12-394292-0.00012-6

Gonzalez-Perez D, Garcia-Ruiz E y Alcalde M, 2012. *Saccharomyces cerevisiae* in directed evolution: An efficient tool to improve enzymes. Bioengineered Bugs, 3(3): 172-177.
http://dx.doi.org/10.4161/bbug.19544

Gonzalez-Perez D y Alcalde M, 2014. Assembly of evolved ligninolytic genes in *Saccharomyces cerevisiae*. Bioengineered, 5: 254263.
http://dx.doi.org/10.4161/bioe.29167

Gonzalez-Perez D, Garcia-Ruiz E, Ruiz-Dueñas FJ, Martinez AT y Alcalde, M, 2014a. Structural determinants of oxidative stabilization in an evolved versatile peroxidase. ACS Catalysis, 4: 3891-3901.
http://dx.doi.org/10.1021/cs501218v

Gonzalez-Perez D, Molina-Espeja P, Garcia-Ruiz E y Alcalde M, 2014b. Mutagenic organized recombination process by homologous *in vivo* grouping (MORPHING) for directed enzyme evolution. PLoS ONE 9:e90919.
http://dx.doi.org/10.1371/journal.pone.0090919

Grinkova YV, Denisov IG, McLean MA y Sligar SG, 2013. Oxidase uncoupling in heme monooxygenases: Human cytochrome P450 CYP3A4 in Nanodiscs. Biochemical and Biophysical Research Communications, 430: 1223-1227.
http://dx.doi.org/10.1016/j.bbrc.2012.12.072

Gröbe G, Ullrich R, Pecyna MJ, Kapturska D, Friedrich S, Hofrichter M y Scheibner K, 2011. High-yield production of aromatic peroxygenase by the agaric fungus *Marasmius rotula*. AMB Express, 2011: 1-31.
http://dx.doi.org/10.1186/2191-0855-1-31

Guallar V y Wallrapp FH, 2010. QM/MM methods: looking inside heme proteins biochemistry. Biophysical Chemistry, 149: 1-11.
http://dx.doi.org/10.1016/j.bpc.2010.03.010

Gupta RD y Tawfik DS, 2008. Directed enzyme evolution via small and effective neutral drift libraries. Nature Methods, 5: 939-942.
http://dx.doi.org/10.1038/nmeth.1262

Gutiérrez A, Babot ED, Ullrich R, Hofrichter M, Martínez AT y del Río JC, 2011. Regioselective oxygenation of fatty acids, fatty alcohols and other aliphatic compounds by a basidiomycete heme-thiolate peroxidase. Archives of Biochemistry and Biophysics, 514: 33-43.
http://dx.doi.org/10.1016/j.abb.2011.08.001

H

Herman A y Tawfik DS, 2007. Incorporating Synthetic Oligonucleotides via Gene Reassembly (ISOR): a versatile tool for generating targeted libraries. Protein Engineering Design and Selection, 20: 219-226.
http://dx.doi.org/10.1093/protein/gzm014

Hidalgo A, Schliessmann A, Molina R, Hermoso J y Bornscheuer UT, 2008. A one-pot, simple methodology for cassette randomisation and recombination for focused directed evolution. Protein Engineering Design and Selection, 21: 567-576.
http://dx.doi.org/10.1093/protein/gzn034

Hofrichter M y Ullrich R, 2006. Heme-thiolate haloperoxidases: versatile biocatalysts with biotechnological and environmental significance. Applied Microbiology and Biotechnology, 71: 276-288.
http://dx.doi.org/10.1007/s00253-006-0417-3

Hofrichter M, Ullrich R, Pecyna MJ, Liers C, Lundell T, 2010. New and classic families of secreted fungal heme peroxidases. Applied Microbiology and Biotechnology, 87: 871-897.
http://dx.doi.org/10.1007/s00253-010-2633-0

Hofrichter M y Ullrich R, 2014. Oxidations catalyzed by fungal peroxygenases. Current Opinion in Chemical Biology, 19: 116-125.
http://dx.doi.org/10.1016/j.cbpa.2014.01.015

Hofrichter M, Ullrich R, Kellner H, Upadhyay RC y Scheibner K, 2014. Fungal Unspecific Peroxygenases: a New Generation of Oxygen-Transferring Biocatalysts. Proceedings of the 8th International Conference on Mushroom Biology and Mushroom Products (ICMBMP8) 2014, 172-181.

Hofrichter M, Kellner H, Pecyna MJ y Ullrich R, 2015. Fungal Unspecific Peroxygenases: Heme-Thiolate Proteins That Combine Peroxidase and Cytochrome P450 Properties. En: Monooxygenase, Peroxidase and Peroxygenase Properties and Mechanisms of Cytochrome P450. Advances in Experimental Medicine and Biology, 851: 341-368. E.G. Hrycay y S.M. Bandiera ed.
ISBN 978-3-319-16008-5.
http://dx.doi.org/10.1007/978-3-319-16009-2

Hong KK y Nielsen J, 2012. Metabolic engineering of *Saccharomyces cerevisiae*: a key cell factory platform for future biorefineries. Cellular and Molecular Life Sciences, 69: 2671-2690.
http://dx.doi.org/10.1007/s00018-012-0945-1

J

Jacobsen EN, 1993. Asymmetric catalytic epoxidation of unfunctionalized olefins. En: Catalytic Asymmetric Synthesis, 1st ed., 159-202. Ojima I, ed, New York, Wiley-VCH.

Jegannathan KR y Nielsen PH, 2013. Environmental assessment of enzyme use in industrial production - a literature review. Journal of Cleaner Production, 42: 228e240. http://dx.doi.org/10.1016/j.jclepro.2012.11.005

Jaguar, version 8.1, Schrödinger, LLC, New York, 2013.

Joo H, Lin Z y Arnold FH, 1999. Laboratory Evolution of Peroxide-Mediated Cytochrome P450 Hydroxylation. Nature, 399: 670-673. http://dx.doi.org/10.1038/21395

Jung ST, Lauchli R y Arnold FH, 2011. Cytochrome P450: Taming a Wild Type Enzyme. Current Opinion in Biotechnology, 22: 809-817. http://dx.doi.org/10.1016/j.copbio.2011.02.008

K

Karich A, Kluge M, Ullrich R yHofrichter M, 2013. Benzene oxygenation and oxidation by the peroxygenase of *Agrocybe aegerita*. AMB Express, 3:5. http://dx.doi.org/10.1186/2191-0855-3-5

Kinne M, Poraj-Kobielska M, Aranda E, Ullrich R, Hammel KE, Scheibner K y Hofrichter M, 2009a. Regioselective preparation of 5-hydroxypropranolol and 4'-hydroxydiclofenac with a fungal peroxygenase. Bioorganic and Medicinal Chemistry Letters, 19: 3085-3087. http://dx.doi.org/10.1016/j.bmcl.2009.04.015.

Kinne M, Poraj-Kobielska M, Ralph SA, Ullrich R, HofrichterM y Hammel KE, 2009b. Oxidative Cleavage of Diverse Ethers by an Extracellular Fungal Peroxygenase. Journal of Biological Chemistry, 284: 29343-29349. http://dx.doi.org/10.1074/jbc.M109.040857

Kinne M, Zeisig C, Ullrich R, Kayser G, Hammel KE y Hofrichter M, 2010. Stepwise oxygenations of toluene and 4-nitrotoluene by a fungal peroxygenase. Biochemical and Biophysical Research Communications, 397: 18-21. http://dx.doi.org/10.1016/j.bbrc.2010.05.036

Kinne M, Poraj-Kobielska M, Ullrich R, Nousiainen P, Sipilä J, Scheibner K, Hammel KE y Hofrichter M, 2011. Oxidative cleavage of non-phenolic ß-0-4 lignin model dimers by an extracellular aromatic peroxygenase. Holzforschung, 65: 673-679.

http://dx.doi.org/10.1515/HF.2011.057

Kiss G, Çelebi-Ölçüm N, Moretti R, Baker D y Houk KN, 2013. Computational enzyme design. Angewandte Chemie International Edition, 52: 5700-5725.
http://dx.doi.org/10.1002/anie.201204077

Kitajima S, Kitamura M y Koja N, 2008. Triple mutation of Cys26, Trp35, and Cys126 in stromal ascorbate peroxidase confers H_2O_2 tolerance comparable to that of the cytosolic isoform. Biochemical and Biophysical Research Communications, 372: 918-923.
http://dx.doi.org/10.1016/j.bbrc.2008.05.160

Kluge M, Ullrich R, Scheibner K y Martin Hofrichter, 2007. Spectrophotometric assay for detection of aromatic hydroxylation catalyzed by fungal haloperoxidase-peroxygenase. Applied Microbiology and Biotechnolpgy, 75: 1473-1478.
http://dx.doi.org/10.1007/s00253-007-0942-8

Kluge M, Ullrich R, Dolge C, Scheibner K y Hofrichter M, 2009. Hydroxylation of naphthalene by aromatic peroxygenase from *Agrocybe aegerita* proceeds via oxygen transfer from H_2O_2 and intermediary epoxidation. Applied Microbiology and Biotechnology, 81: 1071-1076.
http://dx.doi.org/10.1007/s00253-008-1704-y

Kluge M, Ullrich R, Scheibner K y Hofrichter M, 2012. Stereoselective benzylic hydroxylation of alkylbenzenes and epoxidation of styrene derivatives catalyzed by the peroxygenase of *Agrocybe aegerita*. Green Chemistry, 14: 440-446.
http://dx.doi.org/10.1039/c1gc16173c

Kries H, Blomberg R y Hilvert D, 2013. *De novo* enzymes by computational design. Current Opinion in Chemical Biology, 17: 221-228.
http://dx.doi.org/10.1016/j.cbpa.2013.02.012

Krivoruchko A, Siewers V y Nielsen J, 2011. Opportunities for yeast metabolic engineering: lessons from synthetic biology. Biotechnology Journal, 6: 262-276.
http://dx.doi.org/10.1002/biot.201000308

Kudo K, Ohmae T, Uno A, United States Patent 1976, 3,935,282.

Kumar D, Karamzadeh B, Sastry GN y de Visser SP, 2010. What factors influence the rate constant of substrate epoxidation by compound I of cytochrome P450 and analogous iron(IV)-oxo oxidants? Journal of the American Chemical Society, 132: 7656-67.
http://dx.doi.org/10.1021/ja9106176

L

Lewis DFV, 2001. Guide to Cytochromes P450: Structure and Function. Taylor & Francis, London.
ISBN 9780748408979.

Lewis JC y Arnold FH, 2009. Catalysts On Demand: Selective Oxidations By Laboratory-Evolved Cytochrome P450 BM-3. Chimia, 63:309-312.
http://dx.doi.org/10.2533/chimia.2009.309

Lin-Cereghino J, Wong WW, Xiong S, Giang W, Luong LT, Vu J, Johnson SD y Lin-Cereghino GP, 2005. Condensed protocol for competent cell preparation and transformation of the methy-lotrophic yeast *Pichia pastoris*. Biotechniques, 38:44-8.

Linde D, Pogni R, Cañellas M, Lucas F, Guallar V, Baratto MC, Sinicropi A, Sáez-Jiménez V, Coscolín C, Romero A, Medrano FJ, Ruiz-Dueñas FJ y Martínez AT, 2015. Catalytic surface radical in dye-decolorizing peroxidase: a computational, spectroscopic and site-directed mutagenesis study. Biochemical Journal, 466: 253-262.
http://dx.doi.org/10.1042/BJ20141211 253

Lucas F, Babot ED, Cañellas M, del Río JC, Kalum L, Ullrich R, Hofrichter M, Guallar V, Martínez AT y Gutiérrez A, 2016. Molecular determinants for selective C25-hydroxylation of vitamins D2 and D3 by fungal peroxygenases. Catalysis Science & Technology, 6: 288-295
http://dx.doi.org/10.1039/c5cy00427f

Lutz S, 2010. Beyond directed evolution--semi-rational protein engineering and design. Current Opinion Biotechnology, 21: 734-743.
http://dx.doi.org/10.1016/j.copbio.2010.08.011

M

Madadkar-Sobhani A y Guallar V, 2013. PELE web server: atomistic study of biomolecular systems at your fingertips. Nucleic Acids Research, 41: 322-328.
http://dx.doi-org/10.1093/nar/gkt454

Madhavi Sastry G, Adzhigirey M, Day T, Annabhimoju R y Sherman W, 2013. Protein and ligand preparation: parameters, protocols, and influence on virtual screening enrichments. Journal of Computer-Aided Molecular Design, 27: 221-234.
http://dx.doi.org/10.1007/s10822-013-9644-8

Martinez AT, Ruiz-Dueñas FJ, Gutierrez A, del Rio JC, Alcalde M, Liers C, Ullrich R, Hofrichter M, Scheibner K, Kalum L, Vind J y Lund H, 2014. Search, engineering, and

applications of new oxidative biocatalysts. Biofuels, Bioproducts and Biorefining, 8: 819-35.
http://dx.doi.org/10.1002/bbb.1498

Mate DM, García-Burgos C, García-Ruiz E, Ballesteros AO, Camarero S y Alcalde M, 2010. Laboratory Evolution of High-Redox Potential Laccases. Chemistry and Biology, 17: 1030-1041.
http://dx.doi.org/0.1016/j.chembiol.2010.07.010.

Mate DM, Garcia-Ruiz E, Camarero S y Alcalde M, 2011. Directed Evolution of Fungal Laccases. Current Genomics, 12(2): 113-122.
http://dx.doi.org/10.2174/138920211795564322011

Mate DM, Garcia-Ruiz E, Camarero S, Shubin VV, Falk M, Shleev S, Ballesteros AO y Alcalde M, 2013a. Switching from blue to yellow: altering the spectral properties of a high redox potential laccase by directed evolution. Biocatalysis and Biotransformations, 31: 8-21.
http://dx.doi.org/10.3109/10242422.2012.749463

Mate DM, Gonzalez-Perez D, Falk M, Kittl R, Pita M, López De Lacey A, Ludwig R, Shleev S y Alcalde M, 2013b. Blood Tolerant Laccase by Directed Evolution. Chemistry and Biology, 20: 223-231.
http://dx.doi.org/10.1016/j.chembiol.2013.01.001

Mate DM, Gonzalez-Perez D, Kittl R, Ludwig R y Alcalde M, 2013c. Functional expression of a blood tolerant laccase in *Pichia pastoris*. BMC Biotechnology, 13: 38.
http://dx.doi.org/10.1186/1472-6750-13-38

McIntosh JA, Farwell CC y Arnold FH, 2014. Expanding P450 Catalytic Reaction Space Through Evolution and Engineering. Current Opinion in Chemical Biology, 19: 126-134.
http://dx.doi.org/10.1016/j.cbpa.2014.02.001

Meinhold P, Peters MW, Hartwick A, Hernandez AR y Arnold FH, 2006. Engineering Cytochrome P450 BM3 for Terminal Alkane Hydroxylation. Advanced Synthesis & Catalysis, 348: 763-772.
http://dx.doi.org/10.1002/adsc.200505465

Miyazaki-Imamura C, Ohira K, Kitagawa R, Nakano H, Yamane T y Takahashi H, 2003. Improvement of H_2O_2 stability of manganese peroxidase by combinatorial mutagenesis and high-throughput screening using *in vitro* expression with protein disulfide isomerase. Protein Engineering Design and Selection, 16: 423-428.
http://dx.doi.org/10.1093/protein/gzg054

Molander GA, Siddiqui SZ y Fleury-Brégeot N, 2014. Synthesis of 1-Naphthol via Oxidation of Potassium 1-Naphthyltrifluoroborate. Organic Synthesis, 90:153-163.
http://dx.doi.org/10.1002/0471264229.os090.15

Molina-Espeja P, Viña-Gonzalez J, Gomez BJ, Martin-Diaz J, Garcia-Ruiz E y Alcalde M, 2016. Beyond the outer limits of nature by directed evolution. Biotechnology Advances Enviado.

Morawski B, Lin Z, Cirino P, Joo H y Arnold FH, 2000. Functional expression of horseradish peroxidase in *Saccharomyces cerevisiae* and *Pichia pastoris*. Protein Engineering, Design & Selection, 13: 377-84.
http://dx.doi.org/10.1093/protein/13.5.377

N

Nevoigt E, 2008. Progress in metabolic engineering of *Saccharomyces cerevisiae*. Microbiology and Molecular Biology Reviews, 72: 379-412.
http://dx.doi.org/10.1128/MMBR.00025-07

Nothwehr SF y Gordon JI, 1990. Targeting of Proteins into the Eukaryotic Secretory Pathway: Signal Peptide Structure/Function Realtionships. Bioassays, 12: 479-484.
http://dx.doi.org/10.1002/bies.950121005

O

Ortiz de Montellano PR y De Voss JJ, 2005. Substrate oxidation by cytochrome P450 enzymes. En: Cytochrome P450: structure, mechanism, and biochemistry, 3rd ed., 183-245. Ortiz De Montellano PR, ed., Kluwer Academic/ Plenum Publishers, New York.
ISBN: 978-0-306-48324-0
http://dx.doi.org/10.1007/0-387-27447-2_6

Ostrov N, Wingler LM y Cornish W, 2013. Gene assembly and combinatorial libraries in *S. cerevisiae* via reiterative recombination. Methods in Molecular Biology, 978: 187-203.
http://dx.doi.org/10.1007/978-1-62703-293-3_14

P

Packer MS y Liu DR, 2015. Methods for the directed evolution of proteins. Nature Reviews Genetics, 16: 379-394.
http://dx.doi.org/doi:10.1038/nrg3927

Pardo I, Vicente AI, Mate DM, Alcalde M, Camarero S. 2012. Development of chimeric laccases by directed evolution. Biotechnology and Bioengineering, 109: 2978-2986. http://dx.doi.org/10.1002/bit.24588

Paret C, Martin-Diaz J y Alcalde M, 2015. Shuffling the neutral drift of unspecific peroxygenase expressed in yeast. Trabajo fin de Máster en Biología Molecular y Celular, Universidad Autónoma de Madrid.

Pecyna MJ, Ullrich R, Bittner B, Clemens A, Scheibner K, Schubert R y Hofrichter M, 2009. Molecular characterization of aromatic peroxygenase from *Agrocybe aegerita*. Applied Microbiology and Biotechnology 84: 885-897. http://dx.doi.org/10.1007/s00253-009-2000-1

Peisajovich SG and Tawfik DS, 2007. Protein engineers turned evolutionists. Nature Methods, 4: 991-994. http://dx.doi.org/10.1038/nmeth1207-991

Peng L, Wollenberger U, Kinne M, Hofrichter M, Ullrich R, Scheibner K, Fischer A y Scheller FW, 2010. Peroxygenase based sensor for aromatic compounds. Biosensors and Bioelectronics, 26: 1432-1436. http://dx.doi.org/10.1016/j.bios.2010.07.075

Peter S, Kinne M, Wang X, Ullrich R, Kayser G, Groves JT y Hofrichter M, 2011. Selective hydroxylation of alkanes by an extracellular fungal peroxygenase. FEBS Journal, 278: 3667-3675. http://dx.doi.org/10.1111/j.1742-4658.2011.08285.x

Peter S, Kinne M, Ullrich R, Kayser G y Hofrichter M, 2013. Epoxidation of linear, branched and cyclic alkenes catalyzed by unspecific peroxygenase. Enzyme and Microbial Technology, 52: 370- 376. http://dx.doi.org/doi:10.1016/j.enzmictec.2013.02.013

Peter S, Karich A, Ullrich R, Gröbe G, Scheibner K and Hofrichter M, 2014. Enzymatic one-pot conversion of cyclohexane into cyclohexanone: Comparison of four fungal peroxygenases. Journal of Molecular Catalysis B: Enzymatic, 103: 47-51. http://dx.doi.org/10.1016/j.molcatb.2013.09.016

Piontek K, Strittmatter E, Ullrich R, Gröbe G, Pecyna MJ, Kluge M, Scheibner K, Hofrichter M y Plattner DA, 2013. Structural Basis of Substrate Conversion in a New Aromatic Peroxygenase cytochrome P450 functionality with benefits. The Journal of Biological Chemistry, 288: 34767-34776. http://dx.doi.org/10.1074/jbc.M113.514521

Pirakitikulr N, Ostrov N, Peralta-Yahya P y Cornish VW, 2010. PCRless library mutagenesis via oligonucleotide recombination in yeast. Protein Science, 19: 2336-2346. http://dx.doi.org/10.1002/pro.513

Pompon D y Nicolas A, 1989. Protein engineering by cDNA recombination in yeasts: shuffling of mammalian cytochrome P-450 functions. Gene, 15;83(1): 15-24. http://dx.doi.org/10.1016/0378-1119(89)90399-5

Poraj-Kobielska M, Kinne M, Ullrich R, Scheibner K, Kayser G, Hammel KE y Hofrichter M, 2011. Preparation of human drug metabolites using fungal peroxygenases. Biochemical Pharmacology, 82: 789-796. http://dx.doi.org/10.1016/j.bcp.2011.06.020

Poraj-Kobielska M, Kinne M, Ullrich R, Scheibner K y Hofrichter M, 2012. A spectrophotometric assay for the detection of fungal peroxygenases. Analytical Biochemistry, 421: 327-329. http://dx.doi.org/10.1016/j.ab.2011.10.009

Poraj-Kobielska M, 2013. Conversion of pharmaceuticals and other drugs by fungal peroxygenases. PhD Dissertation. Universidad Técnica de Desden, Alemania.

Poraj-Kobielska M, Atzrodt J, Holla W, Sandvoss M, Gröbe G, Scheibner K y Hofrichter, 2013. Preparation of labeled human drug metabolites and drug-drug interaction-probes with fungal peroxygenases. Journal of Labelled Compounds and Radiopharmaceuticals, 56: 513-519. http://dx.doi.org/10.1002/jlcr.3103

Pourmir A y Johannes TW, 2012. Directed evolution: selection of the host organism. Computational and Structural Biotechnology Journal. 2:e201209012. http://dx.doi.org/10.5936/csbj.201209012

Q

QSite, version 5.7, Schrödinger, LLC, New York, 2011.

R

Rai GP, Zong Q y Hager LP, 2000. Isolation of directed evolution mutants of chloroperoxidase resistant to suicide inactivation by primary olefins. Israel Journal of Chemistry, 40: 63-70. http://dx.doi.org/10.1560/264G-UH9K-MEYU-9YHY

Rai GP, Sakai S, Flórez AM, Mogollon L y Hager LP, 2001. Directed Evolution of Chloroperoxidase for Improved Epoxidation and Chlorination Catalysis. Advanced Synthesis and Catalysis, 343: 638-645.
http://dx.doi.org/10.1002/1615-4169(200108)343:6

Rakestraw J, Sazinsky SL, Piatesi A, Antipov E y Wittrup K, 2009. Directed evolution of a secretory leader for the improved expression of heterologous proteins and full-length antibodies in *Saccharomyces cerevisiae*. Biotechnology and Bioengineering, 103: 1192-1201.
http://dx.doi.org/10.1002/bit.22338

Reetz MT, Bocola M, Carballeira JD, Zha D y Vogel A, 2005. Expanding the range of substrate acceptance of enzymes: combinatorial active-site saturation test. Angewandte Chemie International Edition English, 44: 4192-4196.
http://dx.doi.org/10.1002/anie.200500767

Reetz MT y Carballeira JD, 2007. Iterative saturation mutagenesis (ISM) for rapid directed evolution of functional enzymes. Nature Protocols, 2: 891-903.
http://dx,doi.org/10.1038/nprot.2007.72

Renata H, Wang ZJ y Arnold FH, 2015. Expanding the Enzyme Universe: Accessing Non-Natural Reactions by Mechanism-Guided Directed Evolution. Angewandte Chemie International Edition, 54: 3351-3367.
http://dx.doi.org/10.1002/anie.201409470

Ribeiro AJM, Santos-Martins D, Russo N, Ramos MJ y Fernandes PA, 2015. Enzymatic Flexibility and Reaction Rate: A QM/MM Study of HIV-1 Protease. ACS Catalysis, 5: 5617-5626.
http://dx.doi.org/10.1021/acscatal.5b00759

Roibana GD y Reetz MT, 2015. Expanding the toolbox of organic chemists: directed evolution of P450 monooxygenases as catalysts in regio- and stereoselective oxidative hydroxylation. Chemical Communications, 51: 2208-2224.
http://dx.doi.org/10.1039/C4CC09218J

Romanos MA, Scorer CA y Clare JJ, 1992. Foreign gene expression in yeast: a review. Yeast 8: 423-488.
http://dx.doi.org/10.1002/yea.320080602

Romero PA y Arnold FH, 2009. Exploring protein fitness landscapes by directed evolution. Nature Reviews Molecular Cell Biology, 10: 866-876.
http://dx.doi.org/10.1038/nrm2805

Rui L, Kwon YM, Fishman A, Reardon KF y Wood TK, 2004. Saturation Mutagenesis of Toluene ortho-Monooxygenase of Burkholderia cepacia G4 for Enhanced 1-Naphthol Synthesis and Chloroform Degradation. Applied and Environmental Microbiology, 70: 3246-3252.
http://dx.doi.org/10.1128/AEM.70.6.3246–3252.2004

Ruiz-Dueñas FJ, Morales M, Garcia E, Miki Y, Martinez MJ y Martinez AT, 2009. Substrate oxidation sites in versatile peroxidase and other basidiomycete peroxidases. Journal of Experimental Botany, 60: 441-452.
http://dx.doi.org/10.1093/jxb/ern261

Ryan BJ y O'Fagain C, 2007. Effects of single mutations on the stability of horseradish peroxidase to hydrogen peroxide. Biochimie 89: 1029-1032.
http://dx.doi.org/10.1016/j.biochi.2007.03.013

Rydberg P, Sigfridsson E y Ryde U, 2004. On the role of the axial ligand in heme proteins: a theoretical study. Journal of Biological Inorganic Chemistry, 9: 203-223.
http://dx.doi.org/10.1007/s00775-003-0515-y

S

Sakaki T, 2012. Practical application of cytochrome P450. Biological and Pharmaceutical Bulletin, 35: 844-849.
http://doi.org/10.1248/bpb.35.844

Schuster L, Seid B, United States Patent 1979, 4,171,459.

Sebestova E, Bendl J, Brezovsky J, Damborsky J, 2014. Computational tools for designing Smart libraries. En: Directed evolution Library Creation: Methods in Molecular Biology 1179, 291-314. Eds: Gillam EMJ, Copp JN, Ackerley DF. Humana press, Springer NY. ISBN: 978-1-4939-1053-3

Shao ZY, Zhao H y Zhao HM, 2009. DNA assembler, an *in vivo* genetic method for rapid construction of biochemical pathways. Nucleic Acids Research, 37:e16.
http://dx.doi.org/10.1093/nar/gkn991

Shaw PD y Beckwith J, 1960. Chloroperoxidase: a component of the betaketoadipate chlorinase system. Federation Proceedings, 19:47.

Shaw PD y Hager LP, 1959a. An enzymatic chlorination reaction. Journal of the American Chemical Society, 81: 1011-1012.
http://dx.doi.org/10.1021/ja01513a069

Shaw PD y Hager LP, 1959b. Biological chlorination. III. ß- Ketoadipate chlorinase: a soluble enzyme system. Journal of Biological Chemistry, 234: 2565-2569.

Shivange AV, Marienhagen J, Mundhada H, Schenk A y Schwaneberg U, 2009. Advances in generating functional diversity for directed protein evolution. Current Opinion in Chemical Biology 13: 19-25.
http://dx.doi.org/10.1016/j.cbpa.2009.01.019

Shoji O y Watanabe Y, 2014. Peroxygenase reactions catalyzed by cytochromes P450. Journal of Biological Inorganic Chemistry, 19: 529-539.
http://dx.doi.org/10.1007/s00775-014-1106-9

Shuster JR, 1991. Gene expression in yeast: protein secretion. Current Opinion in Biotechnology, 2: 685-690.
http://dx.doi.org/10.1016/0958-1669(91)90035-4

Sygmund C, Santner P, Krondorfer I, Peterbauer CK, Alcalde M, Nyanhongo GS, Guebitz GM y Ludwig R, 2013. Semi-rational engineering of cellobiose dehydrogenase for improved hydrogen peroxide production. Microbial Cell Factories, 12:38.
http://dx.doi.org/10.1186/1475-2859-12-38

T

Tee KL y Wong TS, 2013. Polishing the craft of genetic diversity creation in directed evolution. Biotechnology Advances, 31: 1707-1721.
http://dx.doi.org/10.1016/j.biotechadv.2013.08.021

Torres Pazmino DE, Winkler M, Glieder A, Fraaije MW, 2010. Monooxygenases as biocatalysts: classification, mechanistic aspects and biotechnological applications. Journal of Biotechnology, 146: 9-24.
http://dx.doi.org/10.1016/j.jbiotec.2010.01.021

Torres-Salas P, Mate DM, Ghazi I, Plou FJ, Ballesteros AO y Alcalde M, 2013. Widening the pH Activity Profile of a Fungal Laccase by Directed Evolution. ChemBioChem, 14: 934-937.
http://dx.doi.org/10.1002/cbic.201300102

Tracewell CA y Arnold FH, 2009. Directed enzyme evolution: climbing fitness peaks one amino acid at a time. Current Opinion in Chemical Biology, 13: 3-9.
http://dx.doi.org/10.1016/j.cbpa.2009.01.017

U

Ullrich R, Nüske J, Scheibner K, Spantzel J y Hofrichter M, 2004. Novel Haloperoxidase from the Agaric Basidiomycete *Agrocybe aegerita* Oxidizes Aryl Alcohols and Aldehydes. Applied and Environmental Microbiology, 70: 4575-4581.
http://dx.doi.org/10.1128/AEM.70.8.4575–4581.2004

Ullrich R y Hofrichter M, 2005. The haloperoxidase of the agaric fungus *Agrocybe aegerita* hydroxylates toluene and naphthalene. FEBS Letters 579: 6247-6250.
http://dx.doi.org/10.1016/j.febslet.2005.10.014

Ullrich R y Hofrichter M, 2007. Enzymatic hydroxylation of aromatic compounds. Cellular and Molecular Life Sciences, 64: 271-93.
http://dx.doi.org/10.1007/s00018-007-6362-1

Ullrich R, Dolge C, Kluge M y Hofrichte M, 2008. Pyridine as novel substrate for regioselective oxygenation with aromatic peroxygenase from *Agrocybe aegerita*. FEBS Letters, 582: 4100-4106.
http://dx.doi.org/10.1016/j.febslet.2008.11.006

Ullrich R, Liers C, Schimpke S y Hofrichter M, 2009. Purification of homogeneous forms of fungal peroxygenase. Biotechnology Journal, 4: 1619-1626.
http://dx.doi.org/10.1002/biot.200900076

Urlacher VB y Schmid RD, 2006. Recent advances in oxygenase-catalyzed biotransformations. Current Opinion in Chemical Biology, 10: 156-161.
http://dx.doi.org/10.1016/j.cbpa.2006.02.001

V

Valderrama B, Ayala M y Vazquez-Duhalt R, 2002. Suicide Inactivation of Peroxidases and the Challenge of Engineering More Robust Enzymes. Chemistry & Biology, 9: 555-565.
http://dx.doi.org/10.1016/S1074-5521(02)00149-7

van Beilen JB, Duetz WA, Schmid A, Witholt B, 2003. Practical issues in the application of oxygenases. Trends in Biotechnology, 21: 170-177.
http://dx.doi.org/10.1016/S0167-7799(03)00032-5

van Bloois E, Winter RT, Kolmar H, Fraaije MW, 2011. Decorating microbes: surface display of proteins on Escherichia coli. Trends in Biotechnology, 29: 79-86.
http://dx.doi.org/10.1016/j.tibtech.2010.11.003

Verma R, Schwaneberg U y Roccatano D, 2012. Computer-aided protein directed evolution: a review of web servers, databases and other computational tools for protein engineering. Computational and Structural Biotechnology Journal, 2:e201209008.
http://dx.doi.org/10.5936/csbj.201209008

Viña-Gonzalez J, Gonzalez-Perez D, Ferreira P, Martinez AT y Alcalde M, 2015. Focused Directed Evolution of Aryl-Alcohol Oxidase in *Saccharomyces cerevisiae* by Using Chimeric Signal Peptides. Applied and Environmental Microbiology, 81: 6451-6462.
http://dx.doi.org/10.1128/AEM.01966-15

Voloshchuk N y Montclare JK, 2010. Incorporation of unnatural amino acids for synthetic biology. Molecular BioSystems, 6: 65-80.
http://dx.doi.org/10.1039/b909200p

W

Wang T, Ma X, Zhu H, Li A, Du G y Chen J, 2012a. Available methods for assembling expression cassettes for synthetic biology. Applied Microbiology and Biotechnology, 93: 1853-1863.
http://dx.doi.org/10.1007/s00253-012-3920-8

Wang X, Peter S, Kinne M, Hofrichter M y Groves JT, 2012b. Detection and kinetic characterization of a highly reactive heme-thiolate peroxygenase compound I. Journal of the American Chemical Society, 134: 12897-12900.
http://dx.doi.org/10.1021/ja3049223

Wang X, Peter S, Ullrich R, Hofrichter M y Groves JT, 2013. Driving force for oxygen-atom transfer by heme-thiolate enzymes. Angewandte Chemie International Edition, 52: 9238-9241.
http://dx.doi.org/10.1002/anie.201302137

Wingler LM y Cornish VW, 2011. Reiterative Recombination for the *in vivo* assembly of libraries of multigene pathways. Proceedings of the National Academy of Sciences of the United States of America, 13: 15135-40.
http://dx.doi.org/10.1073/pnas.1100507108

Wong TS, Zhurina D y Schwaneberg U, 2006. The diversity challenge in directed protein evolution. Combinatorial Chemistry & High Throughput Screening, 9: 271-88.
http://dx.doi.org/10.2174/138620706776843192

Wong TS, Roccatano D y Schwaneberg U, 2007. Steering directed protein evolution: strategies to manage combinatorial complexity of mutant libraries. Environmental Microbiology, 9: 2645-2659.
http://dx.doi.org/10.1111/j.1462-2920.2007.01411.x

Y

Yu Y y Lutz S, 2011. Circular permutation: a different way to engineer enzyme structure and function. Trends in Biotechnology, 29: 18-25.
http://dx.doi.org/10.1016/j.tibtech.2010.10.004

Z

Zhao H, Giver L, Shao Z, Affholter JA y Arnold FH, 1998. Molecular Evolution by Staggered Extension Process (StEP) *in vitro* Recombination. Nature Biotechnology, 16: 258-261.
http://dx.doi.org/10.1038/nbt0398-258

Zollinger H, 2004. Diazo Chemistry I: Aromatic and Heteroaromatic Compounds. Wiley-VCH Verlag GmbH & Co. KGaA, 1-13.
http://dx.doi.org/10.1002/3527601724.fmatter

Zumarraga M, Bulter T, Shleev S, Polaina J, Martinez-Arias A, Plou FJ, Ballesteros A y Alcalde M, 2007. *In Vitro* Evolution of a Fungal Laccase in High Concentrations of Organic Cosolvents. Chemistry and Biology, 14: 1052-1064.
http://dx.doi.org/10.1016/j.chembiol.2007.08.010

Zumarraga M, Camarero S, Shleev S, Martínez-Arias A, Ballesteros A, Plou FJ y Alcalde M, 2008. Altering the laccase functionality by *in vivo* assembly of mutant libraries with different mutational spectra. Proteins, 71: 250-260.
http://dx.doi.org/10.1002/prot.21699

ANEXOS

9

ANEXO I

Secuencia de UPOs evolucionadas

```
1    ATG AAA TAT TTT CCC CTG TTC CCA ACC TTG GTC TAC GCA GTG GGG   45
1     M   K   Y   F   P   L   F   P   T   L   V   Y   A   V   G   15

46   GTC GTT GCT TTT CCT GAC TAC GCC TCA TTG GCC GGC CTC AGC CAG   90
16    V   V   A   F   P   D   Y   A   S   L   A   G   L   S   Q   30

91   CAG GAA TTG GAC GCT ATA ATC CCA ACA CTC GAG GCC CGA GAG CCA  135
31    Q   E   L   D   A   I   I   P   T   L   E   A   R   E   P   45

136  GGA TTA CCT CCT GGT CCT CTC GAG AAT AGC TCT GCA AAG TTG GTG  180
46    G   L   P   P   G   P   L   E   N   S   S   A   K   L   V   60

181  AAC GAC GAG GCT CAC CCA TGG AAG CCG CTT CGA CCT GGC GAT ATT  225
61    N   D   E   A   H   P   W   K   P   L   R   P   G   D   I   75

226  CGT GGA CCT TGC CCT GGT CTC AAT ACT CTG GCA TCT CAC GGG TAC  270
76    R   G   P   C   P   G   L   N   T   L   A   S   H   G   Y   90

271  CTC CCG AGA AAT GGC GTT GCA ACC CCG GCG CAA ATA ATA AAC GCG  315
91    L   P   R   N   G   V   A   T   P   A   Q   I   I   N   A  105

316  GTT CAG GAA GGA TTC AAT TTC GAC AAT CAA GCC GCA ATC TTC GCC  360
106   V   Q   E   G   F   N   F   D   N   Q   A   A   I   F   A  120

361  ACA TAT GCG GCC CAC CTT GTG GAC GGC AAT CTC ATT ACG GAC TTG  405
121   T   Y   A   A   H   L   V   D   G   N   L   I   T   D   L  135

406  CTG AGC ATC GGA CGC AAG ACG CGG CTC ACT GGG CCT GAT CCA CCA   50
136   L   S   I   G   R   K   T   R   L   T   G   P   D   P   P   50

451  CCC CCC GCT TCC GTT GGT GGA CTC AAT GAG CAT GGC ACC TTC GAA  495
151   P   P   A   S   V   G   G   L   N   E   H   G   T   F   E  165

496  GGC GAC GCC AGT ATG ACC CGA GGT GAC GCA TTC TTT GGC AAC AAC  540
166   G   D   A   S   M   T   R   G   D   A   F   F   G   N   N  180

541  CAC GAT TTC AAT GAG ACG CTC TTC GAA CAG TTG GTT GAC TAC AGC  585
181   H   D   F   N   E   T   L   F   E   Q   L   V   D   Y   S  195

586  AAC CGA TTT GGA GGA GGA AAA TAC AAT CTT ACC GTC GCG GGG GAG  630
196   N   R   F   G   G   G   K   Y   N   L   T   V   A   G   E  210

631  CTC CGT TTC AAG CGC ATT CAA GAC TCC ATT GCG ACC AAC CCC AAT  675
211   L   R   F   K   R   I   Q   D   S   I   A   T   N   P   N  225

676  TTC TCC TTT GTT GAC TTT AGG TTC TTT ACT GCT TAC GGC GAG ACC  720
226   F   S   F   V   D   F   R   F   F   T   A   Y   G   E   T  240


721  ACC TTC CCC GCG AAT CTT TTT GTG GAT GGG CGC AGG GAC GAC GGC  765
241   T   F   P   A   N   L   F   V   D   G   R   R   D   D   G  255
```

```
766  CAG CTA GAT ATG GAT GCT GCA CGG AGT TTT TTC CAA TTC AGC CGT  810
256   Q   L   D   M   D   A   A   R   S   F   F   Q   F   S   R   270

811  ATG CCT GAC GAT TTC TTC CGC GCA CCC AGC CCG AGA AGT GAC ACA  855
271   M   P   D   D   F   F   R   A   P   S   P   R   S   D   T   285

856  GGA GTC GAG GTA GTT GTA CAG GCT CAT CCT ATG CAG CCC GGA AAA  900
286   G   V   E   V   V   V   Q   A   H   P   M   Q   P   G   K   300

901  AAT GTC GGC AAG ATC AAC AGC TAC ACC GTC GAC CCA ACA TCC TCT  945
301   N   V   G   K   I   N   S   Y   T   V   D   P   T   S   S  315

946  GAC TTT TCC ACC CCC TGC TTG ATG TAC GAG AAA TTC GTC AAC ATA  990
316   D   F   S   T   P   C   L   M   Y   E   K   F   V   N   I  330

991  ACG GTC AAG TCA CTC TAC CCG AAT CCG ACG GTG CAG CTT CGC AAA 1035
331   T   V   K   S   L   Y   P   N   P   T   V   Q   L   R   K  345

1036 GCC CTT AAT ACG AAT CTC GAT TTC TTA TTC CAG GGA GTC GCC GCT 1080
346   A   L   N   T   N   L   D   F   L   F   Q   G   V   A   A  360

1081 GGA TGT ACC CAG GTC TTC CCA TAC GGG CGA GAT TGA   1116
361   G   C   T   Q   V   F   P   Y   G   R   D   *    372
```

Las mutaciones introducidas en el péptido señal aparecen subrayadas y en negrita. La secuencia correspondiente al péptido señal se muestra en rojo.

Las mutaciones aparecidas en la evolución hacia expresión funcional aparecen resaltadas en azul, con el cambio nucleotídico subrayado.

Las mutaciones aparecidas en la evolución hacia producción de 1-naftol se señalan en verde, con el cambio nucleotídico subrayado.

ANEXO II

Publicaciones relacionadas con la Tesis Doctoral

1. Gonzalez-Perez D, Molina-Espeja P, Garcia-Ruiz E y Alcalde M, 2014. Mutagenic organized recombination process by homologous *in vivo* grouping (MORPHING) for directed enzyme evolution. PLoS ONE 9: e90919.
   http://dx.doi.org/10.1371/journal.pone.0090919
2. Molina-Espeja P, Garcia-Ruiz E, Gonzalez-Perez D, Ullrich R, Hofrichter M y Alcalde M, 2014. Directed evolution of unspecific peroxygenase from *Agrocybe aegerita*. Applied and Environmental Microbiology, 80: 3496-3507.
   http://dx.doi.org/10.1128/AEM.00490-14
3. Molina-Espeja P, Ma S, Mate DM, Ludwig R y Alcalde M, 2015. Tandem-yeast expression system for engineering and producing unspecific peroxygenase. Enzyme and Microbial Technology, 73-74:29-23.
   http://dx.doi.org/10.1016/j.enzmictec.2015.03.004
4. Molina-Espeja P, Cañellas M, Plou FJ, Hofrichter M, Lucas F, Guallar V y Alcalde M, 2016. Synthesis of 1-Naphthol by a Natural Peroxygenase Engineered by Directed Evolution. ChemBioChem, 2016, en prensa.
   http://dx.doi.org/10.1002/cbic.201500493

Patentes relacionadas con la Tesis Doctoral

1. Molina-Espeja P, Garcia-Ruiz E, Gonzalez-Perez D, Ullrich R, Hofrichter M y Alcalde M, 2014. Peroxigenasa inespecífica con alta actividad monooxigenasa. P201430595.
2. Molina-Espeja P, Plou FJ y Alcalde M, 2015, Mutantes de la peroxigenasa inespecífica con alta actividad monooxigenasa y sus usos. P201531641.

Publicaciones no relacionadas con la Tesis Doctoral

1. Camarero S, Pardo I, Cañas AI, Molina P, Record E, Martínez AT, Martínez MJ y Alcalde M, 2012. Engineering platforms for directed evolution of laccase from *Pycnoporus cinnabarinus*". Applied and Environmental Microbiology, 78:1370-1384. http://dx.doi.org/10.1128/AEM.07530-11
2. Garcia-Ruiz E, Mate DM, Gonzalez-Perez D, Molina-Espeja P, Camarero S, Martínez AT, Ballesteros AO y Alcalde M, 2013. Directed evolution of ligninolytic oxidoreductases: from functional expression to stabilization and beyond. En: Cascade Biocatalysis: Integrating Stereoselective and Environmentally Friendly Reactions, 1-22, 1st ed. Riva S y Fessner WD eds. Wiley-VCH Verlag GmbH & Co. KGaA.
   ISBN: 978-3-527-33522-0
3. Molina-Espeja P, Viña-Gonzalez J, Gomez BJ, Martin-Diaz J, Garcia-Ruiz E y Alcalde M, 2016. Beyond the outer limits of nature by directed evolution. Biotechnology Advances. Enviado.

Participación en congresos

1. "Directed evolution of a high-redox potential laccase for functional expression in S. cerevisiae." Póster presentado en Oxidative Enzymes as Sustainable Industrial Biocatalysts 1st Conference (Santiago de Compostela, España, 14-15 de Septiembre de 2010).
2. "Evolución molecular dirigida de una lacasa fúngica de alto potencial redox en *S. cerevisiae*." Póster presentado en VI Reunión de la Red Temática Nacional sobre Estructura y Función de Proteínas (Madrid, España, 21-23 de Abril de 2010).
3. "High-redox potencial laccase engineered by directed evolution in *Saccharomyces cerevisiae*." Póster presentado en III Congreso de Microbiología Industrial y Biotecnología Microbiana - CMIBM2010 (Alcalá de Henares, Madrid, España, 17-19 de Noviembre de 2010).

4. "Directed evolution of a high-redox potential laccase for functional expression in *S. cerevisiae*." Póster presentado en Oxidative Enzymes as Sustainable Industrial Biocatalysts 1st Conference (Santiago de Compostela, España, 14-15 de Septiembre de 2010).
5. "*Saccharomyces cerevisiae* in directed evolution: an efficient tool to improve enzymes". Póster presentado en Biotrans (Sicilia, Italia, 2-6 de Octubre de 2011).
6. "High-redox potencial laccase engineered by directed evolution in *Saccharomyces cerevisiae*." Póster presentado en III Congreso de Microbiología Industrial y Biotecnología Microbiana - CMIBM2010 (Alcalá de Henares, Madrid, España, 17-19 de Noviembre de 2010).
7. "Directed evolution of α-factor prepro-leader fusion genes for functional expression in *Saccharomyces cerevisiae*". Póster presentado en Multistep Enzyme-Catalyzed Processes 2012-MECP12 (Graz, Austria, 10-13 de Abril de 2012).
8. "Applications of biocatalysts in sustainable chemistry. Directed evolution and semi-rational approaches". Póster presentado en International Congress on Biocatalysis (Hamburgo, Alemania, 2-6 de Septiembre de 2012).
9. "Expresión funcional y evolución molecular dirigida de la peroxigenasa inespecífica de *Agrocybe aegerita* en *Saccharomyces cerevisiae*." Comunicación oral en la XVI Reunión de la Red Temática Española LignoCel (Biotecnología de Materiales Lignocelulósicos, Pontevedra, España, 26 y 27 de Septiembre de 2013).
10. "Engineering of Unspecific Peroxygenase by Directed Evolution in *Saccharomyces cerevisiae*." Comunicación oral en la VIII Reunión de la Red de Estructura y Función de Proteínas (Madrid, España, 2-4 de Abril de 2014).
11. "Engineering the Unspecific Peroxygenase, a Wide Reaction Range Biocatalyst, by Directed Evolution." Póster presentado en 3rd Multistep Enzyme-Catalyzed Processes 2014-MECP14 (Madrid, España, 7-10 de Abril de 2014).

12. "MORPHING: a random domain mutagenesis method for directed enzyme evolution." Póster presentado en 3rd Multistep Enzyme-Catalyzed Processes Congress 2014 - MECP14 (Madrid, España, 7-10 de Abril de 2014).
13. "Exploring substrate promiscuity of unspecific peroxygenase from *Agrocybe aegerita* by neutral genetic drift". Póster presentado en 3rd Multistep Enzyme-Catalyzed Processes Congress 2014 - MECP14 (Madrid, España, 7-10 de Abril de 2014).
14. "Exploring monooxygenase activity in mutant libraries of unspecific peroxygenase from *Agrocybe aegerita*." Póster presentado en el European Workshop on Lignocellulosics and Pulp 2014 - EWLP 2014 (Sevilla, España, 24-27 de Junio de 2014).
15. "Evolución dirigida de una peroxigenasa inespecífica, un catalizador altamente promiscuo y selectivo." Comunicación oral en el XXXVII Congreso de la Sociedad Española de Bioquímica y Biología Molecular (Granada, España, 9-12 de Septiembre de 2014).
16. "Directed evolution of the ligninolytic consortium." Póster presentado en 4th International Conference on Novel Enzymes (Gent, Bélgica, 14-17 de Octubre de 2014).
17. "Directed evolution of unspecific peroxygenase from *Agrocybe aegerita*." Póster presentado en el Biotrans 2015 (Viena, Austria, 26-30 de Julio de 2015).

DISEÑO DE LA PEROXIGENASA INESPECÍFICA DE *Agrocybe aegerita* MEDIANTE EVOLUCIÓN DIRIGIDA: EXPRESIÓN FUNCIONAL EN LEVADURAS Y SÍNTESIS DE 1-NAFTOL. La peroxigenasa inespecífica (UPO) se considera el relevo de las P450 monooxigenasas para incontables oxifuncionalizaciones C-H de gran interés en síntesis orgánica. Se trata de una enzima hemo-tiolada extracelular y estable que emplea el H_2O_2 tanto como donador de oxígeno como aceptor final de electrones. Haciendo uso de un amplio abanico de herramientas de evolución dirigida, se ha preparado una plataforma para la expresión funcional y sobre-producción en levaduras de mutantes activos y estables, y ha sido finalmente empleada en el diseño una variante UPO altamente eficiente en la producción de 1-naftol.

DESIGN OF THE UNSPECIFIC PEROXYGENASE FROM *Agrocybe aegerita* BY DIRECTED EVOLUTION: FUNCTIONAL EXPRESSION IN YEASTS AND 1-NAPHTHOL SYNTHESIS. The unspecific peroxygenase (UPO) is considered the relief of the P450 monooxygenases to countless C-H oxyfunctionalizations of great interest in organic synthesis. This heme-thiolate, extracellular and stable enzyme uses H_2O_2 both as oxygen donor as well as final electron acceptor. Making use of a wide range of directed evolution tools, a platform for functional expression and over-production in yeasts of active and stable mutants has been prepared, and it has been further used to design an UPO variant highly efficient in the production of 1-naphthol.

ICP
INSTITUTO DE CATÁLISIS Y PETROLEOQUÍMICA

CSIC
CONSEJO SUPERIOR DE INVESTIGACIONES CIENTÍFICAS